UNIVERSITY OF SOUTHAMPTON

THE STABILITY AND EVOLUTION OF AN INTERTIDAL FLAT IN VENICE LAGOON, ITALY.

Sergio Cappucci

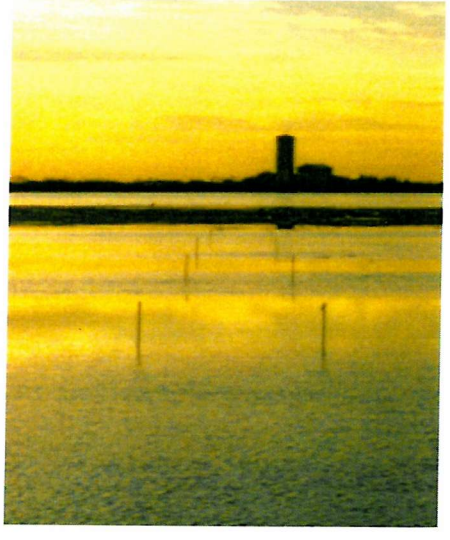

A Thesis submitted to the Faculty of Science in partial fulfilment of the requirements for the degree of Doctor of Philosophy

School of Ocean and Earth Science
Faculty of Science

July 2002

Graduate School of the

Southampton Oceanography Centre

This PhD dissertation by

Sergio Cappucci

has been produced under the supervision of the following persons

Supervisor/s
Dr. Carl Amos

Chair of Advisory Panel
Prof. Michael Collins

Member/s of Advisory Panel

UNIVERSITY OF SOUTHAMPTON

ABSTRACT

FACULTY OF SCIENCE
SCHOOL OF OCEAN AND EARTH SCIENCE

Doctor of Philosophy

THE STABILITY AND EVOLUTION OF AN INTERTIDAL FLAT IN VENICE LAGOON, ITALY.

by Sergio Cappucci

Venice Lagoon is the estuary with the largest area and the greatest microtidal range (1 m spring tide) in the Mediterranean Sea. Presently, the Lagoon is suffering from a sediment loss of ~1 million m^3/a seawards. The consequence of such a deficit in the sediment budget is the progressive destruction of salt marshes and tidal flats. It is estimated that all the salt marshes will have disappeared by 2040 if this trend continues (Consorzio Venezia Nuova, 1996).

In this study, a multidisciplinary investigation was undertaken at two different spatial scales (regional and local) to determine the factors controlling the stability and evolution of Venice Lagoon. A 0-D numerical model, SLIM (Simulation of LIttoral Morphodynamics), was constructed to predict factors responsible for the evolution of mudflats within the Lagoon.
At the regional scale, seven sites were studied during two field campaigns in August 1998 and in February-March 1999 to investigate the temporal and spatial variation of surface sediment properties, sediment stability and environmental characteristics within a range of different habitats (subtidal and intertidal). A new version of the Mini Flume (an erosive device) was deployed *in-situ* for the first time, with the purpose of determining the critical erosion shear stress of surficial sediments under controlled flows. At the local scale, Palude della Centrega, was chosen as a representative cohesive intertidal mudflat in the northern part of the Lagoon. Here sediment stability, sediment properties, elevation and habitat changes were monitored over a period of 16 months, from August 1998 until December 1999. The critical erosion threshold and shear strength of the intertidal sediments were derived using the Cohesive Strength Meter (CSM) and a Tor Vane Shear Meter (TSM), respectively.

Relationships between the critical erosion threshold of the lagoonal sediments and their biological properties reveal that a complex feed-back mechanism exists which enhances the accretion of the intertidal areas in the northern part of the Lagoon. The sediment stability of Palude della Centrega is influenced by changes in sediment bulk density and water content. Palude della Centrega is accreting at a constant rate of 1.52 cm/a. This evolutionary trend is confirmed by investigations of the long-term morphological changes undertaken during the present study, as well as sediment dating carried out in the area by others and is in contrast with the general trend of intertidal mudflats in Venice Lagoon. Sensitivity analyses carried out using SLIM show that accretion of Palude della Centrega is controlled mainly by: 1) sediment input provided by the erosion of the surrounded areas; and 2) biostabilisation of sediments by the micro and macro-phytobenthos which increase the erosion threshold and decrease the bed shear stresses applied by wind-generated waves.

ACKNOWLEDGEMENTS

Firstly I would like to thank my supervisor Dr. Carl Amos for allowing me entry into the F-ECTS project (MAST III - CT97 – 0145, which financially supported this thesis) and for his excellent advice. I am in debt to Dr. Damon O'Brien for the help he provided in all phases of this work. I feel immense gratitude to all members of the Sediment Dynamics Group of SOC who, in different ways, helped me to understand the Philosophy of cohesive sediment dynamics (in particular Dr. Patrick Friend shared with me all the problems of deploying the CSM on cohesive sediments and helped me reviewing the manuscript).

Many people deserve a big "thank you" for their genuine help during my field work: Dr. P. Ciavola, F. Corbani, D. Cloutier, S. Cristante, C. Evarchi, F. Lenci, A. Levy, B. Murphy, B. Wile in particular have been vital for data acquisition. Field work in Venice Lagoon could not have been carried out without the invaluable support of many people from THETIS SpA (particularly to A. Bergamasco and L. DeNat). A big "thank you" also goes to R. Cattellan for his help in the laboratory analyses at THETIS SpA, to C. Piovesan and R. Marascalchi for the technical support and the help provided to fix the instruments before the Winter campaign (without them, the Mini Flume could not have been deployed during the second field programme).

Within the SOC many people, besides my supervisor, have contributed to the development of the numerical model. In particular, Alessio Bellucci, Dr .Daniel Perez and my office mate Taro Hosoe gave me invaluable support in the debugging and the reconstruction of the numerical model that only after a long time started to respond correctly to my commands. (This part of the work has been also funded by the CNR (It): SLIM project - *Bando* 203.21 - *codice* 03). The time-series of tidal currents used to run the model were provided by Dr. Umgiesser from the *Istituto Studio Dinamica Grandi Masse* (ISDGM), Italy.

Thanks to all the PG community of Cardiff University and the SOC for a great time!

Finally, I would like to thank my family for the encouragement that has been vital to the completion of this thesis.

Dedicated to the memory of Dr. A. Cramp
and Lorenzo Cuneo

TABLE OF CONTENTS

ABSTRACT

ACKNOWLEDGEMENTS

INDEX

LIST OF FIGURES

LIST OF TABLES

LIST OF NOTATION AND SYMBOLS

CHAPTER I: INTRODUCTION

Reseach perspective 1
Thesis outline 5

CHAPTER 2: BACKGROUND ON SEDIMENT STABILITY OF INTERTIDAL MUDFLATS.

2.1. Forces acting on particles 6
2.2. The erosion threshold and cohesion 7
2.3. Factors controlling sediment stability 8
Physical control of sediment stability 9
Biological adhesion 11
2.4. Definitions of sediment stability and erodibility 15

CHAPTER 3: BACKGROUND TO VENICE LAGOON

3.1. Introduction to Venice Lagoon 18
3.2. Tide and wave conditions 20
3.3. Sediment supply 25
3.4. Subsidence 28
3.4.1. Natural subsidence 28
3.4.2. Anthropogenic subsidence 28
3.4.3. Relative subsidence due to eustacy 29
3.5. Pollution 31

3.6. Summary 32

CHAPTER 4: IN-SITU STABILITY MEASURED WITHIN VENICE LAGOON.

4.1. Introduction 33
4.1.1. The F-ECTS campaigns 34
4.2. Method 34
4.2.1. Description of sites and environmental conditions 34
4.2.2. Stability measurements 37
Measurements of sediment stability using the Mini Flume 37
Description of the Mini Flume (in-situ apparatus) 38
Mini Flume calibration 38
Data processing 43
4.2.3. Core sampling 45
Gravity cores 45
Syringe cores 46
4.3. Results 46
4.3.1. Environmental conditions 46
4.3.2. Results from the Mini Flume deployments 49
4.3.3. Sediment properties 50
Texture and grain size from the gravity cores 50
Physical and biological properties from the syringe cores 53
4.3.4. Comparison between Mini Flume and Sea Carousel 54
4.3.5. The relationship between erosion threshold and sediment properties in Venice Lagoon 57
4.4. Discussion 57
4.5. Summary 61

CHAPTER 5: SEDIMENT STABILITY OF PALUDE DELLA CENTREGA

5.1. Introduction 63
5.2 Methodology 66
5.2.1. Topographic surveying 66
5.2.2. Sediment strength using the Tor Vane Shear Meter (TSM) 67
5.2.3. Sediment stability using the Cohesive Strength Meter (CSM) 69

5.2.4. Sampling strategy 76
5.2.5. A comparison between the CSM and Mini Flume 76
5.3. Results 79
5.3.1. Absolute elevation and habitat descriptions 79
5.3.2. Sediment strength using the TSM 82
5.3.3. Erosion threshold using the CSM 84
5.3.4. Physical and biological properties of the mudflat 86
5.3.5. Data analysis 90
5.3.6. A comparison of results between the CSM and Mini Flume. 92
5.4. Limitations 94
5.5. Discussion 95
5.5.1. A comparison of Vane Shear Strength and τ_c results. 96
5.5.2. The relationship between erosion threshold and sediment properties from Palude della Centrega 97
5.6. Summary 100

CHAPTER 6: THE EVOLUTION OF PALUDE DELLA CENTREGA

6.1. Introduction and background to the short term and long term studies to investigate morphological changes of Palude della Centrega 101
Short-term bed level changes 101
Long-term morphological changes 102
6.2. Method 105
6.2.1. Monitoring of bed level changes of Palude della Centrega 105
6.2.2. Long-term study of salt marsh distribution in Palude della Centrega 106
6.2.3. Radionuclide analyses 106
6.3. Results 106
6.3.1. Short-term accretion rate of Palude della Centrega 106
6.3.2. Long-term accretion rate of Palude della Centrega 111
6.4. Discussion 113

CHAPTER 7: PREDICTION OF EVOLUTION BY 0-D MODELLING

A background to the modelling of intertidal areas 115
7.1. Description of the SLIM model 117

7.1.2. Calculation of bed shear stress 119
7.1.3. Estimation of erosion rate 121
7.1.4. Evaluation of deposition rate 121
7.2. Modelling of bed level changes in Palude della Centrega 122
7.2.1 Sediment transport under tidal currents. 122
7.2.2. Sediment transport under the combined effect of tidal currents and waves 124
7.3. Model sensitivity analysis 129
7.3.1. Effects of varying erosion thresholds 130
7.3.2. Effects of varying sediment export 131
7.3.3. Effects of varying bed properties on the erosion process 132
7.3.4. Effects of varying sediment input 134
7.3.5. Effects of shear stress reduction due to plant cover 135
7.3.6. Effects of the Bora wind on the migration of Canale Scanello 137
7.4. Results 138
7.5. Model calibration 140
7.6. Summary 141

CHAPTER 8: CONCLUDING REMARKS AND FUTURE WORK

Conclusion 143
Future work 146

REFERENCES 148

APPENDICES

LIST OF FIGURES

Figure 1.1. Mud flat block diagram (from PETHICK, 1990). 1

Figure 1.2. Schematic diagram of the interlinking processes on intertidal mud flats (after DYER; 1996). 2

Figure 2.1. Forces acting on a particle resting on a grain boundary under the effect of fluid motion. F_G = gravity force; F_L = lift force; F_D = drag force; CG is the gravity centre. 6

Figure 2.2. Shields type diagram of mean current velocity (ordinate) necessary to erode uniform material (from HJÜLSTROM, 1939). 9

Figure 2.3. The Shields threshold curve (after MILLER *et al.*, 1977), where θ is the Shields parameter and Re is the Reynolds number. 10

Figure 2.4. Scanning Electronic Micrograph (SEM) showing a diatom-dominated biofilm (from UNDERWOOD *et al.*, 1995). 12

Figure 2.5. Laboratory tests on the effect of diatoms on erosion threshold. Critical velocity is along the ordinate (U_*) and time along the x axis (hours). Lines indicate stability of sediment with (filled lines) and without (dotted line) diatoms. (from VOS *et al.*, 1988). 13

Figure 2.6. Classification of types of cohesive sediment erosion. Type I erosion (top) and type II erosion (centre) can be distinguished by a logarithmic or linear increase of suspended sediment concentration in the water column. They can occur together (bottom) depending on the nature of the sediments and characteristics of the flow (from PATERSON & BLACK, 1999). 16

Figure 2.7. Schematic diagram showing the cohesive sediment erosion process (from DELO & OCKENDEN, 1992). 17

Figure 3.1. A satellite image of Venice Lagoon, Italy. Note the study area is located in the northern part of the Lagoon (dark pattern) where the intertidal mudflats are better preserved (the dotted line marks the dredged Malamocco Canal). 19

Figure 3.2. Two transects across Venice Lagoon represent the situation of the approximate elevation of the Lagoon deposits in 1930 (above) and 1990 (below). The horizontal line represents MSL (from CVN, 1996). 20

Figure 3.3. Tidal range (*A*), tidal current velocities (*B*) and bed shear stress (*C*) applied by tides at the studied area (*Palude della Centrega*). 22

Figure 3.4. Bed shear stress due to wind generated waves at different depths (D) of water. The critical shear stress was estimated between 0.2 and 1 Pa (dotted lines) (from DHI, 1991). 23

Figure 3.5. Typical edge of vegetated salt marshes in Venice Lagoon. Note the position of the imminent failure (white dotted lines). 24

Figure 3.6. *Acqua alta* occurrences. The increased frequencies of inundation (red areas) started after 1950 as a consequence of the lowering in ground level (gl). Increased storminess and the change in the inundation regime resulted in a destabilisation of the intertidal regions (from GATTO & CARBOGNIN, 1981). 25

Figure 3.7. A schematic representation of the river diversion carried out in Venice Lagoon between the 15th and the 19th century (from CVN, 1996). 26

Figure 3.8. Sediment input from rivers (blue line) and the open sea (black line) in the last five centuries (from CNV,1996). 27

Figure 3.9. The relative distribution of water discharge in the northern, central and southern basin of Venice Lagoon. Note that 88% of the river discharge is concentrated in the northern and central basin where the salt marshes and mudflat are better preserved (data obtained from the DRAIN project: ZONTA, 2000). 27

Figure 3.10. Relative sea level changes in Venice Lagoon due to subsidence and eustacy from 1908 to 1980 (GATTO & CARBOGNIN, 1981). After 1975 the trend of subsidence follows the natural rate of about 0.4 mm/a. 29

Figure 3.11. Mean sea level records for the cities of Venice and Trieste between 1896 and 1993 (CARBOGNIN & TARONI, 1996). Note that the greater lowering rate of Venice started around 1930 due to human activities. 30

Figure 4.1. The study region of Venice Lagoon showing the position of the sites occupied by Mini Flume. The 7 sites investigated in August '98 and February March '99 are represented by white dots. 35

Figure 4.2. The barge (A) used to deploy the flumes (B) in Venice Lagoon, Italy. 36

Figure 4.3. The Mini Flume used *in-situ* mounted on a deployment frame. 39

Figure 4.4. The Mini Flume foot print left on the mud after deployment in station V50. 39

Figure 4.5. The relationship between the M value input of the Mini Flume motor and the rotational speed (rev/s) of the lid (A). The relationship between lid speed and the applied bed shear stress was calculated using O'BRIEN (1998) and from LDV data of FUNG (1997; B). 41

Figure 4.6. The relationship between OBS output and SSC derived for (1) low and (2) high gains of the OBS on Mini Flume. 43

Figure 4.7. A typical time-series of the Mini Flume. In this illustration, the erosion threshold was derived using (1) the highest increments of stress, yielding in a τ_c = 2.4 Pa (solid line) and (2) excluding the highest increments of stress, yielding in a τ_c =2.0 Pa (dotted line). Estimate of τ_c are based on the full data set in this study. The data is from site V40 undertaken in the northern Lagoon during summer 1998. 44

Figure 4.8. A schematic representation of the sub-sampling operations before analysis. 46

Figure 4.9. SSC and wind speed measured during the F-ECTS field campaign. Note the high turbidity occurring after 48 - 72 hours of increased wind speed. 48

Figure 4.10. Erosion threshold measured *in-situ* at different sites in Venice Lagoon during the two field campaigns (summer 1998 and winter 1999). Data have been calculated from Mini Flume deployments. Stations V41, V42, V43, V44 were located close to station V40, but aligned across a section of the *Canale Scanello* where sediments did not show any evidence of biostabilisation (measurements in these stations were not replicated during the winter campaign). 50

Figure 4.11. Textural classification of surface sediments in Venice Lagoon. Note the increasing sand content moving from the north (V50) to the south (V60). 52

Figure 4.12. Relationships found between the sand content and the distance from the northern part of the lagoon (O) and from the closest inlet (□) based upon sites investigated during summer campaign of the F-ECTS project. 52

Figure 4.13. The Sea Carousel and the Mini Flume systems in operation. 55

Figure 4.14. A comparison between erosion threshold determined by Sea Carousel and Mini Flume during the two F-ECTS field campaign. The red area indicates the critical shear stress for erosion predicted by DHI (1991). 56

Figure 4.15. Erosion threshold values derived from Mini Flume (MF) and Sea Carousel (SC) deployments during the F-ECTS campaigns. Also illustrated is the 1:1 line between the two parameters. 56

Figure 4.16. Quantitative relationships between erosion threshold (derived by MF) and colloidal carbohydrate (A), chlorophyll *a* (B) and elevation (C) at sites investigated during the F-ECTS campaigns. Note that significant relationships were found during the summer campaign (red line) due to the increase in biological activity of the two intertidal areas: V40 and V50. 56

Figure 4.17. A positive feed-back mechanism illustrated in three steps: A) The subtidal area is vegetated by seagrass which enhances accretion; B) the area accretes to the intertidal level; and C) during tidal exposure a biofilm is produced by micro-organisms which stabilise surface sediment. 60

Figure 5.1. A composite photo aero-photograph of *Palude della Centrega* taken in August 1998. Note that station V40 (white dot) is located at the edge of *Canale Scanello* (courtesy of HR Wallingford). 63

Figure 5.2. A schematic diagram showing the location of sampling stations St1 - St16 on *Palude della Centrega* and the distribution of vegetation during August 1998. *Canale Scanello* is not to scale as bathymetric data were not collected; the darker blue colours indicates deeper water (~3 m). 64

Figure 5.3. Water level (WL) recorded at *Lido* inlet on 22 August 1998 and predicted for *Burano* after GOTTARDO & CAVAZZONI (1981). The two lines clearly show the phase lag of the tidal curve between the studied area (close to the village of *Burano*) and the main inlet of the Lagoon. A reduction of about 11 cm was applied at the time of the topographic survey (11:50 a.m.) with respect to sea level measured at the *Lido* Inlet. 67

Figure 5.4. Principal components of the Tor Vane Shear apparatus (from SEROTA & JAGLE, 1972). 68

Figure 5.5. The relationships between shear stress and shear strength derived from DUNN (1959) and from data published by AMOS *et al.* (1996b). The grey area shows the approximate range of shear strength values found in *Palude della Centrega*. 69

Figure 5.6. The CSM Mk4 onsite (image provided by Ian Black). 70

Figure 5.7. Laboratory image of the vertical jet flow structure (TOLHURST *et al.*, 1999). 70

Figure 5.8. The CSM footprint after deployment (bar length is 3 cm). The scour pit provides visual confirmation that erosion has occurred (TOLHURST *et al.*, 1999). 70

Figure 5.9. Erosion threshold (τ_c) derived at 80% light transmission using the CSM at St5. 72

Figure 5.10. The CSM in the laboratory during calibration of light sensors. 74

Figure 5.11. Light transmission during the CSM calibration (each coloured line represents % of light transmitted at each increment of turbidity). A drop in light transmission in some of the time series was due to the magnet lifting within the chamber and subsequent obstruction of the transmissometer light beam. 74

Figure 5.12. The quadratic relationship between light transmission (%) and turbidity (mg/l) for sediments collected in the studied area. 74

Figure 5.13. A typical time series of bed shear stress (*A*), SSC (*B*) and erosion rate (*C*) from a CSM test. (data are from St1). Note peak erosion rate, measured immediately after the jet pulse is proportional to applied shear stress and is followed by settling in the chamber. 75

Figure 5.14. A) The external wall of Mini Flume is pushed into the stiff clay, filled with water and the natural sediments from V40 are added to create a thick homogeneous layer over the bottom.
B) When settling is completed (about 1-2 hours), the internal wall is added in order to run an experiment with the Mini Flume annulus leaving the central core undisturbed. The water is then removed from the central part so that CSM may be deployed immediately. C) Three tests were performed using the CSM on the soft exposed mud layer in the central part of the Mini Flume. 78

Figure 5.15. The CSM chamber inside the annular flume during comparative experiments. 79

Figure 5.16. The absolute elevation of the south-north profile numbered from St1 to St7 and the west-east profile going from St10 to St16 (below). Note that stability measurements (during the F-ECTS study) were performed at the edge of *Canale Scanello* (east of St16). 80

Figure 5.17. St1, August 1998. The southern part of transect 1 is densely covered by *Salicornia* spp. and *Spartina* spp. which have an average height of about 40 cm. 81

Figure 5.18. St7, August 1998. The *Zostera noltii* community during exposure of the mudflat covering the soft mud (see the footprints in the background) of the northern part of the transect. 81

Figure 5.19. A thick biofilm at the edge of *Palude della Centrega* close to *Canale Scanello*. 81

Figure 5.20. Vane shear strength derived at each station along the N-S transect (*A*) and the W-E transect (*B*). Note that maximum sediment stability was found in the upper part of the mudflat (St1) and lower values close to the tidal creeks (St3, St4 and St13). The sediment strength progressively increases southwards and eastwards along the transects. 83

Figure 5.21. Mean erosion threshold derived using the CSM along the N-S transect (A) and along the E-W transect (B). Note that maximum sediment stability occurred in the upper part of the mudflat (St1and St2) and the minimum in areas colonised by the seagrass. Along the N-S transect the erosion threshold generally decreases southwards. 85

Figure 5.22. Bulk density profiles of the syringe cores collected at the four sites during the summer (red) and winter (blue) campaigns. Note the self-weight consolidated top 1 cm characterising all the samples analysed. Generally, bulk 89

density was found to be higher in summer than in winter (St6 showed higher values during winter 1999).

Figure 5.23. Erosion thresholds derived from the three CSM deployments. Note the rapid drop in light transmission, and the consistency in light transmission values between the three tests performed. 93

Figure 5.24. Erosion thresholds derived from Mini Flume deployments. 93

Figure 5.25. Comparison between the erosion threshold derived using the CSM and the Mini Flume on cohesive sediment from *Palude della Centrega*. 93

Figure 5.26. A schematic diagram showing increasing bulk density with sediment depth. Deeper and denser sediments can increase τ_v. τ_c derived by flume deployments is based on the erosion of the top 1 mm. 94

Figure 5.27. Erosion threshold values derived using the TSM during summer '98 (red dots) and winter '99 (blue dots) using the equation of DUNN (1959) and AMOS *et al.* (1996) are compared against the erosion threshold derived using the CSM. Note that the equation of DUNN (1959) which was used to transform the TSM data gave values of 2.5-3 Pa. 96

Figure 5.28. VSS derived in August 1998 (red dots) and February 1999 (blue dots) versus τ_c derived CSM on a 1:1 line. 97

Figure 5.29. Relationships between the erosion threshold and bulk density found in the present study and by AMOS *et al.* (1996b). 97

Figure 5.30. Possible mechanisms proposed to correlate the reduction of τ_c along the E-W transect with the highest sea grass density cover and the highest water content. During inundation, the reduction of the shear stress applied at the sediment/water interface is controlled by high densities of sea grass which can reduce the bed shear stress westward (A). During exposure the density of macroalgae and seagrass that protected sediments from solar radiation and prevented drainage can reduce evaporation (B). The erosion threshold is influenced by the water content (i.e. bulk density) of superficial sediments (C). 99

Figure 6.1. General scheme of the relationship between human activities and morphological evolution of the intertidal areas of Venice Lagoon (CNV, 1992). 103

Figure 6.2. The two poles and the cross bar used to measure changes in bed level elevation. 105

Figure 6.3. Changes in bed level elevation at stations along the N-S transect (*A*) and E-W transect (*B*). Note that maximum accretion rate was found in the upper part of the studied area (N-S transect) and lower values found close to the tidal creeks. 108

Figure 6.4. Changes in mean bed level elevation through time along the N-S transect. At St1, St2, St3, St4 no data were collected on the 16th October 1998. 109

Figure 6.5. Changes of mean bed level elevation through time along the E-W transect. 110

Figure 6.6. A digital map of *Palude della Centrega* from data collected in 1908. Salt marshes are indicated in grey (their elevation is $0<Z<0.5$ m). 112

Figure 6.7. A digital map of *Palude della Centrega* during 1968. Salt marshes are indicated in grey (their elevation is $0<Z<0.5$ m). 112

Figure 6.8. A schematic representation of the migration westwards of *Canale Scanello* (arrow indicates the direction of migration). Morphological analysis of the studied area suggests long-term migration westwards of the channel. Note that on the western flank of the channel, both the gravity core and bed level changes in St16 revealed erosion. 114

Figure 7.1. The internal sediment redistribution model of Venice Lagoon (SILVA & MOL, 1993). 116

Figure 7.2. A scheme of the input and output values of the model (SLIM) used for simulations. 117

Figure 7.3. A simple representation of the box model (SLIM) showing the boundary conditions of the mass conservation equation. SI represents sediment input, SE represents a sediment export which reduces the SSC in the water column and BF represent the benthic flux which is controlled by intermittent erosion and deposition processes. 118

Figure 7.4. A flow diagram of the model SLIM. 120

Figure 7.5. Bed shear stress and SSC time series (A), eroded and deposited mass (B) bed level elevation (C) simulated under the effect of tidal currents and a sediment input of $3.3x10^4$ t/a. Note the deposited mass goes to zero during the exposure of the tidal flat. 123

Figure 7.6. Results of bed level changes under the effect of tidal currents and different sediment inputs. Note that the accretion rate increases with increases in sediment input. 124

Figure 7.7. A time series of wind speeds measured in *Treporti* station and the bed shear stress computed by the model using the equation 7.1.2.II. 126

Figure 7.8. Bed shear stress (A), SSC (B) and elevation (C) computed on the basis of 4 steady increases in wind steps. In this simulation real tidal data were used. Oscillations of SSC (B) are due to different water depths during the erosion periods. 127

Figure 7.9. A time series of bed shear stress (A), SSC (B) and bed elevation (C) computed by the model on a 30-day simulation using real wind speed data measured at *Treporti* on August 1998. 128

Figure 7.10. A time-series of bed shear stress (A), SSC (B) and bed elevation (C) computed by the model with station at MSL. Note the decrease in elevation during storms and the partial deposition of sediments afterwards due to the loss of material in the subtidal areas. 129

Figure 7.11. Results of bed level changes using different values of erosion threshold. Note that the final eroded depth is inversely related to the erosion threshold. The deposition rate obtained using 1.16 and 2.36 Pa shows exactly the same trend because the critical shear stress of erosion is higher than the maximum shear stress applied by wind generated waves. 131

Figure 7.12. Results of bed level changes using different values of sediment export from Venice Lagoon. Note that the erosion rate found using a sediment export of $7.5x10^5$ t/a and $1.5x10^6$ t/a is the same. 132

Figure 7.13. Results of bed level changes using different values of internal friction angle. Note that the black line represents the bed level simulated using a friction 133

angle of zero degrees.

Figure 7.14. Results of bed level changes using different sediment input rates. Note the increase in the accretion rates between the three storms. 134

Figure 7.15. A time-series of bed level predicted from a reduced bed shear stress. Note that final bed level value is not sensitive to a reduction in bed shear stress of less then 50%. 137

Figure 7.16. Station 6 in winter 1999. Note the unvegetated soft mud. 136

Figure 7.17. Station 14 in summer 1998. Note the high density *Zostera noltii* community. 136

Figure 7.18. Station V40 in August 1998. Note the edge of *Canale Scanello* (boat on the left) characterised by exposed mud passing rapidly to the right into seagrass communities. 136

Figure 7.19. A time series of bed level changes under high wind forcing. Note that the model simulates accretion of the intertidal flat when the erosion threshold is 2.36 Pa and erosion when is it 1.16 Pa. 138

Figure 7.20. A summary of results of bed level changes obtained from the sensitivity analysis of SLIM. The vertical blue line separates the results obtained under the effect of currents only and tidal currents and waves. The horizontal blue line separates the simulations of accretion and erosion. SB = sediment stability; SE = sediment export; FA = friction angle ($0°<\phi<30°$); SI= sediment input; BW = *Bora* wind, TauR = bed shear stress reduction. Note that maximum erosion is obtained by modifying the friction angle. Deposition can occur under the effect of tidal currents or, in the presence of waves, under a decreased elevation of the mudflat, an increase in the erosion threshold and a reduction of the bed shear stress by sea grasses. The actual accretion rate (1.5 cm/a) is represented by the green dotted line and is simulated using a sediment input of ~363000 t/a. 139

Figure 7.21. A summary of the calibration results of bed level changes obtained from the sensitivity analysis under the combined effect of high τ_c , reduction of the shear stress by plants and increase in the river sediment input. The calibration of the model can be obtained using a SI of ~363000 t/a, increasing the τ_c up to 1.16 Pa (SB) and using a SI=148000 t/a, or reducing τ_o (TauR) by 50% in combination with a SI=132000 t/a. The dotted arrows represent the contribution of sediment input to the accretion rate. 141

Figure 7.22. A schematic representation of an ideal E-W transect across *Palude della Centrega* during sea grass colonisation in the summer. Note that all flume measurements were carried out at the edge of the channel (downward arrow indicates erosion). Moving westward, wave attenuation (by sea grasses) takes place (MÖLLER *et al.*, 1999), and deposition is enhanced (upward arrow indicates accretion). 142

LIST OF TABLES

Table 2.1. Selected measurements of biogenic stabilisation from the literature. 14

Table 3.1. Principal categories of habitats in Venice Lagoon, their bathymetry and distribution. The data do not include 90 km^2 of the Lagoon which form isolated fish farming areas (from BETTINETTI *et al.*, 1996). 18

Table 4.1. A summary of site descriptions from the F-ECTS field campaigns. 37

Table 4.2. A list of the principal factors that affect the response of the Optical Backscatter Sensor. The magnitude and the effect on the final results are also indicated in order of importance following the results of SUTHERLAND *et al.* (1999*) and BUNT *et al.* (1999**). 42

Table 4.3. The results of all deployments carried out during the F-ECTS summer campaign (Summer 1998) using Mini Flume. The principal water properties are referenced to the deployment time. Note that highest turbidity value was measured at V44 after four windy days (highlighted). 47

Table 4.4. The results of all deployments carried out during the F-ECTS winter campaign (Winter 1999) using the Mini Flume. Principal water properties were measured at the time of deployment. Note that the highest turbidity was measured in station V30 after two windy days (highlighted). 47

Table 4.5. Values of erosion threshold and peak erosion rates are reported for all Mini Flume deployments carried out during summer and winter field surveys. In site V22, V32, V42, V43, V44 deployments were not carried out during the winter campaign. 49

Table 4.6. Mean values (%) of the grain size distribution, in the upper 21 cm of the bed. Depth of the core is reported and colours (generally fades from dark gray to black) are from the top (COVELLI & CIAVOLA, 2000). 46

Table 4.7. A list of the physical and biological parameters determined for each station from samples collected during summer 1998. 53

Table 4.8. A list of the physical and biological parameters determined for each station from samples collected during winter 1999. 53

Table 4.9. Erosion thresholds derived by the Mini Flume and the Sea Carousel (from AMOS *et al.*, 2000). 55

Table 4.10. Regression equations of erosion threshold (τ_c) on sediment properties in Venice Lagoon during Summer 1998 and Winter 1999. Highlighted cells indicate significant relationships ($p<0.05$). 57

Table 5.1. *In-situ* and laboratory investigations carried out in the present study. Laboratory investigations were carried out to quantify the effect of consolidation on τ_c and to compare the results obtained using two different devices to determine τ_c. 65

Table 5.2. Principal instrument characteristics of the Mini Flume and CSM and parameters which can be derived from their use. 76

Table 5.3. Mean shear strength (kPa) and standard deviation derived using the TSM at each station in *Palude della Centrega*. 82

Table 5.4. Erosion threshold and standard deviation values derived from CSM 84

deployments carried out on *Palude della Centrega* in November 1999.

Tables 5.5. A list of the physical and biological properties determined at each station of *Palude della Centrega* in August 1998. 86

Tables 5.6. A list of the physical and biological properties determined at each station of *Palude della Centrega* in February 1999. 87

Tables 5.7. Physical and biological properties determined at each station of *Palude della Centrega* in November 1999. 87

Table 5.8. Regression equations between erosion threshold (τ_c) and sediment properties along the N-S and E-W profiles during August 1998, February 1999, and November 1999. Significant relationships ($p<0.05$) are highlighted. 90

Table 5.9. A list of the principal parameters that describe the hydrodynamic condition of the incremental bed shear stresses applied by the CSM and the Mini Flume. Highlighted areas indicate the bed shear stress steps under which erosion occurred. 92

Table 6.1. Bed level elevation and accretion/erosion rates calculated for each time interval for data collected along the N-S transect. 107

Table 6.2. Bed level elevation and accretion/erosion rate calculated for each time interval for data collected along the W-E transect. 107

Table 6.3. The areal extent of the supratidal areas of *Palude della Centrega* during the 20^{th} century. 111

Table 7.1. Results of bed level changes under the effect of tidal currents and different sediment inputs. 122

Table 7.2. Results of bed level changes under the effect of tidal currents, waves and different sediment inputs. 125

Table 7.3. Results of bed level changes using different values of erosion threshold. 130

Table 7.4. Results of bed level changes using different values of sediment export from Venice Lagoon. 132

Table 7.5. Results of bed level changes using different values of internal friction angle. Note that the eroded depth increases drastically when $\phi = 0$, suggesting an unrealistic erosion rate of 12.39 cm/a. 133

Table 7.6. Results of bed level changes using sediment input rates between 3.3×10^4 t/a and 3.63×10^5 t/a. 134

Table 7.7. Results of bed level changes for reduced shear stresses. Note that the model simulates an accretion of the intertidal flat starting from a reduced bed shear stress value of 80%. 135

Table 7.8. Results of bed level changes under *Bora* winds (wind speed was multiplied by two) at the edge of the *Canale Scanello*. 138

Table 7.9. Results of bed level changes under the effect of sediment input, bed shear stress reduction and high erosion threshold. The parameters changed in the simulations are in bold. 140

LIST OF NOTATION AND SYMBOLS

a	Annum
A	Adhesion
A_l	Area of Venice Lagoon
A_r	Area of exposed grain
A_t	Radioactive activity at time t
A_o	Radioactive activity of original material
BF	Benthic Flux
BW	*Bora* wind (Figure 7.4.1.& 7.5.1.)
C	Cohesion
C_D	Drag coefficient
C_L	Lift coefficient
CC	Colloidal carbohydrate
CEC	Cation exchange capacity
CG	Centre of gravity
CNR	*Consiglio Nazionale delle Ricerche*
CNV	*Consorzio Venezia Nuova*
CST	Cohesive Sediment Transport
C_{100}	Drag coefficients at heights of 100 above the bed respectively
^{137}Cs	Cesium (relative atomic mass: 137)
D	Deposition rate
D_E	Depth of sediment eroded (Equation 2.6.I)
D_r	Grain diameter
D_w	Average water depth of Venice Lagoon (Equation 2.4.I)
D_{50}	Median grain size
DHI	Danish Hydraulic Institute
e	Void ratio
E	Erosion rate
EPS	Extra-cellular polymeric substances
FA	Friction angle
F_D	Drag force
F_G	Gravity force
F_L	Lift force
g	gravitational force constant
GSCA	Geological Survey of Canada - Atlantic
GE	Glucose equivalent
h	Water depth
h_{p1}	Upper depth of ^{137}Cs peak
h_{p0}	Lower depth of ^{137}Cs peak
h_1	Mean bed level at time 1 (Equation 6.2.I)
h_0	Mean bed level at time 0 (Equation 6.2.I)
H_s	Significant wave height
IGM	*Istituto geografico militare*
IR	Infrared signal
ISEF	*In-Situ* erosion flume
ISIS	Instrument for shear stress i*n-situ*
LDV	Laser doppler velocimeter
LOI	Loss on ignition
M	Motor input speed
MF	Mini Flume
MHWN	Mean high water neaps

MHWS	Mean high water springs
MSL	Mean sea level
MLWN	Mean low water neaps
MLWS	Mean low water springs
n	Sample number
n	Porosity
OBS	Optical backscatter sensor
^{210}Pb	Lead (relative atomic mass: 210)
p	Pore pressure
P	Probability of settling ($P = 1 - \tau_o/\tau_m$)
r^2	Coefficient of determination
^{226}Ra	Radium (relative atomic mass: 226)
Re	Reynolds number
^{222}Rn	Radon (relative atomic mass: 222)
RS232	Serial link cable
S_b	Biostabilisation index $\tau_{bio}/\tau_{sterile}$
SB	Seasonal biostabilisation
SC	Sea carousel
SD	Standard deviation
SE	Sediment export
SET	Sedimentation erosion table
SLIM	Simulation of littoral morphodynamics
SI	Sediment input
Sm	Summer (Figure 3.4.3.)
SOC	Southampton Oceanography Centre
SSC	Suspended sediment concentration
SSC_a	Ambient suspended sediment concentration
SSC_{eq}	Steady-state suspended sediment concentration
SSC_0	Initial suspended sediment concentration
t	Time
T_c	Consolidation time
TauR	Shear stress reduction (Figure 7.4.1.& 7.5.1.)
TSM	Tor vane shear meter
U	Current speed
U_x	Flume radial current speed
U_y	Flume tangential current speed
U(Z)	Horizontal current speed at height Z
U_*	Friction velocity
U_{*cr}	Critical erosion friction velocity
^{238}U	Uranium (relative atomic mass: 238)
V_L	Volume of Venice Lagoon
V_s	Volume of sediment (Equation 2.6.I)
VSS	Vane shear strength
WC	Water content
W_m	Measured settling velocity
W_s	Median settling velocity
W_v	Wind velocity
Wt	Winter (Figure 3.4.3.)
Z	Height above the sediment-water interface
z	Depth below the sediment surface
z_o	Roughness length

ϕ	Internal friction angle
γ	Wet bulk density
γ_d	Dry bulk density
κ	Von Karman's constant
λ	Decay constant (Equation 6.1.II)
ν	Kinematic viscosity
θ	Shields parameter
ρ	Fluid density
ρ_s	Sediment density
σ'	Effective stress below sediment surface (Equation 7.1.II)
τ	Shear stress
τ_{bio}	Erosion threshold calculated *in-situ*
$\tau_{sterile}$	Erosion threshold of abiotic sediments
τ_o	Bed shear stress
τ_e	Excess bed shear stress
τ_c	Critical shear stress for erosion
τ_m	Critical shear stress for total deposition
τ_t	Total shear stress
τ_v	Strength of sediment at the shear point
τ_w	Shear stress applied by wind generated waves

CHAPTER 1: INTRODUCTION

1.1. Research perspective.

Intertidal mudflats are low-sloping, fine sediment deposits, which are submerged (periodically) during the high tide (Fig. 1.1.). Mudflats have a worldwide distribution and due to intermittent flooding and exposure to the atmosphere, are characterised by many different physical and biological processes that can influence their composition, habitats, and evolution (PERILLO, 1995). Generally they are composed of coarser sediment in the subtidal areas (below the low tide level) and finer sediments in the upper part (between the mid tide and the high tide level).

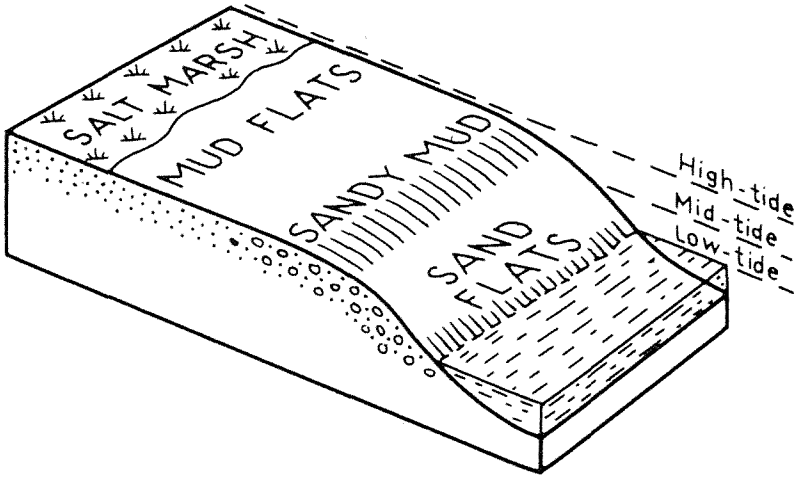

Figure 1.1. Mudflat block diagram (from PETHICK, 1990).

Mudflats are concentrated mostly on the coastlines of mid-latitude, meso- and macro-tidal environments. These flat areas are associated with salt marshes and, in most cases, occur in estuaries, deltas or lagoons (BLACK *et al.*, 1998). On a geological time-scale mudflats are considered as ephemeral. They are short-lived (usually a few thousand years), and characterised by extremely high biological productivity, which plays an important role in the balance between marine and terrestrial ecosystems (BLACK *et al.*, 1998). Intertidal areas provide a source of food for many species of flora and fauna, due to their particular environmental characteristics (subaerial and subtidal exposure). Intertidal mudflats play an important role in protecting the shoreline from erosion by wave action during storms. This is due mainly to the dissipation of wave energy in shallow water, particularly between mean low water neaps (MLWN) and mean high water springs (MHWS).

A classification of mudflats (DYER *et al.*, 1998) considered tidal range, wave energy, sediment supply, mudflat morphology, as well as physical and biological properties as classification parameters. Tidal range is considered one of the most important parameters for the classification of mudflats into different types because of its important role in controlling bed morphology and evolution. However, the sedimentological, biological and oceanographical characteristics of mud flats are still not fully understood (DYER *et al.*, 2000). This lack of comprehension derives from the many interlinking processes acting on the mudflat which can regulate the morphology and evolution of these complex features (Fig. 1.2.).

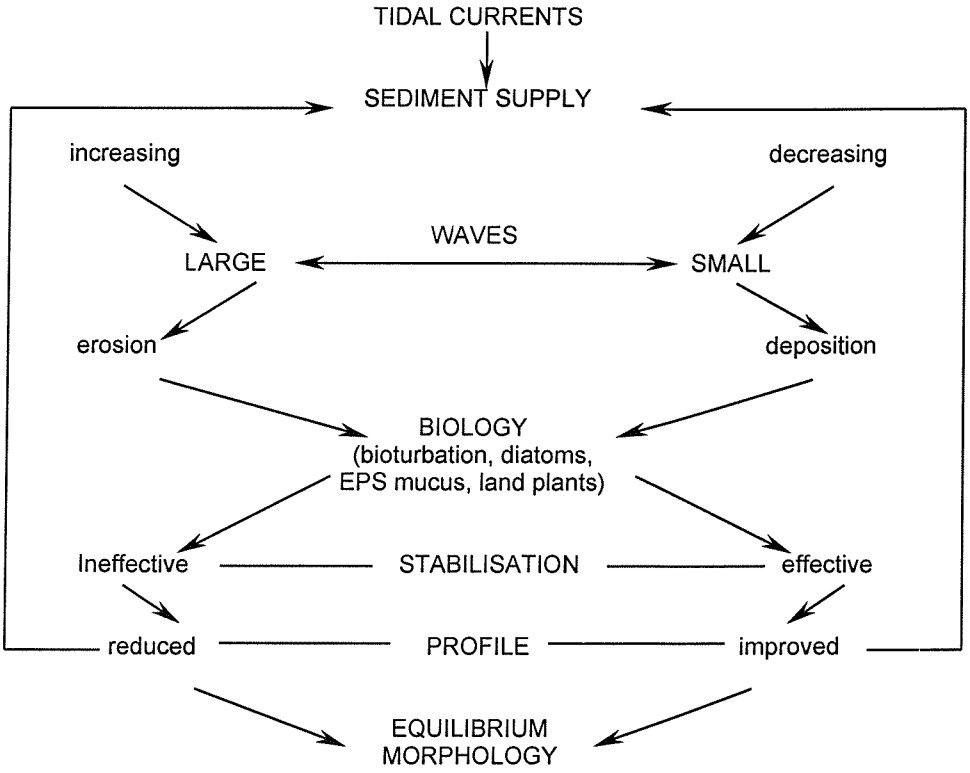

Figure 1.2. Schematic diagram of the interlinking processes on intertidal mud flats (after DYER; 1996).

The complex interactions that exist within and between the different biological species on an intertidal flat are able to modify the environmental conditions of their unique ecosystem. These modifications include changes in the physical processes, which in turn influence sediment transport. Complicated positive and negative feed-back loops occur in estuaries causing non-linear changes to phytobenthic communities as well as the characteristics of overlying water and underlying

sediments. The study of these mechanisms is vital to gain a thorough knowledge of the ecosystem and its interaction with human activities. Fine-grained sediments also accumulate pollutants. Therefore the erosion and deposition of mudflats have implications for the environment, and the prediction of mudflat evolution through time is vital for the coastal zone management (CZM) of estuaries.

Erosion of a bed occurs when the hydrodynamic force at the bed exceeds the resistance to erosion of the sediments that comprise the bed. Many laboratory studies of the erosion process have been undertaken (e.g. VILLARET & PAULIC, 1986; METHA & PARTHENIADES, 1975; OCKENDEN & DELO, 1991). Flumes have the advantage of measuring the response of sediments under controlled conditions of applied shear stress. However, due to the rheology of cohesive sediment it is impossible to transport natural material to a laboratory without substantial changes to its structure (MCCAVE, 1984; TOLHURST, 1999). Therefore, the advantage of *in-situ* investigations of sediment stability is that the spatial and temporal variations caused by the continuous changes of physical and biological conditions can be investigated (PERILLO, 1995; BLACK *et al.*, 1998, HUNTLEY & OLTMAN, 2000). Biological or physical parameters that influence sediment stability may be used as a proxy for the erosion threshold (CHRISTIE *et al.*, 2000). Relationships between sediment properties and stability are of use in remote sensing studies (GRANT & GUST, 1987) and modelling of coastal sediment dynamics when erosion threshold cannot be derived *in-situ* (RIETHMULLER *et al.*, 2000; WIDDOWS *et al.*, 2000). Such relationships have already been used to quantify the interaction between sedimentology, biology and hydrodynamics (DE BROUWER *et al.*, 2000).

In-situ investigations of the erosion process are a key part of sediment transport studies. The erosion process itself has been found to be more complex than laboratory investigations have indicated previously (AMOS *et al.*, 1992a; AMOS *et al.*, 1992b). Recent *in-situ* determinations of the erosion process have been carried out in a large number of research projects (LISP, LISP-UK, INTRMUD, F-ECTS) and several erosion devices have been developed for this purpose (BLACK & PATERSON, 1998).

F-ECTS (***F**eed-backs of **E**stuarine **C**irculation and **T**ransport of **S**ediments on Phytobenthos*), the financial supporter of this project, aimed to investigate mechanisms taking place between phytobenthos, hydrodynamics, and sediment transport in three European estuarine ecosystems (Venice Lagoon, Italy; *Ria*

Formosa, Portugal; and *Roskilde Fjord,* Denmark). The main objectives of F-ECTS were:

- to investigate the role of rooted macrophytes and microflora in modifying their habitats;
- to develop a direct monitoring scheme that will enable the description and evaluation of the feed-back mechanisms between phytobenthos and physical/biological processes; and
- to compare the results obtained in a microtidal environment (Venice Lagoon) with those from other microtidal environments (*Roskilde Fjord* and *Ria Formosa*).

Two fields campaign were carried out in Venice lagoon, the location for the pilot study of the F-ECTS project. Venice Lagoon is unique due to its complexity and importance as a cultural and historical site. The problems of the city, the most notable of which is the occasional flooding of Venice (*Acqua Alta*), have been well publicised. However, other problems affect the Lagoon such as the high rate of industrial, civil and agricultural wastewater discharge, as well as subsidence, and changes in channel and salt marsh morphology which result in a sediment loss of about 1 million m^3/a (CNV, 1996). If the loss of sediment continues at the present rate, all the intertidal areas will have disappeared by 2040. Previous studies have already demonstrated the positive effect of sea grass communities on the sediment deposition process, so the survival of sea grass and the loss of intertidal habitats are strongly related (CNV, 1992). The influence of benthic microalgae on sediment stability (YALLOP *et al.*, 1994) has also been recognised as a primary factor for protection against erosion of the few intertidal areas left in the region (CNV, 1992). Within the context of the F-ECTS programme, the research presented in this thesis has focused on:

- a regional scale investigation of sediment stability in Venice Lagoon;
- a small scale investigation of sediment stability on a single intertidal mudflat (*Palude della Centrega*);
- a study of mudflat evolution through time at different temporal scales; and
- the creation of a numerical model which simulates the sedimentary processes occurring in the area studied.

The main hypothesis of the present study is that processes occurring on a single intertidal mudflat may be used as a proxy for determining which factors are responsible for morphological changes of the whole Lagoon.

Thesis Outline

In the present study, the mudflat properties and evolution, and their mutual interactions are investigated using a multidisciplinary approach. In Chapter 2, the previous research into sediment stability is summarised with particular attention given to the biological and physical properties that are responsible for the temporal and spatial variation of sediment stability. In Chapter 3, background environmental information is provided for Venice Lagoon, with a focus on the factors responsible for environmental degradation and the disappearance of the intertidal flats. In Chapter 4, the methodology to determine sediment properties and stability are defined and the results of two field campaigns carried out in Venice Lagoon as part of the F-ECTS project are presented.

In Chapter 5, a sub-area of the F-ECTS study region is investigated in detail. The morphology, the habitats and the sediment stability of *Palude della Centrega* are presented. In Chapter 6, the evolution of *Palude della Centrega* is investigated through the study of morphological changes, monitoring of erosion/accretion rates and sediment dating. In Chapter 7, a 0-D numerical model is developed. Factors controlling the evolution of the mudflat are investigated based on the coefficients, constants, and thresholds of sedimentation derived from field measurements. Finally, in Chapter 8 the relevant conclusions of this research and suggestion for future work are presented.

CHAPTER 2: SEDIMENT STABILITY OF INTERTIDAL MUDFLATS

Within the context of this thesis, intertidal flat stability is defined as the resistance of sediment comprising the intertidal flat to hydrodynamic forcing. In this chapter, the properties of intertidal mudflats are reported, and a review of the hydrodynamic forcing and sediment properties relevant to Venice Lagoon is provided.

2.1. Forces acting on particles

The stability of the granular material comprising the inter tidal flats of Venice Lagoon is controlled by the balance of forces acting on that material (ARULANDAN, 1975). A schematic diagram (Fig. 2.1.) shows the stabilising and destabilising forces acting on a single grain comprising a plane sediment surface under the effect of a steady current. This is perhaps the simplest relationship expressing the link between bed stability and an applied hydrodynamic force. In the first instance cohesionless effects are discussed.

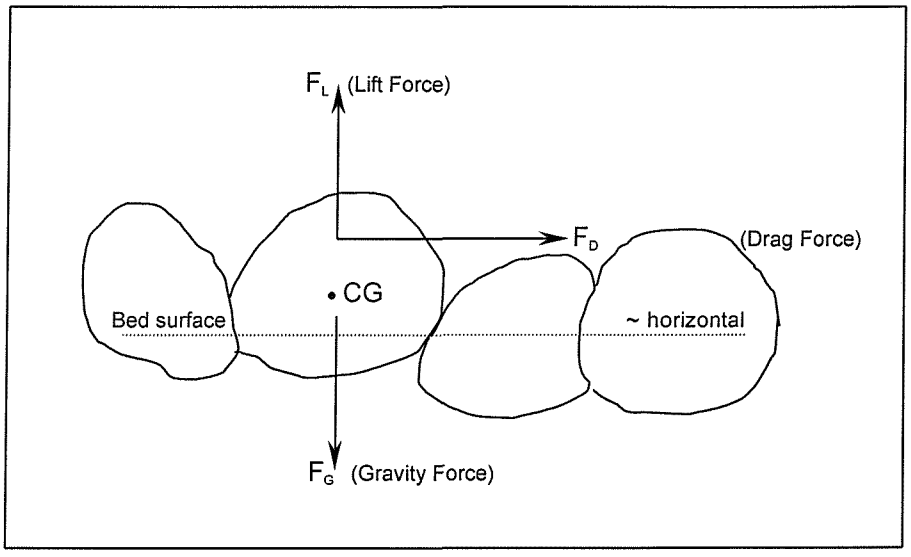

Figure 2.1. Forces acting on a particle resting on a grain boundary under the effect of fluid motion. F_G = gravity force; F_L = lift force; F_D = drag force; CG is the gravity centre.

The forces acting on a bed which cause non-cohesive particles to move depend on the characteristics of the flow. Drag forces between a stationary bed and a moving

fluid apply a bed shear stress (τ_o) that is proportional to the square of the fluid velocity (U^2). This relationship is estimated using the Quadratic Stress Law:

$$\tau_o = \frac{1}{2} C_D \rho U^2 = \rho U_*^2 \qquad 2.1.I$$

where C_D is the drag coefficient (dependent on the particle shape, the height of measurement of U and flow turbulence (KOMAR & REIMENRS,1978)), ρ is the density of the water and U_* is the friction velocity.

As fluid streamlines converge over a particle, a higher fluid velocity results which causes a decrease in pressure resulting in a lift force (F_L) on the particle. This lift force contributes to particle destabilisation and takes the form:

$$F_L = \frac{1}{2} \rho C_L A_r U^2 \qquad 2.1.II$$

where A_r is the cross sectional area of exposed grain ($\frac{1}{4}\pi D_r^2$; where D_r is the grain diameter) and C_L is the lift coefficient.

The tangential component (horizontal pressure gradient) acting on the particle is known as the drag force (F_D); where:

$$F_D = \frac{1}{2} \rho C_D A_r U^2 \qquad 2.1.III$$

The immersed weight or gravity force (F_G) acting on a particle is inversely proportional to the cube of its diameter, its buoyant density (ρ_s-ρ) and the gravitational constant (g):

$$F_G = ma = \pi/6 (\rho_s - \rho) g D_r^3 \qquad 2.1.IV$$

where m is mass, a is acceleration, and ρ_s is the density of the particle.

2.2. The erosion threshold and cohesion

Incipient erosion occurs when the ratio of stabilising and destabilising forces acting on a particle is larger than or equal to 1:

$$F_L / F_G \geq 1 \qquad 2.2.I.$$

Natural fine-grained sediments (≤63μm) are composed of an aggregation of particles with different sizes, shapes, composition, and interparticle attraction (cohesion). Estuarine sediments, which are composed of a mixture of sand, silt and clay are stabilised in part by cohesion (C) between the fine-grained fraction. So, erosion occurs when:

$$F_G+C \leq F_L+F_D \qquad 2.2.\text{II}.$$

Variations in sediment stability may be the result of physical processes (AMOS *et al.*, 1988), or the result of biological processes due to the presence of benthic organisms (or a combination of both). The latter effect is known as biostabilisation and biodestabilisation, which can be caused directly or indirectly by biological activity (PATERSON & DABORN, 1991). The contribution of bio-cohesion to sediment stability is known as adhesion (A). It is the result of bonds between two dissimilar materials: organic compounds and mineral particles (BLACK, 1991). Thus, biostabilised muddy sediments have a threshold of erosion defined by:

$$F_G+C+A \leq F_L+F_D \qquad 2.2.\text{III}$$

where C+A>0.

Equation 2.2.III. demonstrates that sediment stability is controlled by many factors (both biotic and abiotic). It is almost impossible to determine any single contribution to the erosion threshold. Nevertheless, in the last 40 years many relationships between sediment stability and biogeochemical properties have been derived (BLACK *et al.*, 1998).

2.3. Factors controlling sediment stability

There are many factors which influence sediment stability (SARGUMAN, 1973). In this section a short review of the principal physical and biological factors that control the stability of intertidal mudflats is given.

Physical control of sediment stability

The cohesive properties of a sediment are influenced by the grain size distribution and the mineralogy of the clay particles (<40 μm). Most clay particles are plate-like in shape and are attracted by electrostatic forces surrounding the plates BERLAMONT *et al.* (1993). This is due to positive electric charges which occur on the faces of the clay plates, and negative charges at the plate edges (DYER, 1986). The attraction of opposite charges results in an open structure characteristic of clays. Other parameters, such as the cation exchange capacity, the sodium adsorption ratio and the pH of interstitial water can control the intergranular forces affecting the stability of abiotic sediments (BLACK, 1991).

HJÜLSTROM (1939) presented a diagram showing the steady flow speed necessary to erode abiotic sediments of different particle diameters (Fig. 2.2.). Above a grain diameter of about 0.3 mm, the mean flow velocity leading to the erosion of a uniform bed increases with grain size. This behaviour can be explained by the fact that larger particles have a greater submerged weight (F_G). By contrast particles finer than 0.3 mm and in particular clay, show a trend of increasing threshold for movement with decreasing mean grain size. Fine sediment (silt and clay) is thus more stable than fine sand. The reason for this is due to cohesion (C), which is greater than the effect of gravity (F_G) in stabilising sediments.

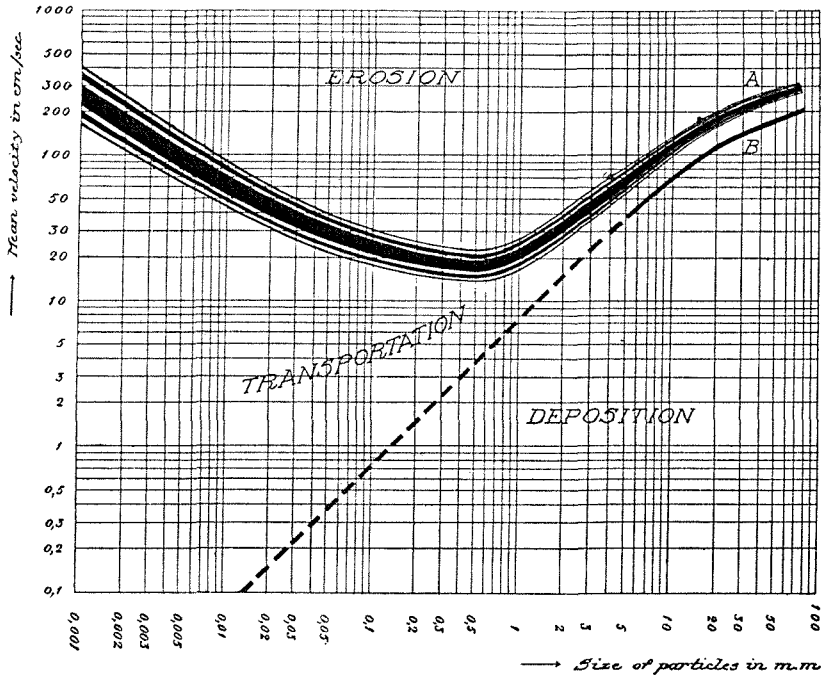

Figure 2.2. Shields type diagram of mean current velocity (ordinate) necessary to erode uniform material (from HJÜLSTROM, 1939).

SHIELDS (1936), provided a major advance in threshold determination of non-cohesive sand by defining a non-dimensional shear stress (Fig. 2.3.). The Shields parameter is expressed as:

$$\theta = \tau_c / (\rho_s - \rho_w)\, g\, D_r$$

where τ_c is the critical shear stress for erosion.

The major contribution of this work was in the derivation of a non-dimensional critical shear stress related to grain Reynolds Number (Re). Due to the heterogeneity of natural sediments, both the Hjülstrom's and Shield's diagram should be used with caution to predict the stability of estuarine muds (BLACK, 1991).

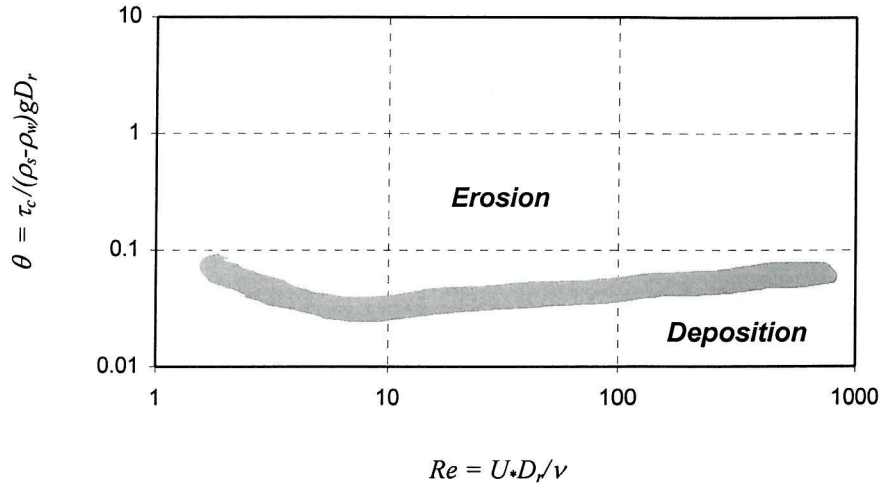

Figure 2.3. The Shields threshold curve (after MILLER *et al.*, 1977), where θ is the Shields parameter and Re is the Reynolds number.

Other properties, for example the packing and shape of grains as well as their orientation can be important. Particle shape can influence the *angle of repose* of sand (KOMAR & LI, 1986) and the void ratio of fines (LAMBE & WHITMAN, 1979). An increase in the bulk density of sediments increases stability and is often due to the consolidation process (OCKENDEN & DELO, 1991). Consolidated sediments have a higher value of bulk density and show higher resistance to erosion (TORFS, 1994). During the exposure of intertidal mudflats, natural dewatering aids the consolidation process, decreasing sediment erodibility (ANDERSON, 1983). YOUNG (1977) found that a decrease of 5 % in water content (WC) increases the erosion threshold by 150-200 %.

Sediment texture is defined as the relative composition of clay, silt and sand, and it has an important effect on sediment stability. Sediment stability increases with increasing mud content (WHITEHOUSE *et al.*, 1999). A 10 % (by weight) clay content is usually sufficient to bind sand particles together. PANAGIOTOPOULOS *et al.* (1997) suggested that when the clay content is about 11-14 %, sand particles are no longer in contact with each other and the mixture behaves cohesively. Cohesion increases significantly when clay content is 10-15 % by weight (METHA & PARTHENIADES, 1982) reaching a maximum at 30 % resulting in a critical shear stress (τ_c) which is 10 times that of pure sand (WHITEHOUSE *et al.*, 1999).

Consolidation can also influence sediment stability, when there is a significant fine-grained fraction present in bottom sediments. Consolidation occurs when sediment is loaded, either artificially or naturally. In natural systems, fine sediments consolidate under the pressure of the accumulated material (geostatic load). The increased pressure breaks the bonds of flocs and floc aggregates. As a consequence, a bed composed of packed flocs develops, with increasing density with depth (PARTHENIADES, 1986). The floc deformation and the decrease of interparticle space changes the density of the sediment through time. This process, known as self-weight consolidation (TOORMAN, 1996a; TOORMAN, 1996b), can increase sediment stability through time (PAPANICOLAOU & DIPLAS, 1999; TEISSON *et al.*, 1993; GUDEHUS & TOORMAN, 1999). The slope of the bed also increases by up to 90 % the erosion threshold because the magnitude of gravity force is increased in the presence of a sloping bed (EVANS & HARDISTY, 1989).

Biological adhesion

Adhesion can be defined as the bonding together of unlike substances. In the case of intertidal flats this applies usually to the bonding of organic and inorganic matter. Seasonal and spatial variation in the organic components of intertidal sand and mud have been widely reported (WEBB, 1966; GRANT, 1988), and are due typically to mucilagenous secretions within intergranular pore spaces (SUTHERLAND *et al.*, 1998a; 1998b). Benthic diatoms and bacteria are common in intertidal and subtidal areas of many estuaries (BLACK *et al.*, 1998). Motile diatoms often dominate benthic microbial assemblages (UNDERWOOD *et al.*, 1995) and secrete large amounts of EPS (Extra-cellular Polymeric Substances; Fig. 2.4.).

Figure 2.4. Scanning Electronic Micrograph (SEM) showing a diatom-dominated biofilm (from UNDERWOOD *et al.,* 1995).

A detailed description of the properties and composition of biofilms produced by micro-organisms is given by DECHO (2000). An increase in organic content is associated with finer sediments (YOUNG, 1977), particularly for silts and clays (CHRISTIE *et al.*, 2000).

EPS is composed, partially, of colloidal carbohydrates. Carbohydrates have been detected to a depth of 3-4 cm in the sediment bed (UNDERWOOD & PATERSON, 1995) and deeper (FRIEND, 2001), but the greatest content is confined typically in the topmost 1-3 mm (MADSEN *et al.*, 1993; YALLOP *et al.*, 1994;). PATERSON *et al.* (2000) demonstrated that the micro-spatial resolution of biological measurements influences the interpretation of biogenic stabilisation of intertidal cohesive sediments and often, processes occurring in the uppermost few μm, may be missed.

Values of carbohydrate content can vary by 1 order of magnitude if measured within the topmost 2 mm (1-2000 $\mu gGE/g_{DW}$) instead of the top 5 mm (1-300 $\mu gGE/g_{DW}$) (PATERSON *et al.*, 2000). In cohesive sediments, an exponential decrease in chlorophyll *a* and carbohydrate concentration usually occurs in the top 1 mm; in non-cohesive sediments the decrease is usually linear with depth.

Muco-polysaccharides secreted by micro-organisms for attachment and mobility, form long-chain polymers that have an adhesive effect between sediment particles

and aggregates, thus increasing sediment stability (PATERSON, 1989). A benthic diatom biofilm increases resistance to erosion and reduces bed roughness (DADE *et al.*, 1990). This is particularly evident during diatom blooms when the erodibility of sediments can be influenced heavily by the biota, leading to an increase in the erosion threshold (YALLOP *et al.*, 1994; VOS *et al.*, 1988; Fig. 2.5.).

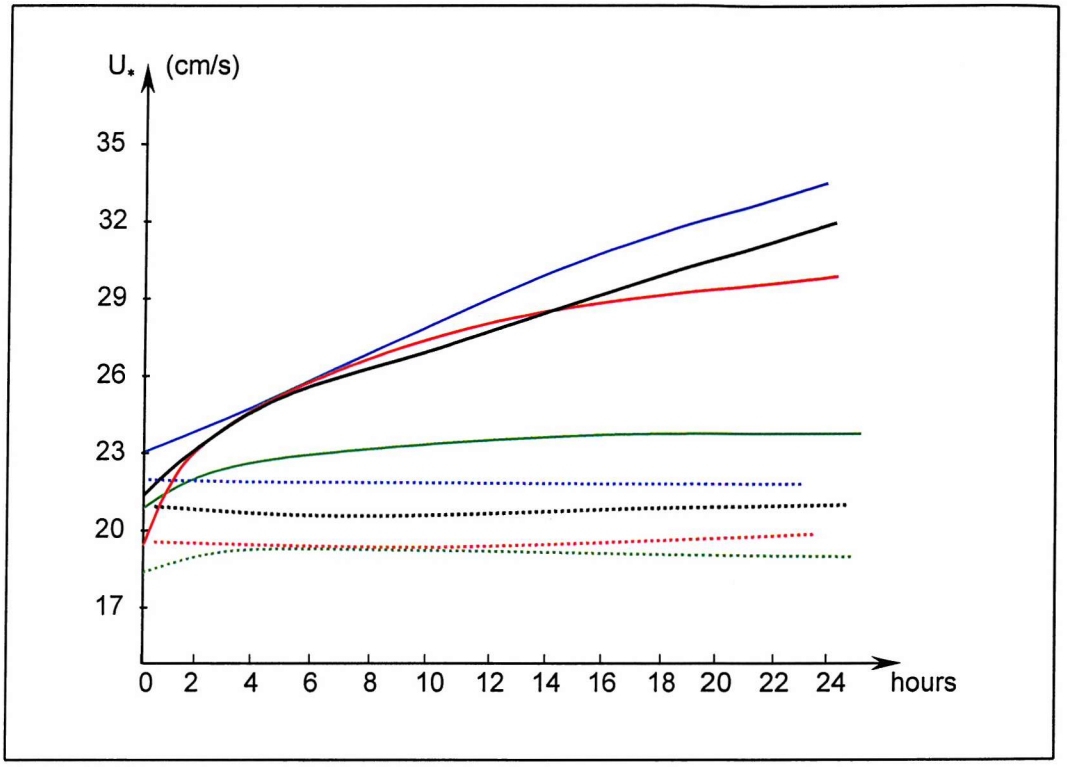

Figure 2.5. Laboratory tests on the effect of diatoms on erosion threshold. Critical velocity is along the ordinate (U*) and time along the x axis (hours). Lines indicate stability of sediment with (filled lines) and without (dotted line) diatoms. (from VOS *et al.*, 1988).

A useful index of biostabilisation is the ratio of biotic to abiotic sediments (MANZENRIEDER, 1983). The biostabilisation index (S_b) is defined as follows:

$$S_b = \tau_{bio}/\tau_{sterile} \qquad 2.3.1$$

where τ_{bio} is the *in-situ* (biotic) erosion threshold calculated *in-situ*, and $\tau_{sterile}$ is the erosion threshold of the sterilised (abiotic) inorganic sediments. Many studies have attempted to quantify the contribution of biological activity to sediment stabilisation. The percentage increase in sediment stability based on the ratio of 'biotic' to 'abiotic' responses determined by several authors is illustrated (Table 2.1.).

Source	*Biota*	S_b
Non-cohesive	***Sediment type***	***(%)***
NEUMAN *et al.* (1970)	Algae/cyanobacteria	500
HOLLAND *et al.* (1974)	Diatoms	(100)
MANZENRIEDER (1983)	Bacteria/algae	300-700
GRANT & GUST (1987)	Sulphur bacteria	390
GRANT & GUST (1987)	Cyanobacteria	350
VOS *et al.* (1988)	Diatoms	100
DADE *et al.* (1990)	Bacteria	200
PATERSON & UNDERWOOD (1990)	Diatoms/bacteria	400
MADSEN *et al.* (1993)	Diatoms/cyanobacteria	300
YALLOP *et al.* (1994)	Diatoms/cyanobacteria	>960
Cohesive	***Sediments type***	***(%)***
HOLLAND *et al.*(1974)	Diatoms	45
BLACK (1991)	Diatoms/bacteria	500
YALLOP *et al.*(1994)	Diatoms/bacteria	300

Table 2.1. Selected measurements of biogenic stabilisation from the literature.

From Table 2.1., it appears that the contribution of microphytobenthos to sediment stabilisation is relatively high compared to the contribution of the remaining physical components (F_D and C). All these factors (C, F_D, A) are interdependent and their relative effects are indistinguishable. For example, AMOS & MOSHER (1985) found the highest values of τ_c for sediments with the lowest bulk density values. In that case, the sediments had a high clay content which increased interparticle cohesion.

The bed shear stress (τ_o) also influences sediment stability. The erosion threshold can increase by about 20 - 30 % due to the stress history of the fluid (GOMEZ, 1996). When a flow is applied to a bed for enough time it can adjust the grains and therefore the packing of particles.

The presence of a smooth biofilm which covers sediment particles (Fig. 2.4.) can influence the roughness of the bed (i.e. the drag coefficient and the turbulence of the flow) resulting in a complex relationship between bed evolution and shear stress (AMOS *et al.*, 2000).

2.4. Definitions of sediment stability and erodibility

Sediment stability is expressed usually by a single parameter known as the erosion threshold (τ_c in Pa), which is determined by the strength of the sediment fabric at the point of incipient motion. Many methods can be used to determine the erosion threshold, the choice of method depending on the erosion device employed. The erosion threshold, as an index of bed stability, is valid for the sediment-water interface only; its use does not consider the fate of the bed once the erosion process has begun (erosion rate). The erosion rate defines the mass of sediment released from the bed per unit area over time. Bedload or suspended load transport can occur after the critical shear stress of erosion is exceeded by the flow. The erosion type can be defined on the basis of qualitative information depending on how the erosion proceeds over time (MEHTA & PARTHENIADES, 1982). VILLARET & PAULIC (1986) distinguished two erosion types: I and II. The type of erosion is a function of time and excess bed shear stress (τ_e); it may be either asymptotically diminishing with time (type I) or constant (type II) (Fig. 2.6.).

Type I erosion occurs as resuspension "particle by particle" of sediments up to a certain depth where binding forces are strong enough to resist the pressure applied by the eroding flow. Type II erosion is a "mass failure" of flocs and aggregates characterised by failure along planes of weakness and is not constrained by the consolidation profile. Type I was further subdivided into type Ia and type Ib by AMOS *et al.* (1992b) and described as follows: **type Ia** *..."characterised by an asymptotically decreasing erosion rate with time, diagnostic of floc or pellet resuspension"...* **type Ib** *..."shows asymptotically decreasing erosion with time, diagnostic of bed failure occuring as a rip-up clasts (aggregates) but which is constrained in depth by a higher than normal consolidation profile in the sediment"...*

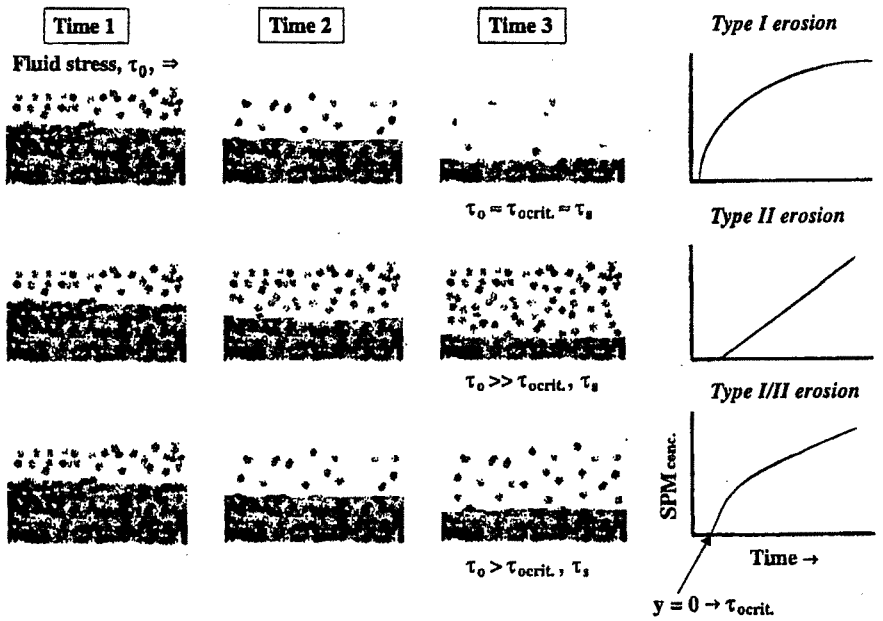

Figure 2.6. Classification of types of cohesive sediment erosion. Type I erosion (top) and type II erosion (centre) can be distinguished by a logarithmic or linear increase of suspended sediment concentration in the water column. They can occur together (bottom) depending on the nature of the sediments and characteristics of the flow (from PATERSON & BLACK, 1999).

The distinction between different types of erosion can provide useful information about the rheological properties of the substratum or the hydrodynamic characteristics of the eroding fluid. Fig. 2.7. is a schematic representation of how sediments behave under the effect of an eroding fluid.

Differences in the erosion process reported above are not easily distinguished by *in-situ* investigations (particularly with regards to cohesive sediments which are found usually in highly turbidity water characterised by low visibility). This is the reason why measures of suspended sediment concentration (SSC) are often used to detect changes in turbidity and to determine the type of erosion (BLACK & PATERSON, 1996).

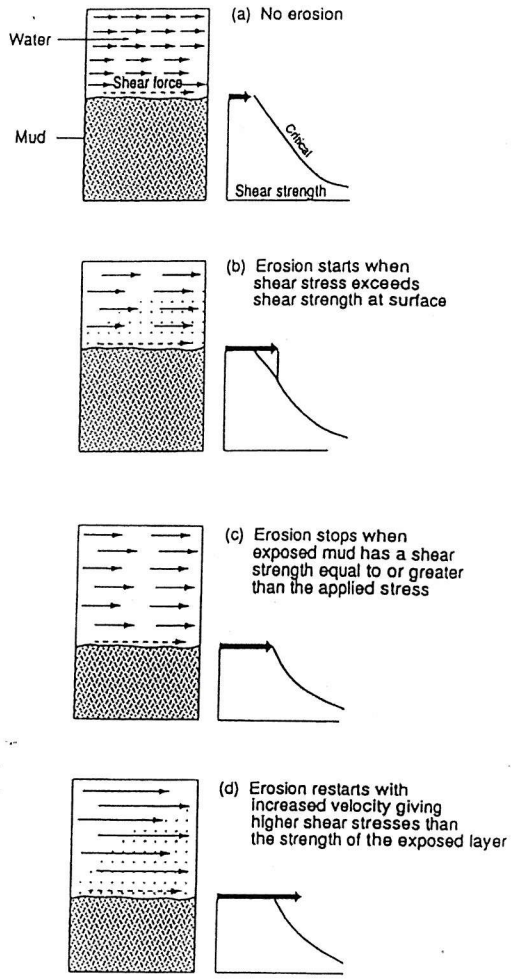

Figure 2.7. Schematic diagram showing the cohesive sediment erosion process (from DELO & OCKENDEN, 1992).

CHAPTER 3: BACKGROUND TO VENICE LAGOON

3.1. Introduction to Venice Lagoon

Venice Lagoon is a shallow coastal embayment located along the northern part of the Adriatic Sea (north-eastern Italy) at 45° N, 12 E°. It is restricted, according to the definition of KJERFE (1994), arched in shape, 8-14 km wide and a with shore-parallel orientation. The Lagoon is separated from the open sea by a 50 km long barrier island. Its total area is about 550 km^2 (Fig 3.1.). Water exchange takes place across three large inlets: *Chioggia* in the south, *Malamocco* in the centre and *Lido* in the north. It has a strong tidal circulation driven by phase changes across the Lagoon influenced by winds (UMGIESSER, 2000). It is a well-mixed estuary (PRICHARD, 1989) with a residence time of about 24 hours (CNV, 1996) and exhibits brackish water to open sea salinity.

Human activities have modified the environment of the Lagoon in several ways during the last five centuries. A drastic change has occurred in the hydrological regime of the rivers flowing into the Lagoon. In addition, the dredging of channels for navigation purposes and the more recent construction of concrete breakwaters to protect each inlet have had a negative impact on the sediment balance, and therefore on the Lagoon morphology. This modern morphology has been created by a variety of human activities and is classified in to five categories (Table 3.1.).

Habitat categories	Bathymetry (m)	Surface (km^2)
Islands	*>0.5*	*100*
Intertidal marshes	*from 0.0 to 0.5*	*30*
Intertidal flats	*from -0.3 to 0.0*	*40*
Shallow areas	*from -2.0 to -0.3*	*230*
Channels	*< -2.0*	*60*

Table 3.1. Principal categories of habitats in Venice Lagoon, their bathymetry and distribution. The data do not include 90 km^2 of the Lagoon which form isolated fish farming areas (from BETTINETTI *et al.*, 1996).

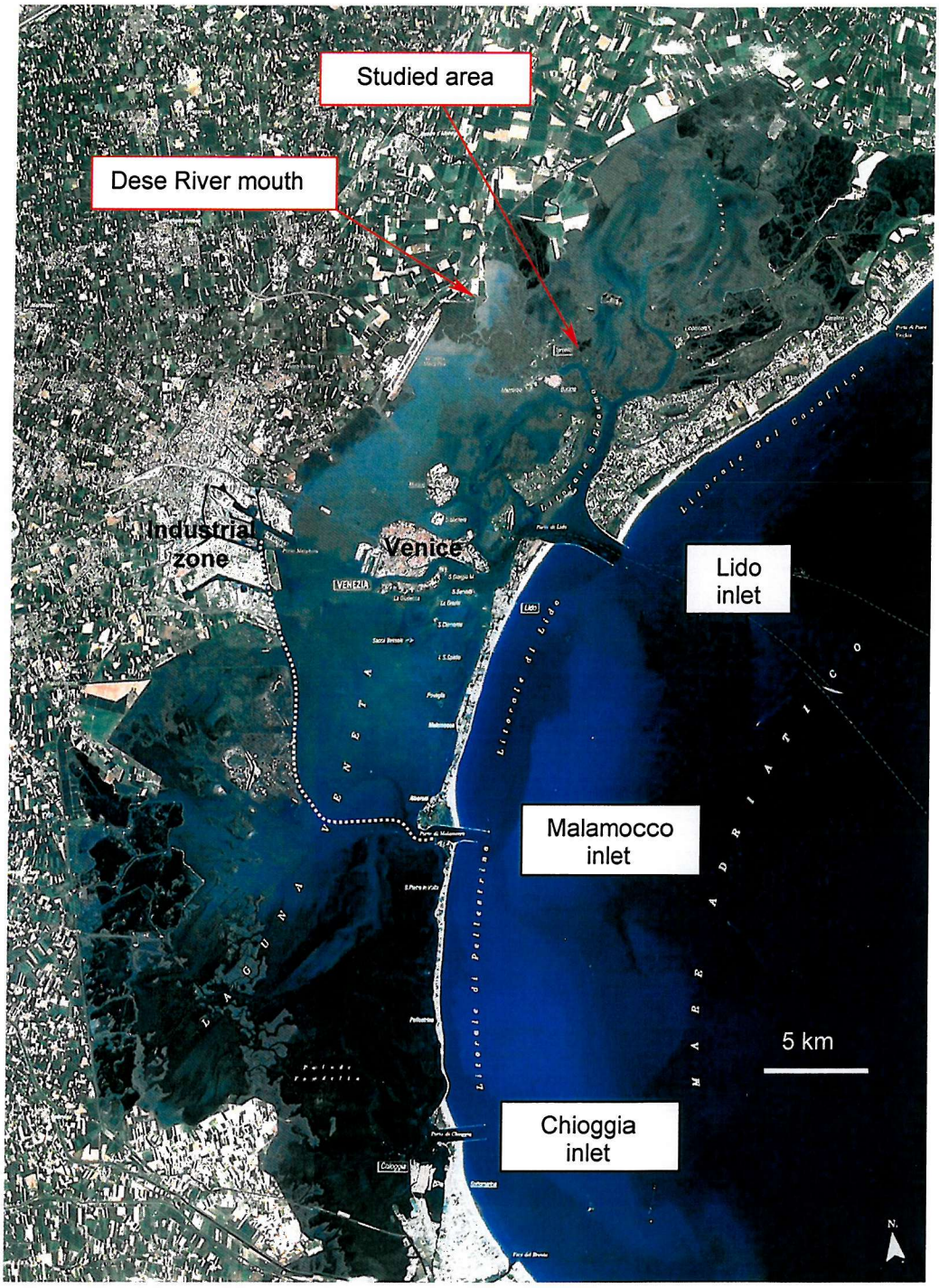

Figure 3.1. A satellite image of Venice Lagoon, Italy. Note the study area is located in the northern part of the Lagoon (dark pattern) where the intertidal mudflats are better preserved (the dotted line marks the dredged Malamocco Canal).

The area of salt marshes in the Lagoon has fallen drastically during the last century mainly due to subsidence and reduced sediment input. It was reduced from 90 km^2 in 1901 (CARBOGNIN & CECCONI, 1997), to 72 km^2 in 1930, and to 47 km^2 in 1990. As a consequence, the erosion of mud flats and salt marshes has resulted in an increase in the average water depth (Fig. 3.2.). At present, the estimated annual deficit of sediment (transported to the sea) is about 1.1 million m^3 (CNV, 1996).

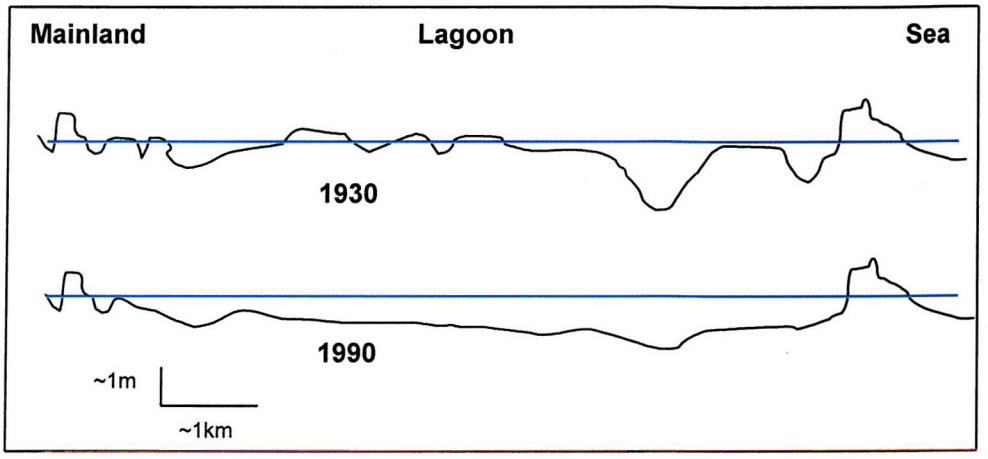

Figure 3.2. Two transects across Venice Lagoon represent the situation of the approximate elevation of the Lagoon deposits in 1930 (above) and 1990 (below). The horizontal line represents MSL (from CVN, 1996).

3.2. Tide and wave conditions

Venice Lagoon is a micro-tidal environment in which the neap tide is 30 cm, the mean tidal range is 55 cm and the spring tide is 110 cm (CARBOGNIN & CECCONI, 1997). Tides are semidiurnal and asymmetric in form. They are characterised by shorter ebb flows at the southern inlets and a longer ebb flow in the northern part of the Lagoon (GOTTARDO & CAVAZZONI, 1981). A reduction of the tidal range caused by the propagation of the tide into the Lagoon is accentuated particularly in the northern part of the basin, moving landward from the entrance of the estuary (GOTTARDO & CAVAZZONI, 1981). As a consequence, the tidal range measured at the tidal inlets has different characteristics to that inside Venice Lagoon.

CAVAZZONI (1977) also found that dredging of tidal channels for navigation purposes, caused feedback mechanisms affecting the hydrology and morphology of the Lagoon floor. The increased section of the channels for navigation increased

the propagation speed of the tide into the basin, changing the current speed and inundation time of many areas.

A time series of the tidal range, the tidal current and the derived bed shear stress in the study area of *Palude della Centrega* is shown in Fig. 3.3., illustrating the output of a 2-D finite element hydrodynamic model of Venice Lagoon presently under development (UMGIESSER, 2000).

Waves in Venice Lagoon are the most important factor for resuspension of sediments in the shallow areas (CAVALERI, 1980). They occur episodically and are wind driven (CAVALERI & HUBBARD, 1981, CNV, 1992). The strongest wind velocities occur usually during *Bora* events, which are characterised by winds from the north, and can form significant waves up to H_s = 0.5 m within the Lagoon (CAVALERI & MALANOTTE RIZZOLI, 1981). These waves can generate oscillatory shear stresses that exceed the critical shear stress for bed erosion, estimated by Danish Hydraulic Institute (DHI; 1991) to be between 0.2 to 1 Pa. The shear stresses applied by waves depend on wind speed and water depth (Fig. 3.4.). They are considered responsible for the erosion of most of the intertidal region of the southern and central Lagoon.

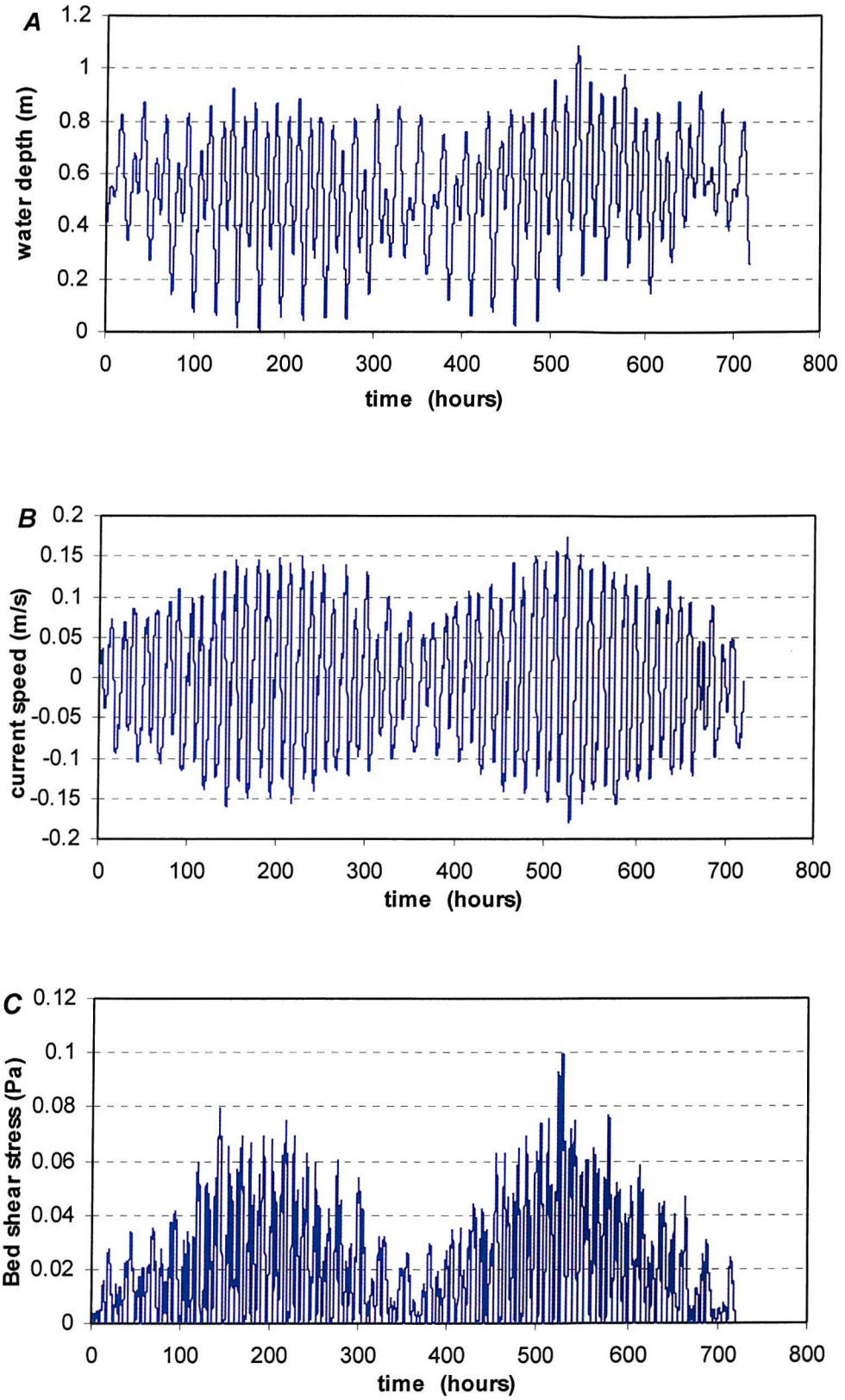

Figure 3.3. Tidal range (*A*), tidal current velocities (*B*) and bed shear stress (*C*) applied by tides at the studied area (*Palude della Centrega*).

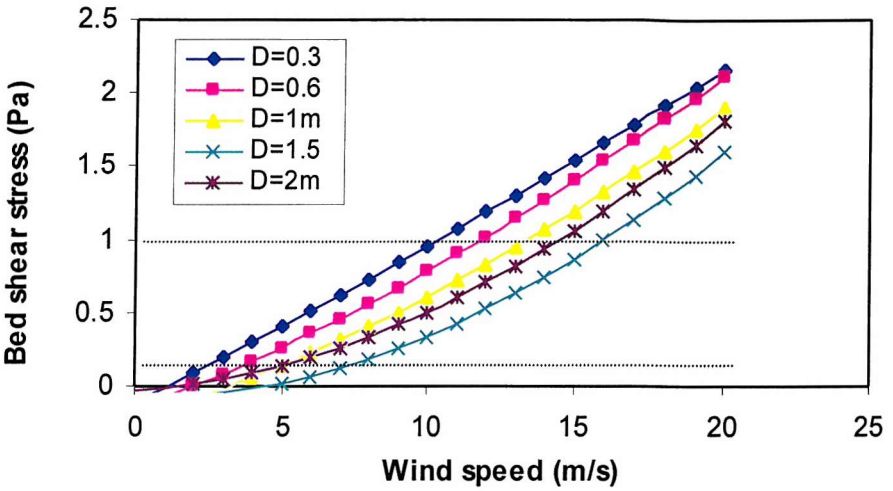

Figure 3.4. Bed shear stress due to wind generated waves at different depths (D) of water. The critical shear stress was estimated between 0.2 and 1 Pa (dotted lines) (from DHI, 1991).

The implication of wind-induced bed shear stresses for sediment transport is that waves erode the sediments and increase the turbidity of the water column, meanwhile the tidal currents transport the resulting suspended sediments until they redeposit on the bed or are exported to the open sea. Wave motion affects slope stability and is considered to be the main cause of soil failure (CRAIG, 1992; MCCARTHY, 1993) in the intertidal areas. Slumping has been observed at the edge of salt marshes all around Venice Lagoon (Fig. 3.5.) and hence has a significant impact on channel stability.

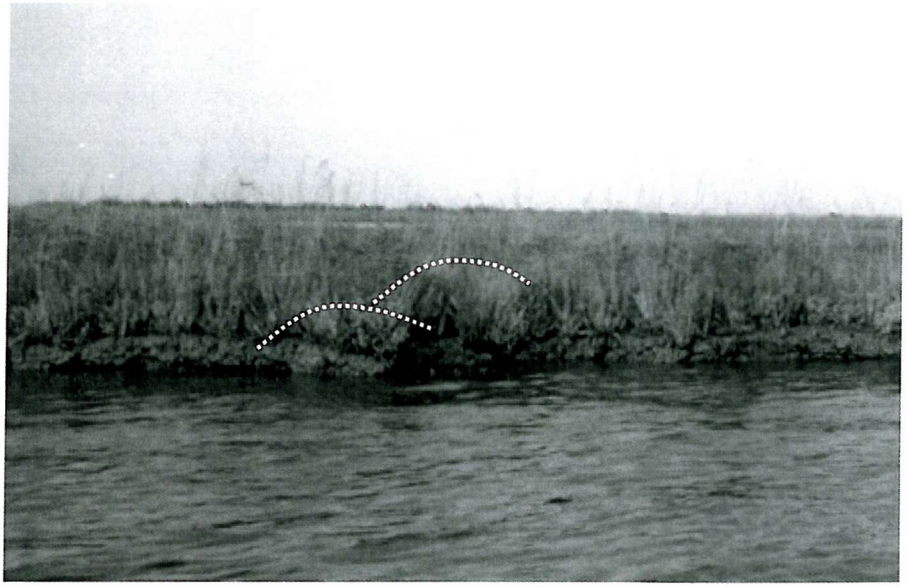

Figure 3.5. Typical edge of vegetated salt marshes in Venice Lagoon. Note the position of the imminent failure (white dotted lines).

Plant roots, animal burrows, microbial and meiofauna communities can contribute to stabilise intertidal slopes (SHAKH *et al.,* 1998). CNV (1992) reported that the initiation of slumping occurs during low tide, when waves break on the edge of exposed and poorly consolidated sediments (as shown in Fig. 3.5.).

Wave motion is also generated by motorised traffic in the Lagoon and City canals. Boat-induced waves breaking on canal sides cause erosion of the shoals (DHI, 1991) and damage the foundation of buildings and monuments in the City of Venice (PULLIERO, 1987). The effect of motorised boat and ship-induced wave motion has been identified as one of the possible causes of salt marsh erosion and pollution release. As part of the F-ECTS project, turbidity sensors were deployed on shoal areas near the *Malamocco* Canal (oil-channel). Resuspension takes place with the passage of slow, large ferries as well as from smaller, faster recreational craft, which have a big impact on bed erosion (CIAVOLA, *pers comm.*; DHI, 1991).

Finally, atmospheric forcing, wind set up and seasonal variation of MSL can occasionally increase high water levels in Venice Lagoon. The phenomenon of high water is better known as *Acqua Alta*. It is responsible for the flooding of the city of Venice and should not be confused with an normal high tide. The recurrence of *Acqua Alta* has increased since the fifties due to ground subsidence (GATTO & CARBOGNIN, 1981; Fig. 3.6.).

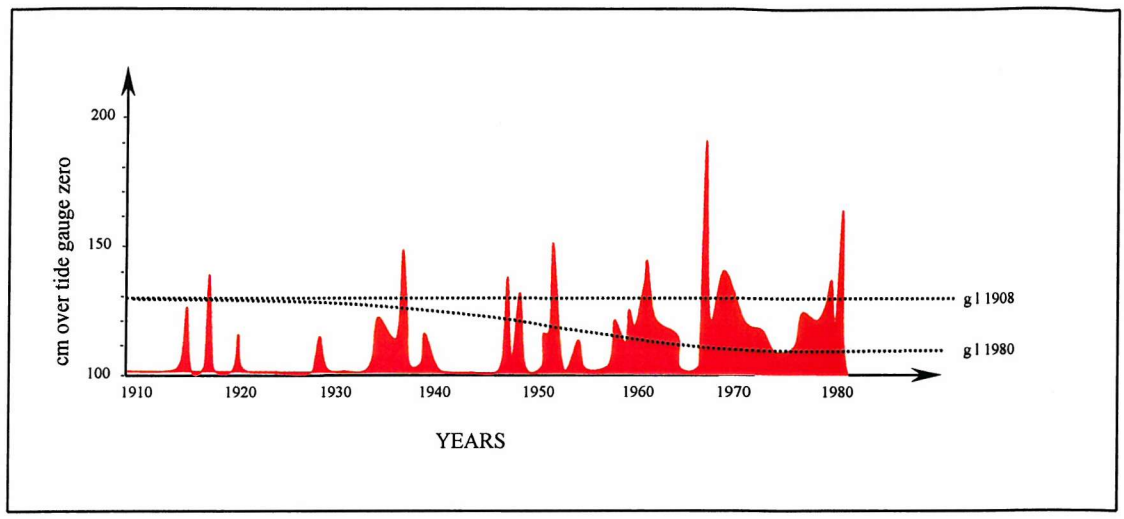

Figure 3.6. *Acqua alta* occurrences. The increased frequencies of inundation (red areas) started after 1950 as a consequence of the lowering in ground level (gl). Increased storminess and the change in the inundation regime resulted in a destabilisation of the intertidal regions (from GATTO & CARBOGNIN, 1981).

3.3. Sediment supply

The sediment supply to Venice Lagoon has been restricted artificially over the past five centuries by controlling river discharge and by the construction of inlet jetties in order to prevent natural silting of the Lagoon. The *Brenta*, *Piave* and *Sile* rivers that once flowed into the Lagoon, now flow directly into the sea and only a few small rivers presently discharge into the Lagoon (Fig. 3.7.). Mean freshwater discharge is about 30-40 m^3/s and the drainage basin is 1830 km^2 (THETIS, 1997). The quantity of sediment brought into the Lagoon from the hinterland has been reduced drastically from $7x10^5$ m^3/a in 1500 AD to $30x10^3$ m^3/a today (CNV, 1996; Fig. 3.8.).

More recent results from the DRAIN project (***DeteRmination of pollutAnts INput from the drainage basin to the Venice Lagoon***) indicated that the estimated sediment input is about $33x10^3$ t/a (ZONTA, 2000) confirming the previous study of the CNV (1996). Sediment input was calculated assuming that the river discharge was equally distributed over the entire volume (V_L) of the Lagoon:

$$V_L = A_L D_W = 6 \times 10^6 \quad m^3 \qquad 3.3.1.$$

where A_L is the area of the Lagoon (5.5×10^6 m^2) and D_W is the average depth at MSL of about 1.1 m.

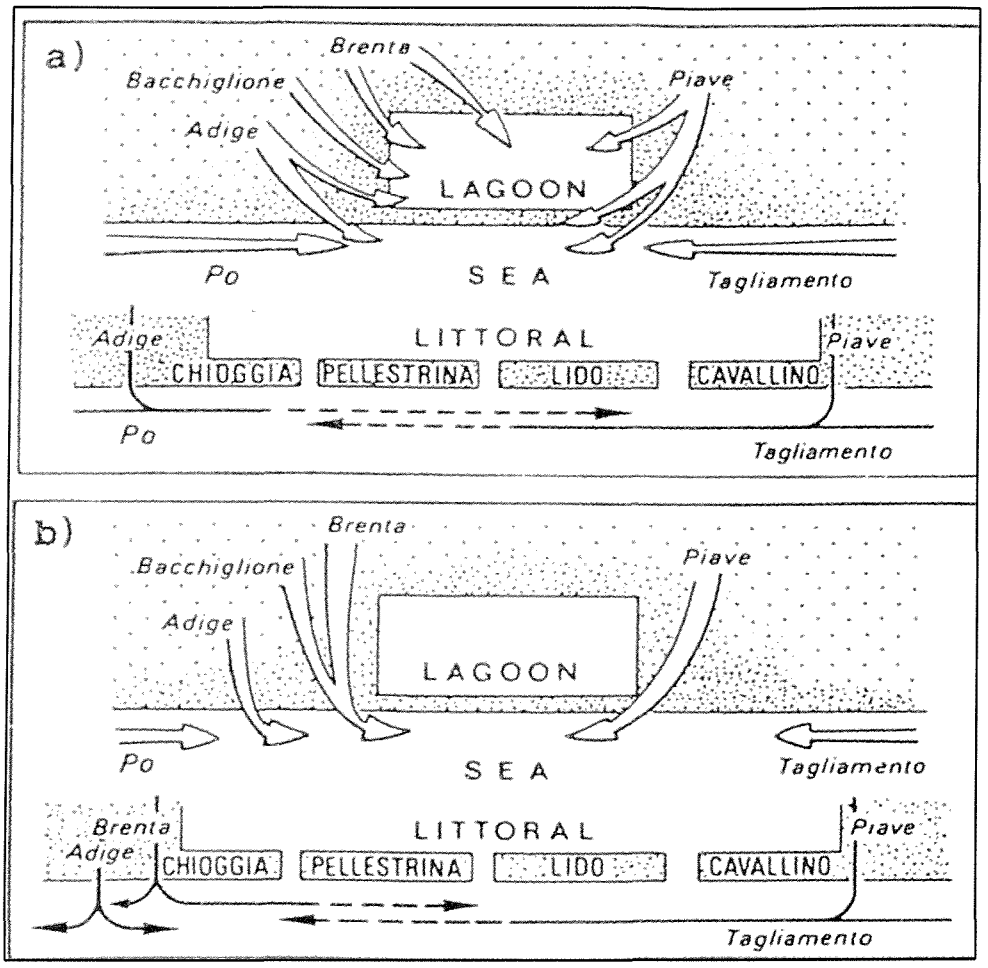

Figure 3.7. A schematic representation of the river diversion carried out in Venice Lagoon between the 15th and the 19th century (from CVN, 1996).

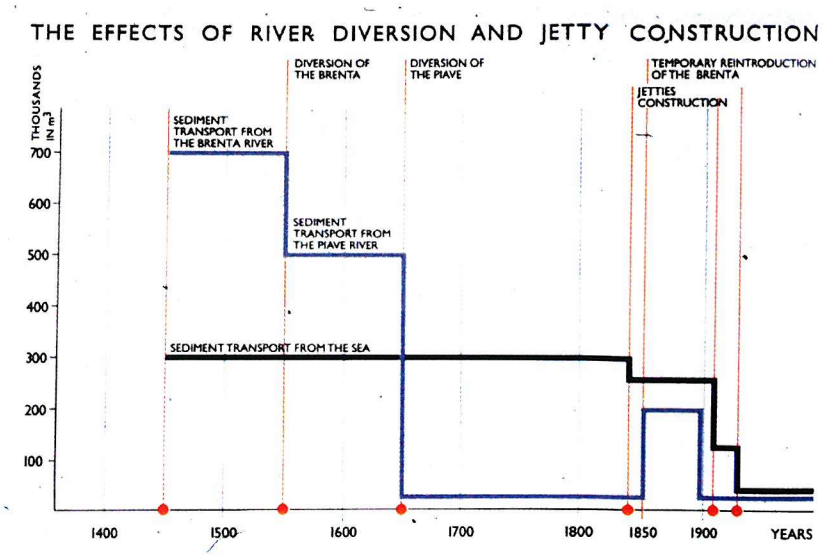

Figure 3.8. Sediment input from rivers (blue line) and the open sea (black line) in the last five centuries (from CNV,1996).

The assumption that sediment input from rivers into Venice Lagoon is distributed homogeneously must be taken with caution for two main reasons:

1) more than 50 % of the overall water discharge from rivers is concentrated in the northern basin of the Lagoon (Fig. 3.9.; ZONTA, 2000);

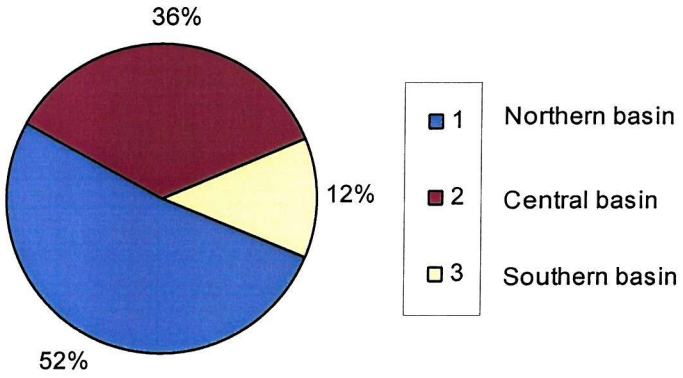

Figure 3.9. The relative distribution of water discharge in the northern, central and southern basin of Venice Lagoon. Note that 88% of the river discharge is concentrated in the northern and central basin where the salt marshes and mudflat are better preserved (data obtained from the DRAIN project: ZONTA, 2000).

2) UMGIESSER (2000) has predicted that the residual currents in Venice Lagoon, which provide an effective mechanism of sediment redistribution between the central and the northern parts, are strongly controlled by wind direction. UMGIESSER

(2000) underlines also the importance of wind forcing by *Bora* and *Scirocco* winds on the redistribution of suspended load inside the Lagoon. In effect, this means that it is impossible at present to predict the transport pathways of sediments within the Lagoon.

3.4. Subsidence

Subsidence is defined as the lowering of the ground level with respect to MSL. Subsidence has played a major role in the formation and evolution of Venice Lagoon, and has been caused by several factors (both natural and anthropogenic). The rate of lowering has varied through time (CARBOGNIN *et al.*, 1976; GAMBOLATI *et al.*, 1974) as a function of the characteristics of the soil (1993; CARBOGNIN *et al*, 1993), climatic conditions (CARBOGNIN *et al.*, 1981) and human activities (CARBOGNIN *et al.*, 1996). Detailed studies of subsidence in Venice Lagoon are found in CARBOGNIN *et al.* (1984), POLAND *et al.* (1984), BORTOLAMI *et al.* (1985), TEATINI *et al.* (1995), CARBOGNIN *et al.* (1995a) and CARBOGNIN *et al.* (1995b).

3.4.1. Natural subsidence

Natural subsidence is caused by the consolidation of fine-grained deposits due to a positive excess load, resulting in a reduction in the void ratio between the particles over time and therefore a decrease in their original volume (LAMBE & WHITMAN, 1979). Natural subsidence in Venice Lagoon has been estimated at 0.4 mm/a. Authors using different methods or databases, have recorded different values of subsidence. Discrepancies between results are small and have been explained by the diversion of the rivers (CARBOGNIN *et al.*, 1976) which may have modified the natural trend of subsidence in many ways; (GATTO & CARBOGNIN, 1981).

3.4.2. Anthropogenic subsidence

After 1925, pumping of ground water increased considerably. The highest rates of pumping occurring between 1950 and 1969 (a period of industrial growth). Acquifer depletion led to subsidence which reached critical levels in the late seventies (Fig. 3.10.). From 1969, the ground water pumping strategy was changed

in order to re-establish the original pressure within the aquifer. Piezometric levels have been improved and the original aquifer pressure was attained in 1978, unfortunately only 15 % of the compaction was recovered (CARBOGNIN, 1987; DAZZI *et al.*, 1984). Man-induced subsidence has been the main factor in the lowering of Venice and of the Lagoon bottom (estimated at about 10 cm, including rebound). At present, subsidence is not a major problem (CARBOGNIN & CECCONI, 1997; see Fig. 2.6.).

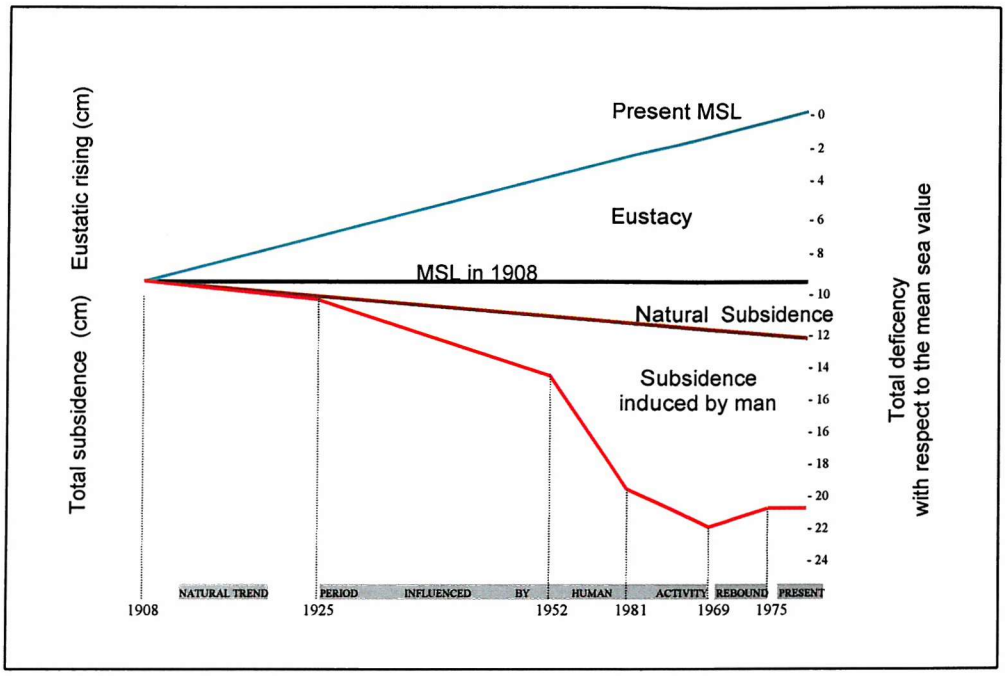

Figure 3.10. Relative sea level changes in Venice Lagoon due to subsidence and eustacy from 1908 to 1980 (GATTO & CARBOGNIN, 1981). After 1975 the trend in subsidence follows the natural rate of about 0.4 mm/a.

3.4.3. Relative subsidence due to eustacy

WARRICK & OERLEMANS (1990) proposed that MSL will rise 35-70 cm over the next 100 years. This phenomenon, better known as eustacy, has strong implications for coastal sites, particularly Venice Lagoon. The effect of eustacy has been studied in many areas of the north Adriatic Sea affected by subsidence (e.g. City of Venice) and in stable areas (e.g. City of Trieste). An average rate of MSL rise of 1.27 mm/a has been determined from these studies (GATTO & CARBOGNIN, 1981; CARBOGNIN & TARONI, 1996). The authors also describe a "quiescent period" of sea level change between 1970 and 1993 (Fig. 3.11.).

Relative subsidence during the 20th century has induced a lowering of the ground surface by about 22 cm (GATTO & CARBOGNIN, 1981; CARBOGNIN & TARONI, 1984). In Venice, the current estimated rate of sea level rise ranges from +1.1 mm/a (RUSCONI *et al.*, 1993) to +1.3 mm/a (PIRAZZOLI, 1987). The total rate (due to natural subsidence plus eustacy) is about 1.7 mm/a.

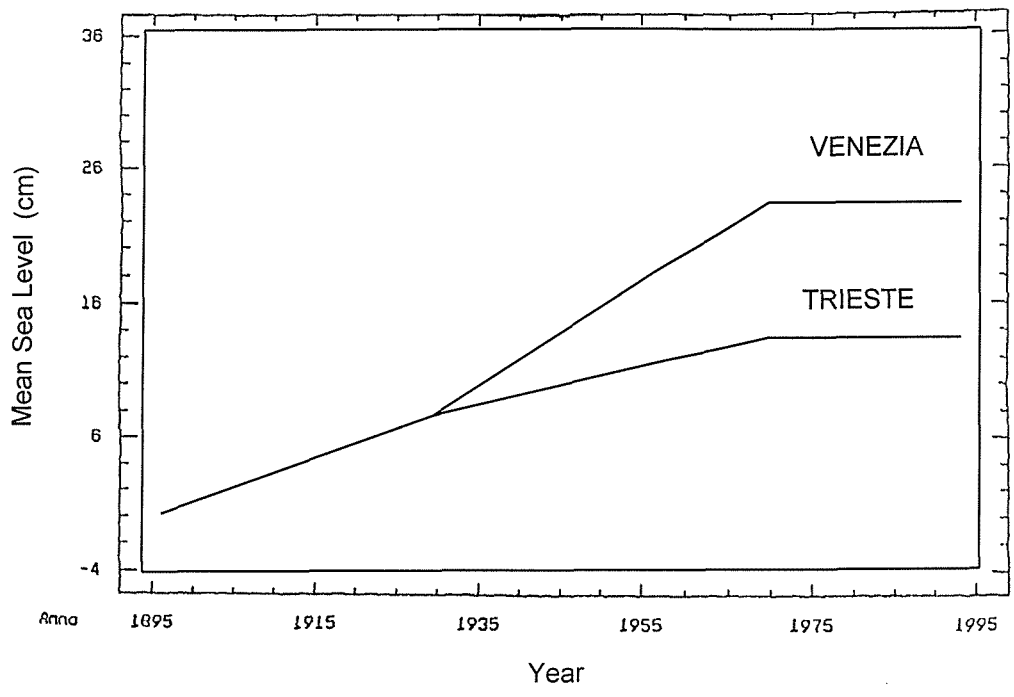

Figure 3.11. Mean sea level records for the cities of Venice and Trieste between 1896 and 1993 (CARBOGNIN & TARONI, 1996). Note that the greater lowering rate of Venice started around 1930 due to human activities.

3.5. Pollution

Pollution, due to the introduction of heavy industrial as well as urban and agricultural wastewater load, is one of the biggest problems of the Venice Lagoon ecosystem (CNV, 1996). Pollution problems are particularly significant in estuaries where fine-grained sediment is abundant, such as Venice Lagoon (because pollutants are better adsorbed by small particles). From the 1950's, a big Italian petrochemical centre was built (the largest in the Adriatic Sea) in the *Marghera* and *Mestre* areas. Every year more then 10 million tonnes of crude oil and petroleum products are treated and transported through Venice Lagoon along the *Malamocco-Marghera* Channel (Fig. 3.1.). The industrial centre of *Marghera* has been clearly identified as one of the principal sources of heavy metal contamination in Venice Lagoon (ALBEROTANZA *et al.*, 1991a; GHERMANDI *et al.* 1993; ZAGO *et al.*, 1994; ZONTA *et al.*, 1994b; ZAGGHIA & ZONTA, 1997). Other studies have focused on the concentration of heavy metals and their interactions with the sediments and water (ALBEROTANZA *et al.*, 1991b; RAMASCO, 1991; ARGESE *et al.*, 1992; ZONTA *et al.*, 1994a; ZONTA *et al.*, 1995; ZAGGHIA *et al.*, 1996).

Wastewater from Venice, Chioggia and other small villages contribute a large amount of phosphorous and nitrogen to the Lagoon. The agricultural wastewater discharge is concentrated in the northern part of the Lagoon (close to the studied area; Fig 3.9.). Investigations carried out before 1991 indicated that the annual nutrient discharge at that time was about 7-9x10^6 kg N/a and 1x10^6 kg P/a (THETIS, 1997). Many studies have also been carried out to evaluate nutrient levels in relation to resuspension and macrophyte dynamics (MOSS, 1989; FLINDT, 1994; FLINDT *et al.*, 1997; GENNARO *et al.*, 1994; SFRISO *et al.*, 1991; SFRISO & PAVONI, 1994; PAVONI *et al.*, 1997; DE CASABIANCA *et al.*, 1997). The discharge of nutrients in the Venice Lagoon basin is particularly important because it controls the bloom of algae.

3.6. Summary

Salt marshes (*barene*) and mudflats (*velme*) are largely found in the northern part of the Lagoon because they are less affected by boat traffic and better protected from *Bora* winds. By contrast, subsidence and man-induced modifications have destroyed these environments in the central and southern parts. Channel excavation over the last five centuries has enhanced the transversal transport of sediments from the intertidal areas to the channels resulting in a loss of sediments to the open sea. The greatest rate of morphological deterioration within Venice Lagoon has occurred over the last 100 years. Assuming that: (1) the export of sediment (1.1 million m^3/a) is constant; (2) the area of the Lagoon is about 500 km^2; and (3) erosion is distributed homogeneously throughout the Lagoon, it is possible to estimate the future eroded depth using the following relation:

$$D_E = V_S/A_L \qquad m \qquad 3.5.1$$

where V_S is the volume of sediment (m^3) that will be exported per unit time, A_L is the area of the Lagoon (m^2), D_E is the depth (m) of sediments eroded on the entire area.

From the above consideration, it is estimated that erosion to a depth of about 10 cm will occur within the next 40 years if no remedial action is taken, resulting in a reduction in the complexity and diversity of the ecosystem. This prediction is conservative as it does not include changing bathymetry within the Lagoon, the spatial variation of sediment properties (i.e. their stability) and the effect of an increasing inundation period.

If this trend continues, by 2040 all the salt marshes and mudflats will have probably disappeared (LABORATORIO VENEZIA, 1996). In order to reduce the rate of sediment loss from the mudflats, sediments dredged from the channels over the last 10 years were used to nourish salt marshes and create artificial islands (about 280 ha) in different parts of the Lagoon (CNV, 1996).

Venice Lagoon is affected by serious environmental deterioration (LASSERRE & MARZOLLO, 2000). The area is affected by high concentrations of pollutants, high nutrient discharges leading to eutrophication (a decrease of oxygen content in the water due to the algal blooms), and changes in the chemical and physical characteristics of the sediments.

CHAPTER 4: *IN-SITU* SEDIMENT STABILITY WITHIN VENICE LAGOON

4.1. Introduction

The work carried out as part of the EU-funded F-ECTS project is presented. The objective of F-ECTS was to evaluate the role of estuarine phytobenthos on sediment stability in order to acquire information on the feed-back mechanisms between the biology and the sedimentology within the Lagoon. Venice Lagoon, as in many other estuaries, is a habitat for a variety of species of micro- and macroalgae (LASSERRE & MARZOLLO, 2000). Sediment stability and the effect of biostabilisation was investigated previously in Venice Lagoon by CNV (1992). Diatom abundance was measured at 86 stations in order to monitor spatial distribution by CNV (1992), but the diatom effect on erosion threshold (even if it was recognised) has not been investigated until the present study and has never been related to sediment stability. However, some areas of uncertainty requiring further research were indicated by CNV (1992). These are: (1) the investigation of *in-situ* sediment stability; (2) the determination of the best predictor of sediment stability (if any); (3) the effect of microphytobenthos activity in subtidal areas; and (4) the correlation between the erosion threshold and sediment properties.

In the present study, all the points listed above were investigated. The results of *in-situ* measurements carried out in the northern and central part of the Lagoon are presented. The aim of this large-scale investigation was dictated by a lack of understanding of seasonal and spatial variation of sediment stability at different sites throughout Venice Lagoon (intertidal, subtidal and channels areas). Furthermore, use of a larger scale investigation was of benefit to the site-specific study carried out in *Palude della Centrega* enabling it to be interpreted in the context of the whole Lagoon.

In particular, the present study focuses on the effects of the microphytobenthos on sediment biostabilisation, and how, where and when organisms can change the resistance and eventual protection of the sediments against erosion.

4.1.1. The F-ECTS campaigns

Extensive field programmes were undertaken in summer 1998 and winter 1999. The locations of the investigated sites are shown in Fig. 4.1. Sediment stability was investigated using an *in situ* benthic flume: the Mini Flume (MF).
Deployments of the Mini Flume were carried out around Venice Lagoon by moving the equipment on a barge (Fig. 4.2.) from one site to another to reduce the time interval between measures. The erodibility of the sea bed was defined by calculating erosion thresholds, erosion rate and the peak erosion rates.
Sediment samples were collected during both campaigns in order to determine physical (i.e. grain size, water content and bulk density), biochemical (chlorophyll *a* and colloidal carbohydrate) and biological (organic content) parameters. Erosion threshold was correlated with the main physical and biological sediment properties to determine which parameter was significant at each location through time and which could be used as a proxy to predict (indirectly) sediment stability.

4.2. Method

The sites investigated during F-ECTS were selected to include some variability in water depth, sediment composition, and phytobenthos assemblage. For each investigated site, environmental data were collected at the time of Mini Flume deployments. At some sites, more than one experiment was carried out to replicate MF measures or to investigate areas covered by different vegetation. This approach was particularly useful during the summer campaign when higher spatial heterogeneity (patchiness) in algal cover occurred. Sediment samples (gravity and push cores) were collected as close to the instruments as possible (when Mini Flume deployments were completed), in order to determine coupled sediment characteristics and correlate them with the stability of the seabed.

4.2.1. Description of sites and environmental conditions

A brief description of each site is reported in Appendix II and site locations (Fig. 4.1.) and sediment characteristics are listed in Table 4.1.

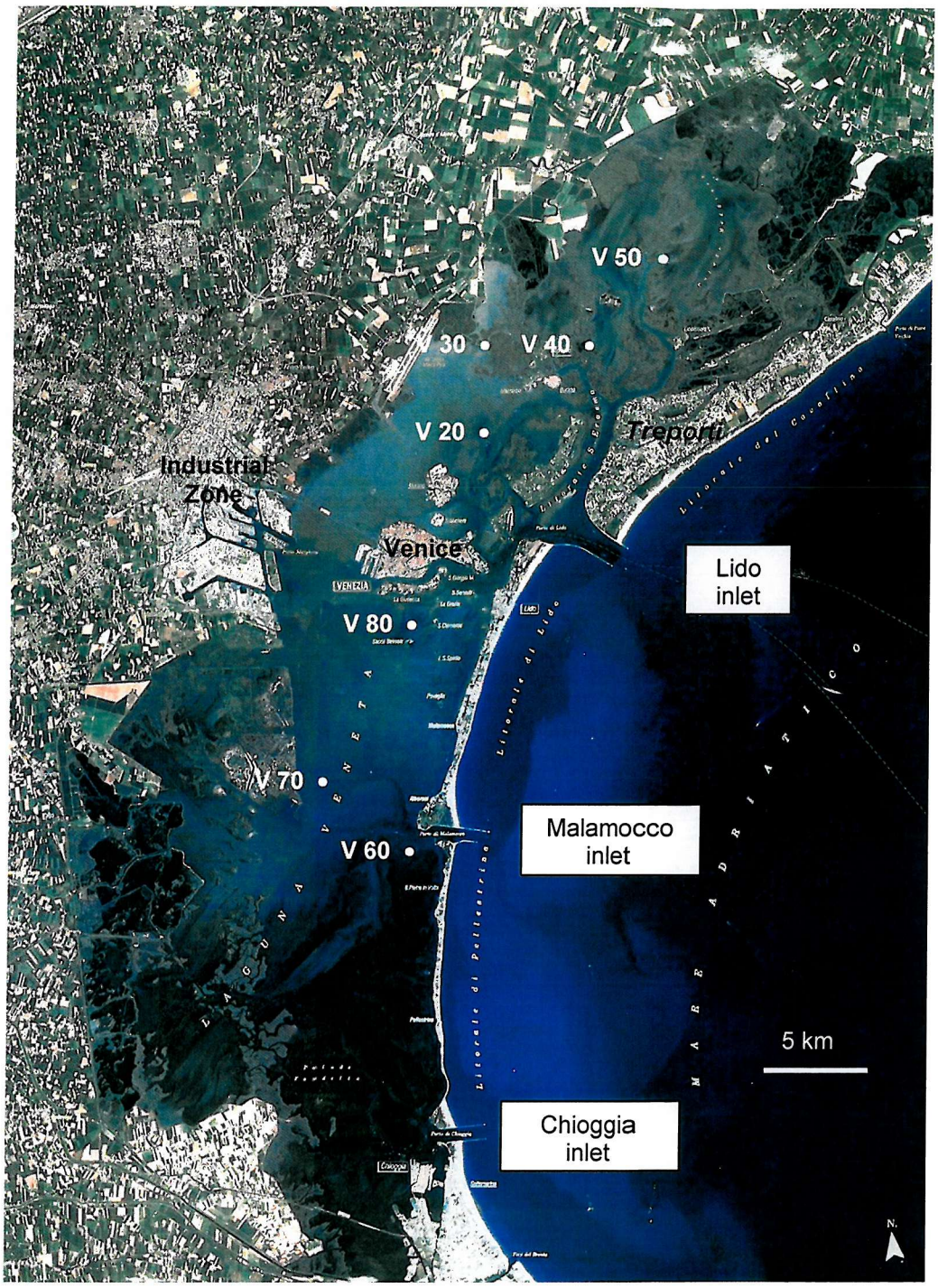

Figure 4.1. The study region of Venice Lagoon showing the position of the sites occupied by Mini Flume. The 7 sites investigated in August 1998 and February March 1999 are represented by white dots.

A

B

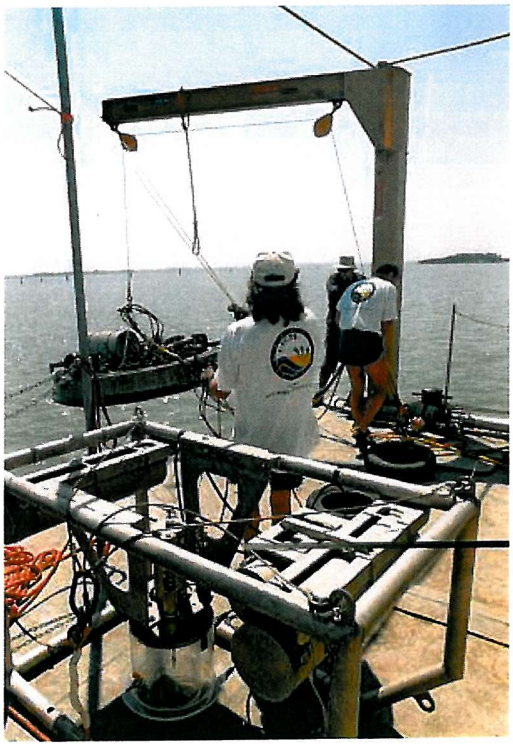

Figure 4.2. The barge (A) used to deploy the flumes (B in Venice Lagoon, Italy.

Site	Name	Latitude	Longitude	Depth (m)	Sub-Basin	Sediment	Typology	Covering
V 20	S.Giacomo	45° 28' 31"	12° 23' 11"	1	Northern	Sandy silt	Subtidal	Biofilm and macroalgae
V 30	Cona	45° 30' 30"	12° 23' 12"	1.4	Northern	Clayey silt	Subtidal	Macroalgae
V 40	Centrega	45° 29' 40"	12° 26' 23"	0.2	Northern	Clayey silt	Intertidal	Biofilm, Zostera noltii, Spartina
V 50	Saline	45° 30' 34"	12° 28' 28"	0.2	Northern	Clayey silt	Intertidal	Zostera noltii
V 60	S.Maria del Mare	45° 19' 58"	12° 18' 13"	2	Central	Silty sand	Subtidal	Cymodocea nodosa, Zostera noltii
V 70	S.Leonardo	45° 21' 25"	12° 15' 45"	2.4	Central	Silty sand	Subtidal	Bare
V 80	S.Spirito	45° 24' 08"	12° 20' 10"	1.7	Central	Clayey silt	Subtidal	Ulva

Table 4.1. A summary of site descriptions from the F-ECTS field campaigns.

Environmental (water depth, temperature, salinity, turbidity and wind speed) data were collected to assist interpretation of the results and expand the background information at each site.

Water temperature and salinity were measured when deployments started. Turbidity values were calculated as an average value of SSC recorded by the optical backscatter sensor (OBS) of the flume before erosion started. Wind speed data were obtained from the Ministry of Public works (measured at *Treporti* in the northern part of the Lagoon). Wind speeds are reported for the same time as turbidity measurements (i.e. start of the Mini Flume deployments).

4.2.2. Stability measurements

Measurements of sediment stability using Mini Flume

The erosion threshold was derived for each site where Mini Flume deployments were carried out. At some sites, more than one experiment was carried out to replicate measures or to investigate areas covered by different vegetation. This approach was particularly useful during the summer campaign when high spatial heterogeneity of algae was observed.

Description of the Mini Flume (in-situ apparatus)

The Mini Flume (MF) is an annular flume composed of two concentric acrylic cylinders 30 cm high (Fig. 4.3.). It is open at the base, enclosed at the top and has a test section of about 0.036 m^2 (Fig. 4.4.). It is an autonomous device fully pre-programmed before deployment and the data collected can be evaluated after recovery. The system is not interactive, which often limited the quality of the results. The flume is mounted on a tubular aluminium frame which supports a digital Sony® video camera, a 70 watt light, two battery pack housings, and an electronics housing. The flume is designed to be lowered onto a cohesive bed encapsulating the local bed properties as well as those of the near-bed waters.

The MF is mounted with springs that maintain a downward pressure on the annulus lid (about 10 Kg) once on the bed. The speed and acceleration of the flume paddles are controlled by a Compumotor digital DC stepping motor that is powered by a bank of 90 D-cell (1.5 volt) batteries. The motor is controlled by a Tattletale® 7 data logger that is located in the electronics housing and connected through an RS232 serial link.

A Seapoint® Optical Backscatter Sensor (OBS) monitors turbidity at a height of 12 cm above the base. Low and high sensor gains can be chosen before deployments, depending on the turbidity levels of the ambient water. The OBS is interfaced to the Tattletale® 7 data logger which logs and stores data on a 20 Mbyte hard drive at a rate of 1 Hz. A sample port is situated at the height of the OBS for purposes of sensor calibration. A digital Sony® video camera was used to monitor the erosion process at the bed. The camera is capable of storing about 1 hour of imagery on internal memory.

Mini Flume calibration

FUNG (1997) has accurately measured the velocity structure within the Mini Flume. He determined the velocity distribution in the flume at three lid speeds (0.2, 0.6 and 1 rev/s). Bed shear stress was calculated by O'BRIEN (1998) from the logarithmic section of the bottom boundary layer using the Law of the wall:

$$U(z) = \frac{U_*}{k} \ln\left(\frac{z}{z_0}\right) \qquad \text{m/s} \qquad 4.2.2.1$$

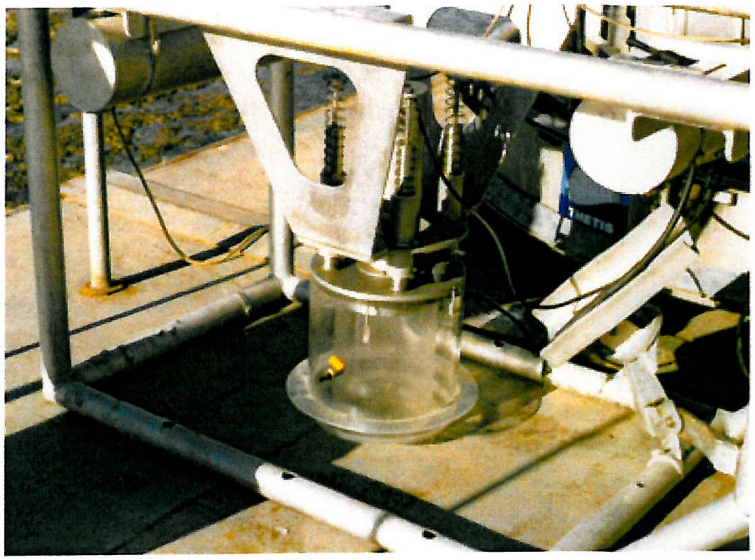

Figure 4.3. The Mini Flume used *in- situ* mounted on a deployment frame.

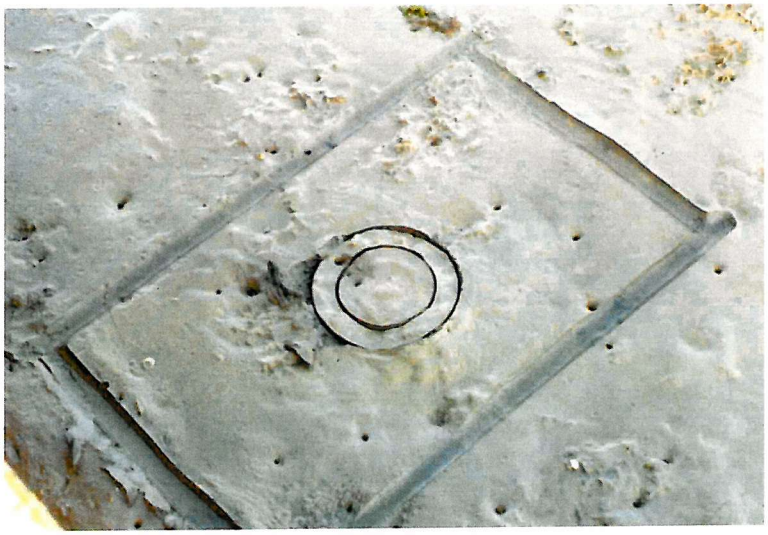

Figure 4.4. The Mini Flume foot print left on the mud after deployment in station V50.

therefore,

$$U_* = \frac{U(z)\,k}{\ln(\frac{z}{z_o})} \qquad \text{m/s} \qquad 4.2.2.\text{II}$$

and

$$\tau_o = C_D\,\rho\,U^2 = \rho\,U_*^2 \qquad \text{Pa} \qquad 4.2.2.\text{III}$$

where z is the height above base of flume (m), U(z) is the mean current velocity at height z (m/s), U_* is the friction velocity (m/s), z_0 is the roughness length (m), k is von Karman's constant (0.4) and ρ is the fluid density (kg/m^3).

U(z) was measured for each step at three positions across the section of the flume (close to the outer wall, the centre and the inner wall of the annulus). Results showed that the radial velocity (U_x) of the flow is roughly 10 % of the tangential velocity (U_y) at 1 cm above the base.

O'BRIEN (1998) found a relationship between current speed and the friction velocity using the data set of FUNG (1997) and particle tracking analysis carried out by AMOS (*pers. comm*). The relationship is reported below:

$$\tau_o = 4.39\,U_r^{\,2} - 0.36\,U_r \qquad \text{Pa} \qquad 4.2.2.\text{IV}$$

where M is the motor speed expressed in rev/s Fig. 4.5.B.

In the present study, τ_o has been calculated from the motor speed rather than current speed. Stress reduction due to turbidity was not accounted for during the experiments. A calibration between lid speed (U_r) and motor input (M) shows a strong linear trend (Fig. 4.5.A). The Mini Flume shows a linear response between M-value (below M=1500) and lid speed (equation 4.2.2.v). Above 0.23 rev/s, the response of the motor is given by the following relation:

$$U_r = 2\text{x}10^{-4}\,M - 0.002 \qquad \text{rev/s} \qquad 4.2.2.\text{V}$$

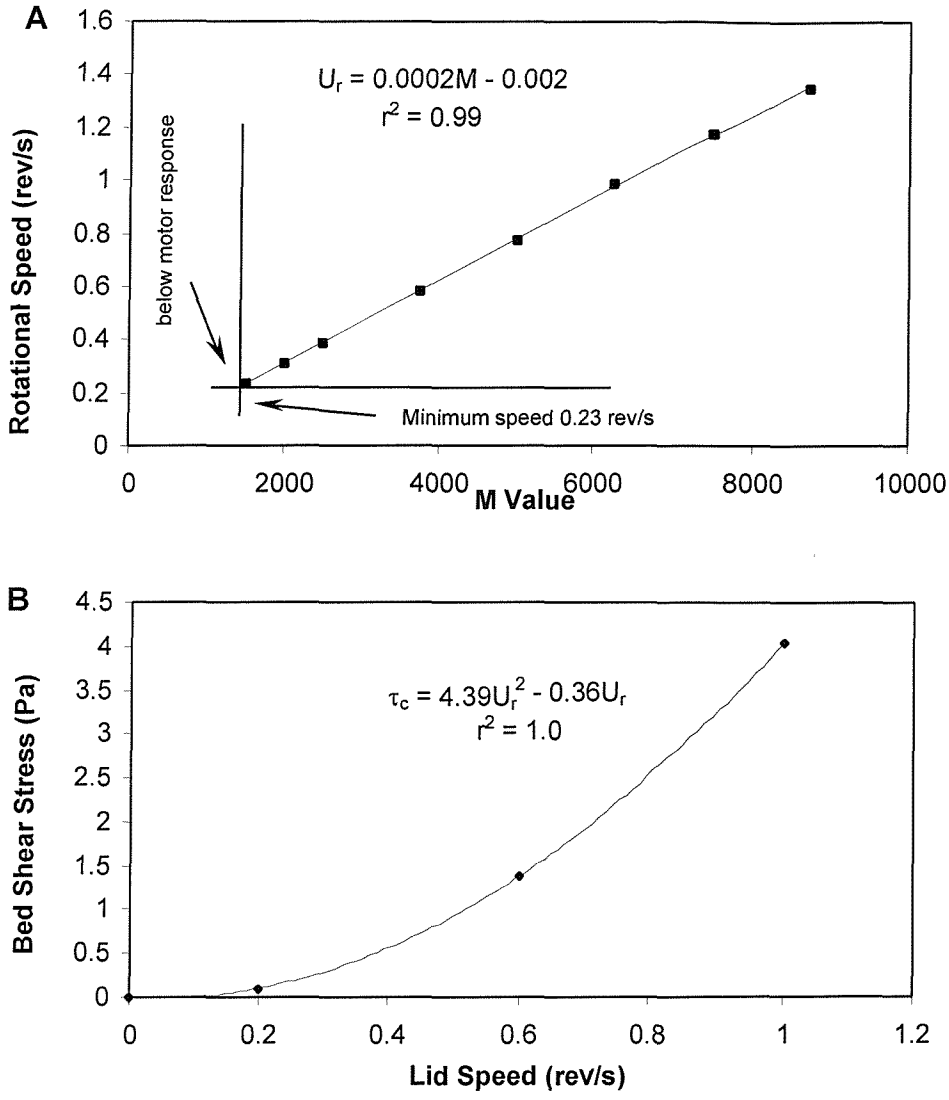

Figure 4.5. The relationship between the M value output of the Mini Flume motor and the rotational speed (rev/s) of the lid of the Mini Flume (A). The relationship between lid speed and the applied bed shear stress calculated using O'BRIEN (1998) and from LDV data (FUNG, 1997; B).

Optical instruments have been used in studies of sediment dynamics for many years. OBS manuals usually provide standard calibrations for mud and sand. Nevertheless, many scientists and OBS users have focused research on the response of OBS to backscatter from natural sediments in field and laboratory experiments (GREEN & BOON, 1993; XU, 1997; HATCHER *et al.*, 2000). BUNT *et al.* (1999) and SUTHERLAND *et al.* (1999) provide good reviews of the response of OBS

devices to variations in suspended particulate matter. BUNT *et al.* (1999) showed that sediment properties (size and shape) can influence OBS response. These problems are amplified when the sensors are used to measure long time series. SUTHERLAND *et al.* (1999) focused on the effect of varying darkness levels on the calibration of the OBS for suspended sediments. The authors showed that the OBS is sensitive to variations in Munsell value and not Munsell hue or chroma. They also suggested that the level of blackness of particles acts to absorb the near-infrared signal of the OBS, modifying its response and hence the calibration. This effect is equal to, if not greater than, the effect of particle size.

Considering the studies mentioned above the most important factors affecting OBS response are: (1) the blackness of particles in suspension (which is influenced by anoxia); (2) multimodal and spatially variability of sediments (e.g. estuaries); (3) sediment dynamics variation through time (e.g. estuaries and surf zones); (4) the time varying grain size due to flocculation of fine-grained sediment (e.g. tidal creeks, coastal zones and mangrove swamps); (5) the time varying plankton or organic matter content (e.g. mangrove swamps, tidal creeks, coastal zones); and (6) the variation in mineralogy of the SPM. The importance of each factor varies depending upon the environmental setting (hydrodynamics, biological and sedimentological conditions; see Table 4.2.).

FACTOR	*EFFECT on OBS*	*MAGNITUDE*
Colour (*)	Inc/dec	Unknown
Grain size (**)	Inc/dec	Over **100** times
Shape (**)	Increase	**2** times
Surface roughness (**)	Increase	**10** times
Particle flocculation (**)	Inc/dec	**2** times
Plankton (**)	Increase	**4** times
Bubbles (**)	Increase	**2** times

Table 4.2. A list of the principal factors that affect the response of the Optical Backscatter Sensors. The magnitude and the effect on the final results are also indicated in order of importance following the results of SUTHERLAND *et al.* (1999;*) and BUNT *et al.* (1999;**).

The OBS sensor on the Mini Flume was calibrated using discrete samples drawn over a large concentration range and over a full range of flow conditions. Samples were filtered using Millipore ® 47mm diameter 0.45 μm filters (see Appendix I).

Calibration was carried out using a tank in which an artificial flow was created by controlled rotation of a propeller placed on the bottom. A turbulent flow was generated before the calibration was started and was maintained constant over time. Turbulence was sufficient to maintain all particles in suspension without the formation of bubbles in the water column. Sediment was added at known time intervals and OBS output was recorded until saturation. The results of the calibration show a linear response of the sensor (Fig. 4.6.):

HIGH GAIN	SSC = 7.39 OBS + 91.99	mg/l	4.2.2.VIa
LOW GAIN	SSC = 1.92 OBS + 93.83	mg/l	4.2.2.VIb

Sediment used in the calibration was collected at Station V40, and was considered representative of the northern part of Venice Lagoon.

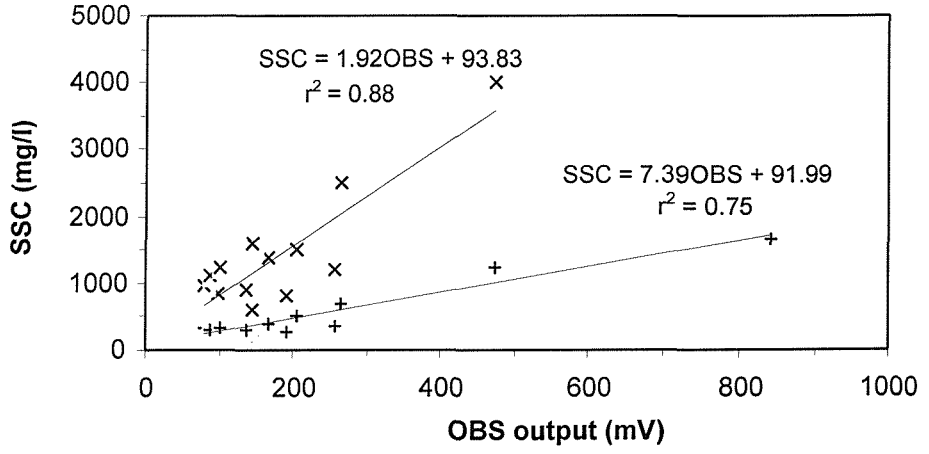

Figure 4.6. The relationship between OBS output and SSC derived for (1) low and (2) high gains of the OBS on Mini Flume.

Data processing

The OBS outputs and the M-value were converted to SSC (mg/l) and bed shear stress (Pa) respectively using equations 4.2.2.IV. and 4.2.2.VI. A time series of time-averaged values were generated. All subsequent calculations and analyses were completed using MS Excel (Fig. 4.7.).

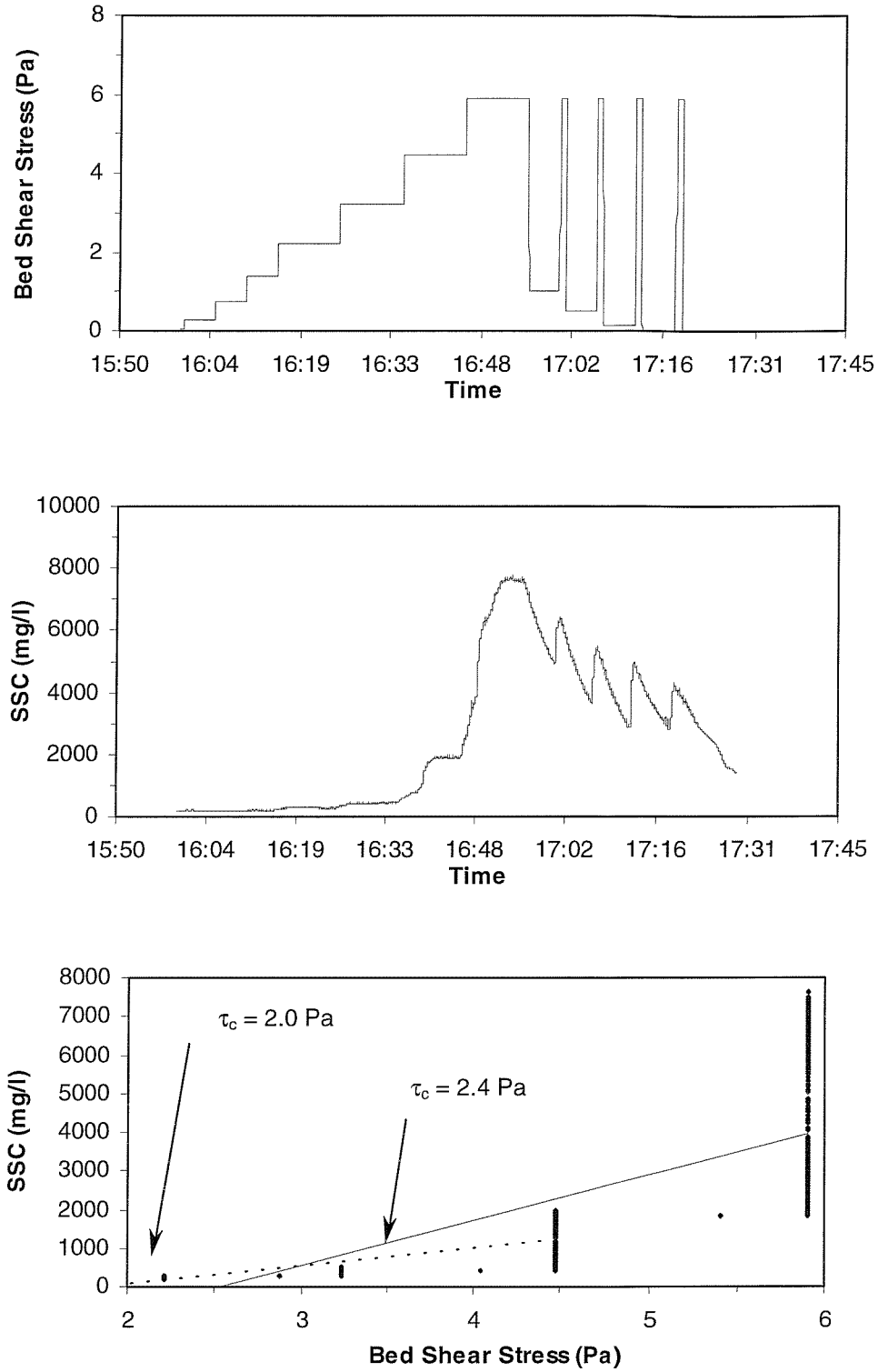

Figure 4.7. A typical time-series of the Mini Flume. In this illustration, the erosion threshold was derived using (1) the highest increments of stress, yielding in a τ_c = 2.4 Pa (solid line) and (2) excluding the highest increments of stress, yielding in a τ_c =2.0 Pa (dotted line). Estimate of τ_c are based on the full data set in this study. The data is from site V40 undertaken in the northern Lagoon during summer 1998.

EROSION THRESHOLD (τ_c) was calculated from all the stress increments where erosion was evident. The best-fit line, derived from least squares regression, is sensitive to different ranges of bed shear stress used in the data analyses (Fig. 4.7.) because the scatter in SSC increases as a function of applied stress. In this study, the erosion threshold was defined as the value of the bed stress at which SSC reaches ambient values (SSC_a) in a regression plot of SSC and bed shear stress (SUTHERLAND, 1996). AMOS & GIBSON (1994), from results of the Sea Carousel, found that the reproducibility of this technique to calculate the *in-situ* erosion threshold was of ±14 % (therefore it was assumed for the purpose of this study that the same accuracy applies in the case of the Mini Flume). SSC_a was calculated as the average value of SSC before erosion started. Usually, when the flume lid started to rotate the SSC was still decreasing due to slight previous disturbance to particles during flume positioning. This decreasing trend does not significantly influence the final estimation.

EROSION RATE (E) was calculated using the equation:

$$E = (dSSC/dt)h \qquad kg/m^2/s \qquad 4.2.1$$

where E is the erosion rate and h is the depth of the water in the annulus.

EROSION TYPE was defined from visual observation of the erosion rate time series. All sites were of type I erosion (after VILLARET & PAULIC, 1986).

4.2.3. Core sampling

Gravity cores

Seventeen cores were collected using the gravity corer of the Geological Survey of Canada during the summer campaign. The corer penetrated 1 metre into the Lagoon sediments. Sediment cores were stored in a cold room at -5 °C before undergoing x-ray analysis and splitting by CIAVOLA & COVELLI (2000).

Syringe cores

Surficial samples were collected manually using 60-ml syringe cores, immediately frozen in liquid nitrogen and stored at –20°C until analysis. Bulk density (the average value of the top 1 cm) was determined from frozen syringes by x-ray computed tomography (AMOS *et al.*, 1996a). Syringe cores were sub-sampled by dividing the top 1 cm into four equal parts (Fig. 4.8.). Sub-samples were used to determine chlorophyll *a*, carbohydrate, water and organic content following the scheme presented below; one subsample was stored for extra analyses. Definitions of the above parameters, together with the analytical methods are reported in Appendix I.

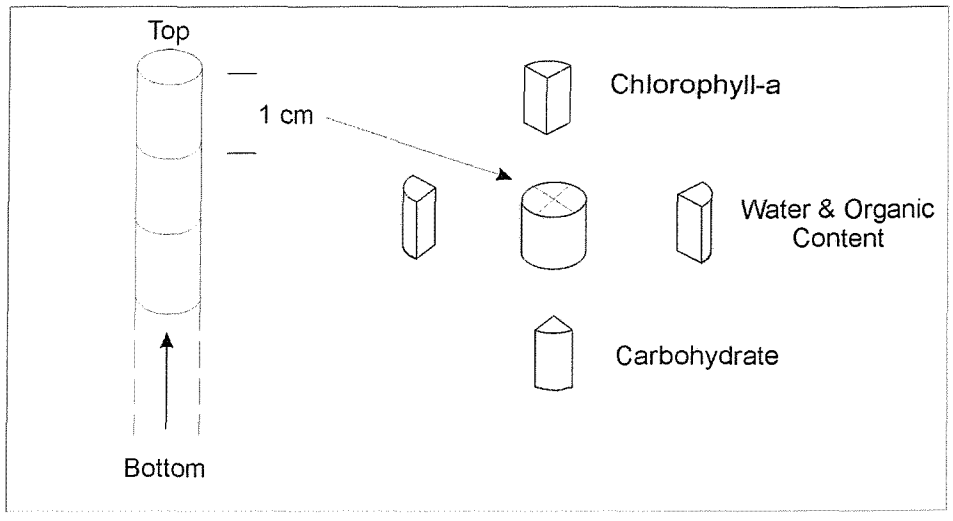

Figure 4.8. A schematic representation of sub-sampling before biochemical or biological analysis.

4.3. Results

4.3.1. Environmental conditions

The sampling programme and basic ambient environmental conditions are summarised in Tables 4.3. and 4.4. respectively. Campaigns are referred to as summer 1998 and winter 1999. Replicates at the same site were placed at few meters apart and consecutive numbers within the same decade indicate them.

Site	Date	Depth	Temperature	Salinity	Turbidity	Wind speed
No.	D/M	M	°C	S	(mg/l)	(km/h)
V 20	11/8	1	29	36	64	10
V 21	12/8	1	27.4	31	19	6
V 22	13/8	1	27	30	163	12
V 30	8/8	1.4	27	28	51	2
V 31	9/8	1.4	27	28	74	8
V 32	10/8	1.4	27	28	75	8
V 40	4/8	0.2	29	33	9	25
V 41	5/8	0.2	30	33	74	38
V 42	5/8	0.2	30	33	113	21
V 43	6/8	0.2	27	36	118	20
V 44	7/8	0.2	26	36	253	9
V 50	2/8	0.2	28	30	15	13
V 60	18/8	2	27	35.7	10	15
V 62	18/8	2	24.9	34	7	14
V 70	19/8	2.4	26.5	35.7	42	6
V 80	17/8	1.7	28	34	14	12

Table 4.3. The results of all deployments carried out during the F-ECTS summer campaign (Summer 1998) using Mini Flume. The principal water properties are referenced to the deployment time. Note that highest turbidity value was measured at V44 after four windy days (highlighted).

Site	Date	Depth	Temperature	Salinity	Turbidity	Wind speed
No.	D/M	M	°C	S	(mg/l)	(km/h)
V 20	27/2	1	6.5	35	32	7
V 21	27/2	1	6.5	35	12	8
V 30	25/2	1.4	6.5	20	103.4	12
V 31	26/2	1.4	7.8	20	37.8	17
V 40	23/2	0.2	9.0	33	21.4	26
V 41	24/2	0.2	9.0	32	15.2	26
V 50	21/2	0.2	5.3	36	19.8	3
V 51	22/2	0.2	5.3	36	12.4	4
V 60	02/3	2	7.2	36	64	5
V 61	03/3	2	6.8	38	63	11
V 70	04/3	2.4	7.7	37	94	5
V 71	05/3	2.4	7.5	37	72	9
V 80	01/3	1.7	7.3	36	89	5

Table 4.4. The results of all deployments carried out during the F-ECTS winter campaign (Winter 1999) using the Mini Flume. Principal water properties were measured at the time of deployment. Note that the highest turbidity was measured in station V30 after two windy days (highlighted).

The time series of wind velocity and turbidity are illustrated (Fig. 4.9.). The limitations of this comparison are that turbidity was measured near the bed at

different water depths, whilst wind speed data were recorded at one point close to the barrier islands (*Treporti*; Fig. 4.1.). Therefore, SSC values were influenced by:

- the vertical profile of τ applied by wind generated waves at different water depths (Fig. 3.4.).
- the different of wind speed regime (lower) in the internal part of the Lagoon with respect to the location where the wind speed data were collected. To correct this, a decrease of 85-90% of the wind speed has been applied (see the study of DHI, 1991).

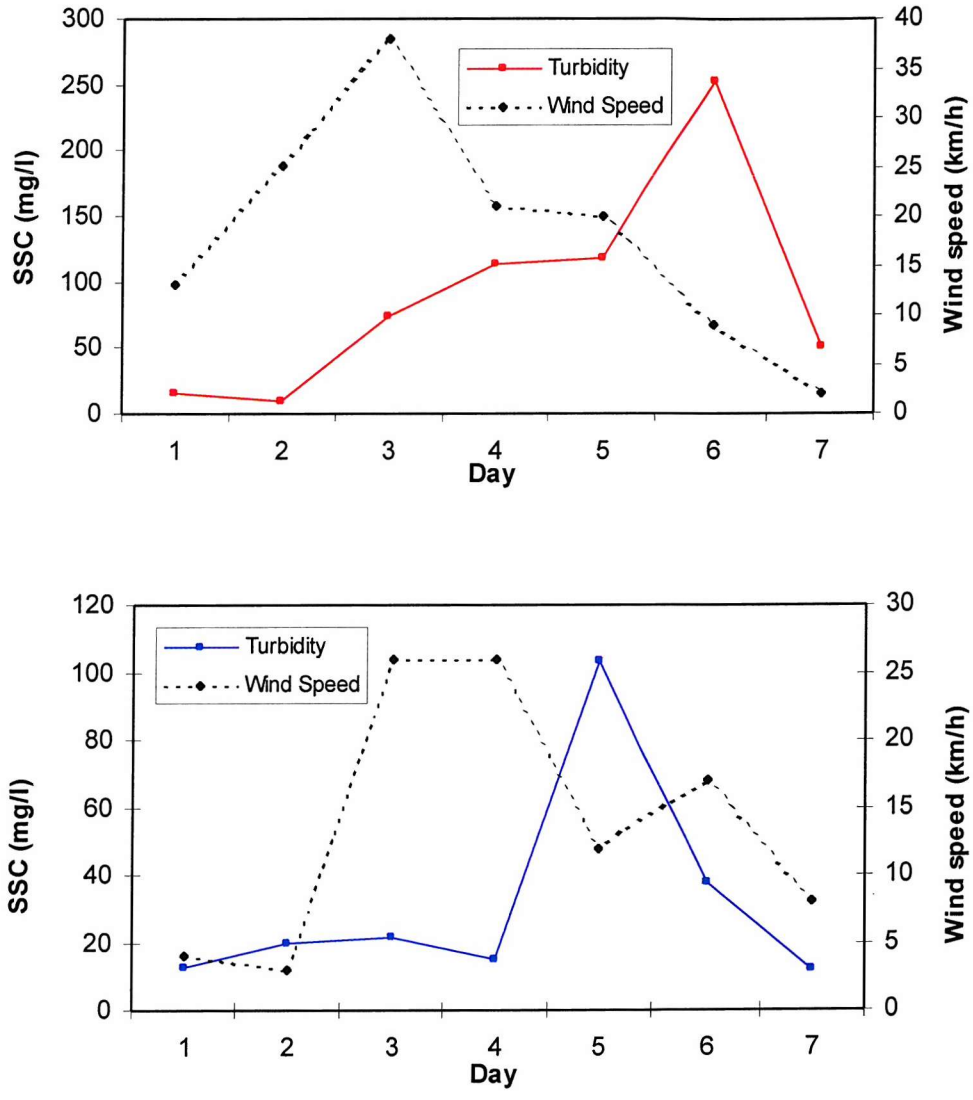

Figure 4.9. SSC and wind speed measured during the F-ECTS field campaign. Note the high turbidity occurring after 48 - 72 hours of increased wind speed.

4.3.2. Results from the Mini Flume deployments

A total of 28 deployments were performed at the 7 sites; 3 deployments failed for technical reasons. Results of the erosion threshold and the peak erosion rate derived for each experiment carried out during F-ECTS campaigns are reported in Table 4.5.

	Summer 1998			Winter 1999		
Site	Date	Erosion Threshold	Peak Erosion Rate	Date	Erosion Threshold	Peak Erosion Rate
No.	D/M/Y	Pa	(kg/m²/s)	D/M/Y	Pa	(kg/m²/s)
V 20	11/8/98	0.31	0.0008	27/2/99	0.73	0.00007
V 21	12/8/98	0.31	0.0005	27/2/99	1.12	0.00015
V 22	13/8/98	0.43	0.0005	-	-	-
V 30	8/8/98	0.59	0.003	Failed		
V 31	9/8/98	0.23	0.0009	26/2/99	0.69	0.00085
V 32	10/8/98	0.18	0.0002	-	-	-
V 40	4/8/98	2.36	0.009	23/2/99	1.16	0.001
V 41	5/8/98	0.34	0.008	Failed		
V 42	5/8/98	0.31	0.0025	-	-	-
V 43	6/8/98	0.29	0.0005	-	-	-
V 44	7/8/98	0.29	0.003	-	-	-
V 50	Failed			Failed		
V 51	2/8/98	1.98	0.0015	22/2/99	0.58	0.0007
V 60	18/8/98	0.38	0.0001	02/3/99	0.6	0.00009
V 62	18/8/98	0.65	0.0009	03/3/99	0.74	0.0007
V 70	19/8/98	0.56	0.001	04/3/99	0.37	0.0005
V 80	17/8/98	0.62	0.0005	01/3/99	0.7	0.0009

Table 4.5. Values of erosion threshold and peak erosion rates are reported for all Mini-Flume deployments carried out during summer and winter field surveys. In site V22, V32, V42, V43, V44 deployments were not carried out during the winter campaign.

The erosion threshold data derived from the Mini Flume deployments show that the sediment stability in Venice Lagoon has a strong spatial and temporal variability (Fig. 4.10.). Spatial variability is manifested by higher sediment stability in the northern Lagoon (see stations V40 and V51).

A clear temporal variation of sediment stability was also found in the northern part of the Lagoon where the highest critical erosional shear stress was measured during the summer. The central and southern part of the Lagoon showed a lower stability

reason for such a trend is unknown, and it will be discussed later (see discussion 4.4.).

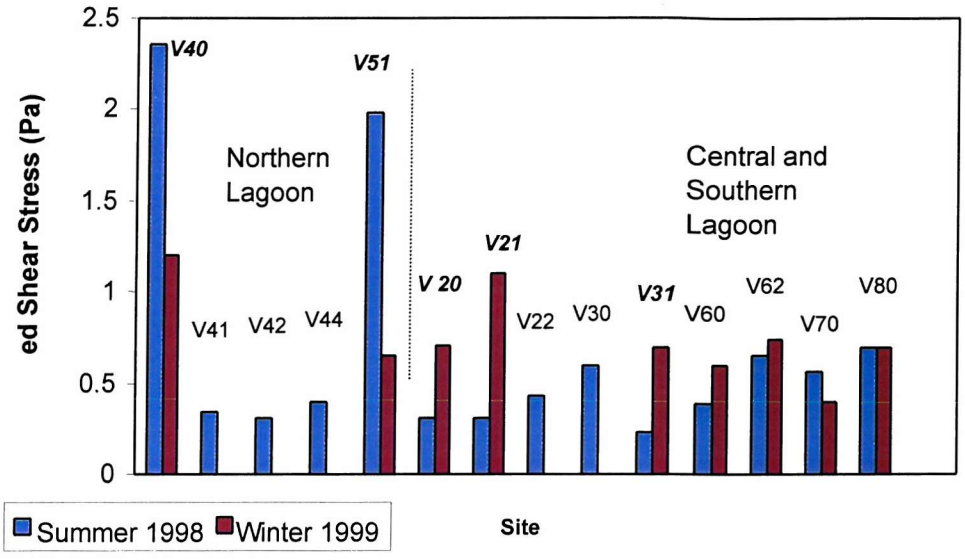

Figure 4.10. Erosion threshold measured *in-situ* at different sites in Venice Lagoon during the two field campaigns (summer 1998 and winter 1999). Data have been calculated from Mini Flume deployments. Stations V41, V42, V43, V44 were located close to station V40, but aligned across a section of the *Canale Scanello* where sediments did not show any evidence of biostabilisation (measurements in these stations were not replicated during the winter campaign).

4.3.3. Sediment properties

The textural properties determined from the gravity cores were used to classify sediments according to a new method proposed by FLEMMING (2000). Physical and biological properties determined from the top 1 cm syringe cores are reported in this section.

Texture and grain size from the gravity cores

Many authors have studied the importance of texture on the erodibility of natural sediments, most recently MITCHNER *et al.* (1996). Sediment texture from the gravity cores collected in Summer 1998 is shown in Table 4.6. Mud % was considered as the sum of the silt and clay content.

Site	Core	Sand%	Silt%	Clay%	Mud%	Colour	Classification	Classification
No.	cm	<4.00ϕ	4.50-9.00ϕ	>9.00ϕ	>4.50ϕ	Munsell	Shepard (1954)	Flemming (2000)
V 20	111	18.8	66.2	15.0	81.2	5Y 3/1	Sandy silt	D-II
V 30	101	15.4	63.0	21.6	84.6	5Y 2.5/1	Clayey silt	D-III
V 40	131	13.4	66.4	20.2	86.6	5Y 5/1	Clayey silt	D-II
V 50	141	4.3	67.9	27.8	95.7	5Y 5/1	Clayey silt	E-III
V 60	101	71.8	21.4	6.8	28.2	5Y 2.5/1	Silty sand	B-II
V 70	61	45.4	45.8	8.8	54.6	5Y 3/2	Silty sand	C-II
V 80	31	15.1	69.5	15.4	84.9	5Y 2.5/1	Clayey silt	D-II

Table 4.6. Mean values (%) of the grain size distribution in the upper 21 cm of the bed. Depth of the core is reported and colours (generally fades from dark gray to black) are from the top (COVELLI & CIAVOLA, 2000).

The colour of sediment has also been reported as it can affect the response of the OBS's (see paragraph 4.2.2.). A ternary diagram of sediment texture classification (Fig 4.11.) shows the sand : silt : clay ratio. The sand fraction increased from the northern (V50) to the southern (V60) sites and decreased with distance from the nearest inlet of the Lagoon (Fig. 4.12.). BARILLARI (1981), MERLIN *et al.* (1978) and BARILLARI (1978) attributed the concentration of coarser sediments close to the inlets to strong tidal currents in these areas.

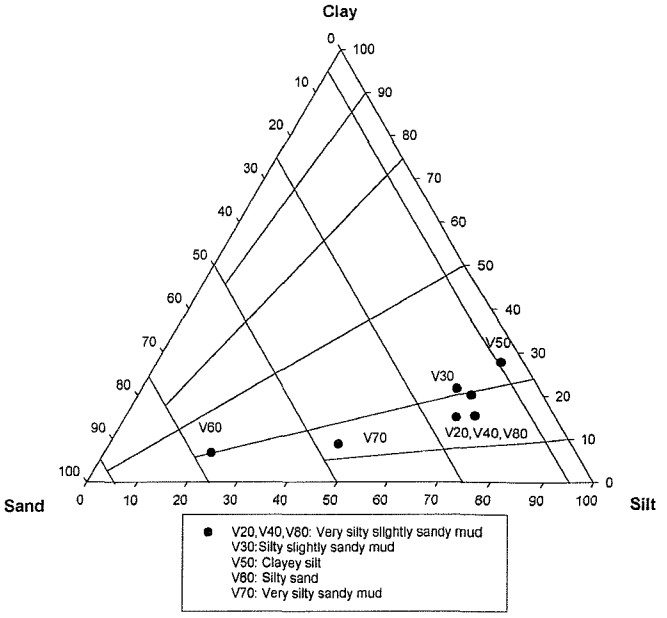

Figure 4.11. Textural classification of surface sediments in Venice Lagoon. Note the increasing sand content moving from the north (V50) to the south (V60).

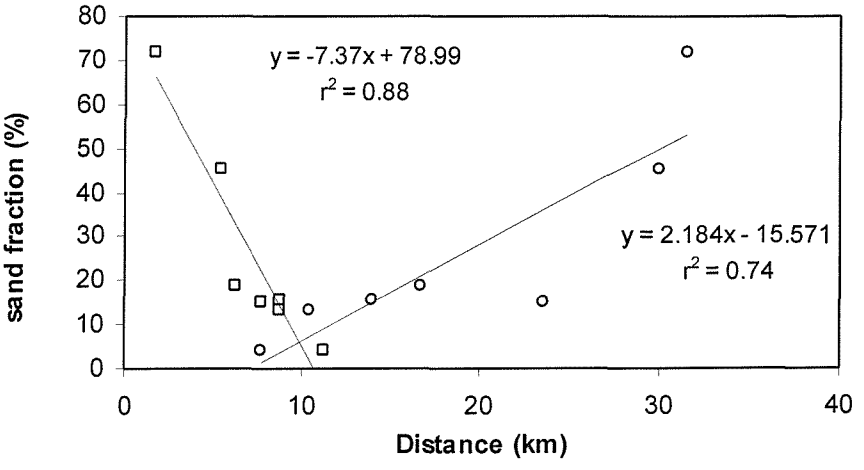

Figure 4.12. Relationships found between the sand content and the distance from the northern part of the Lagoon (○) and from the closest inlet (□) based upon sites investigated during summer campaign of the F-ECTS project.

Physical and biological properties from the syringe cores

Physical and biological properties were determined from samples collected during summer 1998 and winter 1999. Results are reported in Tables 4.7. and 4.8.

Station	Bulk density	Water content	Organic content (LOI)	Chlorophyll a content	Carbohydrate Content
No.	(kg/m^3)	%	%	($\mu gGE/g_{DW}$)	($\mu gGE/g_{DW}$)
V 20	1900	31.7	3.7	24	26
V 21	-	30.7	3.7	25	43
V 22	-	29.9	3.2	-	-
V 30	-	43.5	5.1	-	-
V 31	1850	-	-	-	-
V 32	-	27.8	2.2	43	35
V 40	1750	36.6	2.3	126	130
V 41	1850	29.7	3.8	-	-
V 42	-	31.7	3.9	-	-
V 43	-	-	-	-	-
V 44	-	37.4	4.1		-
V 50	1700	35.7	5	60	86
V 60	1750	25.9	2.7	69	-
V 62	-	25.7	2.8	27	40
V 70	1750	26.1	2.9	19	29
V 80	2000	34.8	3.3	20	38

Table 4.7. A list of the physical and biological parameters determined for each station from samples collected during summer 1998.

Station	Bulk Density	Water Content	Organic content (LOI)	Chlorophyll a Content	Carbohydrate content
No.	(kg/m^3)	%	%	($\mu g/g_{DW}$)	($\mu g/g_{DW}$)
V 20	1800	41.1	1.9	32	58
V 21	-	-	-	-	-
V 30	-	-	-	-	-
V 31	1650	44.5	2.5	69	126
V 40	1700	42.7	2.7	29	91
V 41	-	-	1.1	-	-
V 50	1700	42.4	2.9	37	58
V 51	1850	-	2.3	13	-
V 60	1700	30.7	2.6	10	33
V 61	-	-	-	-	-
V 70	1700	40.4	2.6	5	56
V 71	-	-	-	-	-
V 80	1950	32.5	2.4	10	19

Table 4.8. A list of the physical and biological parameters determined for each station from samples collected during winter 1999.

The biological properties displayed a strong seasonal and spatial variation. A higher content of both chlorophyll *a* and colloidal carbohydrate content existed at stations V40 and V50 (located in the northern part of the Lagoon) during the summer campaign. Very similar values for BD and WC of surficial sediments were found at different sites within Venice Lagoon. There was little seasonal variation in water content between samples. However, lower values (about 7 % less) were found during the summer compared to the winter. As a consequence, sediment during the summer campaign had a higher bulk density (about 2 %).

4.3.4. Comparison between the Mini Flume and Sea Carousel

The Mini Flume and Sea Carousel were deployed simultaneously at each site during F-ECTS campaign (Fig. 4.13.), therefore, sediment properties and environmental conditions responsible for sea bed stability were considered equivalent for both devices during all deployments. Results of the erosion thresholds derived from deployments carried out using MF (in the present study) and SC (by AMOS *et al.*, 2000) are reported in Table 4.9. and Fig. 4.14.

No significant statistical relationships were found between in the erosion threshold values derived from the Sea Carousel and the Mini Flume during the winter and summer campaigns (Fig. 4.15.), although the range in thresholds appears to be very similar. The largest difference between erosion thresholds derived from the Mini Flume and Sea Carousel deployments was found in the intertidal regions (where erosion threshold was much higher than that expected from the literature; Fig. 4.14.). Results between the two devices were particularly different at sites: V31, V40, V41 and V50 (Table 4.9.). In sites V31 and V41 such differences were due probably to technical failure of the Mini Flume, therefore data collected at these sites were not included in Fig. 4.15. At sites V40 and V51 differences in the erosion threshold data were attributed to the patchiness of the biofilm distribution.

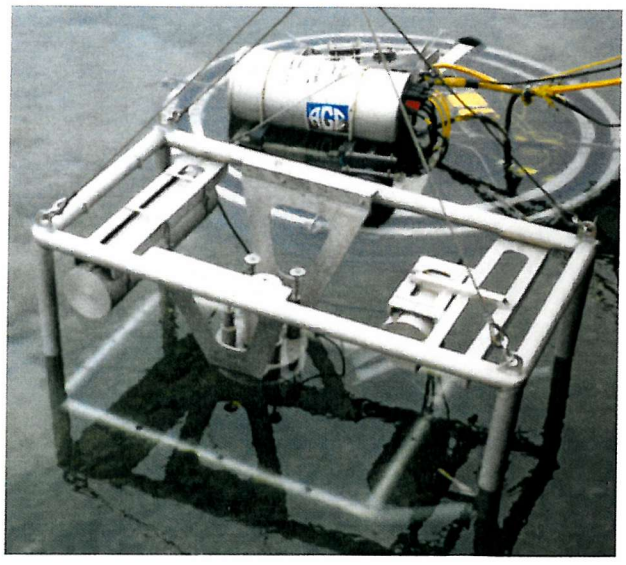

Figure 4.13. The Sea Carousel and the Mini Flume systems in operation.

	Summer 1998		Winter 1999	
Site	Erosion Threshold Mini Flume (Pa)	Erosion Threshold Sea Carousel (Pa)	Erosion Threshold Mini Flume (Pa)	Erosion Threshold Sea Carousel (Pa)
No.				
V 20	0.31	0.35	0.73	1.16
V 21	0.31	0.22	1.12	0.57
V 22	0.43	-	-	-
V 30	0.59	0.80		0.36
V 31	0.23	1.90	0.69	0.75
V 32	0.18	-	No	
V 40	2.36	3.06	1.16	0.73
V 41	0.34	1.51		1.29
V 42	0.31	-	-	-
V 43	0.29	-	-	-
V 44	0.29	-	-	-
V 50		1.42		0.68
V 51	1.98	1.51	0.58	0.62
V 60	0.38	0.36	0.6	0.68
V 62	0.65	-	0.74	-
V 70	0.56	0.59	0.37	1.00
V 80	0.62	0.85	0.7	0.51

Table 4.9. Erosion thresholds derived by the Mini Flume and the Sea Carousel (from AMOS *et al.*, 2000).

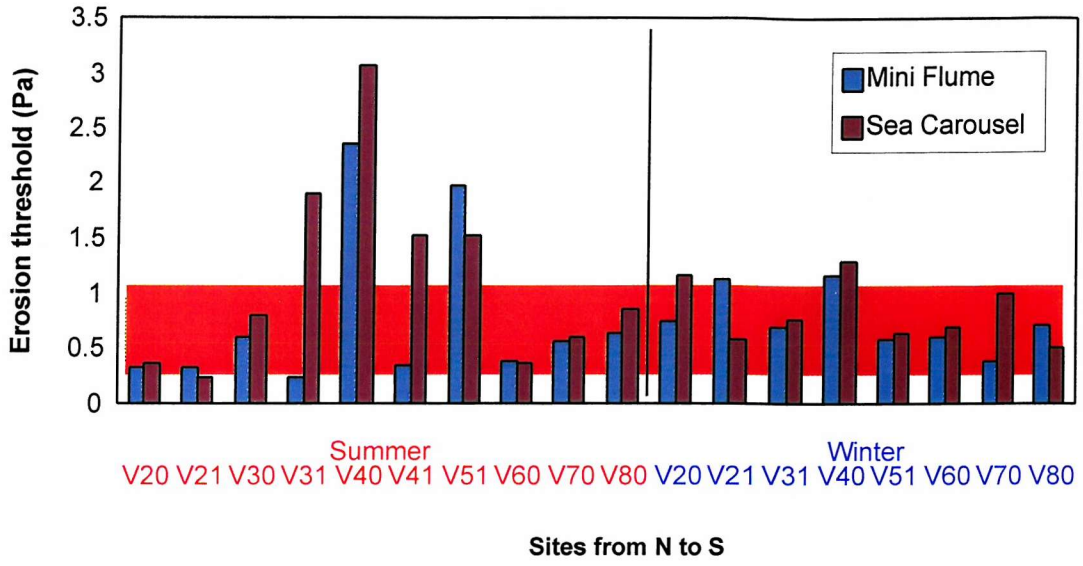

Figure 4.14. A comparison between erosion thresholds determined by Sea Carousel and Mini Flume during the two F-ECTS field campaigns. The red area indicates the critical erosional shear stress predicted by DHI (1991).

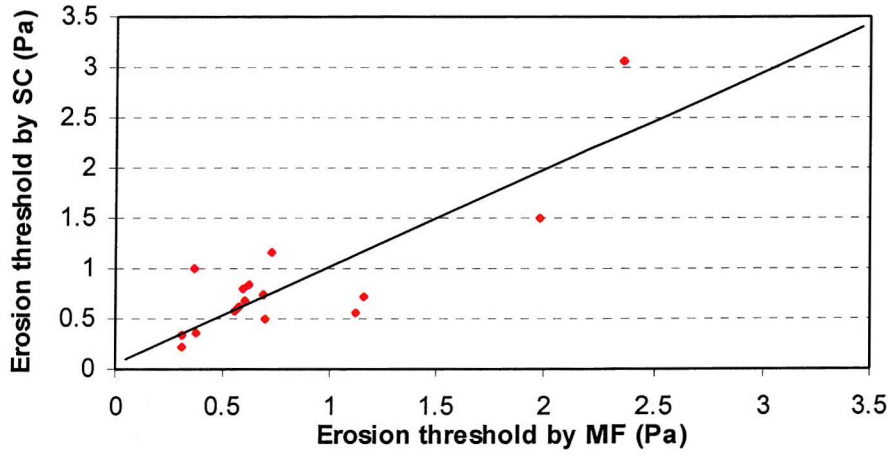

Figure 4.15. Erosion threshold values derived from the Mini Flume (MF) and the Sea Carousel (SC) deployments during the F-ECTS campaigns. Also illustrated is the 1:1 line between the two parameters.

4.3.5. The relationship between erosion threshold and sediment properties in Venice Lagoon

Quantitative relationships between the erosion threshold and sediment properties were derived through a least-squares regression analysis. Results are reported in Table 4.10.

	Summer 1998		Winter 1999	
Parameters (x)	Regression eq (7<n<13)	correlation	Regression eq (7<n<13)	correlation
Elevation	τ_c = -0.79 x + 1.98	r^2 = 0.66 p = 0.02	τ_c = -0.02 x + 0.93	r^2=0.44 p = 0.10
Carbohydrates	τ_c = 0.02 x + 0.02	r^2 = 0.83 p = 0.002	τ_c = 0.00 x + 0.0.54	r^2 = 0.12 p = 0.44
Chlorophyll *a*	τ_c = 0.01 x + 0.16	r^2 = 0.87 p = 0.02	τ_c = -0.01 x + 0.57	r^2 = 0.16 p = 0.43
Bulk density	τ_c = -0.00 x + 7.17	r^2 = 0.43 p = 0.27	τ_c = -0.00 x + 1.75	r^2 = 0.067 p = 0.57
Water Content	τ_c = 0.01 x + 0.17	r^2 = 0.02 p = 0.66	τ_c = 0.01 x + 0.09	r^2 = 0.05 p = 0.64
LOI	τ_c = 0.01 x + 0.61	r^2 = 0.00 p = 0.94	τ_c = 0.27 x + 0.68	r^2 = 0.02 p = 0.85

Table 4.10. Regression equations of erosion threshold (τ_c) on sediment properties in Venice Lagoon during Summer 1998 and Winter 1999. Highlighted cells indicate significant relationships ($p<0.05$).

4.4. Discussion

Wet bulk density values are relatively high compared with other intertidal regions e.g. the Fraser Delta, Canada (AMOS *et al.*, 1997) or with sediments used in laboratory tests (OCKENDEN & DELO, 1991). The reason for the high wet bulk density of surface sediments can be attributed to the fact that there is a constant loss of sediment from the Lagoon to the sea. This exposes the underlying consolidated material to the effect of currents and wave motion. This process may also explain the higher erosion thresholds derived during the winter campaign in subtidal regions characterised by stations V20, V21 and V31.

In summer 1998, the highest chlorophyll *a* and colloidal carbohydrate contents occurred at stations V40 and V50 (the only two intertidal sites investigated). During this period, the correlation between the critical shear stress and colloidal carbohydrate content was statistically significant (r^2=0.83; p=0.002) (Fig. 4.16.A).

The best correlation (r^2=0.87; p=0.02) was found between the erosion threshold and chlorophyll *a* (Fig. 4.16.B). In addition, a significant (r^2=0.67; p=0.02) negative linear relationship existed between the erosion threshold and the elevation of the stations where the Mini Flume deployments were carried out (Fig. 4.16.C).

In contrast, during the winter 1999 F-ECTS campaign, no significant relationships between biological parameters and sediment stability were found (Table 4.10.). Results suggest that a feed-back mechanism, mediated by microphytobentos influences, causes biostabilisation of sediments and thus may explain the exceptional preservation of the intertidal mudflats in the northern part of the Lagoon. Such a mechanism can be summarised in three different steps (which are illustrated in Fig. 4.17.).

STEP A) Subtidal areas, which are colonised by sea grass, are better protected against erosion. The ability of vegetation to reduce the applied bed shear stress may enhance deposition. STEP B) Through time, vertical accretion can occur; bottom sediments are elevated from a subtidal to an intertidal environment. STEP C) Micro-organisms which are more abundant in intertidal environments start to colonise the substrata producing EPS (particularly during summer and intertidal exposure) and increasing the erosion threshold.

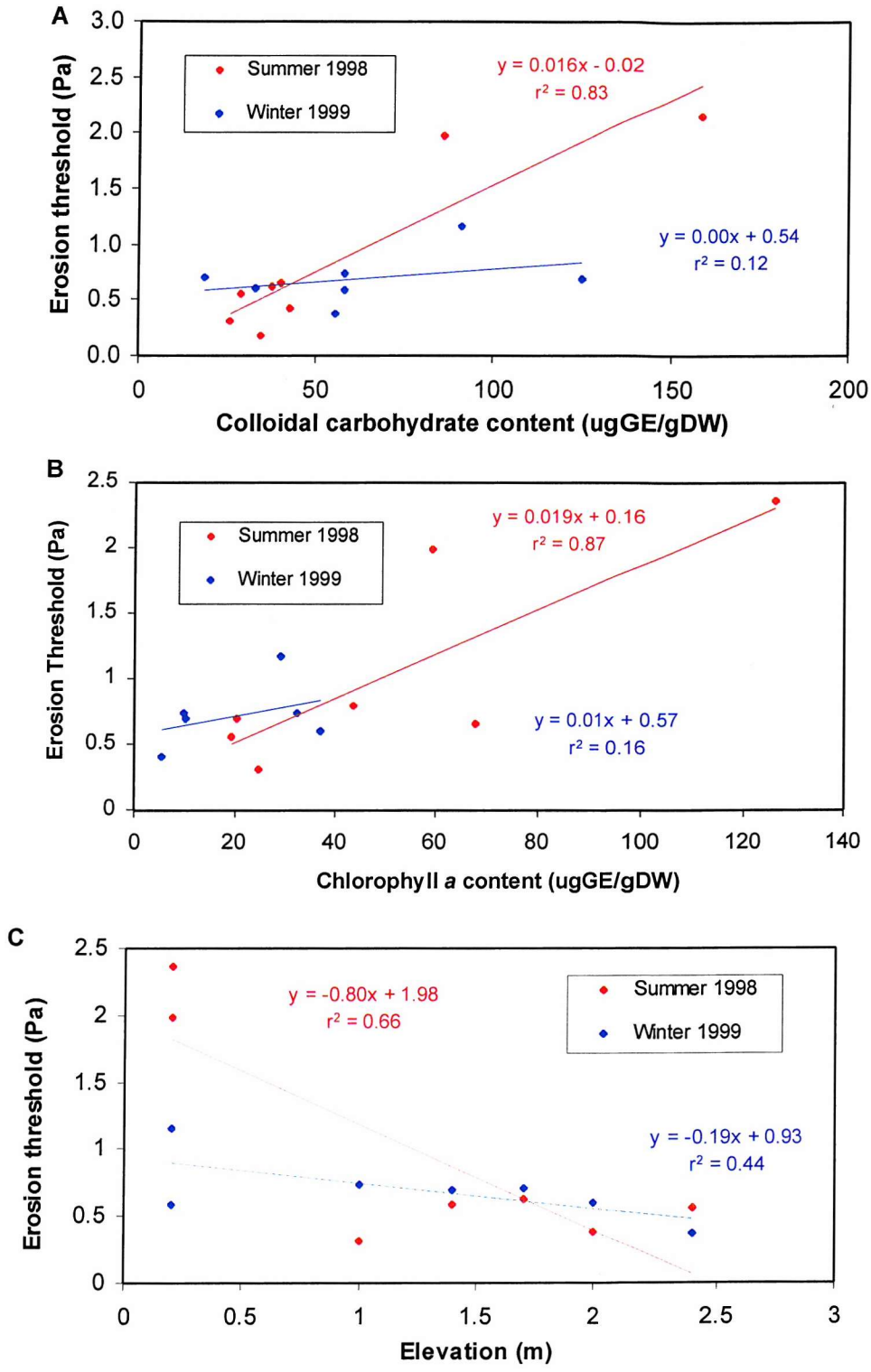

Figure 4.16. Quantitative relationships between erosion threshold (derived by MF) and colloidal carbohydrate (A), chlorophyll *a* (B) and elevation (C) at sites investigated during the F-ECTS campaigns. Note that significant relationships were found during the summer campaign (red line) due to the increase in biological activity of the two intertidal areas: V40 and V50.

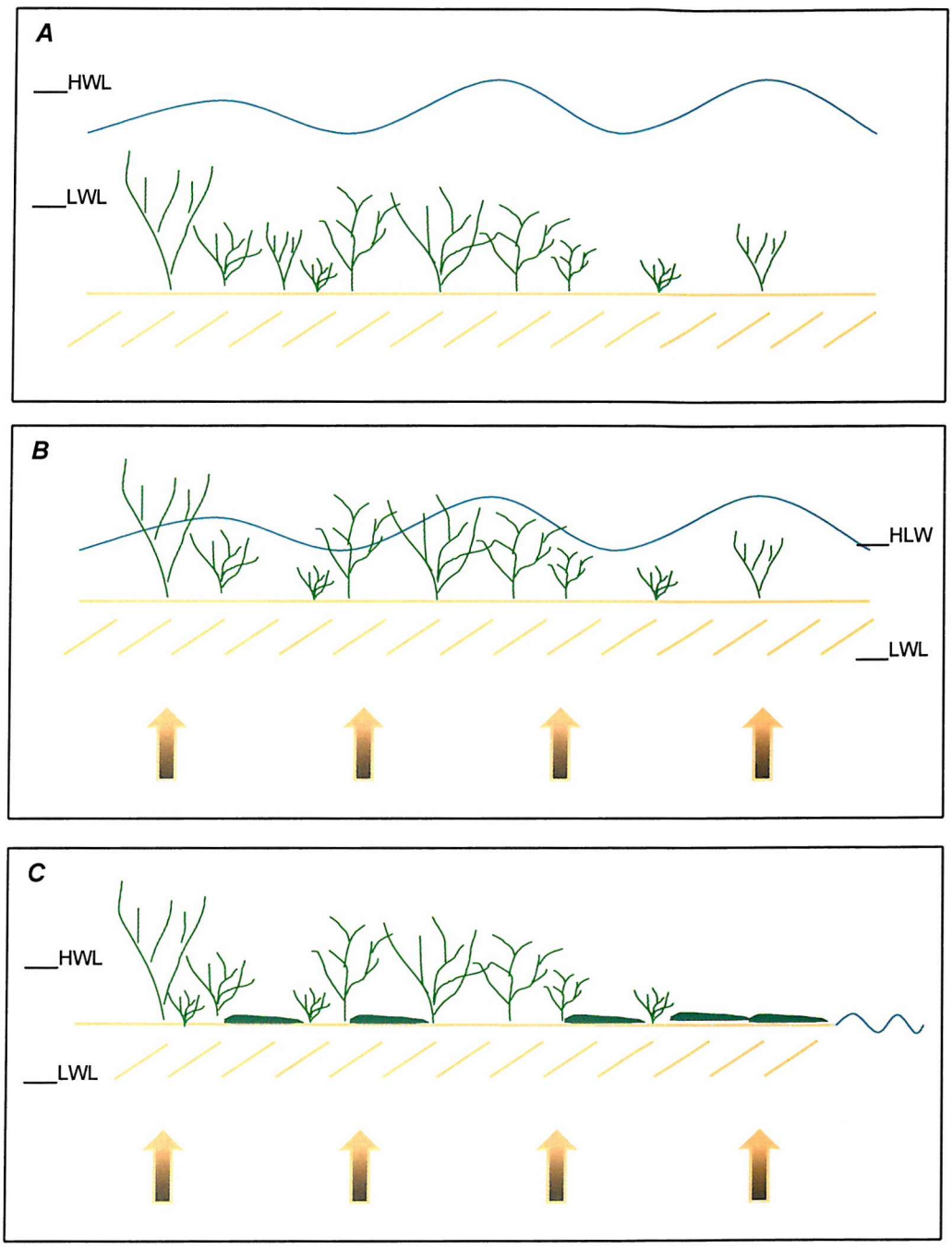

Figure 4.17. A positive feed-back mechanism illustrated in three steps: A) The subtidal area is vegetated by seagrass which enhances accretion; B) the area accretes to the intertidal level; and C) during tidal exposure a biofilm is produced by micro-organisms which stabilise surface sediment.

4.5. Summary

A brief summary of this chapter is reported as follows:

- The greatest stability was found in the northern part of the Lagoon (where sediments have a higher clay fraction), the least stability was found in the central and southern regions where sediments are dominated by fine sand.

- A strong seasonal fluctuation in stability was found in the northern intertidal areas of the Lagoon. The northern part of the Lagoon was dominated by well-preserved intertidal flats where biological activity increased during the summer (and which exhibit the highest erosion threshold).

- No significant variation in physical or biological activity was detected in the subtidal regions between the summer and the winter campaigns.

- Chlorophyll *a*, carbohydrate content and elevation were good predictors of erosion threshold derived during the summer, but physical properties such as bulk density or water content played a secondary role in sediment stability.

- Mini Flume and Sea Carousel deployments indicated a critical shear stress of erosion higher than 1 Pa in the northern Lagoon, showing that previous work under-estimated sediment stability in Venice Lagoon (Fig. 3.4.).

- A significant agreement in results of the erosion threshold values obtained from deployments of Mini Flume and the Sea Carousel was found. In some cases the difference in the erosion threshold derived from the two devices (for example at sites V40 and V50 during the summer campaign) was probably due to the natural spatial heterogeneity of the biofilm in the intertidal areas.

- During both field campaigns, the maximum value of turbidity was found after two (site V30) and three (site V44) windy days, underlying the primary importance of wave resuspension. Sediments resuspended in this way are early disperses within the Lagoon before exporting it to the sea.

- Salinity is very high (~35 S) throughout the Lagoon except in site V30 (~20 S) which is close to the Dese river mouth, in the northern part of the Lagoon.

CHAPTER 5: SEDIMENT STABILITY OF PALUDE DELLA CENTREGA

5.1. Introduction

The sediment stability of *Palude della Centrega* intertidal mudflat was investigated by (1) repeat field campaigns and (2) by simulations in the laboratory version of the Mini Flume. The mudflat is close to V40 of the F-ECTS campaigns, and is located in the northern part of Venice Lagoon near the villages of *Burano* and *Torcello* (Fig. 5.1.).

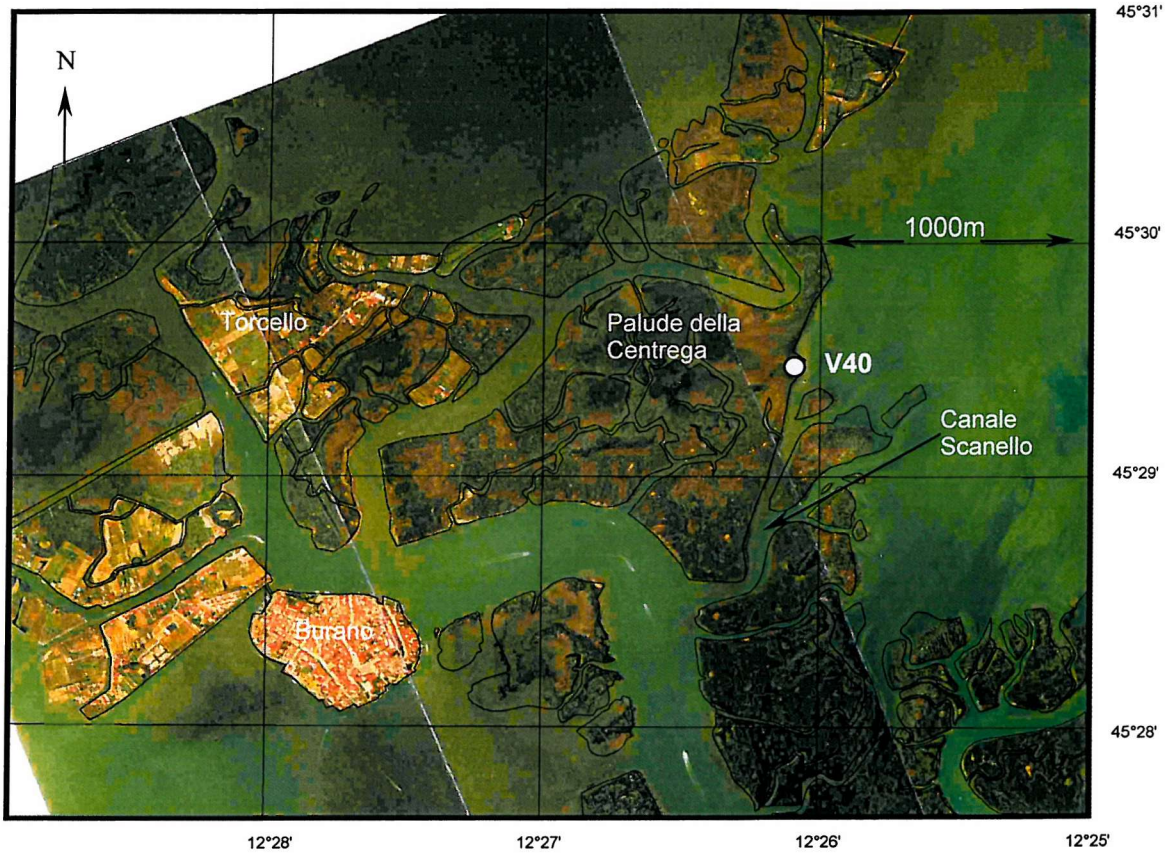

Figure 5.1. A composite photo aero-photograph of *Palude della Centrega* taken in August 1998. Note that station V40 (white dot) is located at the edge of *Canale Scanello* (courtesy of HR Wallingford).

Station V40 is to the west of *Canale Scanello* and its position (45°29.67 N; 12°26.18 E; ± 50m) was considered representative of the studied area. On *Palude della Centrega,* two sets of 7 stations were placed at 25 m intervals in order to monitor bed level elevation, sediment stability and properties of the surface sediments. The stations were located along two perpendicular transects (orientated

in N-S and E-W directions) in order to obtain representative samples of different habitat areas dominated by *Spartina* spp., *Zostera* spp. and micro-organisms (Fig. 5.2.). Station positions and habitat distribution were mapped during a topographic survey. No bedforms were present in *Palude della Centrega*. The study area was drained by a tidal creek, the presence of which may have influenced the sediment stability results obtained. This is discussed in section (5.5.).

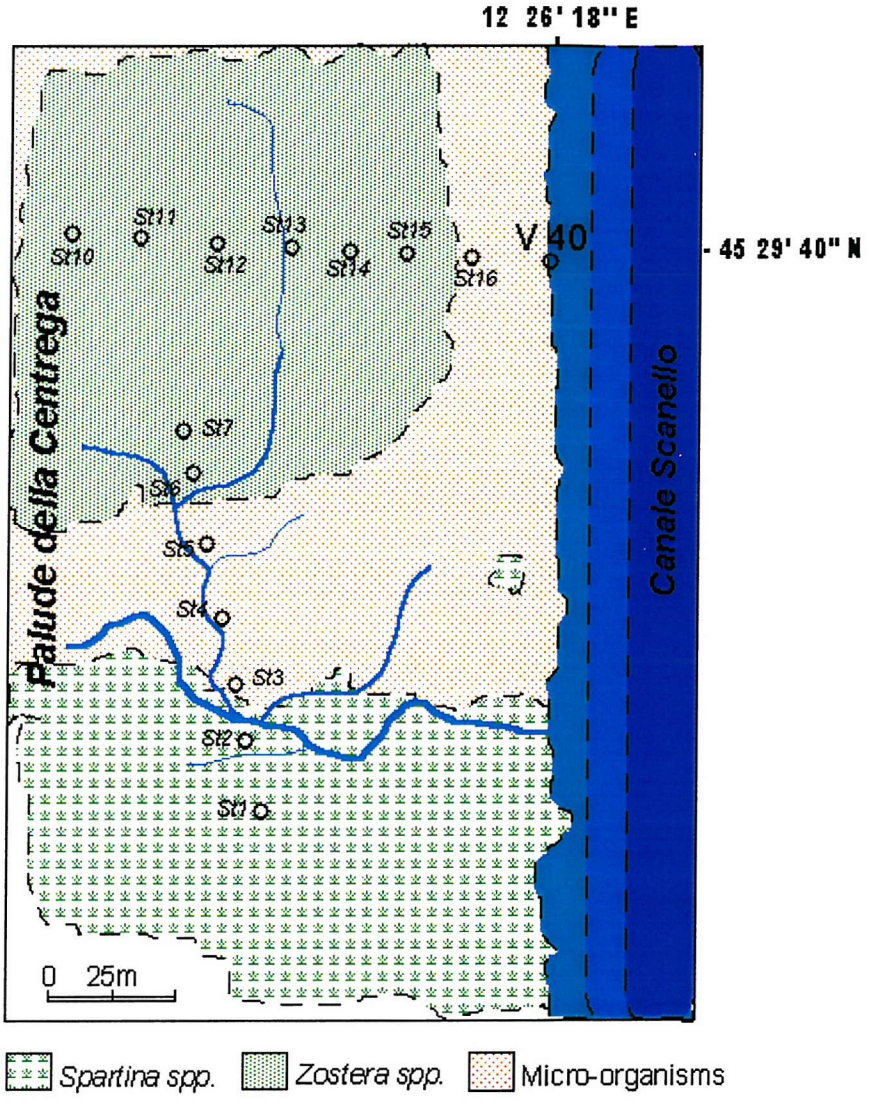

Figure 5.2. A schematic diagram showing the location of sampling stations St1 - St16 on *Palude della Centrega* and the habitat distribution during August 1998. *Canale Scanello* is not to scale as bathymetric data were not collected; the darkest blue colour indicates deeper water (~3 m).

Spatial and temporal variations in sediment stability in the study region were monitored in August 1998, February 1999 and November 1999. Two erosion

devices were used: the Tor Vane Shear Meter (TSM) and the Cohesive Strength Meter (CSM; www.sediment.co.uk).

A summary of the work carried out is illustrated in Table 5.1.

	In-situ			*Laboratory*	
Month Year	***August 1998***	***February 1999***	*November 1999*	***Autumn 1998***	***Autumn 1999***
Device used to investigate sediment stability	*TSM (14 sites)*	*TSM (14 sites)*	*CSM (in 9 sites)*	-	-
Sediment properties determined	*D_{50}, BD, WC, LOI, Chl a, Carbo (14 sites)*	*D_{50}, BD, WC, LOI, Chl a, Carbo (14 sites)*	*D_{50}, BD, WC, LOI, Chl a, Carbo (9 sites)*	-	-
Bulk density profile	*Using CT scanner technique (4 sites)*	*Using CT scanner technique (4 sites)*	-	-	-
Statistical analysis	*X*	*X*	*X*		
Study of the consolidation effect on τ_c	-	-	-	*X*	-
Comparison of CSM and MF	-	-	-	-	*X*

Table 5.1. *In-situ* and laboratory investigations carried out in the present study. Laboratory investigations were undertaken to quantify the effect of consolidation on τ_c and to compare the results obtained using two different devices to determine τ_c.

In-situ monitoring of τ_c was undertaken to determine: temporal and spatial changes in sediment stability at each station on *Palude della Centrega*; and to test whether: (1) spatial changes in sediment stability are related to elevation, plant cover and proximity to the tidal channel; and (2) if any sediment properties (physical or biological) could be used as a proxy to predict the erosion threshold.

Vane Shear Strength (VSS) was measured during the two field campaigns. This instrument allowed comparison with other sedimentological (O'BRIEN, 1998) and ecological studies (MEADOWS & TAIT, 1989; MUSKANANFOLA, 1994). *In-situ* measurements with the TSM were made at each of the 14 stations along the two

transects (Fig. 5.2.). The Mini Flume and Sea Carousel were deployed at station V40, near the edge of *Canale Scanello*, as part of the F-ECTS field campaign.
In November 1999, the stability of the surface sediment was investigated using the CSM at 9 of the 14 stations located along the two transects in order to determine spatial variability. In this instance the CSM was selected to derive τ_c, whilst VSS, derived using TSM, is more representative of the strength of the surface sediments. Physical and biological sediment properties were determined for each station based on surface samples collected during deployments (see Appendix I). In addition, 60-ml syringe cores were collected at four of the stations (two for each transect) for bulk density profiling of the top 10 cm of the sediment column. Finally, statistical analysis of all sediment parameters was performed to examine which parameters could be used as a proxy for sediment stability. A comparative laboratory study was carried out to quantify differences in τ_c derived using the CSM and the Mini Flume.

5.2 Methodology

5.2.1. Topographic surveying

Absolute elevation of the mud flat was measured during topographic surveys along the two transects. A total station GEODIMETER 422 L.R. (accuracy ±1 mm) was placed on *Burano* Island (~1.5 km from the mudflat). Data (x.y.z.) were processed using AutoCAD "12" software. As the mudflat elevation is fundamental to the calculation of the inundation time, the absolute elevation was derived by considering the influence of tide propagation through Venice Lagoon on tidal range (WHITHAM, 1974). A correction to the elevation data collected in *Palude della Centrega* was applied, reducing the water elevation measured during the survey by 11 cm with respect to the water level at *Lido* inlet (Fig. 5.3.). GOTTARDO & CAVAZZONI (1981) have defined the time of propagation of the tide into Venice Lagoon using empirical equations (Fig. 5.3.).

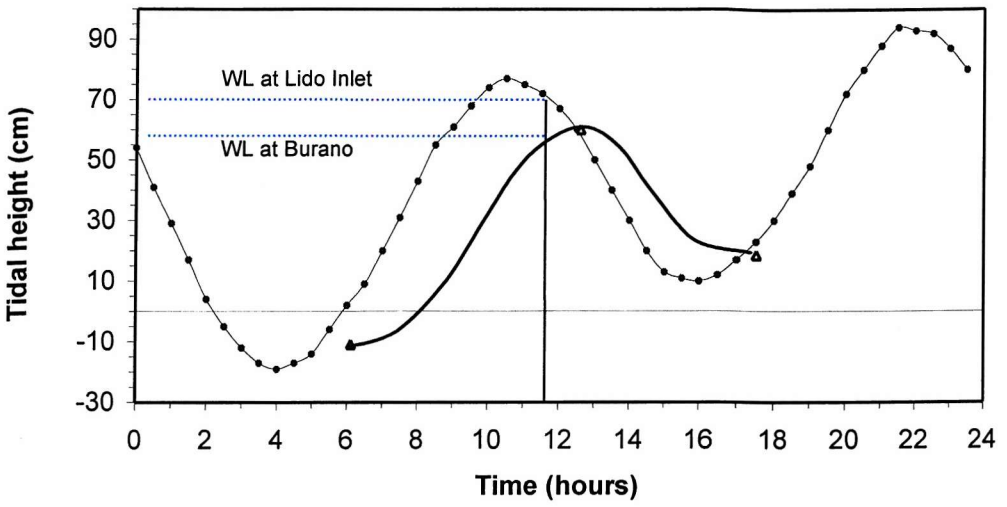

Figure 5.3. Water level (WL) recorded at *Lido* inlet on 22 August 1998 and predicted for *Burano* after GOTTARDO & CAVAZZONI (1981). The two lines clearly show the phase lag of the tidal curve between the studied area (close to the village of *Burano*) and the main inlet of the Lagoon. A reduction of about 11 cm was applied at the time of the topographic survey (11:50 a.m.) with respect to sea level measured at the *Lido* Inlet.

5.2.2. Sediment strength using the Tor Vane Shear Meter (TSM)

In-situ measurements of sediment strength were determined using the TSM. The TSM is a portable device composed of a small shaft with four vanes at the end of a torsion spring that records the force necessary to rotate the shaft (Fig. 5.4.). The Vane is pushed into the sediment and the head is rotated at constant radial speed of about 6 degree/min (~0.1 degree/s). The calibrated spring defines the strength of the sediment at the shear point (τ_v) which is expressed in kPa. The operation of the TSM is based on the concept that resistance of cohesive soils to erosion can be determined by the unconfined compressive strength of saturated undisturbed sediments (SEROTA & JAGLE, 1972).

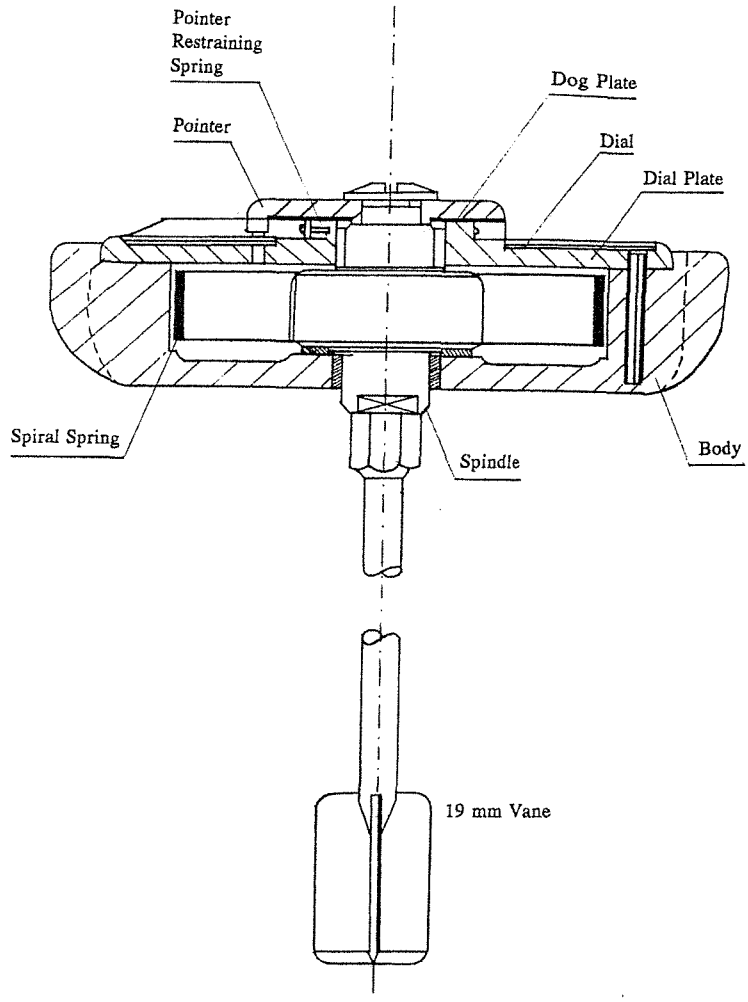

Figure 5.4. Principal components of the Tor Vane Shear apparatus (from SEROTA & JAGLE, 1972).

The *in-situ* measurements of τ_v were used for the first time to predict τ_c by DUNN (1959). The author correlated a series of underwater vane shear tests with current meter measurements within a tidal channel from which bed shear stress values were calculated. MUSKANANFOLA (1994) used a linear relation between shear stress and strength found by DUNN (1959) to derive sediment stability on an intertidal sandy mudflat in Solent Breezes, Southampton Water, UK. A second relationship was derived from the data collected by AMOS *et al.* (1996b) on the basis of a study carried out in Hudson Bay (Canada) on subarctic fine-grained estuarine sediment (using the Sea Carousel). In the latter case a different linear relationship was found between τ_v and τ_c.

These relations (Fig. 5.5.) can be used to convert τ_v into τ_c and are reported as follows:

DUNN (1959)	$\tau_c = 1.6 \times 10^{-4} \tau_v + 2.23$	Pa	5.2.1.I
AMOS *et al.* (1996b)	$\tau_c = 3 \times 10^{-4} \tau_v - 0.4$	Pa	5.2.1.II

where τ_v is in kPa.

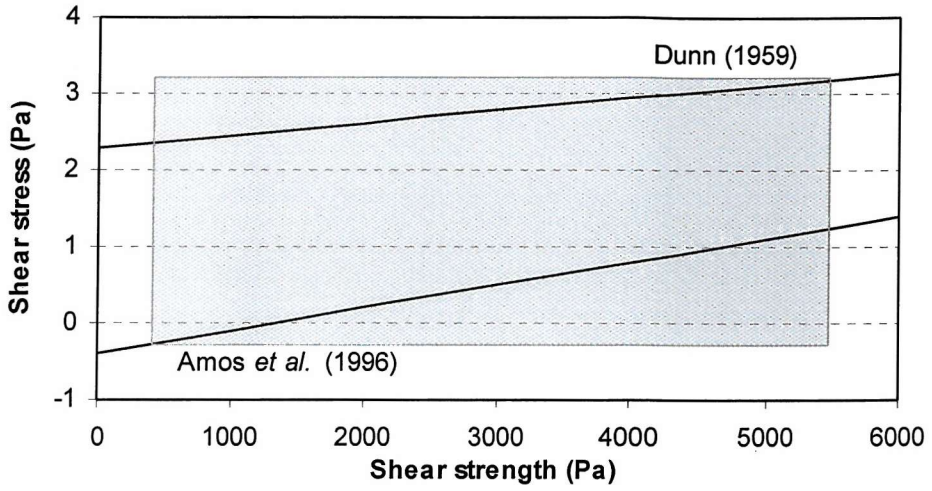

Figure 5.5. The relationships between shear stress and shear strength derived from DUNN (1959) and from data published by AMOS *et al.* (1996b). The grey area shows the approximate range of shear strength values found in *Palude della Centrega*.

Due to the different nature of τ_c and τ_v derived using the TSM and CSM, Tor Vane measurements in the present study were not converted into τ_c and results are reported in kPa.

5.2.3. Sediment stability using the Cohesive Strength Meter (CSM)

The CSM has been used extensively in several multi-disciplinary intertidal flat studies (e.g. CLIMEROD, INTRMUD, BIOPTIS, LISP-UK; see TOLHURST *et al.*, 1999).

The CSM is an *in-situ* erosion device (Fig. 5.6.), which uses the stress induced by a vertical jet of water (Fig. 5.7.) fired at the sediment surface in short-duration pulses to cause erosion (PATERSON, 1989; TOLHURST *et al.*, 1999). The use of a vertical jet in erosion devices was introduced by DUNN (1959), and subsequently adopted by MOORE & MASCH (1962) and SUTHERLAND (1967). A series of pre-programmed tests control the pressure of the water jet in the CSM erosion chamber, which has been

Figure 5.6. The CSM Mk4 onsite (Image provided by Ian Black).

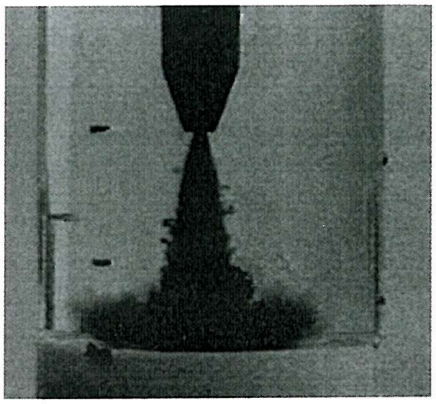

Figure 5.7. Laboratory image of the vertical jet flow structure (TOLHURST *et al.*, 1999).

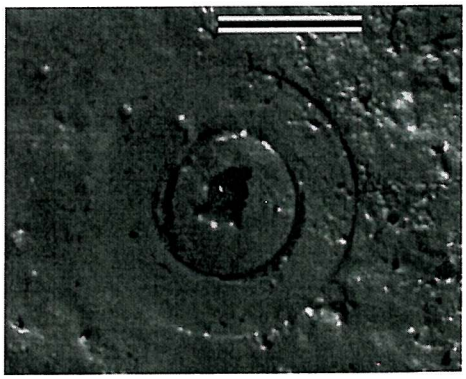

Figure 5.8. The CSM footprint after deployment (bar length is 3 cm). The scour pit provides visual confirmation that erosion has occurred (TOLHURST *et al.*, 1999).

calibrated accurately to derive the appropriate bed shear stress at each incremental step (TOLHURST *et al.,* 1999).

The CSM test chamber consists of two concentric plastic cylinders. At the beginning of each test, the internal chamber is filled gently with ambient sea water (using an appropriate fill tube) and light transmission is recorded. A reduction in light transmission (%) indicates resuspension of sediment in the chamber. The CSM jet usually, but not necessarily, leaves a scour pit in the surface sediment (Fig 5.8.). The scour pit is often smaller than the entire foot print area, indicating an irregular distribution of shear stress in the CSM chamber (greatest under the jet).

The jet pressure values of the CSM (kPa) were calibrated by (TOLHURST *at al.*, 1999) against the onset of the suspension of sand predicted by the equation of BAGNOLD (1966), and modified subsequently by MCCAVE (1971):

$$\theta \geq \frac{CW_s^{\,2}}{gD_{50}} \qquad 5.2.3.\text{I.}$$

where θ is the Shields parameter for the suspension of sand grains, C is a constant (0.19), W_s is the settling velocity, g is the acceleration due to gravity, and D_{50} is the median grain diameter. Sand settling velocity was calculated using the relation of GIBBS *et al.* (1971) modified by BABA & KOMAR (1981):

$$W_m = 0.977\, W_s^{0.913} \qquad \text{m/s} \qquad 5.2.3.\text{II}$$

where W_m is the measured settling velocity of natural quartz sand grains and W_s is the settling velocity of a quartz sphere. The equivalent horizontal bed shear stress was derived from θ using the equation:

$$\tau_o = \theta\,(\rho_s\text{-}\rho)\, g\, D_{50} \qquad \text{Pa} \qquad 5.2.3.\text{III}$$

The best-fit empirical equation between the threshold jet pressures for resuspension and the horizontal bed shear stress, derived by TOLHURST *et al.* (1999) is:

$$\tau_o = [67*(1-e^{(-x/310)})]+[(-195)*(1-e^{(-x/1623)})] \quad \text{Pa} \quad 5.2.3.\text{IV}.$$

where x is the eroding pressure (kPa) of the water jet.

Equation 5.2.3.IV permits conversion of the eroding pressure to U_*, using the relationship :

$$U_* = \sqrt{\frac{\tau_o}{\rho}} \quad \text{m/s}$$

The CSM chamber houses two opposed infrared diodes mounted 1 cm above the sediment-water interface. Light is transmitted at frequencies of about 940 nm.
When the jet pressure is high enough to cause particle resuspension, a drop in light transmission is recorded. A typical example of how the erosion threshold is calculated using the CSM is reported in Fig. 5.9.
TOLHURST *et al.* (1999) defined the erosion threshold as the equivalent horizontal shear stress at the first pressure increment below the 90% transmission value. However, visual inspection of the erosion profile for a particular set of tests may require the erosion threshold to be determined at different light transmissions (TOLHURST, *pers comm.*). In the present study, for example, a light transmission value of 80% was used to identify the erosion threshold due to the immediate drop in light transmission found in the majority of the tests (Fig. 5.9.).

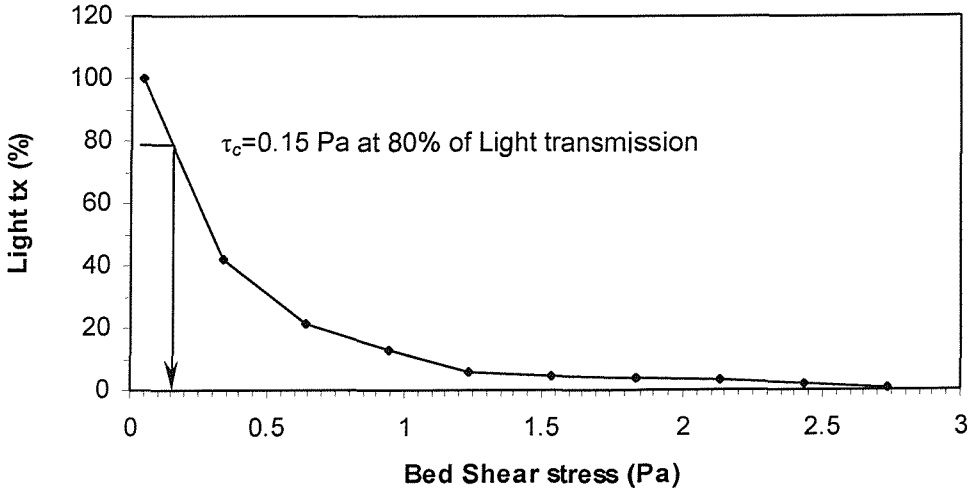

Figure 5.9. Erosion threshold (τ_c) derived at 80 % light transmission using the CSM at St5.

In the present study the CSM light sensor was calibrated in order to quantify the erosion rates resulting from different jet pulses. Calibration of the light sensor involved evaluation of: (1) sensitivity with respect to different levels of SSC; and (2) the maximum value of SSC detected by the CSM using sediment from *Palude della Centrega*.

During calibration, the jet pipe was removed from the chamber in order to maintain a constant volume of water (Fig. 5.10.). The chamber was filled with water and placed on a magnetic stirrer in order to ensure continual particle resuspension. Sediment from station V40 was diluted in 10 ml of water and added at regular time steps through a fill tube into the chamber until the sensor became saturated (0 % light transmission). Fig. 5.11. shows that the light sensor has an extremely stable signal (constant output through time) and was very sensitive to small variations of SSC in the water. The light sensor is capable of detecting turbidity for a maximum of 2 g/l (Fig 5.12.). The following quadratic relationship was found between light transmission and SSC:

$$SSC = 0.18\ tx^2 - 35.99\ tx + 1880 \qquad mg/l \qquad 5.2.3.v$$

where tx is the light transmission (%).

After calibration of the light sensor a time series of bed shear stress and SSC were measured in order to obtain a comparative data set with results of the Mini Flume. An example is illustrated in Fig. 5.13., where the bed shear stress and SSC are plotted as a time series from which erosion threshold is derived, suggesting a possible new method to derive the critical shear stress for resuspension. The time series of the erosion rate has also been derived. This shows that the erosion rate measured after the jet pulse is directly proportional to the applied bed shear stress.

Figure 5.10. The CSM in the laboratory during calibration of light sensors.

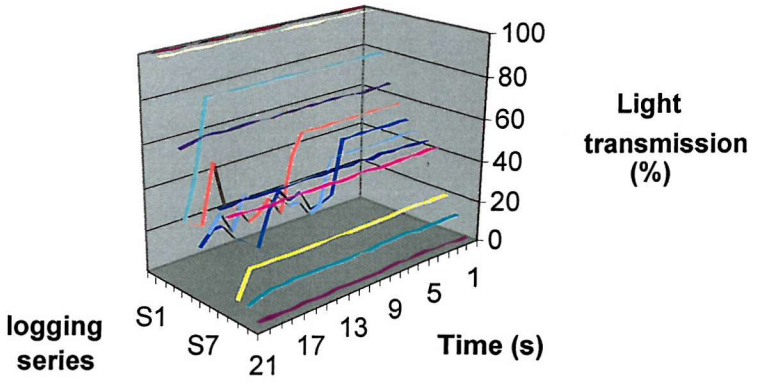

Figure 5.11. Light transmission during the CSM calibration (each coloured line represents % of light transmitted at each increment of turbidity). A drop in light transmission in some of the time series was due to the magnet lifting within the chamber and subsequent obstruction of the transmissometer light beam.

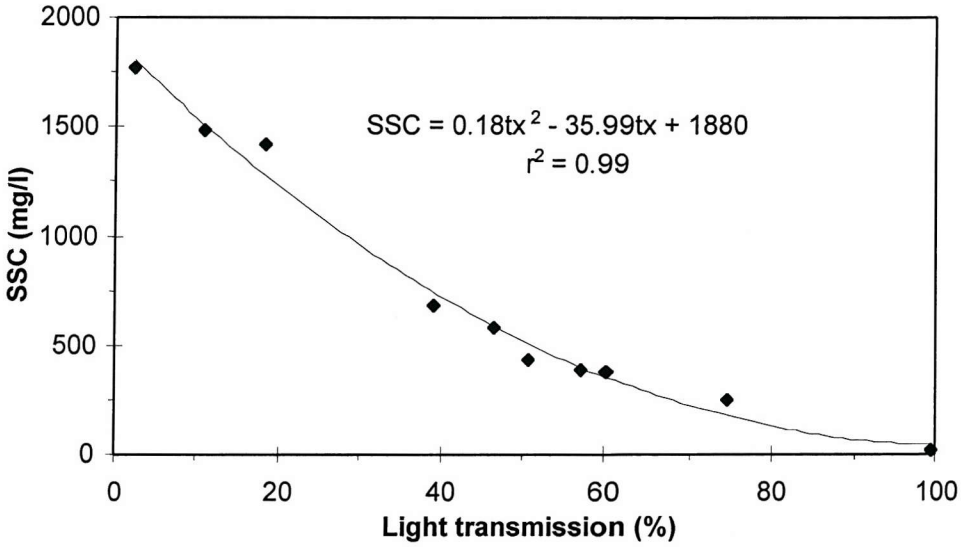

Figure 5.12. The quadratic relationship between light transmission (%) and turbidity (mg/l) for sediments collected in the studied area.

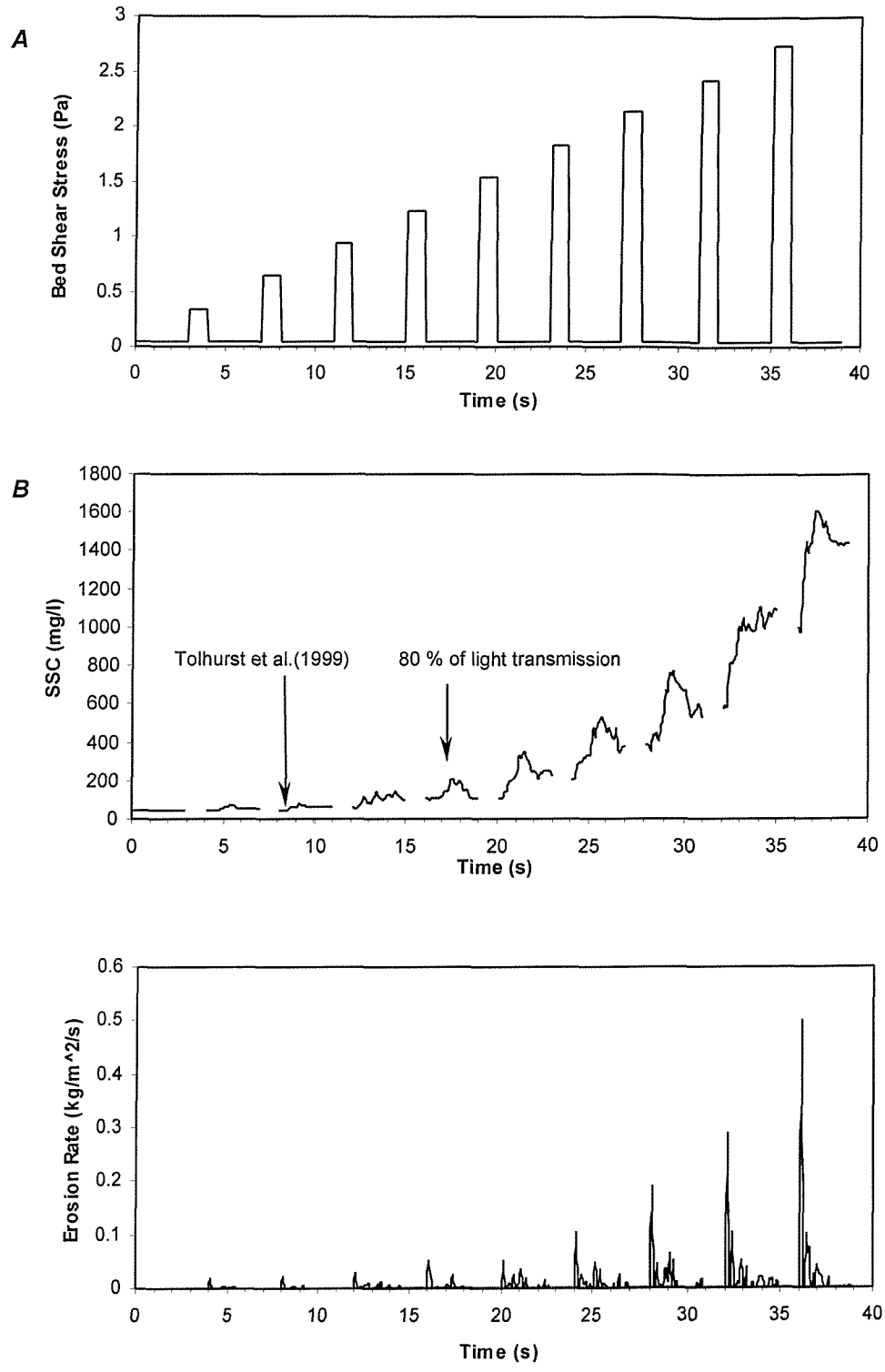

Figure 5.13. A typical time series of bed shear stress (*A*), SSC (*B*) and erosion rate (*C*) from a CSM test. (data from St1). Note peak erosion rate, measured immediately after the jet pulse is directly proportional to applied shear stress, and is followed by settling in the chamber.

5.2.4. Sampling strategy

Surface scrape sediment samples were collected at each station during all three field campaigns to determine water content, bulk density, organic content, sand/mud ratio, chlorophyll *a* content and colloidal carbohydrate content. The methodology used for sampling operations and analysis is the same as that described in Chapter 4 and reported in Appendix I.

At four stations (St1, St6, St12, St15) syringe cores were collected in Summer 1998 and Winter 1999 for bulk density profiling of the top 10 cm of the sediment column. Syringe cores were frozen in liquid nitrogen after sampling, and stored in a freezer at -25 °C until analysis using a CT scanner. Bulk density values were obtained following the method of AMOS *et al.* (1996a) (see Appendix I). The advantage of the CT technique is that very high resolution profiles of bulk density values are obtained at the mm scale.

5.2.5. A comparison between the CSM and Mini Flume

As there is no unique method to derive erosion threshold, a comparison of critical shear stress values is essential when τ_c is derived using different methodologies and different erosion devices (BLACK & PATERSON, 1996). TOLHURST *et al.* (2000) compared the CSM with three other devices (Microcosm, SedErode and ISEF) using the results of a large number of *in-situ* deployments carried out during the INTRMUD project.

In the present study an innovative approach was used to compare shear stress values of the CSM and the Mini Flume, because of the many differences between the two devices (see Table 5.2.), as well as the spatial variation of sediment stability discussed in Chapter 4. A comparison between the CSM and the Mini Flume was carried out in a laboratory study using sediment collected in *Palude della Centrega* and the laboratory version of the Mini Flume (SUTHERLAND, 1996).

Instrument	Mini Flume	CSM
Type	*Annular*	*Jet*
Foot print area (m^2)	*0.036*	*0.0007*
Water volume (l)	*7.5*	*0.021*
Shear stress steps (Pa)	*~0.1*	*0.32*
Time step (min)	*10*	*0.05*

Erosion threshold (Pa)	*Yes*	*Yes*
Erosion rate ((kg/m²/s)	*Yes*	*Yes*
Deposition threshold (Pa)	*Yes*	*No*
Deposition rate ((kg/m²/s)	*Yes*	*No*

Table 5.2. Principal instrument characteristics of the Mini Flume and CSM, and parameters which can be derived.

An homogeneous layer of clay was flattened onto a smooth surface and the external wall of the Mini Flume was gently pushed into it (THOMPSON & AMOS, in press). This was then gently filled with filtered sea water and sediments from V40 were mixed with the water and left to deposit over the clay. The internal wall of the Mini Flume was then pushed into the clay to form the annular flume, which was 4.5 cm wide. After measurements, the CSM was deployed on the undisturbed sediments left in the internal part of the Mini Flume. Three CSM replicate tests were performed. Schematic representations of the operational steps and an illustration of the two erosion devices are shown (Fig. 5.14. and Fig. 5.15.).

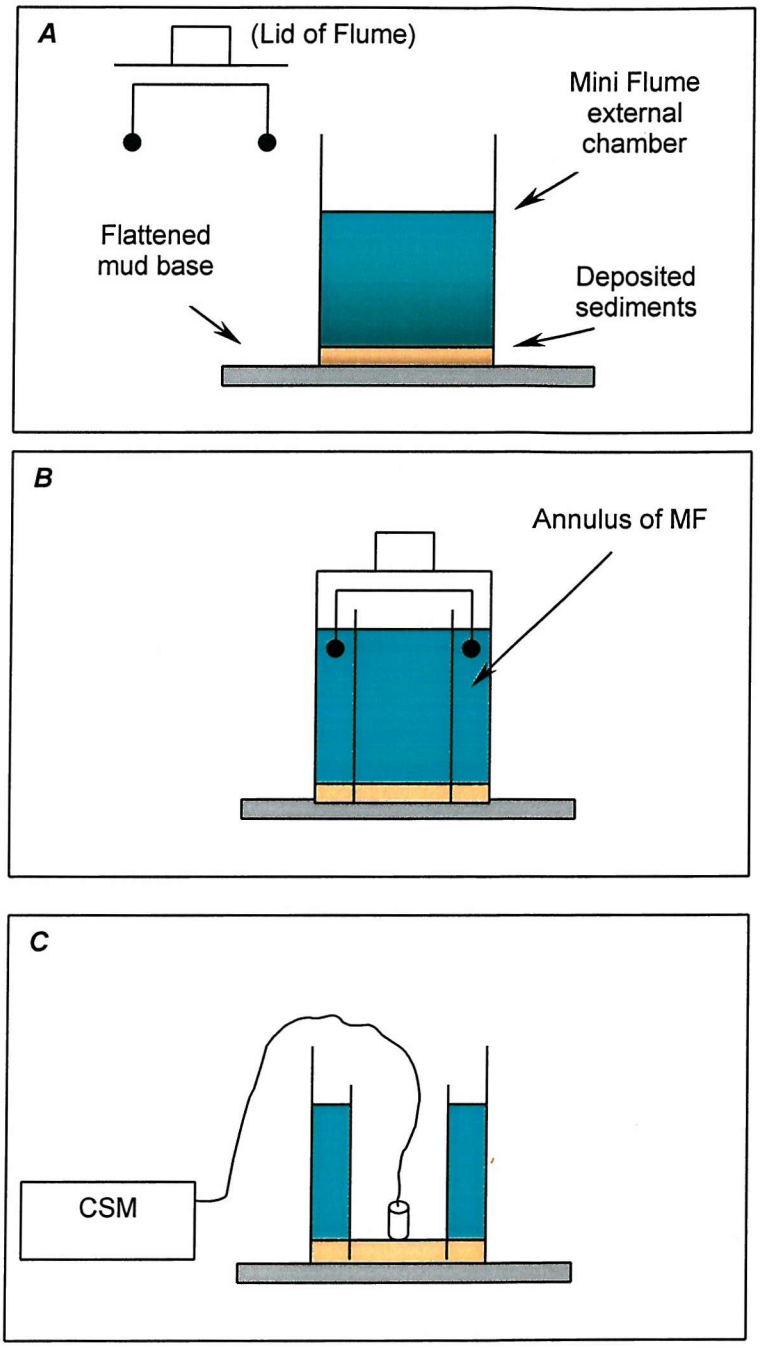

Figure 5.14. A) The external wall of Mini Flume is pushed into the stiff clay, filled with water and the natural sediments from V40 are added to create a thick homogeneous layer over the bottom. B) When settling is completed (about 1-2 hours), the internal wall is added in order to run an experiment with the Mini Flume annulus leaving the central core undisturbed. The water is then removed from the central part so that CSM may be deployed immediately. C) Three tests were performed using the CSM on the soft exposed mud layer in the central part of the Mini Flume.

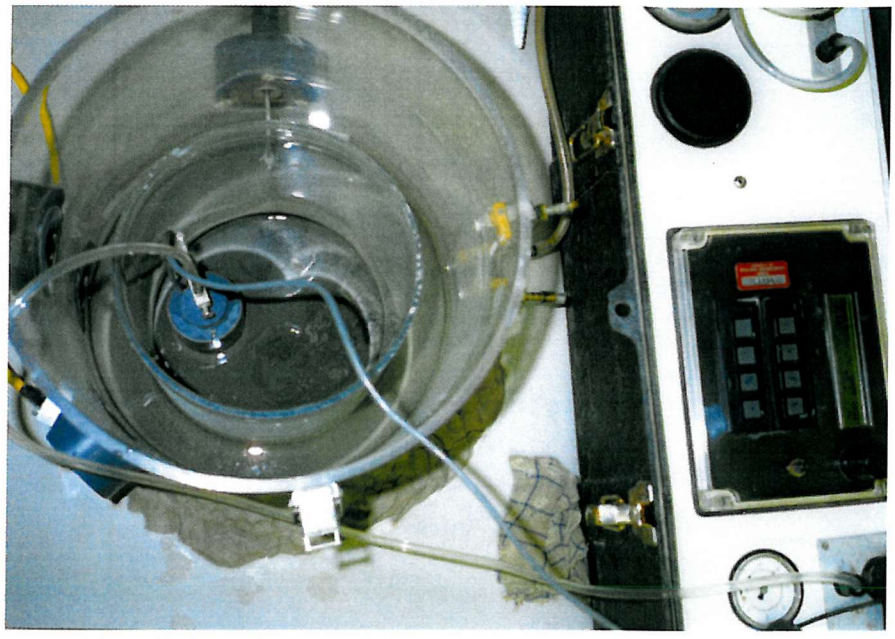

Figure 5.15. The CSM chamber inside the annular flume during comparative experiments.

5.3. Results

5.3.1. Absolute elevation and habitat descriptions

Results of the topographic survey (Fig. 5.16.) show that *Palude della Centrega* has a very low slope which causes rapid inundation of the intertidal flat by the flood tide. Elevation is very close to MSL, particularly along the E-W transect.

The N-S transect is formed of 7 stations, progressively numbered from St1 (southern) to St7 (northern). The transect intersects a series of tidal creeks and is characterised by a gradual northward decrease in elevation (from 25 cm above the MSL at St1 to MSL at St7). A significant habitat change with elevation exists on the mudflat. *Spartina* spp. and *Salicornia* spp. occurred at St1 and St2 (Fig. 5.17.). A dense *Zostera noltii* community colonised the mudflat from St5 to St7 (Fig. 5.18.) during summer.

The E-W transect is flat and MSL can be considered as the representative elevation of the entire profile. The area is seasonally covered by a highly vegetated community of *Zostera noltii* in the western and central part (from St10 to St16) and a

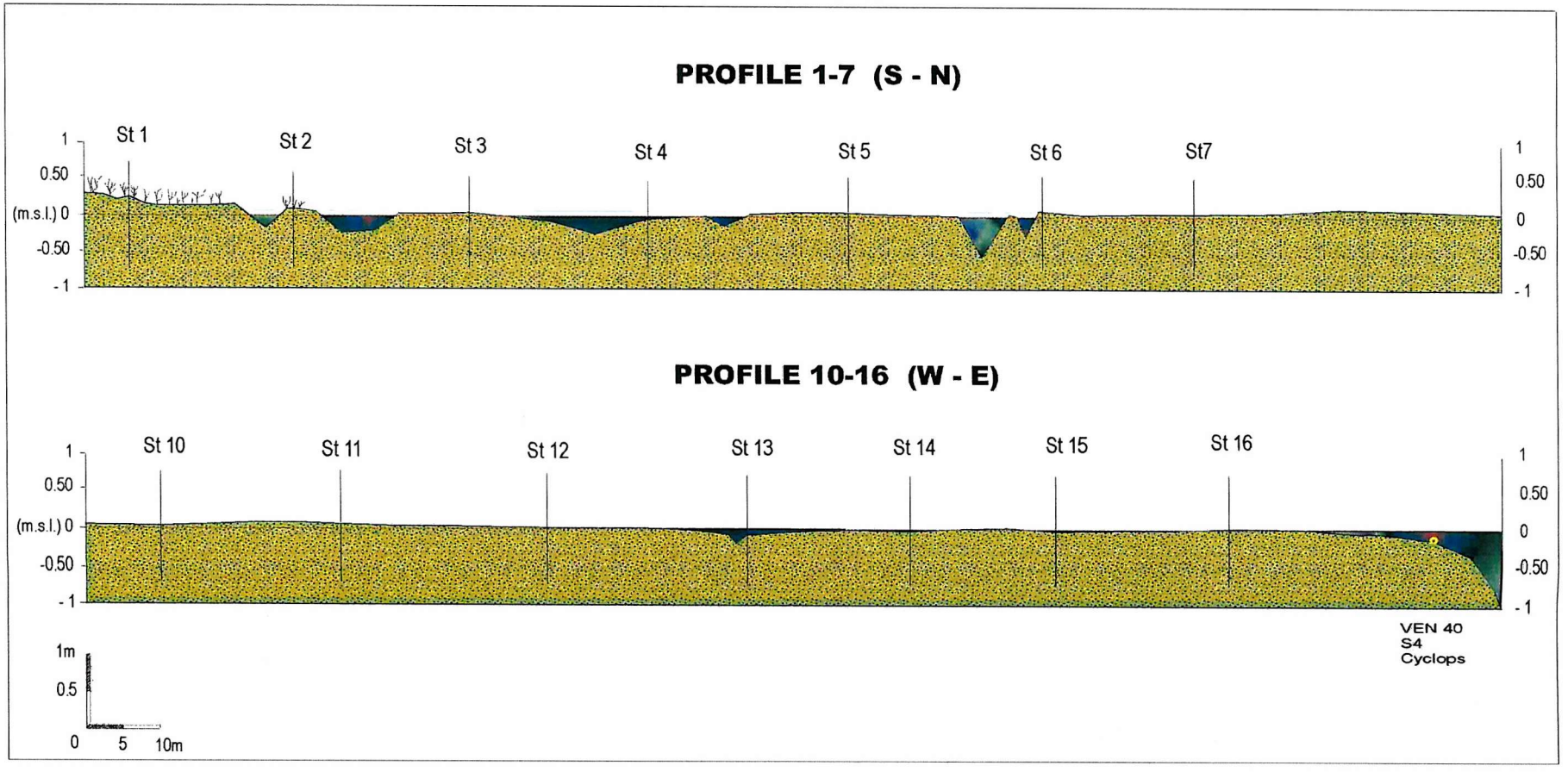

Figure 5.16. The absolute elevation of the south-north (S-N) profile numbered from St1 to St7 and the west-east profile going from St10 t St16 (below). Note that stability measurements (during the F-ECTS study) were performed at the edge of *Canale Scanello* (east of St16).

Figure 5.17. St1, Summer 1998. The southern part of N-S transect is densely covered by *Salicornia* spp. and *Spartina* spp. which have an average height of about 40 cm.

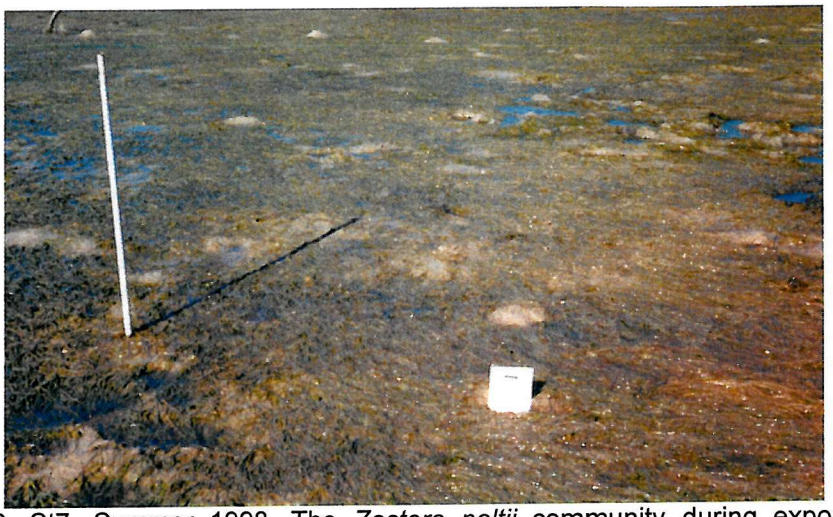

Figure 5.18. St7, Summer 1998. The *Zostera noltii* community during exposure of the mudflat covering the soft mud (see the footprints in the background) of the northern part of the transect.

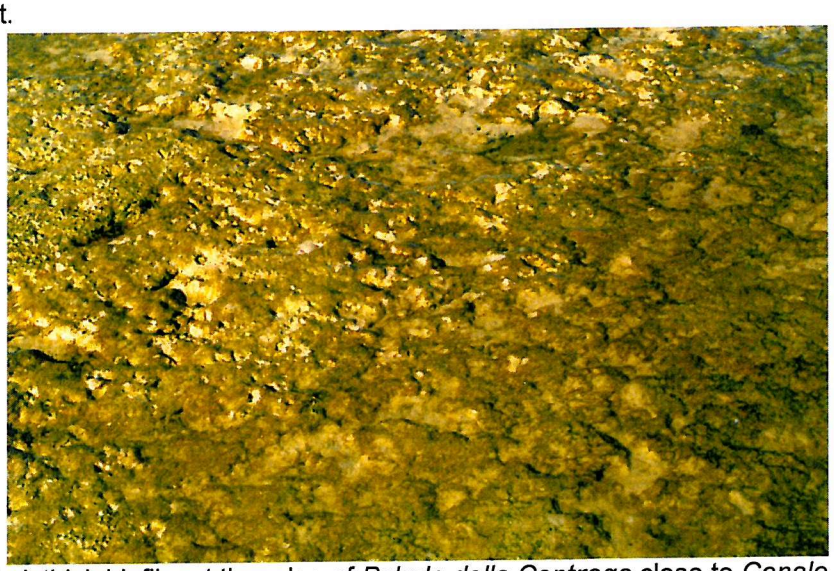

Figure 5.19. A thick biofilm at the edge of *Palude della Centrega* close to *Canale Scanello*.

thick biofilm of microphytobenthos (Fig. 5.19.) on the edge of the channel where station V40 is located.

5.3.2. Sediment strength using the TSM

Vane shear strength was measured across the two transects of *Palude della Centrega* with five replicates carried out at each station. Results are presented in Table 5.3. and in Fig. 5.20. The relatively small standard deviation in most areas indicates that the TSM gives consistent results and appears insensitive to small variations in sediment properties.

	Summer 1998			Winter 1999		
Station	Date	Mean Shear Strength	Standard deviation	Date	Mean Shear Strength	Standard deviation
No.	D/M/Y	kPa	kPa	D/M	KPa	kPa
St 1	6/8/98	4.68	0.55	23/2/99	4.16	0.45
St 2	6/8/98	2.28	0.08	23/2/99	2.76	0.61
St 3	6/8/98	1.56	0.59	23/2/99	1.42	0.55
St 4	6/8/98	0.7	0.25	23/2/99	1.08	0.55
St 5	6/8/98	2.12	0.24	23/2/99	1.98	0.58
St 6	6/8/98	1.96	0.22	23/2/99	1.52	0.78
St 7	6/8/98	1.78	0.08	23/2/99	1.42	0.43
St 10	6/8/98	1.79	0.19	23/2/99	1.16	0.42
St 11	6/8/98	2	0.23	23/2/99	1.92	0.11
St 12	6/8/98	2.7	0.82	23/2/99	2.14	0.13
St 13	6/8/98	0.51	0.57	23/2/99	1.69	0.47
St 14	6/8/98	2.58	0.72	23/2/99	2.04	0.22
St 15	6/8/98	2.08	0.16	23/2/99	1.94	0.11
St 16	6/8/98	2.78	0.78	23/2/99	2.41	0.39

Table 5.3. Mean shear strength (kPa) and standard deviation derived using the TSM at each station in *Palude della Centrega*.

Maximum vane shear strength values were found in the inner part of the mudflat (St1) during both the summer and winter campaigns. Lower values occurred in stations colonised by micro-organisms (with minima close to the tidal creeks: St4 and St13). This trend suggests that the intertidal flat elevation plays an important role in sediment stability, by controlling the inundation time of the area and consequently the water content of sediment (lower in the upper part and higher close to the channels). The roots of *Spartina* spp. may have contributed to an

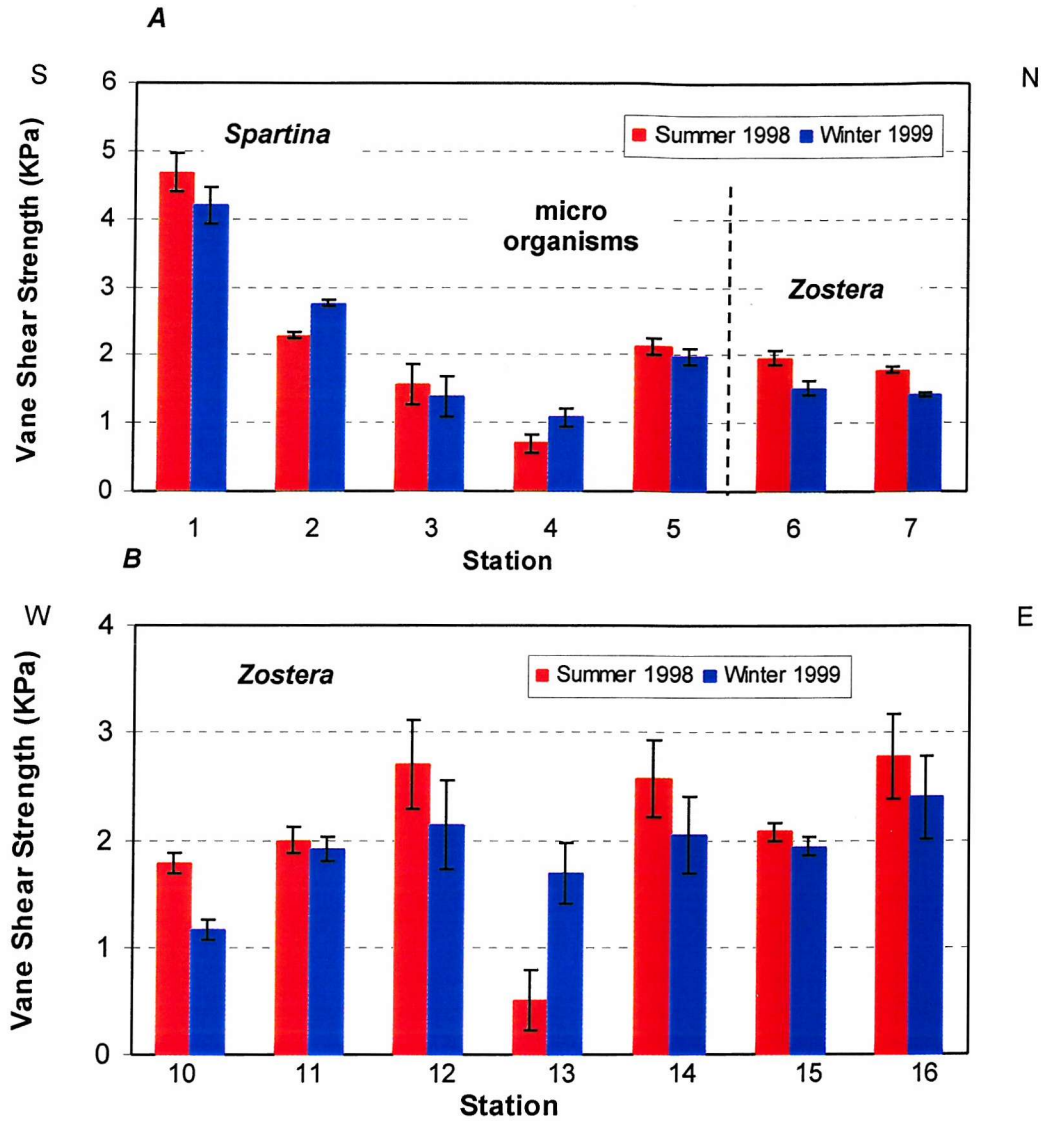

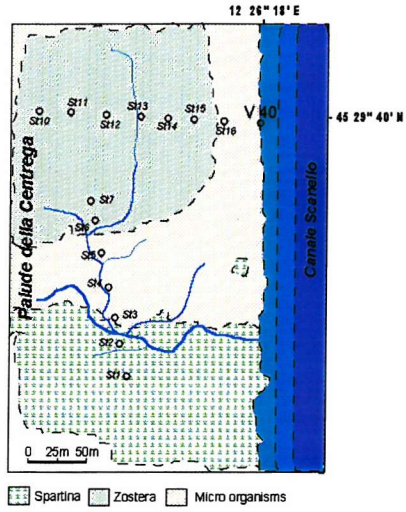

Figure 5.20. Vane shear strength derived at each station along the N-S transect (*A*) and the W-E transect (*B*). Note that maximum sediment stability was found in the upper part of the mudflat (St1) and lower values close to the tidal creeks (St3, St4 and St13). The sediment strength progressively increases southwards and eastwards along the transects.

increase in the strength of sediments and prevented the rotation of the vane during some of the tests. In addition, during the two campaigns the sediment stability along the E-W transect was found to decrease eastward (in the central part of *Palude della Centrega*). During the winter campaign, lower stability was observed in most of the stations.

5.3.3. Erosion threshold using the CSM

The CSM was deployed at 9 sites located along the two transects in November 1999. At each site, three replicate tests were carried out. Results of the mean erosion threshold and standard deviation derived from *Palude della Centrega* are reported in Table 5.4. and Fig. 5.21.

Site	*Date*	*Mean Erosion Threshold*	*Standard Deviation*
No.	*D/M/Y*	*Pa*	*Pa*
St 1	*6/11/99*	*0.89*	*0.76*
St 2	*6/11/99*	*0.88*	*0.60*
St 3	*6/11/99*	*0.69*	*0.28*
St 4	*6/11/99*	*?*	-
St 5	*6/11/99*	*0.12*	*0.03*
St 6	*6/11/99*	*0.88*	*0.86*
St 7	*6/11/99*	*0.25*	*0.10*
St 10	*6/11/99*	*0.14*	*0.01*
St 12	*6/11/99*	*0.23*	*0.11*
St 15	*6/11/99*	*0.44*	*0.17*

Table 5.4. Erosion threshold and standard deviation values derived from CSM deployments carried out on *Palude della Centrega* in November 1999.

Along the N-S transect, maximum erosion threshold values were found in the inner part of the mudflat (St1 and St2). Along the E-W transects, sediment stability decreased eastwards. Such trends in sediment stability (Pa) agree with the results of the investigation carried out on the sediment strength (kPa) using TSM.

At St4, it was not possible to deploy the CSM due to the presence of filamentous algae that prevented insertion of the chamber into the soft sediment without destruction of the sediment fabric. At St6 the relatively high τ_c value was probably due to erosion of the surficial sediments before the fieldwork, and subsequent exposure of consolidated and denser sediments.

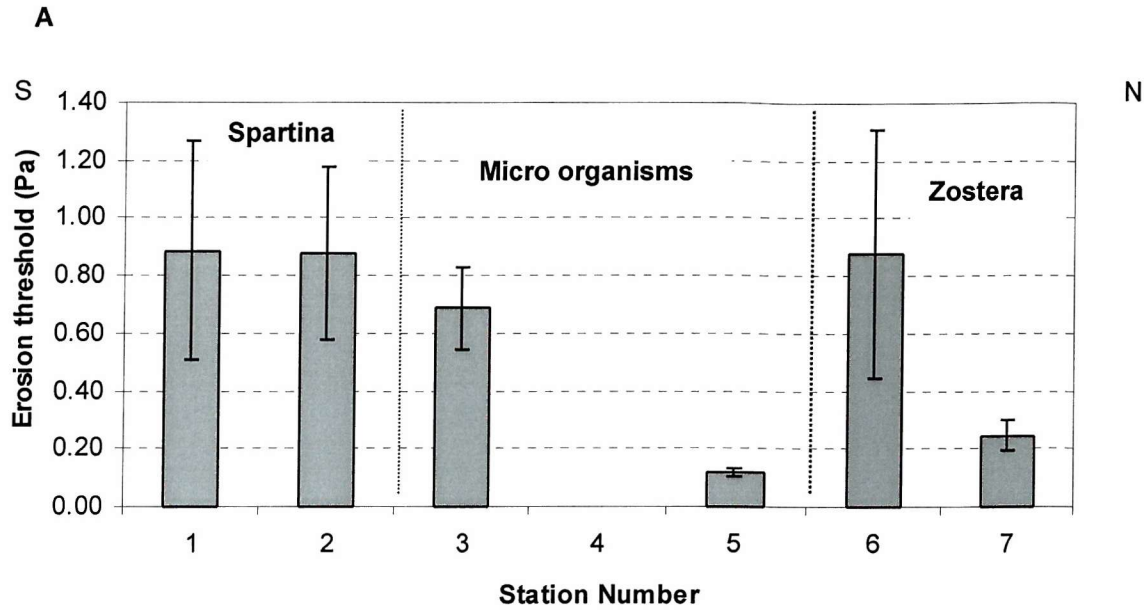

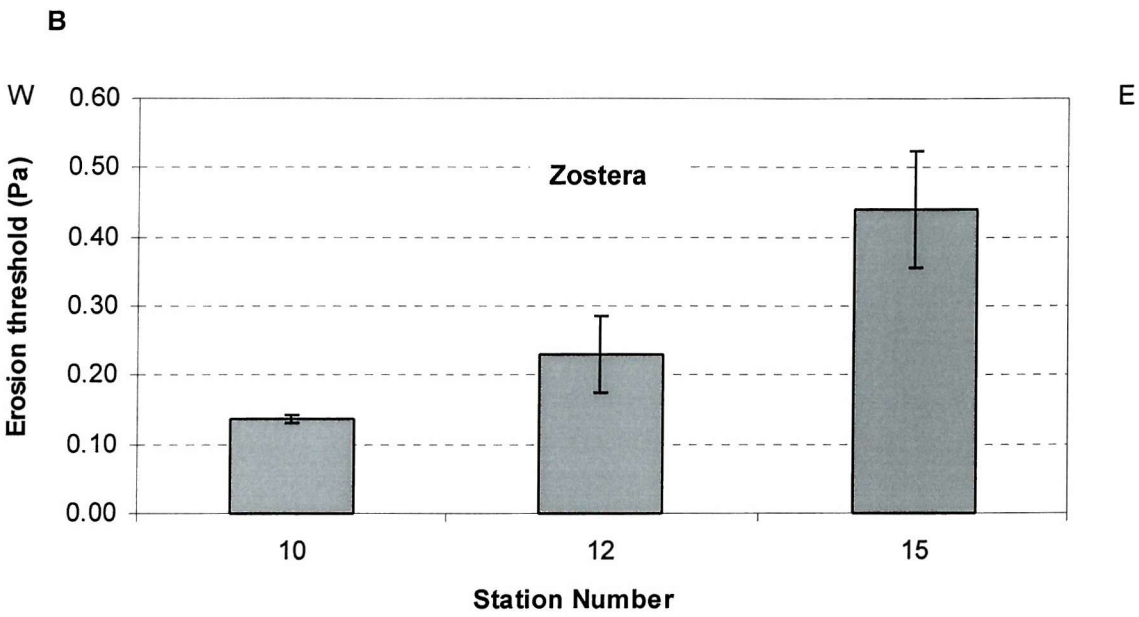

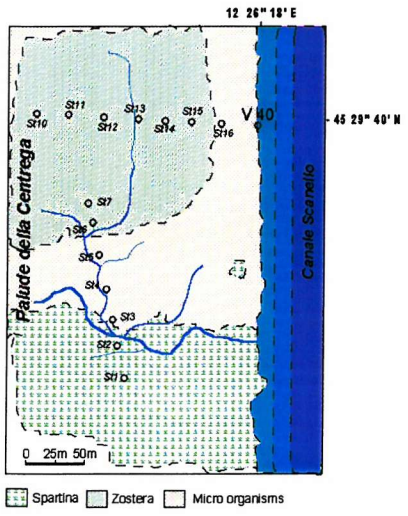

Figure 5.21. Mean erosion threshold derived using the CSM along the N-S transect (A) and along the E-W transect (B). Note that maximum sediment stability occurred in the upper part of the mudflat (St1 and St2) and the lowest in areas colonised by the seagrass. Along the N-S transect the erosion threshold generally decreases southwards.

The standard deviation of sediment stability values derived by using the CSM is higher compared with those derived using the TSM. This suggests that the accuracy is higher compared with those derived using the TSM. This suggests that the accuracy of the CSM to determine the erosion threshold on cohesive sediments could be improved.

Along the E-W transect, τ_c was lower compared with the N-S transect and increased eastward (towards the main channel). Such increases in erosion threshold were probably controlled by the sea grass *Zostera noltii* which colonised the area at the time of deployments. Visual observations indicated that the increase in seagrass density westwards was related to an increase in the water content and a subsequent increase in the bulk density of the sediment, reported below (section 5.3.4.).

5.3.4. Physical and biological properties of the mudflat

Palude della Centrega is characterised by a *"silty slightly sandy mud"* according to the classification of FLEMMING (2000) (Fig. 4.11.). The surface 0.5 cm of sediment was grey (Mansell's colour scale: 5y5/1) and overlapped black anoxic sediment. The physical and biological properties of *Palude della Centrega* are reported in Tables 5.5. (August 1998), 5.6. (February 1999) and 5.7. (November 1999). The mean disaggregated grain size was 41 μm in the summer and 38 μm in the winter. The average sand : silt : clay ratio was 13 : 66 : 20. This composition is within the range characterised by cohesive behaviour (see section 2.4.).

Station	Mean grain size	Bulk density	Water content	Organic content (LOI)	Chlorophyll a content	Carbohydrate content
No.	(μm)	(kg/m^3)	%	%	($\mu gGE/g_{DW}$)	($\mu gGE/g_{DW}$)
North-South Transect						
St1	41.96	2120	19.9	1.9	92	268
St 2	28.80	1720	35.0	3.0	117	90
St 3	35.58	1760	33.6	1.9	50	76
St 4	50.53	1830	31.0	2.6	74	132
St 5	37.78	1750	33.9	1.9	95	91
St 6	57.82	1780	32.8	1.7	80	188
St 7	36.30	1470	44.6	3.7	64	527
East-West Transect						
St 10	33.08	1660	37.4	3.1	200	107
St 11	59.05	1770	33.1	3.0	165	326
St 12	45.76	1890	28.6	2.8	122	184
St 13	60.61	1575	40.6	3.6	359	74
St 14	38.47	1870	29.4	2.6	63	101

St 15	*44.68*	*1725*	*34.9*	*2.2*	*192*	*97*
St 16	*28.99*	*1800*	*32.0*	*3.2*	*93*	*90*
V40	*21.23*	*1750*	*36.6*	*2.3*	*59*	*130*

Tables 5.5. The physical and biological properties at each station on *Palude della Centrega* in August 1998.

Station	***Mean grain size***	***Bulk density***	***Water content***	***Organic content (LOI)***	***Chlorophyll-a content***	***Carbohydrate content***
No.	*(μm)*	*(kg/m^3)*	*%*	*%*	*(μgGE/g$_{DW}$)*	*(μgGE/g$_{DW}$)*
North-South Transect						
St1	*45.75*	*1870*	*29.5*	*2.8*	*40*	*41*
St 2	*40.75*	*1930*	*27.1*	*2.4*	*25*	*22*
St 3	*33.40*	*1700*	*35.9*	*2.4*	*14*	*150*
St 4	*29.30*	*1820*	*31.4*	*2.0*	*20*	*234*
St 5	*45.05*	*1850*	*30.2*	*2.1*	*22*	*123*
St 6	*41.10*	*1840*	*30.3*	*2.0*	*24*	*19*
St 7	*40.30*	*1520*	*42.7*	*2.9*	*85*	*41*
East-West Transect						
St 10	*38.78*	*1690*	*36.0*	*2.8*	*29*	*44*
St 11	*27.08*	*1600*	*39.4*	*2.9*	*79*	*19*
St 12	*36.35*	*1550*	*41.3*	*3.5*	*71*	*139*
St 13	*40.28*	*1560*	*41.0*	*2.8*	*73*	*41*
St 14	*48.73*	*1670*	*36.7*	*2.9*	*56*	*170*
St 15	*32.62*	*1660*	*37.4*	*2.9*	*61*	*160*
St 16	*43.49*	*1660*	*37.3*	*1.7*	*18*	*28*
V40	*33.45*	*1700*	*42.6*	*2.6*	*19*	*91*

Tables 5.6. The physical and biological properties at each station on *Palude della Centrega* in February 1999.

Station	***Bulk density***	***Water content***	***Organic content (LOI)***	***Chlorophyll-a content***	***Carbohydrate content***
No.	*(kg/m^3)*	*%*	*%*	*(μgGE/g$_{DW}$)*	*(μgGE/g$_{DW}$)*
North-South Transect					
St1	*1340*	*49.4*	*6.2*	*97*	*185*
St 2	*1655*	*37.5*	*3.4*	*35*	*134*
St 3	*1485*	*43.9*	*4.3*	*20*	*112*
St 4	*1340*	*49.4*	*3.8*	*35*	*124*
St 5	*1515*	*42.7*	*4.0*	*48*	*88*
St 6	*1605*	*39.5*	*4.3*	*41*	*89*
St 7	*1500*	*43.4*	*9.3*	*31*	*138*
East-West Transect					
St 10	*1475*	*44.3*	*3.5*	*47*	*147*
St 12	*1500*	*43.4*	*6.8*	*44*	*133*
St 15	*1570*	*40.7*	*4.2*	*20*	*100*

Tables 5.7. The physical and biological properties at each station on *Palude della Centrega* in November 1999.

Little difference in grain size was observed between summer and winter measurements. The bulk density of the surface 1 mm sediments varied between 1300-1900 kg/m^3. An increasing density with depth was found in all profiles (Fig. 5.22.), evidence that the sediment was undergoing self-weight consolidation. Higher bulk density values were found generally during August 1998, and lower values during February 1999, suggesting that deposition of soft, unconsolidated sediments typical of areas with an accretionary trend occurred during the winter period. The only exception was at St6 (located at the edge of a tidal creek) where higher bulk densities were detected during February 1999.

Large seasonal differences were found in the biological properties of sediments. The overall mean chlorophyll *a* and colloidal carbohydrate content were 65 % and 47 % lower respectively in February 1999 (~88 $\mu gGE/g_{DW}$ and ~44 $\mu gGE/g_{DW}$) compared with August 1998 (~126 $\mu gGE/g_{DW}$ and ~168 $\mu gGE/g_{DW}$). These data confirm the general results of the regional investigation of the F-ECTS project on the seasonal fluctuation of biological activity in the intertidal areas of Venice. Particularly high chlorophyll *a* values were found during both campaigns at St13, which is close to a tidal creek. It is believed that these were due to the presence of detrital fragments of *Ulva* spp. and other floating algae incorporated into the sediment.

A decrease in colloidal carbohydrate content was observed in November 1999 at St5 and St6 as well as an increase in bulk density. This suggests that the surface sediment is eroded before sampling, exposed denser material. The water content decreased with increasing elevation southward and with increasing density of *Zostera noltii* westwards.

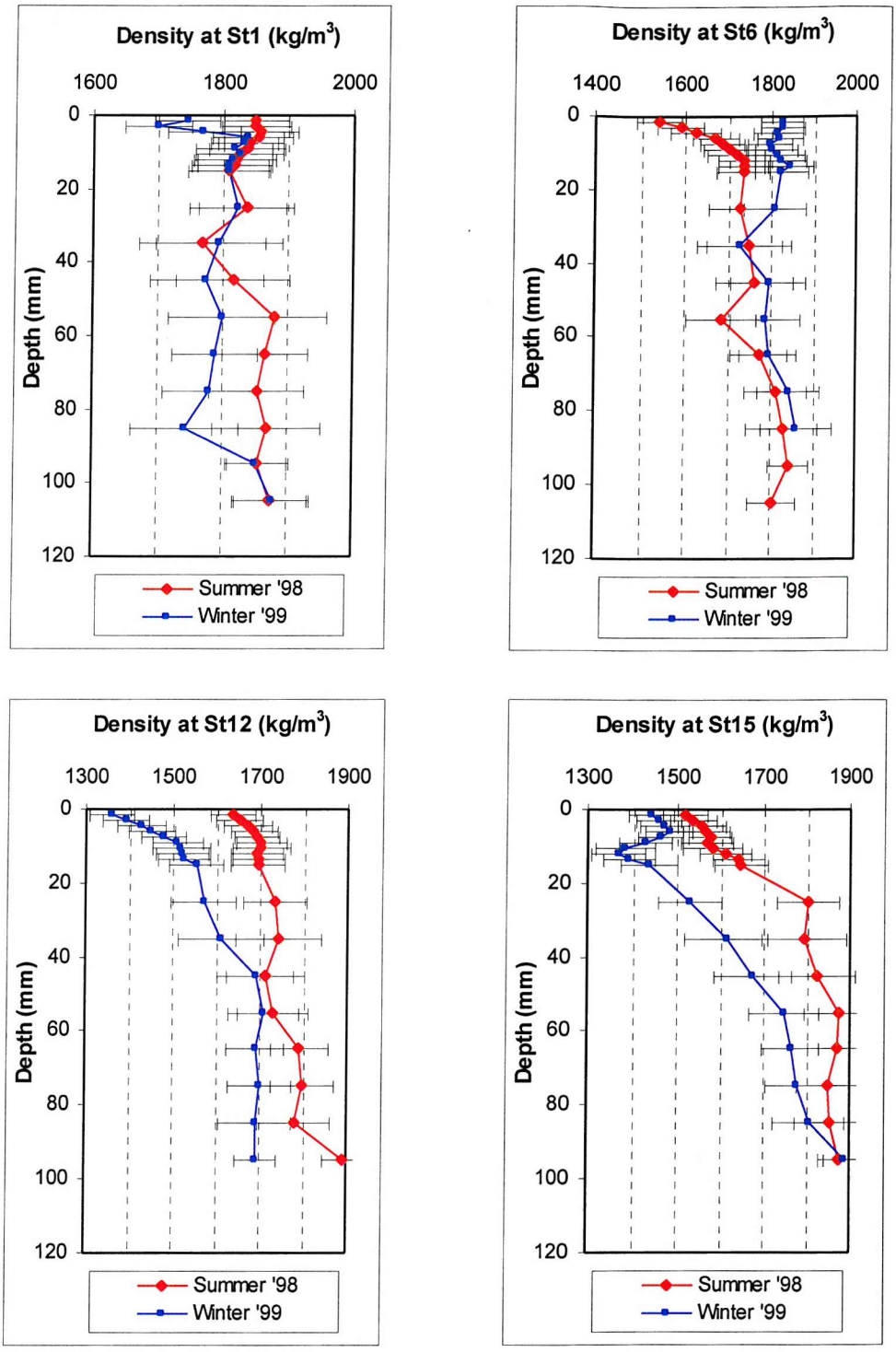

Figure 5.22. Bulk density profiles of the syringe cores collected at the four sites during the summer (red) and winter (blue) campaigns. Note the self-weight consolidated top 1 cm sediment characterising all the samples analysed. Generally, bulk density was found to be higher in summer than in winter (St6 showed higher values during winter 1999).

5.3.5. Data analysis

Quantitative relationships between the erosion threshold and sediment properties were derived through a least-squares regression analysis (Table 5.8.).

Parameters	*N-S transect*		*E-W transect*	
Tor Vane Shear August 1998	Regression eq (n=7)	Coefficient	Regression eq (n=7)	Coefficient
Elevation	$\tau_c = 0.041x + 0.347$	$r^2 = 0.828$ p = 0.005	$\tau_c = -0.076x + 2.494$	r^2=0.121 p = 0.444
Bulk density	$\tau_c = 0.001x - 1.566$	$r^2 = 0.097$ p = 0.496	$\tau_c = 0.005x - 5.538$	$r^2 = 0.608$ p = 0.039
Water Content	$\tau_c = -0.033 x + 1.735$	$r^2 = 0.097$ p = 0.496	$\tau_c = -0.121x + 6.704$	$r^2 = 0.608$ p = 0.039
Loss on ignition	$\tau_c = -0.146 x + 1.000$	$r^2 = 0.300$ p = 0.203	$\tau_c = -0.015x + 2.484$	$r^2 = 0.010$ p = 0.828
Carbohydrate	$\tau_c = 0.001 x + 0.566$	$r^2 = 0.333$ p = 0.175	$\tau_c = -0.011x + 2.721$	$r^2 = 0.150$ p = 0.389
Chlorophyll *a*	$\tau_c = 0.007 x + 0.0829$	$r^2 = 0.027$ p = 0.725	$\tau_c = -0.001x + 0.867$	$r^2 = 0.124$ p = 0.437
Tor Vane Shear February 1999	Regression eq (n=7)	Coefficient	Regression eq (n=7)	Coefficient
Elevation	$\tau_c = -0.002x+0.643$	$r^2 = 0.588$ p = 0.044	$\tau_c = -0.017x+0.643$	$r^2 = 0.123$ p = 0.441
Bulk density	$\tau_c = 0.004x - 4.737$	$r^2 = 0.232$ p = 0.272	$\tau_c = 0.001x + 4.407$	$r^2 = 0.048$ p = 0.526
Water Content	$\tau_c = -0.100x + 5.313$	$r^2 = 0.232$ p = 0.272	$\tau_c = -0.006x + 0.775$	$r^2 = 0.048$ p = 0.634
Loss on ignition	$\tau_c = 1.424x - 1.345$	$r^2 = 0.282$ p = 0.278	$\tau_c = -0.061x + 0.714$	$r^2 = 0.085$ p = 0.526
Carbohydrate	$\tau_c = -0.007x + 2.657$	$r^2 = 0.248$ p = 0.255	$\tau_c = 0.001x + 0.478$	$r^2 = 0.017$ p = 0.606
Chlorophyll *a*	$\tau_c = 0.002x + 1.987$	$r^2 = 0.002$ p = 0.928	$\tau_c = -0.001x + 0.593$	$r^2 = 0.001$ p = 0.945
CSM November 1999	Regression eq (n=6)	Coefficient	Regression eq (n=3)	Coefficient
Elevation	$\tau_c = 0.001x+0.421$	$r^2 = 0.186$ p = 0.392	$\tau_c = -0.056x +0.347$	r^2=0.999 p = 0.06
Bulk density	$\tau_c = 0.001x - 0.025$	$r^2 = 0.016$ p = 0.809	$\tau_c = 0.004x - 5.304$	$r^2 = 0.997$ p = 0.030
Water Content	$\tau_c = 0.095x + 0.969$	$r^2 = 0.016$ p = 0.809	$\tau_c = -0.098x + 4.479$	$r^2 = 0.997$ p = 0.030
Loss on ignition	$\tau_c = 0.053x + 0.841$	$r^2 = 0.143$ p = 0.459	$\tau_c = 0.005x +0.32$	$r^2 = 0.002$ p = 0.969
Carbohydrate	$\tau_c = 0.026x + 0.243$	$r^2 = 0.096$ p = 0.549	$\tau_c = 0.007x + 1.27$	$r^2 = 0.999$ p = 0.005

Chlorophyll *a*	τ_c = 0.003 x + 0.440	r^2 = 0.058 p = 0.643	τ_c = -0.012x + 0.75	r^2 = 0.966 p = 0.118

Table 5.8. Regression equations between erosion threshold (τ_c) and sediment properties along the N-S and E-W profiles during August 1998, February 1999, and November 1999. Significant relationships ($p<0.05$) are highlighted.

The best correlation (r^2=0.83; P=0.005) between VSS and intertidal flat station elevation was found along the N-S transect in August 1998. It is believed that it was due to higher solar radiation during summer (typical in lower latitudes), which plays an important role in the evaporation and desiccation of surface sediments (PARTHENIADES & PAASWELL, 1970). It is possible that the higher amounts of colloidal carbohydrate at St1 and St2, on the inner part of the intertidal flats, are secreted by diatoms to protect their cells against solar radiation (DABORN, 1993; SUNDBÄCK *et al.*, 1997) during summer time.

Significant relationships (r^2=0.61; P=0.04) were found between τ_c and physical parameters (BD and WC) along the E-W transect during summer. However, this trend was not evident during winter 1999 when no relationship was found between τ_c and any of the physical or biological sediment properties. The reasons for this result are unknown but may be due to seasonally changing habitats in *Palude della Centrega,* and their time-varying influence on sedimentary processes. For example, the central part of the studied region was characterised by soft mud and there was no visible evidence of micro- and macro-algae during winter (see 5.3.1. for details).

The best regression coefficients between τ_c, bulk density, water content and colloidal carbohydrate were found along the E-W transect in November 1999, however the high correlation coefficients (r^2=0.99; P<0.03) were probably due to the low number of stations (n=3) investigated along that transect at that time.

5.3.6. A comparison of results between the CSM and Mini Flume

Results of the laboratory deployments carried out to compare the CSM and the Mini Flume are shown in Fig. 5.2.3. and Fig. 5.2.4. Details of the hydrodynamic conditions under which sediment erosion takes place are reported in Table 5.9. A drop in light transmission was found in most of the CSM tests, indicating that the incremented steps in the shear stress were too large. When the first steps are large, the erosion threshold may not be observed accurately and the derived value of critical erosion shear stress may be over-estimated (Fig. 5.13.). An erosion threshold of 0.2 Pa was derived using a threshold of 80 % in the light transmission as a reference value (CAPPUCCI *et al.*, 2000). Using the Mini flume on the same sediments, an erosion threshold of about 0.52 Pa was found.

The comparison between the two devices shows that the erosion threshold derived using the CSM was about 50 % less than that erosion threshold derived using the Mini Flume (Fig. 5.25.).

CSM				Mini Flume			
Jet Pressure	Jet Pressure	τ_0	U.	M Value	Lid Speed	τ_0	U.
PSI	*KPa*	*Pa*	*(cm/s)*		*(rev/s)*	*Pa*	*(cm/s)*
0	*0*	*0*	*0*	*0*	*0*	*0*	*0*
0.5	*3.45*	*0.327*	*1.786*	*2000*	*0.148*	*0.044*	*0.825*
1	*6.9*	*0.647*	*2.512*	*3000*	*0.218*	*0.132*	*1.275*
1.5	*10.35*	*0.96*	*3.059*	*4000*	*0.288*	*0.263*	*1.725*
2	*13.8*	*1.266*	*3.513*	*5000*	*0.358*	*0.437*	*2.175*
2.5	*17.25*	*1.565*	*3.905*	*6000*	*0.428*	*0.654*	*2.625*
3	*20.7*	*1.856*	*4.253*	*7000*	*0.498*	*0.914*	*3.075*
3.5	*24.15*	*2.141*	*4.568*	*8000*	*0.568*	*1.216*	*3.525*
4	*27.6*	*2.419*	*4.856*	*9000*	*0.638*	*1.562*	*3.975*
4.5	*31.05*	*2.691*	*5.121*	*10000*	*0.708*	*1.952*	*4.425*

Table 5.9. A list of the principal parameters that describe the hydrodynamic condition of the incremental bed shear stresses applied by the CSM and the Mini Flume. Highlighted areas indicate the bed shear stress steps under which erosion occurred.

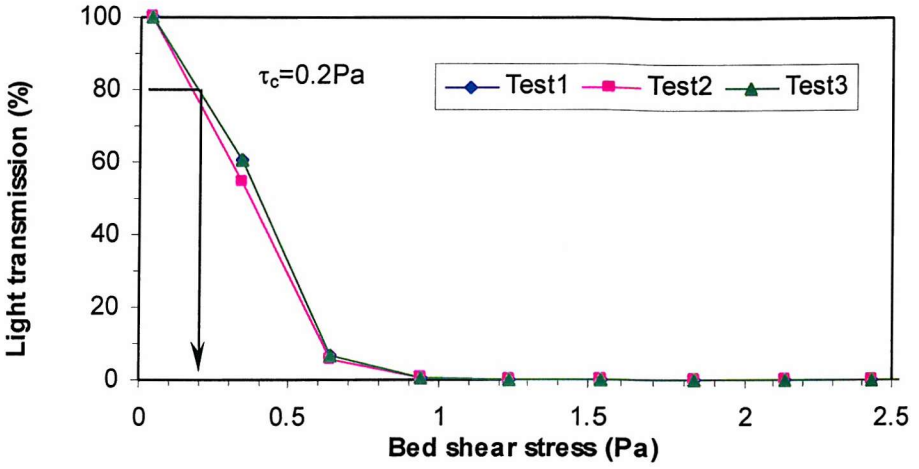

Figure 5.23. Erosion thresholds derived from the three CSM deployments. Note the rapid drop in light transmission, and the consistency in light transmission values between the three tests performed.

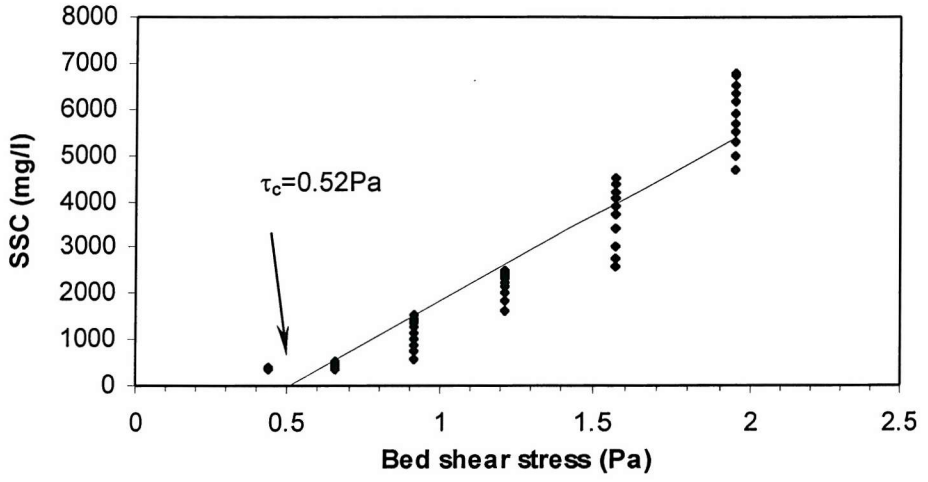

Figure 5.24. Erosion thresholds derived from the Mini Flume deployments.

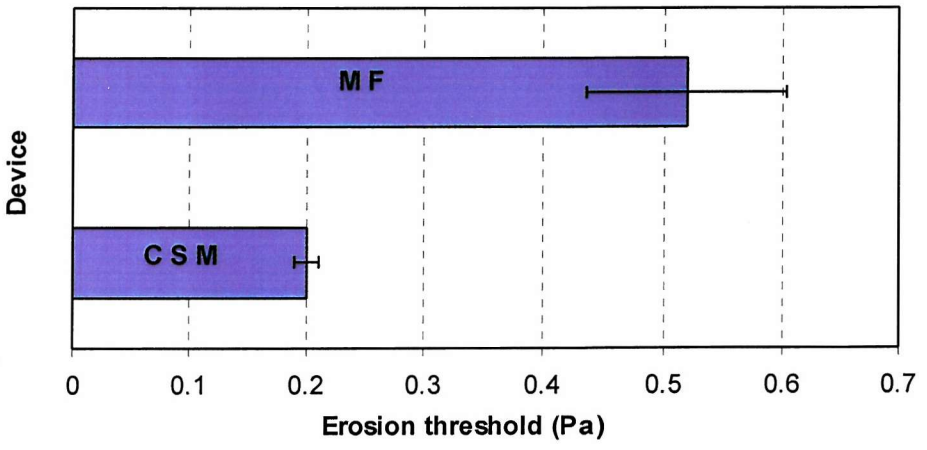

Figure 5.25. Comparison between the erosion threshold derived using the CSM and the Mini Flume on cohesive sediment from *Palude della Centrega*.

5.4. Limitations

The τ_v (kPa) is three orders of magnitude bigger than τ_c (Pa) derived with both the MF and the CSM. Such a difference in the results is explained using the "pack of cards" example described by AMOS *et al.* (1996b): *"It is much easier to slide each card (analogous to fluid shearing) than to tear the whole deck (analogous to a vane shear test)"*. In the present study the fluid shearing is the erosion threshold (τ_c) and the deck is related to the bulk sediment shear strength (τ_v).

The TSM has been used largely in geotechnical studies (LAMBE & WHITMAN, 1979) and applied successfully in sedimentological studies of MUSKANANFOLA (1994) and O'BRIEN (1998). The TSM rotates in a vertical section of about 2 cm and is effected by the higher density (i.e. strength) of the sediment across the depth of the vane illustrated in Fig. 5.26. Therefore relationships between the vane shear strength and physical or biological parameters of surface sediments should be treated with caution.

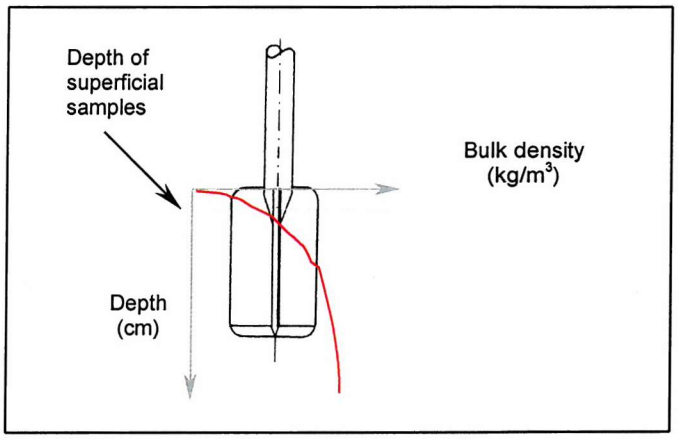

Figure 5.26. A schematic diagram showing increasing bulk density with sediment depth. Deeper and denser sediments can increase τ_v, meanwhile the τ_c derived by flume deployments is based on the erosion of the top 1 mm.

The CSM has some operational limitations, the most significant of which is the big increment of bed shear stress produced by the jet pulse reduces the accuracy of the determination of the erosion threshold (Fig. 5.9.). A modified version of the CSM software is now available, enabling the instrument to be deployed with greater accuracy on cohesive sediments (TOLHURST, *pers. comm.*). The new version of the CSM software is able to pressurize water jets with a higher precision creating

smaller increases in horizontal shear stress, capable of providing a better control of resuspension conditions (i.e. erosion threshold).

Further limitations of the CSM concern the calculation of the erosion rate. A time series of the erosion rate provides an accurate description of the erosion process. Generally, it permits an understanding of how the erosion process proceeds through time and depth within the sediment column. Furthermore, it helps to determine the critical shear stress with greater accuracy, particularly if compared with the time series of turbidity (Fig. 5.13.).

Calculation of the erosion rate with the CSM must be treated with caution because the nature of the jet pulses into the chamber means that sediment is not resuspended homogeneously within the foot print of the instrument (Fig. 5.8.). Therefore, the area used to estimate erosion rate is unknown, and is very often under-estimated by more than 50 %. Finally, even if a good relationship existed between τ_c and the physical properties, further work is required to validate the results, because:

- data analysis is based on a single campaign (carried out in November 1999) (therefore results are not considered representative of sediment stability through the year); and
- the τ_c values derived from the CSM carried out along the E-W transect are very low, and are close to the limit of detection (see Fig. 5.21.).

5.5. Discussion

The *in-situ* derivation of critical erosional shear stress remains a difficult task, particularly in micro-tidal environments where many intertidal deposits cannot be investigated properly due to the logistics of deployment. Devices like the Mini Flume and the Sea Carousel are too large to be transported over the intertidal flats particularly in microtidal environments when depth of water at the high tide remain relatively shallow. Small, easily portable devices like the TSM and the CSM are subject to very low levels of accuracy, and the derived τ_c of the cohesive sediments must be treated with caution. The method proposed in the present study (to derive τ_c from a SSC time series after the calibration of the light sensor of the CSM) is very similar to that used for other flumes and provides a good representation of the erosion process (Fig. 5.13.).

5.5.1. A comparison of VSS and τ_c results

VSS and τ_c data derived using the TSM and the CSM from the same stations were plotted against 1:1 line in order to compare the results of sediment stability. Sediment strength data (kPa) were transformed using equations 5.2.1.I. and 5.2.1.II. This comparison shows clear differences in results (Fig. 5.27.) because of the higher values of erosion threshold (between 2 and 3 Pa) derived from the equation of DUNN (1959).

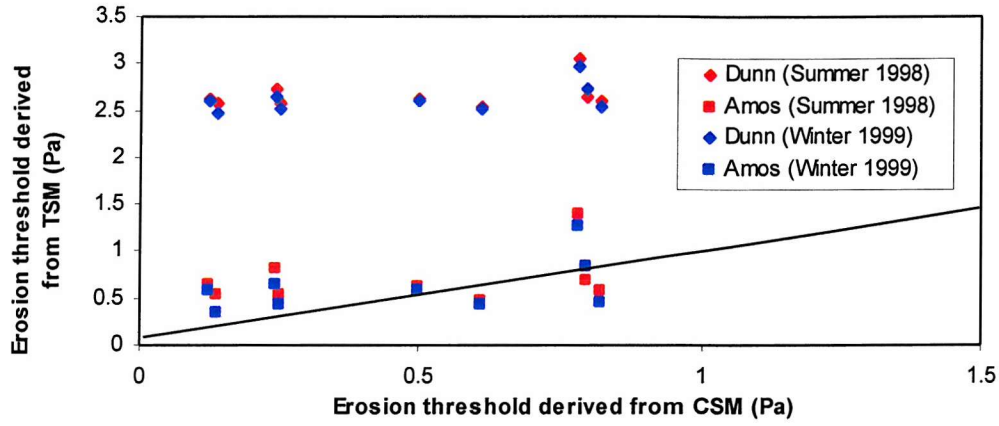

Figure 5.27. Erosion threshold values derived using the TSM during summer 1998 (red dots) and winter 1999 (blue dots) using the equation of DUNN (1959) and AMOS *et al.* (1996) are compared against the erosion threshold derived using the CSM. Note that the equation of DUNN (1959) transforms TSM data between 2.5 and 3 Pa.

A comparison between τ_c derived from CSM (Pa) and the VSS derived from the TSM (kPa) is also presented in Fig. 5.28. As expected, data derived by the CSM and TSM deployments and collected during different field campaign are not related.

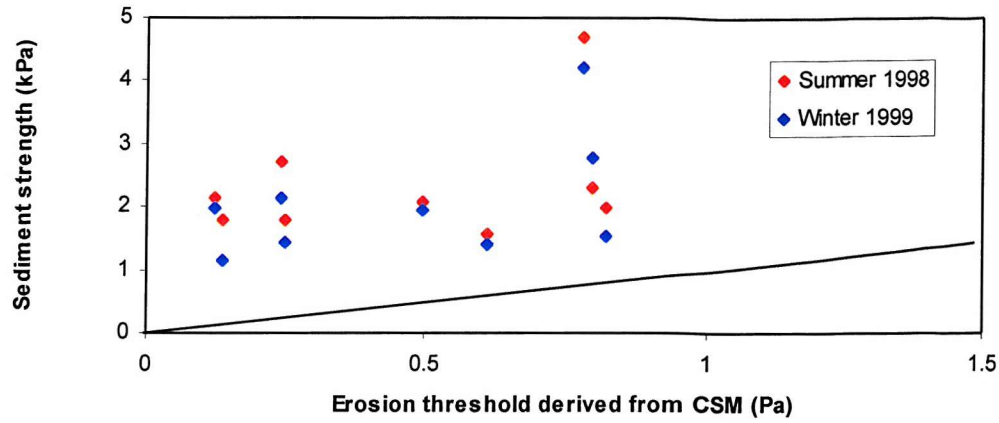

Figure 5.28. VSS derived in August 1998 (in red) and February 1999 (in blue) and versus τ_c derived CSM on a 1:1 line.

5.5.2. The relationship between erosion threshold and sediment properties in Palude della Centrega

Despite all the instrumental differences and limitations, the τ_c values derived from TSM and CSM deployments show the same spatial variation of sediment stability along both the N-S and E-W directions. Along the N-S direction, τ_c increases southwards. Along the E-W direction, the sediment stability increases eastwards. The relationships between erosion threshold and bulk density found in the present study and by AMOS *et al.* (1997) are illustrated in Fig. 5.29. This trend was strongly influenced by the bed elevation and the bulk density which are particularly important in small-scale stability investigations.

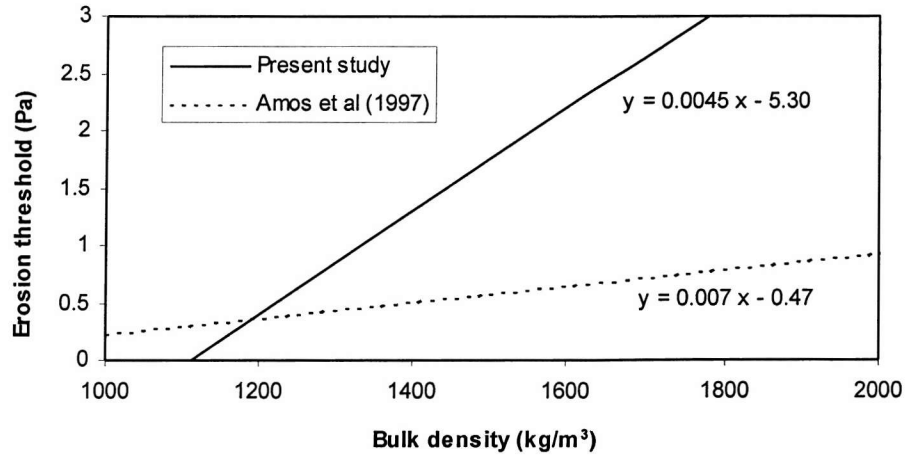

Figure 5.29. Relationships between the erosion threshold and bulk density found in the present study and by AMOS *et al.* (1997).

A conceptual model linking the sedimentology, the biology and the hydrodynamics acting along the E-W transect of the studied area is proposed, although the data analysis was based on a relatively restricted number of samples and stability measurements. This model shows how vegetation can control the sediment stability during exposure of the intertidal mudflat. The process can be summarised in three different steps which are illustrated in Fig. 5.30.

Step A) During high tide, the areas of the intertidal mudflat which are covered by sea grass are better protected against erosion, and the ability of vegetation to reduce the applied bed shear stress may enhance deposition (NEUMEIER & CIAVOLA, 2001).
Step B) During low tide, the sea grass can entrap water between the soft leaves. This reduces the drainage of water and evaporation compared with the unvegetated exposed areas.
Step C) When sediment stability is measured during exposure of the intertidal area (using for example the CSM), the water content of surficial sediments is reduced less by solar radiation in areas colonised by sea grass. Therefore an increase in bulk density and sediment stability is observed.

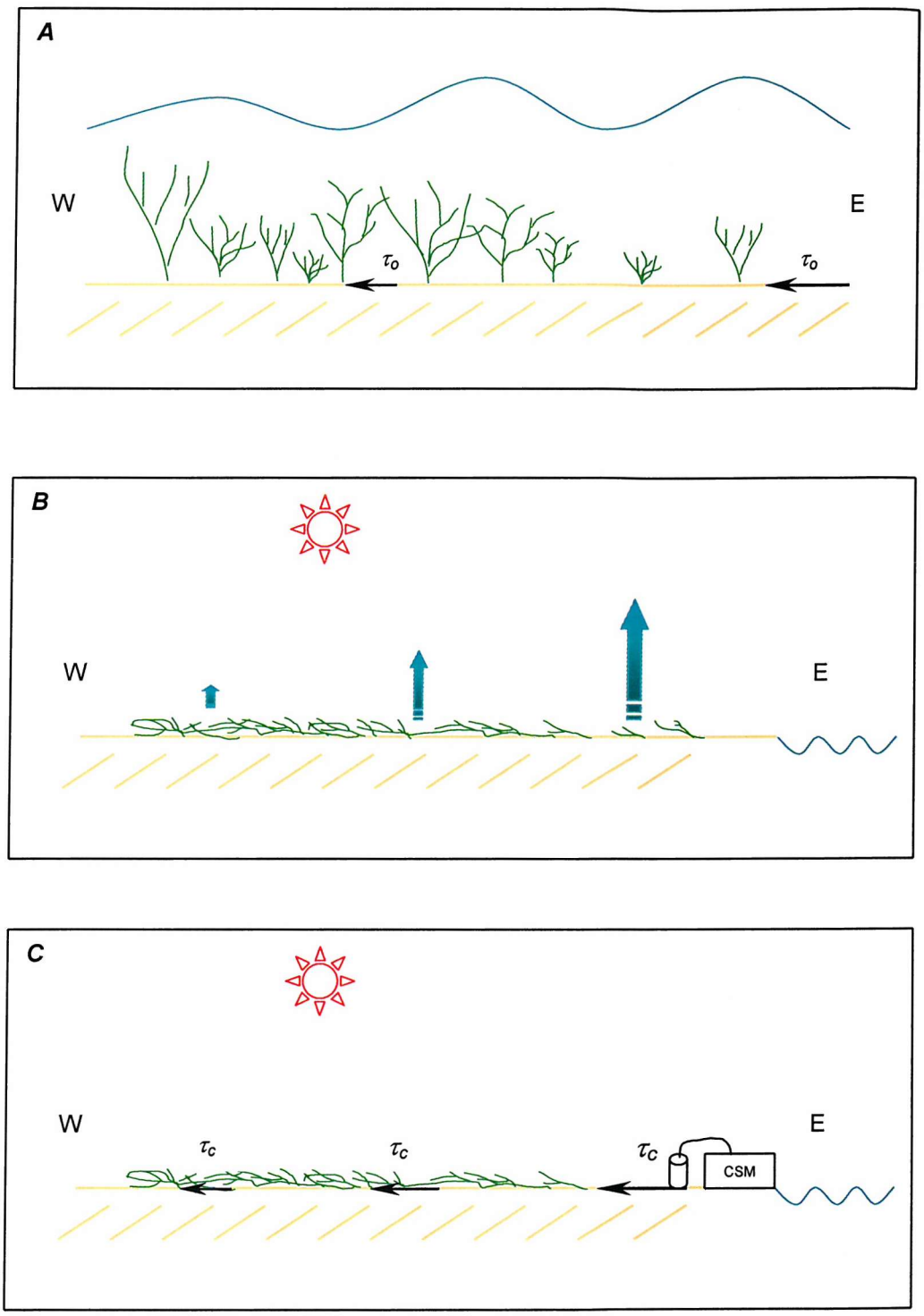

Figure 5.30. Conceptual model of the possible mechanisms proposed to correlate the reduction of τ_c along the E-W transect with the highest sea grass density cover and the highest water content. During inundation, the reduction of the shear stress applied at the sediment/water interface is controlled by high densities of sea grass which can reduce the bed shear stress westward (A). During exposure the density of macroalgae and seagrass that protected sediments from solar radiation and prevented the drainage can reduce evaporation (B). The erosion threshold is influenced by the water content (i.e. bulk density) of surficial sediments (C).

5.6. Summary

- The elevation of *Palude della Centrega* is close to the MSL. The elevation varies from 0 to 25 cm and is characterised by three different seasonally dependent habitats. These are: (1) *Spartina* spp.; (2) *Zostera noltii* spp. (absent in the winter) and (3) microphytobenthos.

- No significant changes were found in the mean grain size of sediment between summer and winter deployments. Significant increases in chlorophyll *a* and colloidal carbohydrate content were found during the summer, suggesting higher biological activity.

- The VSS varies from 1.16 to 4.68 kPa and was 6.33 % higher during August 1998 (average value 2.11 kPa) than during February 1999 (average value 1.97 kPa) suggesting a biological influence on sediment stabilisation.

- The average value of erosion threshold derived in November 1999 using the CSM was 0.47 Pa.

- Despite all technical limitations of the TSM (from which the VSS is derived) and CSM (from which τ_c is derived), a clear trend emerged in the spatial variation of sediment stability. The best predictors of the VSS and τ_c are elevation and bulk density (sediment stability was generally higher between the *Spartina* spp. canopy along the N-S transect).

- A conceptual model has been proposed to explain the variation of τ_c along the E-W transect in relation to different bulk densities (Fig. 5.5.4.), in relation to habitat, hydrodynamics and sediment exposure.

- A comparison carried out on an homogenous layer of sediment revealed that the τ_c derived by using the CSM is about 50% less than the τ_c derived using the MF.

CHAPTER 6: THE EVOLUTION OF PALUDE DELLA CENTREGA

6.1. Introduction and background to the short-term and long-term studies to investigate morphological changes of Palude della Centrega

The salt marsh area is decreasing in Venice Lagoon at a rate of about 1 km^2/a (CNV, 1996; DAY *et al.*, 1999). As a result, many studies have been conducted to determine the short-term (DAY *et al.*,1998a; DAY *et al.*,1998b), and long-term (FRIGNANI, 1999, COCHRAN *et al.*, 1998; BATTISTON *et al.*, 1987), evolution of intertidal areas in different parts of Venice Lagoon. The evolution of *Palude della Centrega* which was unknown prior to this work, was examined using a variety of techniques to evaluate long-term (decadal) and short-term (annual) trends. The area is not subject to the erosive trends evident further to the south. The primary objective of this chapter is to quantify the evolutionary trend of the site, and to quantify accretion/erosion rates in the area.

Short-term bed level changes

Intertidal deposits are extremely susceptible to short-term changes in elevation (PETHICK, 1992) due to frequent inundation by high-energy shallow waters and the high mobility of fine-grained particles (WHITEHOUSE & WILLIAMSON, 1996). For example, O'BRIEN *et al.*, (2000) demonstrated that the mudflats of the Severn Estuary have a multi-timescale combination of periodic and episodic events; erosion by waves was observed during winter and deposition of a 10 cm thick, soft mud layer observed by tidal currents took place during summer.

Due to the dynamic nature of intertidal sediments, *in-situ* monitoring of changes in bed level can be an effective way to determine short-term trends. This method provides quantitative information from which mass balance estimates may be made. In turn, the mass balance can be used to calibrate numerical simulations of tidal flat evolution (KIRBY, 1990; 2000).

Many factors can effect changes in mudflat elevation, the most important of which are: sediment input (AMOS *et al.*, 1996b); consolidation (SCHIFFMAN *et al.*, 1985); surface erosion (O'BRIEN, 1998); chemical and biological processes (FRIEND, 2001); and the formation/migration of bedforms (WHITEHOUSE *et al.*, 2000).

Many intertidal accretion/erosion studies have used single poles to measure bed level (RANWELL, 1964; FROSTICK & MCCAVE, 1979; BALE *et al.*, 1985; KIRBY *et al.*, 1993). By using two poles the effect of scouring is reduced (O'BRIEN, 1998). The method is a fast, cheap and accurate way of determining bed level elevation on intertidal mudflats, if there is no settlement of the poles.

An alternative method of determining the accretion rate of intertidal deposits in Venice Lagoon was achieved by marking an horizon using a buried tracer (FRIGNANI, 1999). Small sediment cores were then collected and the accretion rate was derived from the varying depth through time of the marker in the sediment column. This method gives good results only if the bioturbation by macro fauna is low. Vertical migration of organisms and growth of plant roots can mix the sediments very effectively.

DAY *et al.* (1998a; 1999) monitored bed level changes using the Sedimentation Erosion Table (SET) described by BOUMANS & DAY (1993). The authors investigated soil accretionary dynamics on varying time scales in six wetlands of Venice Lagoon and showed that only three of the studied areas have an accretion rate sufficient to offset relative sea level rise.

Long-term morphological changes

Morphological changes over time within *Palude della Centrega* are amongst the most important indicators of the long-term evolutionary trend of intertidal mudflats (KIRBY, 1990). Since colonisation of Venice Lagoon by humans, significant morphological changes have taken place (such as sea defence, navigation, channel dredging, aquaculture). In the 20th century, the impact of human activities on the morphological evolution of the Lagoon has increased (FAVERO, 1992). Some of the inpacts on the ecosystem (water extraction, dredging of channels, intense navigation, etc.) have had negative effects on the stability and conservation of the intertidal areas. Other changes have had a positive feed-back on their evolution e.g. the discharge of nutrients and pollutants has increased vegetation growth in some areas stabilising the sediments (PIGNATTI, 1966; RUNCA *et al.*, 1993). A general scheme, which summarises how human activities are linked to the morphological evolution of the intertidal mudflats in Venice Lagoon, is shown in Fig. 6.1. (after CNV, 1992).

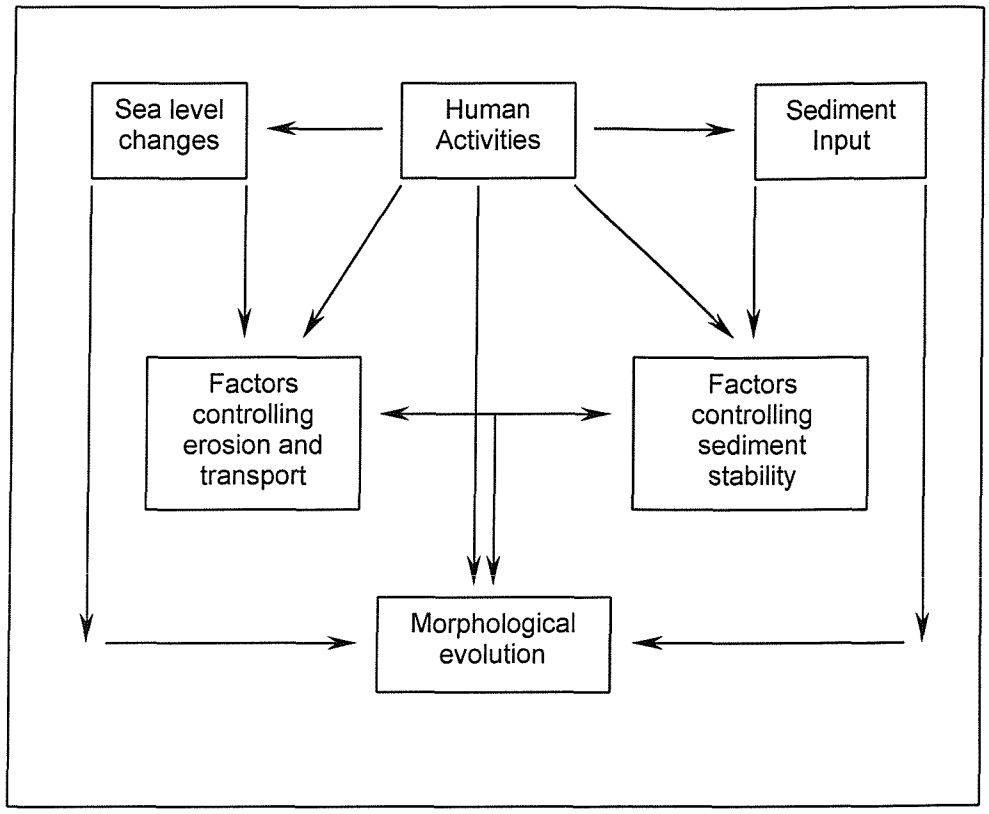

Figure 6.1. General scheme of the relationship between human activities and morphological evolution of the intertidal areas of Venice Lagoon (CNV, 1992).

In order to evaluate the erosion/accretion of the study site over a time-scale equivalent to the period during which detailed charts of the Lagoon were produced, the sediments of *Palude della Centrega* were dated by detection of radionuclides: ^{137}Cs and ^{210}Pb. ^{137}Cs has a half-life of about 30 years. It was introduced into the atmosphere in the 1950's by nuclear tests (SHARMA *et al.*, 1987) and started to become incorporated in sediment after 1952, reaching peak fallout in 1963. A second peak resulted from the release of ^{137}Cs into the atmosphere in 1986 after the Chernobyl nuclear station accident. A time lag of about 6-12 months exists between the atmospheric fallout and accumulation of radionuclides in sediment (RITCHIE *et al.*, 1973) as a result of processes that control the erosion and deposition of sediment.

The long-term sedimentation rate can be determined from the distance between the ^{137}Cs peaks found in the sediment column using the following relation:

$$\frac{dh_P}{dt} = \frac{h_{P1} - h_{P0}}{t_1 - t_0} \qquad \text{cm/a} \qquad 6.1.\text{I}.$$

Where dh_P/dt is the long-term accretion rate, h_{P1} is the depth of the upper ^{137}Cs peak and h_{P0} is the depth of the lower ^{137}Cs peak. t_1 is 1986 and t_0 is 1963.
After introduction into the sediments, concentration peaks of ^{137}Cs can vary due to many chemical, biological and physical factors. These include migration, reworking and bioturbation (CUNDY & CROUDACE, 1996).

^{210}Pb has an half-life of 22.3 years and is a decay product of ^{222}Rn which is a rare atmospheric gas (a volatile decay-product of Uranium present in the earth's crust). It is usually found in sediments where it is adsorbed by clay particles, and is buried within the sediment. Similarly, ^{210}Pb is removed from the atmosphere by precipitation. ^{210}Pb can also be found directly trapped in sediment as a decay product of ^{222}Rn (a decay product of ^{226}Ra and ^{238}U). As it is a radionuclide, ^{210}Pb follows an exponential decay rate that is used to estimate the accumulation rate in a sediment column. The decay law is defined as:

$$A_t = A_o e^{-\lambda t} \qquad \text{Bq/g} \qquad 6.1.\text{II}$$

where A_t is the activity at time t, A_o is the activity in the original material (Bq/g), λ is a decay constant (0.3114 for a 22.3 year half-life) and t is the time since the decay began. ^{210}Pb is usually measured as excess ^{210}Pb.

Both ^{137}Cs and ^{210}Pb are valuable indicators of recent accumulation rates of accretionary deposits and they have been successfully used to date sediment from different coastal environments (BERGER, 1987; BRIKER-URSO *et al.*, 1989, CROUDACE & CUNDY, 1995; CUNDY *et al.*, 1998). However, the accretion rate derived using equations 6.4.I and 6.4.II does not consider the influence of erosion events, which may occur in the area (PETHICK, 1992). In Venice Lagoon, ^{137}Cs and ^{210}Pb sediment dating techniques were applied by MARCOMINI *et al.*, (1997), FRIGNANI *et al.*, (1997) and COCHRAN *et al.*, (1998) in order to determine the accretion rate of different salt marshes. The results showed that accretion rate varied from 0.3 to 2.3 cm/a depending on the position within the Lagoon, the vegetation cover and the changes of sediment input.

6.2. Method

6.2.1. Monitoring of bed level changes of Palude della Centrega

Short-term evolution was evaluated from changes in bed elevation measured at 13 of the 14 stations of *Palude della Centrega* (Fig. 5.16.). Steel poles (2 cm diameter and 1.5 m long). These poles were driven approximately 0.75 m into the mudflat and a cross bar was placed on the top of the two poles (Fig. 6.2.).

Figure 6.2. The two poles and the cross bar used to measure changes in bed level elevation.

The distance to the mud surface from the cross bar was measured every 15 cm along the bar. Measurements were repeated six times; approximately every two months from August 1998 to February 1999, then in June and November 1999. Data collected at St13 (Fig. 5.16.) were not included in the work because the poles were placed across a laterally migrating tidal creek and the accretion rate derived at that site was not considered representative of the vertical accretion of the mudflat.

The rate of change of the local bed level $\frac{dh}{dt}$ between periods of measurements was calculated using the following equation:

$$\frac{dh}{dt} = \frac{h_1 - h_0}{t_1 - t_0} \quad \text{cm/a} \qquad 6.2.1$$

where h_1 is the mean bed level at t_1, h_0 is the mean bed level at time t_0, t_1 is time 1 and t_0 is time 0 (i.e. beginning of monitoring).

6.2.2. Long-term study of salt marsh distribution in Palude della Centrega

Long-term evolution of the salt marsh was assessed from morphological changes that occurred during the 20th century evident from topographic charts (scale 1:25000 and 1:10000) of *Palude della Centrega*. Charts were produced in 1908, 1931, 1968, 1977 and 1980 by the *Istituto Geografico Militare* (IGM). The extent of the tidal flats between *Canale Scanello* and *Canale S'Antonio* was determined using an electronic digital planimeter PLANIX 5000. It was not possible to use charts produced before 1908 as the topographic data were not referenced to MSL (DENEIX, 1896) and therefore the extent of tidal flats illustrated on these early charts is considered unreliable.

6.2.3. Radionuclide analyses

^{137}Cs and ^{210}Pb activity was measured in the top 50 cm of a 1.3 m-long gravity core collected in station V40 in August 1998. The gravity core was stored at 5 °C immediately after collection. The cores were x-rayed and described visually then subsampled at 1 cm intervals (CIAVOLA & COVELLI, 2000). Samples were analysed at the University of Southampton using the facilities of the Geoscience Advisory Unit (http://www.soton.ac.uk/socfac).

6.3. Results

6.3.1. Short-term accretion rate of Palude della Centrega

The overall mean increase in bed level across all stations was 2.03 cm during the 16 month study period. This corresponds to an overall mean accretion rate of 1.52 cm/a. Along the N-S transect the maximum accretion rate (5.6 cm/a) was measured at St3 and the minimum (-2.14 cm/a) at St6 (Fig. 6.3.A); the average accretion rate was 2.36 cm/a. Along the E-W transect, the accretion rate decreased to the east. The maximum accretion rate (+2.70 cm/a) was measured at St12 and the minimum (-0.39 cm/a) at St16 (Fig. 6.3.B.); average accretion rate was 0.95 cm/a. Results of the short-term relative changes in bed level elevation measured in this study are reported in Tables 6.1. and 6.2. The time series of bed level elevation is illustrated in Fig. 6.4. (N-S transect) and Fig. 6.5. (E-W transect).

Elevation

Station	9/8/98	16/10/1998	18/12/98	24/2/99	21/6/99	11/3/99
Num	cm	cm	cm	cm	cm	cm
1	-	-	+1.6	+2.1	+2.3	+3.9
2	-	-	+1.3	+1.8	+1.5	+3.1
3	-	-	+4.4	+4.4	+3.8	+7.1
4	-	-	+0.8	-0.4	+2.6	+4.3
5	-	-	+0.7	+1.5	+0.9	+0.8
6	-	-0.2	+1.5	+1.9	+1.4	-2.7
7	-	+0.9	+3.9	+4.5	+3.8	+3.8
Average	-	+0.3	+2.0	+2.3	+2.3	+2.9
Rate of change in elevation						
Num	cm	cm/a	cm/a	cm/a	cm/a	cm/a
1	-	-	+9.2	+2.5	+0.7	+4.5
2	-	-	+7.4	+2.8	-1.0	+4.7
3	-	-	+25.3	+0.3	-1.8	+9.4
4	-	-	+4.8	-5.9	+8.9	+4.9
5	-	-	+4.2	+3.9	-1.9	-0.1
6	-	-1.3	+9.8	+2.1	-1.4	-11.9
7	-	+5.5	+17.5	+2.8	-2.2	+0.0
Average		+3.0	+11.2	+11.1	-0.1	+ 1.6

Table 6.1. Bed level elevation and accretion/erosion rates calculated for each time interval for data collected along the N-S transect.

Elevation

Station	9/8/98	16/10/1998	18/12/98	24/2/99	21/6/99	11/3/99
Num	cm	cm	cm	Cm	cm	cm
10	-	-0.5	+0.8	+1.3	+1.7	+1.7
11	-	-1.0	+0.7	+1.3	+1.3	+0.7
12	-	-0.6	+2.1	+2.1	+2.1	+3.4
13	-	-	-	-	-	-
14	-	+1.0	+2.7	+3.1	+3.5	+1.4
15	-	-0.8	+1.3	+1.6	+1.6	+0.2
16	-	-0.9	-0.2	-0.3	-0.7	-0.5
Average		-0.5	+1.2	+1.5	+1.6	+1.2
Rate of change in elevation						
Num	cm	cm/a	cm/a	cm/a	cm/a	cm/a
10	-	-2.8	+7.3	+2.4	+1.3	+0.0
11	-	-6.1	+9.8	+3.4	-0.3	-1.5
12	-	-3.5	+15.6	-0.2	+0.2	+3.6
13	-	-	-	-	-	-
14	-	+5.9	+10.0	+1.9	+1.1	-5.8
15	-	-5.0	+12.2	+1.9	-0.2	-3.9
16	-	-5.7	+4.4	-0.7	-1.0	+0.5
Average	-	-2.9	+9.9	-1.4	-0.2	+ 1.2

Table 6.2. Bed level elevation and accretion/erosion rate calculated for each time interval for data collected along the W-E transect.

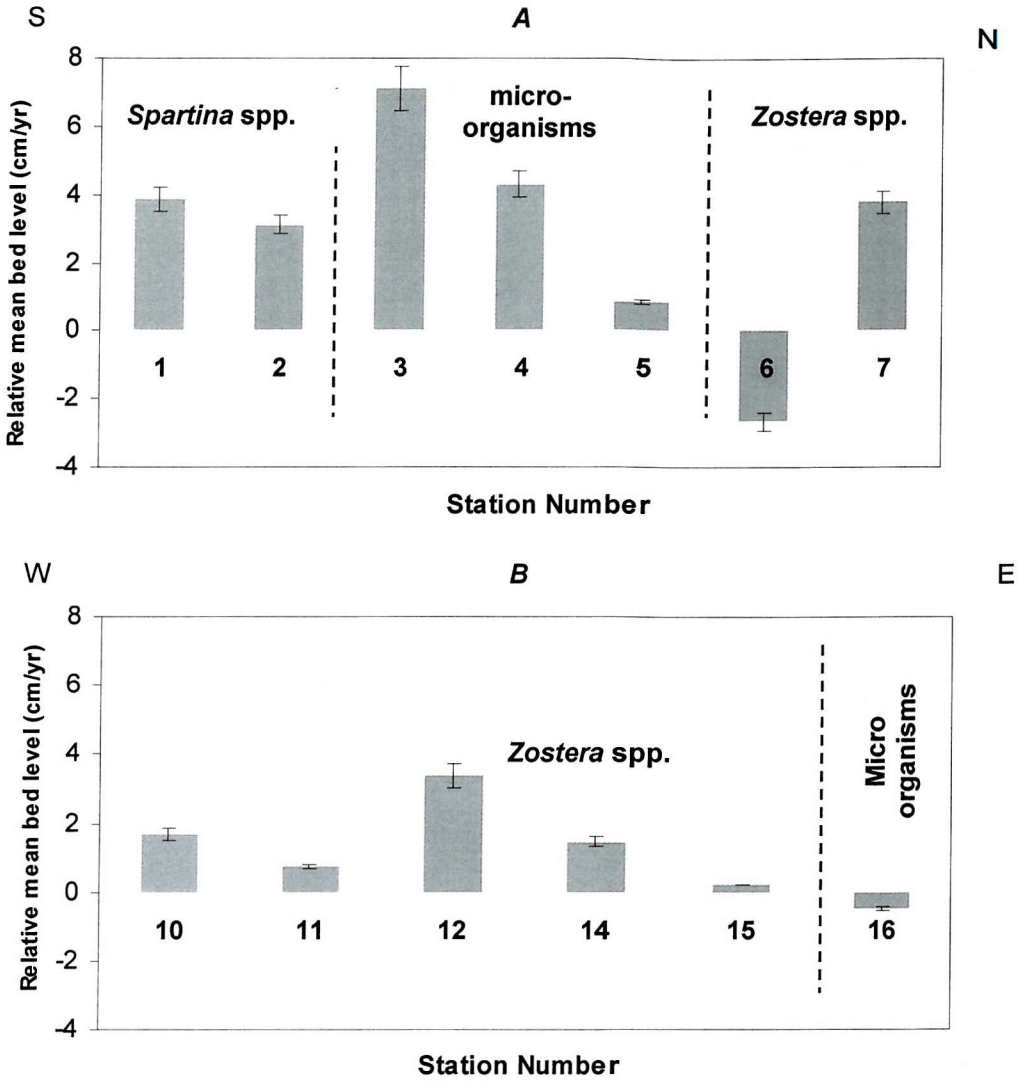

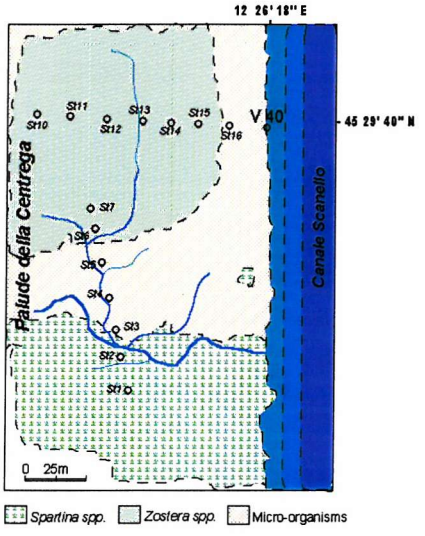

Figure 6.3. Changes in bed level elevation at stations along the N-S transect (*A*) and E-W transect (*B*). Note that maximum accretion rate was found in the upper part of the studied area (N-S transect) and lower values found close to the tidal creeks.

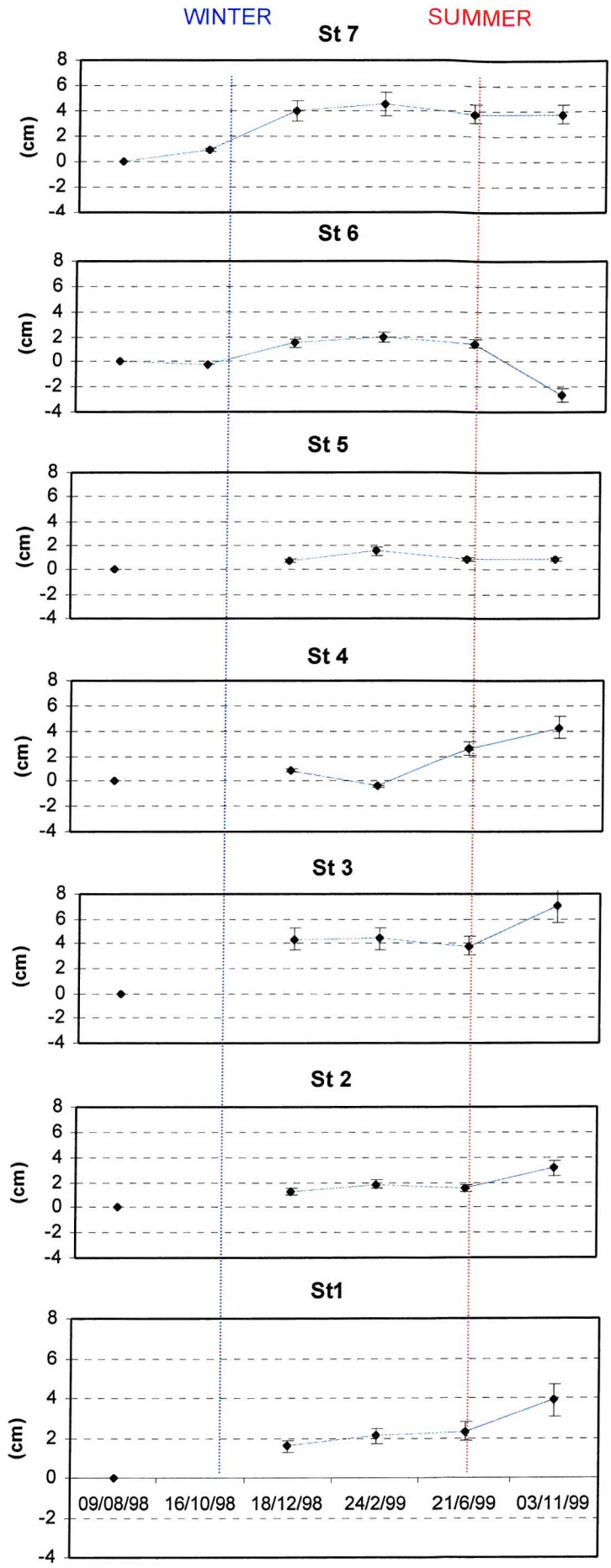

Figure 6.4. Changes in mean bed level elevation through time along the N-S transect. At St1, St2, St3, St4 no data were collected on the 16th October 1998.

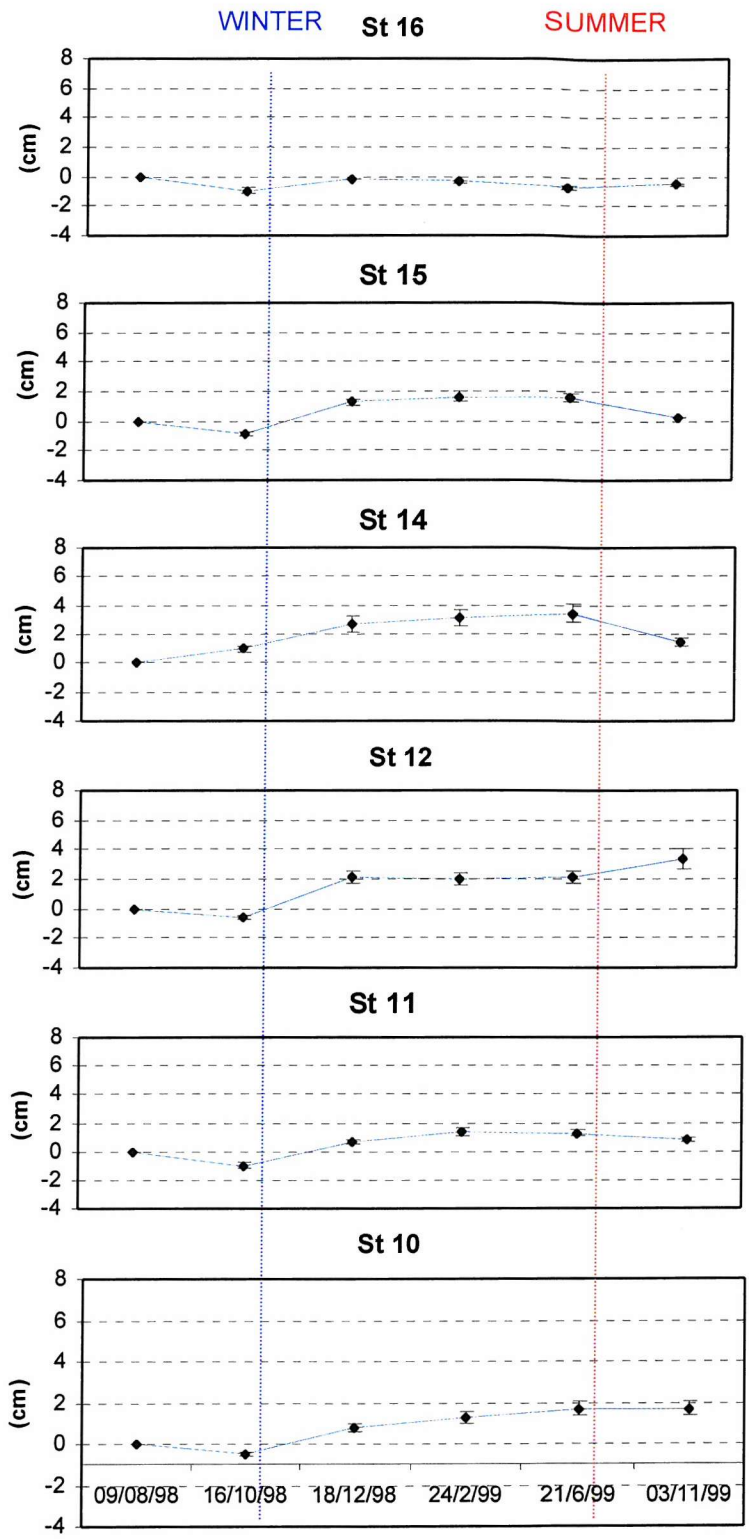

Figure 6.5. Changes in mean bed level elevation through time along the E-W transect.

6.3.2. Long-term accretion rate of Palude della Centrega

Results of the comparison between charts are summarised in Table 6.3. These show an increase in the supratidal saltmarsh area of *Palude della Centrega* of about $2.5x10^{-4}$ km^2/a since 1908.

Date	Source and scale	Extent of tidal flats (km^2)
1908	Chart (1:25000)	~0.427
1931	Chart (1:25000)	~0.494
1968	Chart (1:25000)	~0.562
1977	Chart (1:10000)	~0.579
1980	Chart (1:25000)	~0.61

Table 6.3. The areal extent of the supratidal areas of *Palude della Centrega* during the 20th century.

Two of the most representative images showing the change in morphology of the studied area are illustrated in Fig. 6.6. and 6.7. which show that a westward migration of *Ghebo* (channel) *Scanello* took place in the 20th century. It was originally mapped as a single channel having an arcuate NE-SW orientation (Fig. 6.6.). Subsequently, a new channel formed (CAVAZZONI, 1977) flowing in from the north (Fig. 6.7.). The bathymetric evolution of the surrounding channels could have been included in this study in order to define changes in the morphological evolution of the subtidal areas of *Palude della Centrega* (e.g. siltation; migration of channels bars; CNV, 1996).

It was not possible to obtain an accretion rate from the dating analysis, because levels of the radionuclides ^{210}Pb and ^{137}Cs were below normal background level.

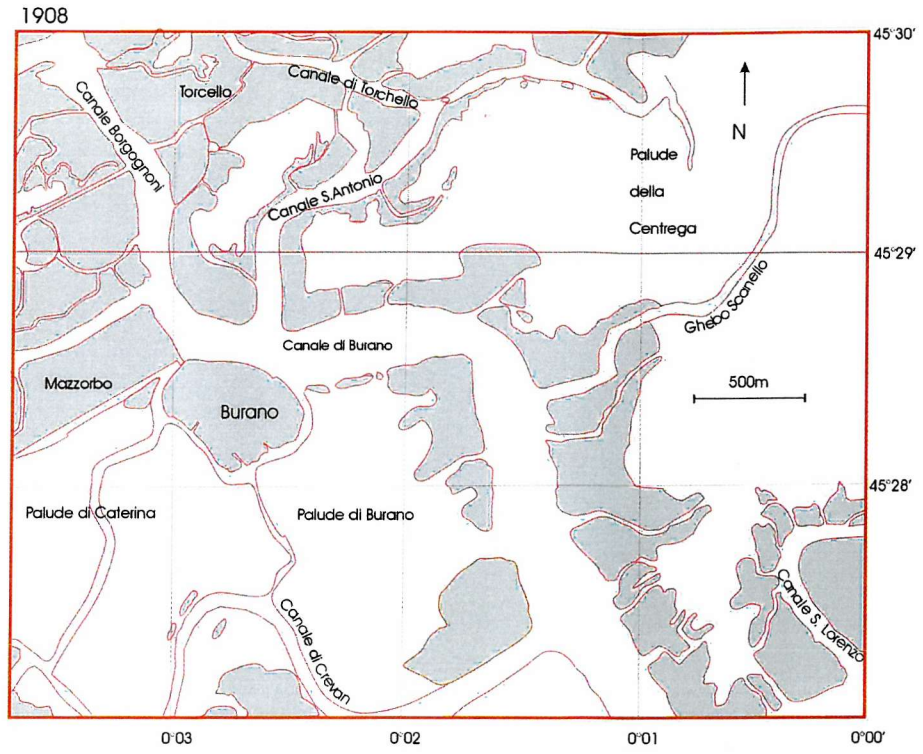

Figure 6.6. A digital map of *Palude della Centrega* from data collected in 1908. Salt marshes are indicated in grey (their elevation is 0<Z<0.5 m).

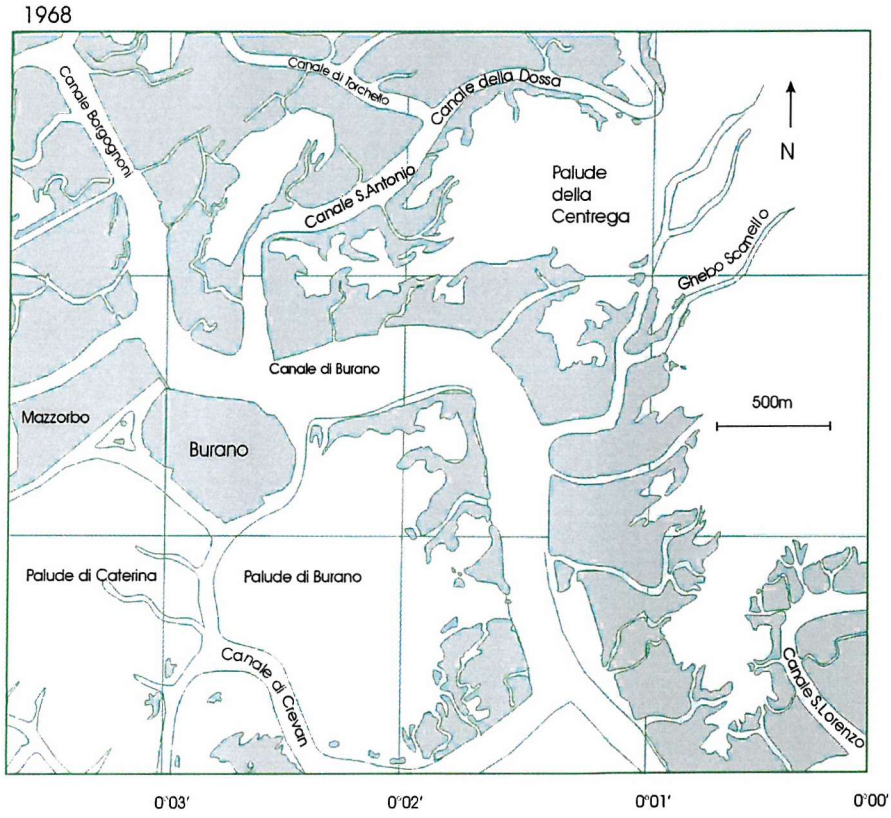

Figure 6.7. A digital map of *Palude della Centrega* during 1968. Salt marshes are indicated in grey (their elevation is 0<Z<0.5 m).

6.4. Discussion

Morphological analysis shows that the western fringes of *Palude della Centrega* were protected with a series of containment pilings at the beginning of the 20th century. This artificial protection prevented sediments from being eroded by breaking waves and promoted accretion (DAY *et al.*, 1998b). As a consequence sedimentation took place and the areal extent of the salt marshes increased during the last century.

A mean accretion rate of 1.52 cm/a was considered representative of *Palude della Centrega* for the purposes of this study. This value compares well with the accumulation rates found by DAY *et al.* (1998a), FRIGNANI *et al.* (1997) and DONAZZOLO *et al.* (1982) in other areas of Venice Lagoon. Net accretion rates of 2.84 cm/a, 1.47 cm/a, 1.52 cm/a were found in areas colonised by *Spartina* spp., *Zostera* spp. and the micro-phytobenthos respectively, showing the clear effect of the rooted vegetation in promoting deposition. No significant differences were found in the seasonal fluctuations of bed level changes, but the highest accumulation of sediments was observed in the inner part of the intertidal flat and the lowest on the marsh front located close to *Canale Scanello* (St16). This suggests that the channels are migrating through bank erosion (Fig. 6.8.). DAY *et al.* (1998a) found very similar results after two years of short-term sedimentation/erosion monitoring on a salt marsh in the southern part of Venice Lagoon; the marsh front was being eroded vertically at a rate of 4.12 cm/a whereas, on the inner part, accretion of 2.32 cm/a was taking place.

Lack of any detectable sedimentation rates from the radionuclide analysis was attributed to the location of the gravity core, collected at the edge of a migrating tidal channel (Fig. 6.8.). More recently, CIAVOLA *et al.* (in press) derived an accretion rate of 1.32 cm/a from a ^{210}Pb profile of the sediment collected in the upper part of a *Spartina* spp. vegetated salt marsh on *Palude della Centrega*.

This value is similar to the average short-term accretion rate derived from the bed level elevation measurements. This accumulation rate is high compared with other sites in Venice Lagoon. However, it is compatible with the accretion rate proposed by FRIGNANI *et al.* (1997) and DONAZZOLO *et al.* (1982).

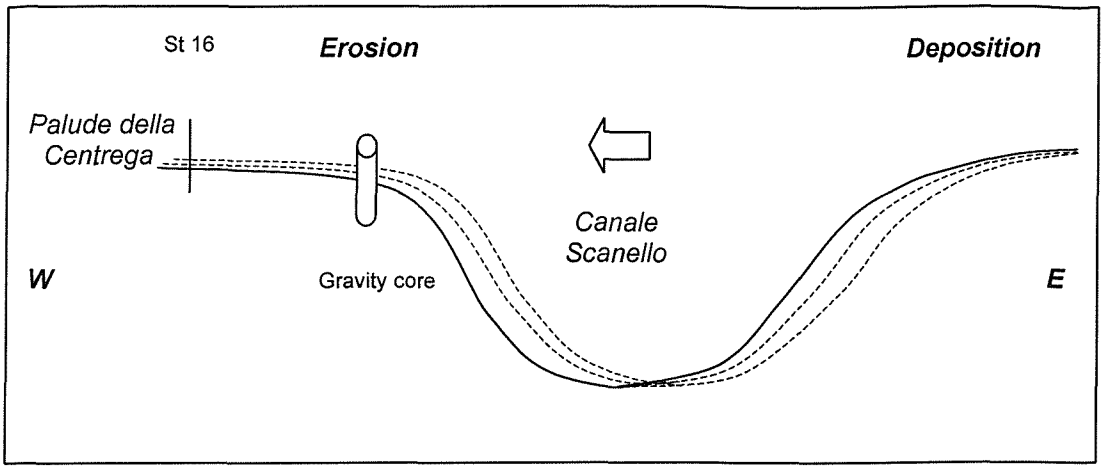

Figure 6.8. A schematic representation of the migration westwards of *Canale Scanello* (arrow indicates the direction of migration). Morphological analysis of the studied area suggests long-term migration westwards of the channel. Note that on the western flank of the channel, both the gravity core and St16 revealed erosion.

CHAPTER 7: PREDICTION OF TIDAL FLAT EVOLUTION

A background to the modelling of intertidal areas

The factors controlling the evolution of muddy intertidal areas is a large unresolved problem in coastal management. However, models to predict the evolution of mudflats are evolving rapidly. In the last 10 years, many complex new processes have been found to simulate cohesive sediment transport (CST) (MCANALLY & METHA, 2001). ROBERTS & WHITEHOUSE (1997) have presented a complete literature review concerning the evolution of intertidal cohesive sediments, highlighting many reasons why it is difficult to develop a realistic model. The most significant problems are:

- sediment properties in suspension (changes of floc strength and dimension through time; changes in settling velocity with SSC);
- the rate of self-weight consolidation and deposition;
- the modes of mud transport: (1) in suspension; (2) as bedload; and (3) as mud clasts moving across the bed;
- the unpredictable behaviour of a sand-mud mixture (as mudflats are rarely composed of pure mud);
- changes to sediment properties during subaerial exposure;
- the patchiness of sediment stability due to bioturbation/biostabilisation;
- the complex hydrodynamics of the flooding and drying of mudflats, especially when the slope of the intertidal area is sub-horizontal as in the microtidal estuaries; and
- the determination of shear stresses applied by the combined action of wave motion and tidal currents.

Despite these problems many models are available which can be subdivided (in order of complexity) into zero dimensional (0-D), one dimensional (1-D), two dimensional (2-D) and three dimensional (3-D) models. One of the biggest limitation of simulating CST is the computer capacity which restricts model runs to short periods (up to a few days) if many processes are included (particularly in 2-D and 3-D models; MCANALLY & METHA, 2001).

In Venice Lagoon, DI SILVIO & GAMBOLATI (1990) proposed a 2-D model to predict the long-term morphological evolution from a non-uniform grain size distribution. The authors distinguished the shoals from the channels, using different grain sizes. It was assumed that net transport through the Lagoon was zero and that the average concentration in the water column was almost the same across the Lagoon.

SILVA & MOL (1993) have applied a 0-D procedure to Venice Lagoon. They modelled the sediment budget of the entire Lagoon on the basis of an average concentration of sediment in shallow areas and canals over a full year. A rooted vegetation coefficient was included to model the biological protection by seagrass and benthic fauna in Venice Lagoon, but it was a major uncertainty in their model. The authors simulated erosion of shallow water areas and salt marshes; at the same time as sedimentation of natural and artificial channels following a scheme reported in Fig. 7.1.

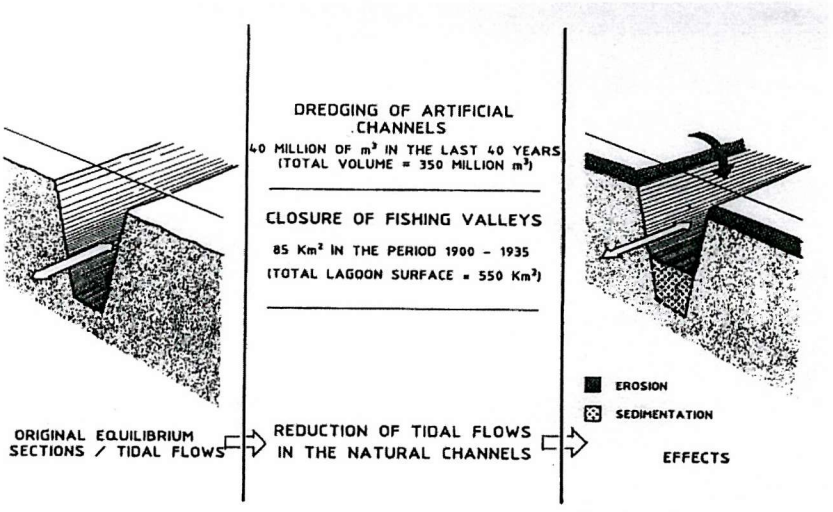

Figure 7.1. The internal sediment redistribution model of Venice Lagoon (SILVA & MOL, 1993).

In the present study, a new 0-D sediment transport model called SLIM (Simulation of LIttoral Morphodynamics) was developed with the advantage of looking at multiple scenarios.

7.1. Description of the SLIM model

The sediment transport model SLIM is written in Quick Basic (QB)45. It can be defined as a "bed stability model" in the sense that sediment transport is controlled by thresholds of erosion and deposition. It provides a time series output of bed level response based upon a set of input parameters. The model was used to calculate the bed shear stress, the SSC, the eroded and deposited mass, the variation of erosion threshold through time and the bed level for a given time series (Fig. 7.2.).

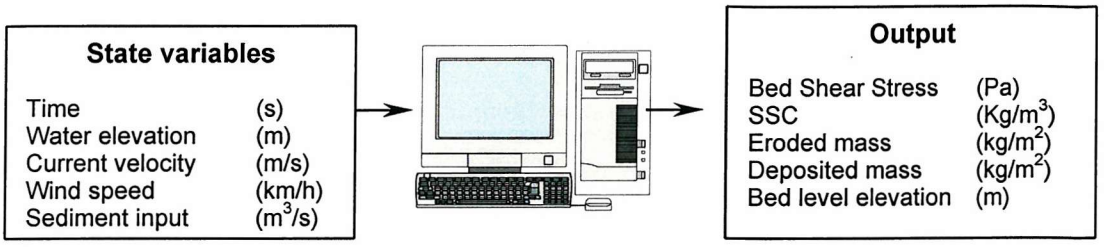

Figure 7.2. A scheme of the input and output values of the SLIM model used for simulations.

All parameters were time-stepped at increments of 5 minutes. A total of 9506 steps were undertaken in order to run the simulation over a time of 792 hours using 30 days of real data and 3 days of no forcing conditions.

The equation for the conservation of mass is:

$$\frac{dM}{dt} = \boldsymbol{BF} + \boldsymbol{SI} - \boldsymbol{SE} \qquad 7.1.1$$

where dM/dt represents changes in the suspended Mass (M), BF represent the benthic flux (deposited - eroded masses), and SI and SE represent a positive and negative sediment input respectively from advected sources.
A schematic representation of the inputs is shown in Fig. 7.3. and a flow diagram representing the detailed structure of the model is shown in Fig. 7.4.

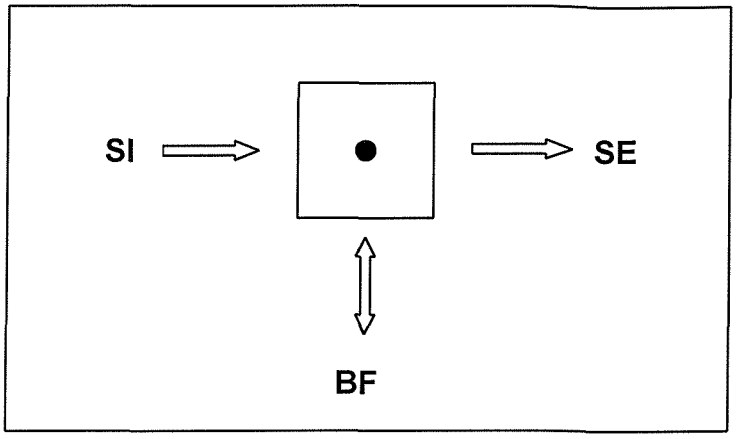

Figure 7.3. Simple representation of the box model (SLIM) showing the boundary conditions of the mass conservation equation. SI represents sediment input, SE represents sediment export which reduces the SSC in the water column and BF represents the benthic flux which is controlled by intermittent erosion and deposition processes.

The bed shear stress applied by waves and tidal currents is first computed for the duration of the time series. If the stress is above the erosion threshold, sediments are resuspended. If it is below the deposition threshold, sediments are deposited. If between the two values, sediments are transported with no deposition or erosion. Erosion and deposition rates are calculated as a function of the excess shear stress using the relationship proposed by SHENG & LICK (1979) and KRONE (1962).

The increase of τ_c with depth was simulated in the model using the following equations (after BAGNOLD, 1956; p 240):

$$\Delta\tau_c = \tau_{cs} + \Delta\sigma' \tan(\phi) \qquad 7.1.\text{II}.$$

and

$$\Delta\sigma' = \gamma_d z - p = (\rho_s - \rho_w)\, gz - p \qquad 7.1.\text{III}.$$

where ϕ is the internal friction angle, τ_{cs} is the erosion threshold at sediment surface, σ' is the effective stress, z is the depth (m), p is excess pore pressure. The excess pore pressure was set at zero in this study.

When the water elevation is below MSL the erosion and deposition processes can increase or decrease the concentration in the water column without changing the bed level elevation of the exposed mudflat (which in this specific study is above MSL). The concentration values can also vary under the effect of the input/export of sediment from the water column, which can be set up at different rates in order to simulate different scenarios. When the deposition processes are simulated during the exposure of the mudflat (low tide), sediments are deposited in the subtidal areas without contributing to the accretion of the area. Finally, changes in elevation are

computed from the integration of the mass eroded and deposited on the mudflat during flooding. The final value of the station elevation is transformed into an erosion/accretion rate (cm/a) and is written in an output file created at the end of the run.

7.1.2. Calculation of bed shear stress

The model includes the effects of tidal currents and waves on bed erosion in the calculation of the bed shear stress. The bed shear stress applied by tidal currents (τ_t) was calculated from the depth-averaged water velocity as follows (see Fig. 3.3.C):

$$\tau_t = \rho C_D U^2 \qquad \text{Pa} \qquad 7.1.2.\text{I}$$

where ρ is the water density (1026 kg/m^3), C_D is the drag coefficient (3X10^{-3} for a measurement at 100 cm above bed), U (m/s) is the depth-averaged water velocity (see Fig. 3.3.B).

The wave contribution was modelled by transforming wind speed into bed shear stress using the relation of DHI (1991). The bed shear stress of the wind generated waves (τ_w) was derived using the following equation ROLINSKI & SÜNDERMANN (2001):

$$\tau_w = 0.0007203 * Wv^2 + 0.099206\, Wv - 0.11125 \qquad \text{Pa} \qquad 7.1.2.\text{II}$$

where Wv is the wind velocity (m/s). Changes in bed shear stress due to time variation in the bed roughness and different water depths have not been included in this study.

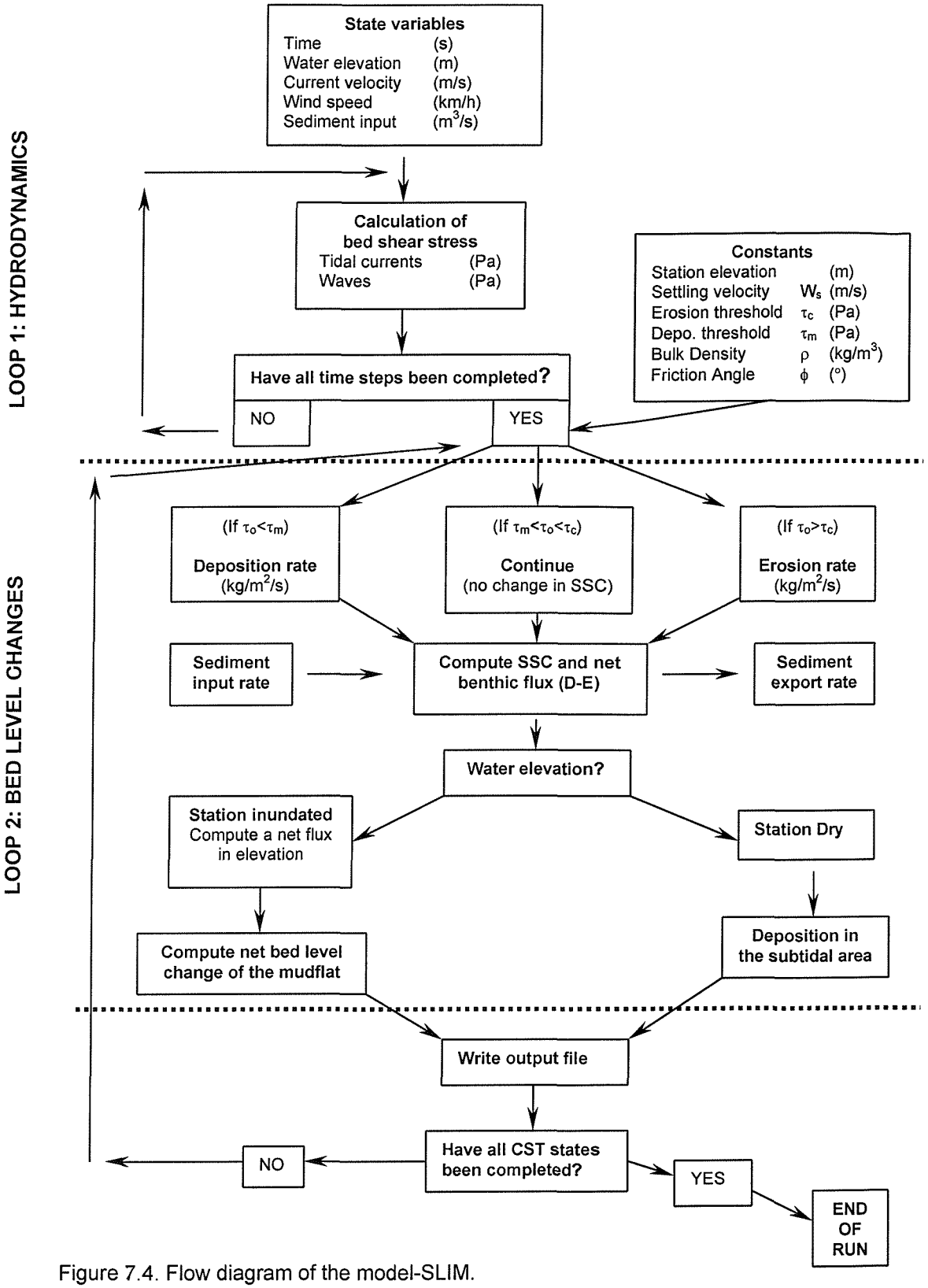

Figure 7.4. Flow diagram of the model-SLIM.

7.1.3. Estimation of erosion rate

An erosion subroutine is invoked when the predicted bed shear stress exceeds the erosion threshold (τ_c). The erosion rate was determined using the following relation from PARTHENIADES (1971):

$$E = \frac{dm}{dt} = M\left[\tau_o - \tau_c\right] \qquad \text{kg/m}^2\text{/s} \qquad 7.1.3.\text{I}$$

where dm/dt is the erosion rate M is an empirical coefficient (4.12×10^{-4} kg/N/s) after SHENG LICK (1979).

7.1.4. The evaluation of deposition rate

A deposition subroutine is invoked to calculate the deposition rate (D) when the predicted bed shear stress is below the minimum shear stress for deposition (τ_m) (METHA & PARTENIADES, 1975). In the present study, the minimum shear stress for deposition was determined from a series of flume experiments using sediment collected at station V40, and was found to be equal to 0.13 Pa.

The deposition rate was determined using the equation of KRONE (1962) and is equal to the product of settling velocity and concentration:

$$D = \frac{dm}{dt} = SSC \cdot Ws \cdot P \qquad \text{kg/m}^2\text{/s} \qquad 7.1.4.\text{I}$$

where $P = 1 - \frac{\tau_o}{\tau_m}$ is the probability of settling, W_s is the mean settling velocity under still water condiutions (1×10^{-4} m/s), and dt is the time step increment (5 minutes). The settling velocity was derived from the Mini Flume experiments using the following equation:

$$Ws = D \cdot \frac{1}{SSC} \qquad \text{m/s} \qquad 7.1.4.\text{II}$$

7.2. Modelling of bed level changes in Palude della Centrega

The assumption made in the present study is that the accretion rate of about 1.52 cm/a measured *in-situ* could be used for the calibration of SLIM. In the present study the simulation ran for 30 days. Therefore, the expected accretion rate, which would validate the model, is about 1.25 mm/month if the accretion rate of the area is considered constant through time. Spatial variation in the accretion rate over the mudflat was not taken into consideration.

7.2.1 Sediment transport under tidal currents

Four simulations were carried out to study the evolutionary behaviour of an intertidal flat without including the effect of wind generated waves in the calculation of the total shear stress. Under the effect of tidal currents, all material at the starting concentration (SSC_o = 80 mg/l) is deposited within 24 hours. Thereafter the water has a very low concentration which fluctuates in phase with changes of water depth (Fig. 7.5.A). Adding an input of sediment of about $3.3x10^4$ t/a, the turbidity shows an average value of about 2 mg/l throughout the simulation resulting in an accretion rate of about 0.5 cm/a (Fig. 7.5.C). A sediment input of $1.32x10^5$ t/a gives an accretion rate on the tidal flat of about 1.55 cm/a (Table 7.1. and Fig. 7.6.) which is close to the average accretion rate measured in the studied area.

Tide	*Waves*	*Erosion threshold*	*Friction angle*	*Sediment export*	***Sediment input***	*Sea level changes*	***Bed level variation***
(Pa)	*(Pa)*	*(Pa)*	*(ϕ)*	*(t/a)*	*(t/a)*	*(cm)*	*(cm/a)*
Yes	No	0.5	10	0	**$3.3x10^4$**	No	**0.459**
Yes	No	0.5	10	0	**$6.6x10^4$**	No	**0.775**
Yes	No	0.5	10	0	**$9.9x10^4$**	No	**1.164**
Yes	No	0.5	10	0	**$1.32x10^5$**	No	**1.552**

Table 7.1. Results of bed level changes under the effect of tidal currents and different sediment inputs.

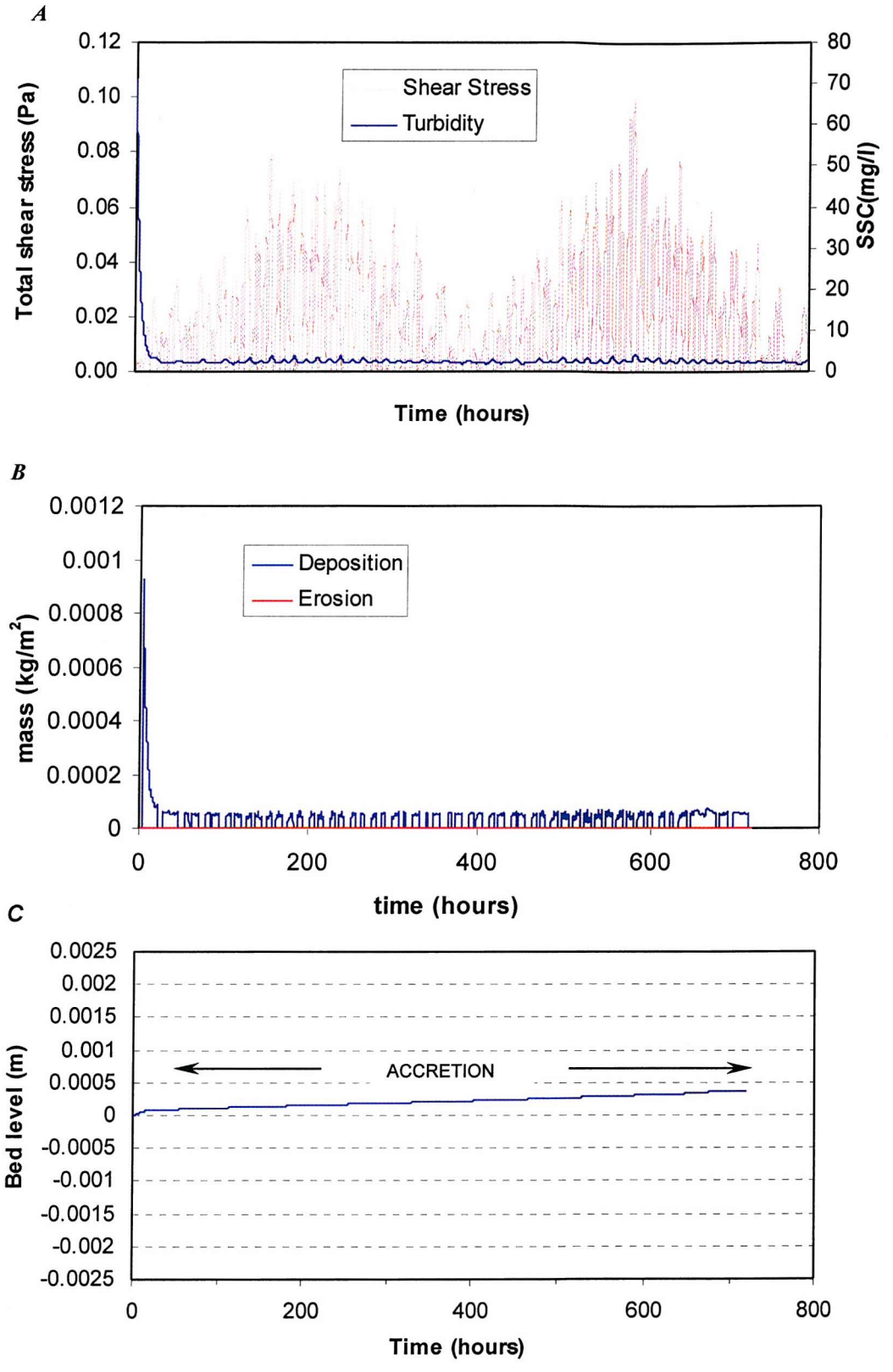

Figure 7.5. Bed shear stress and SSC time series (A), eroded and deposited mass (B) bed level elevation (C) simulated under the effect of tidal currents and a sediment input of 3.3×10^4 t/a. Note the deposited mass goes to zero during the exposure of the tidal flat.

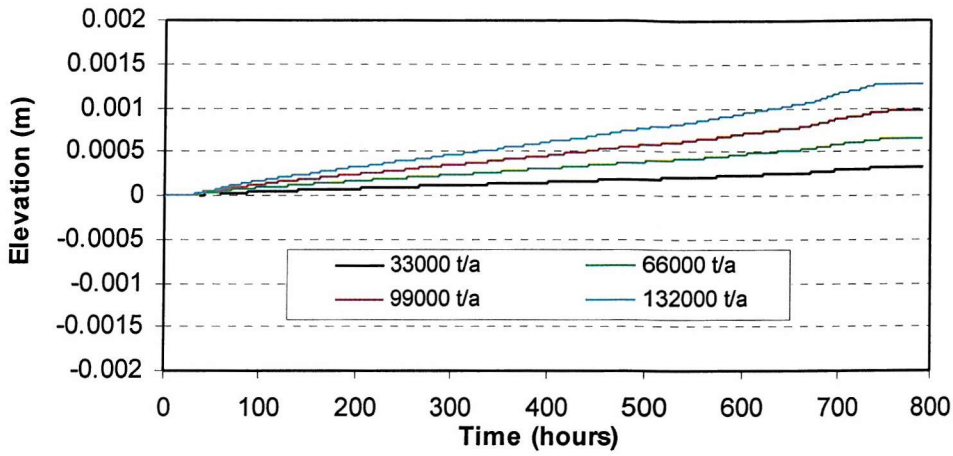

Figure 7.6. Results of bed level changes under the effect of tidal currents and different sediment inputs. Note that the accretion rate increases with increases in sediment input.

Results show that there is no resuspension under the effect of tidal currents on *Palude della Centrega*. This means that without wave motion all suspended mass is deposited resulting in a very low value of turbidity which constrains the mudflat accretion to a constant rate. However, such simulations are valid only for quiet water conditions, and yet resuspension in storms due to waves has been observed.

7.2.2. Sediment transport under the combined effect of tidal currents and waves

There are two main sources of waves in Venice Lagoon: boat traffic and wind generated waves. As *Palude della Centrega* is isolated, it has been considered unaffected by boat waves. Therefore, the bed shear stress resulting from wave motion was derived from a transform of wind speed presented by DHI (1991; see Fig. 3.4.). Results for three of the many experiments carried out to test the model are reported herein. The starting parameters of those experiments are specified in Table 7.2.

Test	Tide	Waves	Erosion threshold	Friction angle	Sediment export	Sediment input	Station depth	Initial concentration
N	**(Pa)**	**(Pa)**	**(Pa)**	**(ϕ)**	**(t/a)**	**(t/a)**	**(m)**	**(mg/l)**
1	Yes	Yes	0.5	10	0	0	< 0.5	0
2	Yes	Yes	0.5	10	0	0	< 0.5	0
3	Yes	Yes	0.5	10	0	$3.3x10^4$	0	0.459

Table 7.2. Results of bed level changes under the effect of tidal currents, waves and different sediment inputs.

The first test was run using an input file characterised by four steps of high wind speed (50 km/h), alternated by calm periods; this was created in order to simulate the effect of erosion and deposition processes in the subtidal areas.

The second test was run under the same boundary conditions as the first, but using real wind velocity data that were measured at *Treporti* (1 km from the studied area) in August 1998. A maximum wind speed of 40 km/h was recorded at that time and this was considered representative of the simultaneous wind speed pattern in Venice Lagoon (CNV, 1992). In these two experiments, changes in sediment concentration due to sediment export or import in the water column were not included.

The third test was run in order to simulate the effect of wave resuspension on an intertidal mudflat with an elevation of 0 cm (MSL), using a sediment input of $3.3x10^4$ t/a which simulates the influence of the river discharge.

A strong linear relationship (r^2=0.97) between the wind speed and the bed shear stress was found (Fig. 7.7.) suggesting that the contribution of tidal currents to the total bed shear stress is small. The results of the simulations are presented in Fig. 7.8., Fig. 7.9. and Fig. 7.10.

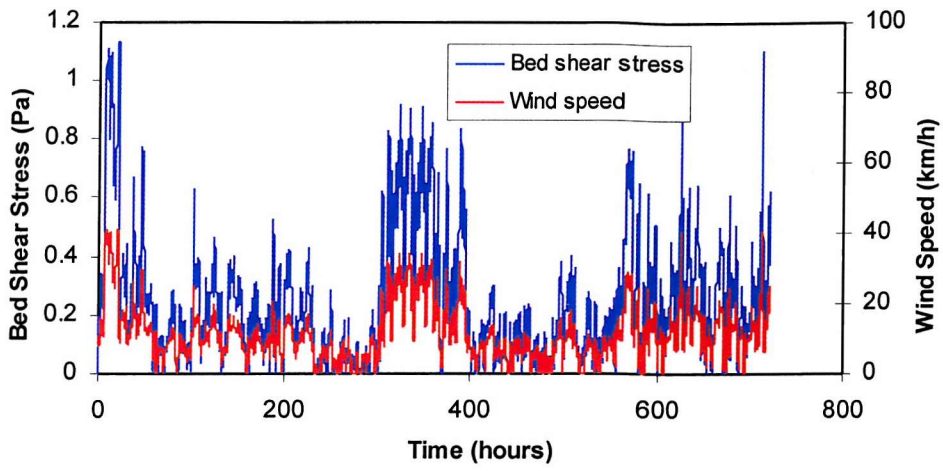

Figure 7.7. A time series of wind speeds measured in *Treporti* station and the bed shear stress computed by the model using the equation 7.1.2.II.

Using the real wind speed data, three main erosional events followed by deposition were predicted (Fig. 7.9. & Fig. 7.10.). The time series of SSC shows an increase in turbidity when the value of erosion threshold is exceeded by the bed shear stress. The elevation of the mud flat reaches a minimum during peaks of turbidity. At that time, only the maximum bed shear stress erodes the dense sediment exposed to the flow. The bed level variations in all of the runs show a decrease in elevation during storms, followed by an increase during subsequent calm conditions. After the storm, sediments are fully (Fig. 7.9.) or partially (Fig. 7.10.) re-deposited depending on the elevation of the station relative to MSL.

The different elevations of the station used in test 2 and test 3 show the influence of exposure time of the mudflat on the computation of bed level changes. Elevation plays a key role in the prediction of mud flat evolution because the period of deposition of material is shortened with increasing elevation of the station. Therefore the deposited mass of material is usually reduced with increasing station elevation.

7.3. Model sensitivity analysis

Computation of the bed level changes of *Palude della Centrega* were carried out in order to undertake a sensitivity analysis of SLIM using data and constants determined in the present study and/or those published by other authors. The sensitivity analysis was undertaken to determine the influence of different variables

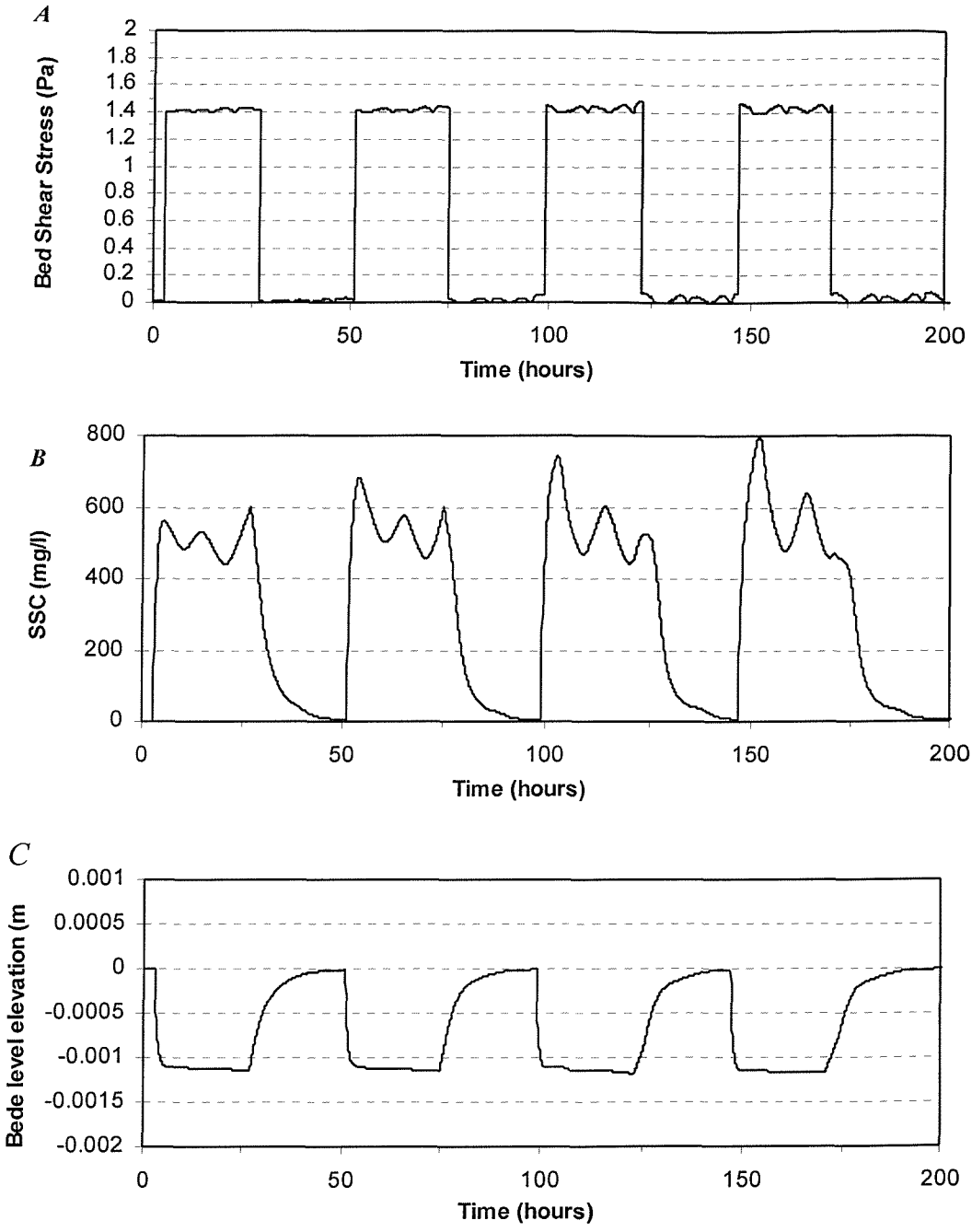

Figure 7.8. Bed shear stress (A), SSC (B) and elevation (C) computed on the basis of 4 steady increases in wind steps. In this simulation real tidal data were used. Oscillations of SSC (B) are due to different water depths during the erosion periods.

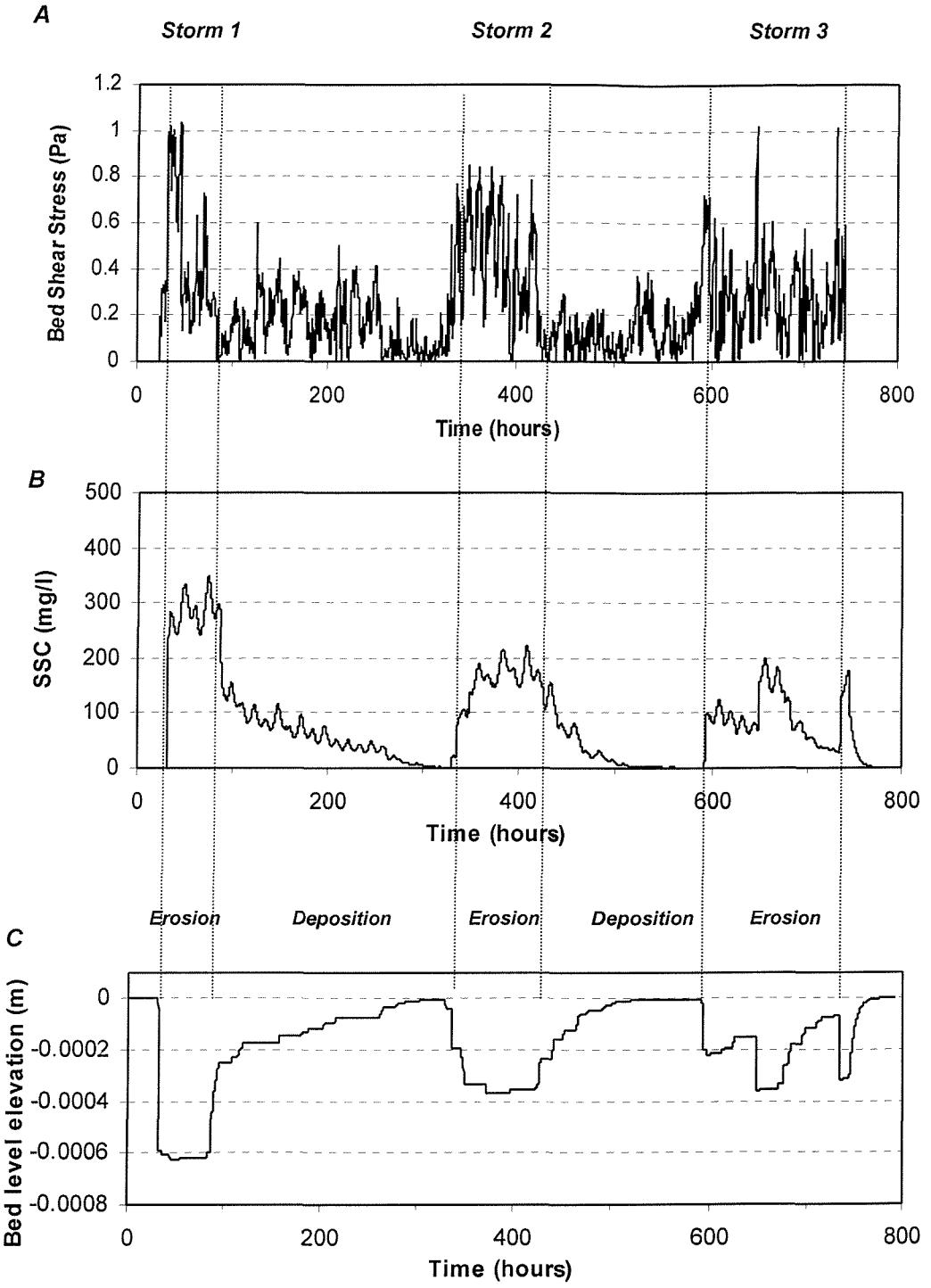

Figure 7.9. A time series of bed shear stress (A), SSC (B) and bed elevation (C) computed by the model on a 30-day simulation using real wind speed data measured at *Treporti* on August 1998.

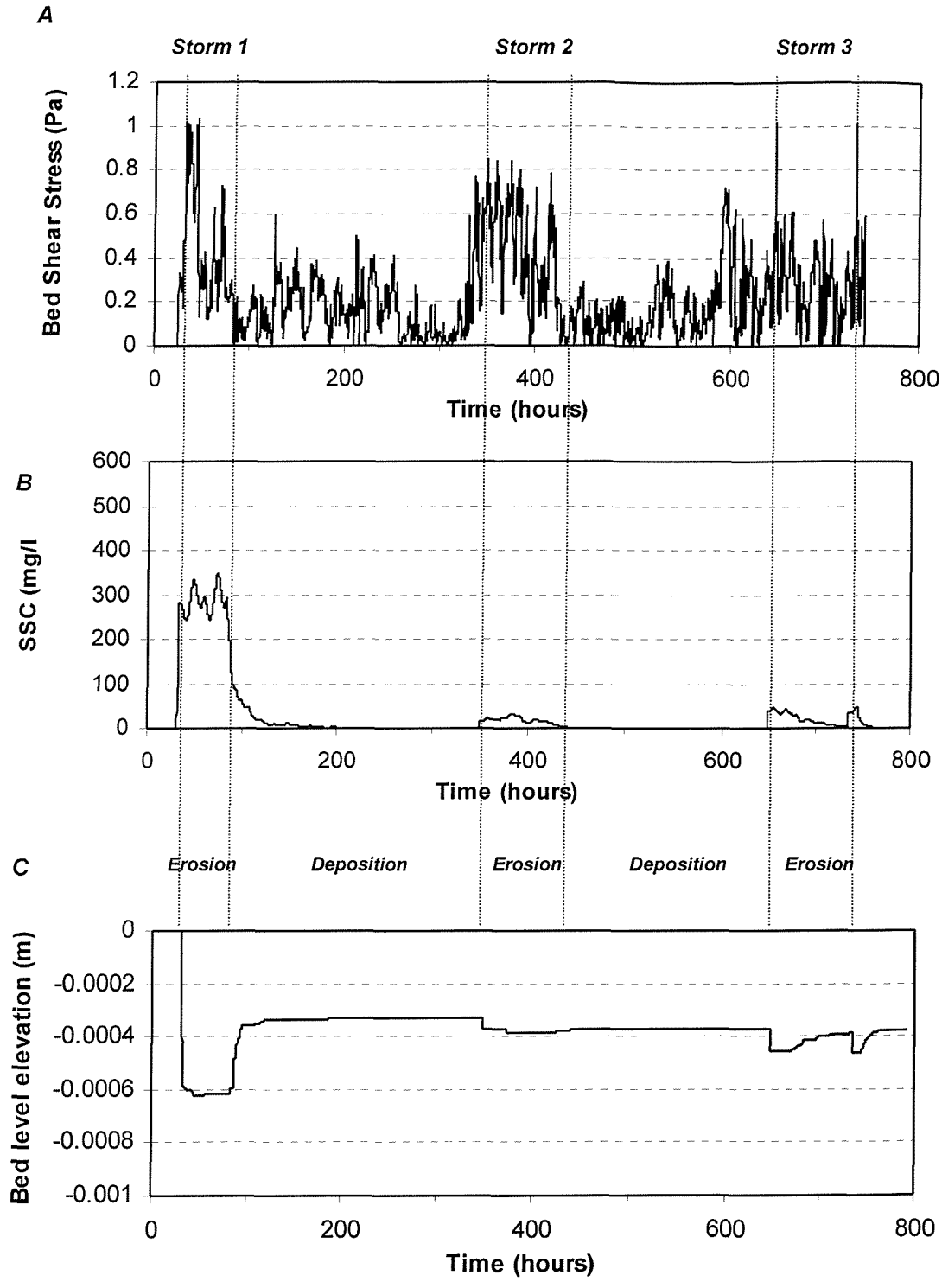

Figure 7.10. A time series bed shear stress (A), SSC (B) and bed elevation (C) computed by the model with a station at msl. Note the decrease in elevation during storms and the partial deposition of sediments afterwards due to the loss of material in the subtidal areas.

on the evolution of the intertidal flats using specific boundary conditions suitable for Venice Lagoon. The simulated conditions were:

- sediment export from the Lagoon to the sea;
- internal friction angle (to evaluate the effect of depth-varying bed properties on the erosion process);
- elevation of the station;
- erosion threshold (in order to quantify the effect of different erosion thresholds);
- reduction of the bed shear stress (to quantify the damping effect of sea grasses on wave motion); and
- river input of sediment (according to the present value of discharge from rivers)

7.3.1. Effects of varying erosion thresholds

Bed stability at *Palude della Centrega* varies through space and time. The impact of these changes on bed level was examined by undertaking five simulations. The erosion threshold was varied between 0.2 and 2.36 Pa which represent the maximum and the minimum values of critical shear stress for erosion derived in the present study. The choice of the erosion threshold values has a strong influence on the number and magnitude of resuspension events caused by storms. The wind speed dataset used in this study shows an erosive trend for τ_c values of 0.2 and 0.5 Pa and an accretionary trend for τ_c values above 0.8 Pa (Table 7.3.).

The eroded depth at the end of the simulation was inversely related to the erosion threshold (Fig. 7.11.); meanwhile no differences in results were observed using τ_c values of 1.16 and 2.36 Pa because these are higher than the maximum shear stress generated by the wind generated waves.

Tide	*Waves*	***Erosion threshold***	*Friction angle*	*Sediment export*	*Sediment input*	*Sea level changes*	***Bed level variation***
(Pa)	*(Pa)*	*(Pa)*	*(ϕ)*	*(t/a)*	*(t/a)*	*(cm)*	*(cm/a)*
Yes	Yes	**0.2**	10	0	$3.3x10^4$	No	**-0.599**
Yes	Yes	**0.5**	10	0	$3.3x10^4$	No	**-0.187**
Yes	Yes	**0.8**	10	0	$3.3x10^4$	No	**0.183**

Yes	Yes	**1.12**	10	0	$3.3x10^4$	No	**0.355**
Yes	Yes	**2.36**	10	0	$3.3x10^4$	No	**0.355**

Table 7.3. Results of bed level changes using different values of erosion threshold.

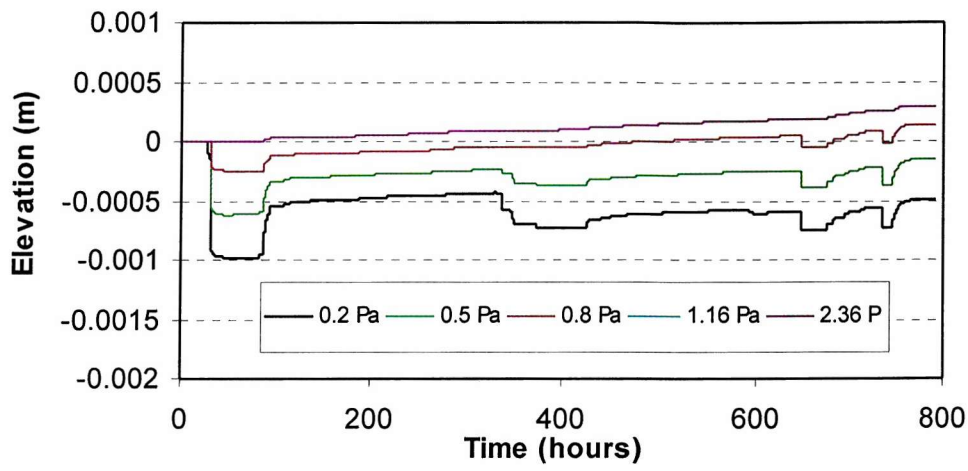

Figure 7.11. Results of bed level changes using different values of erosion threshold. Note that the final eroded depth is inversely related to the erosion threshold. The deposition rate obtained using 1.16 and 2.36 Pa shows exactly the same trends because the critical shear stress for erosion is higher than the maximum shear stress applied by wind-generated waves.

7.3.2. Effects of varying sediment export

Venice Lagoon is suffering a loss of sediment at a rate of 1.1×10^6 m^3/a (CNV, 1996). To examine the influence of changes in this sediment loss, a series of tests were undertaken, reducing the concentration of the suspended mass. A sediment export between 0 t/a (no dispersion) and $1.5x10^6$ t/a were used in order to simulate the flushing of material from the Lagoon to the sea; meanwhile the sediment input by rivers was set at $3.3x10^4$ t/a.

A summary of results is given in Table 7.4. The predicted time series of bed elevation is shown in Fig. 7.12. When sediment export is greater than the sediment input the model is not sensitive to different sediment export rates because SSC cannot be negative. Therefore the simulations carried out using an export of $7.5x10^5$ t/a and $1.5x10^6$ t/a show the same results (Fig. 7.12.).

Tide	*Waves*	*Erosion threshold*	*Friction angle*	***Sediment export***	*Sediment input*	*Sea level changes*	***Bed level variation***
(Pa)	***(Pa)***	***(Pa)***	***(ϕ)***	***(t/a)***	***(t/a)***	***(cm)***	***(cm/a)***
Yes	Yes	0.5	10	**0**	$3.3x10^4$	No	**-0.187**
Yes	Yes	0.5	10	**$7.5x10^5$**	$3.3x10^4$	No	**-0.761**
Yes	Yes	0.5	10	**$1.5x10^6$**	$3.3x10^4$	No	**-0.763**

Table 7.4. Results of bed level changes using different values of sediment export from Venice Lagoon.

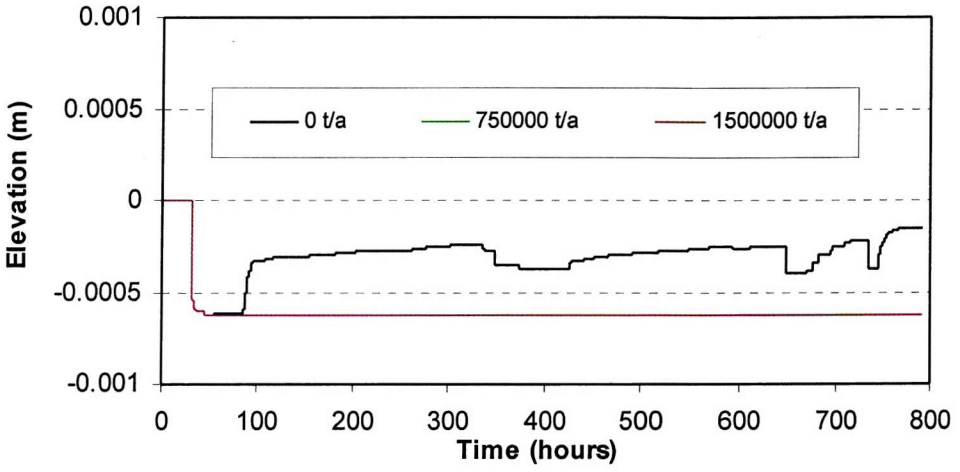

Figure 7.12. Results of bed level changes using different values of sediment export from Venice Lagoon. Note that the erosion rate found using a sediment export of $7.5x10^5$ t/a and $1.5x10^6$ t/a is the same.

7.3.3. Effects of varying bed properties on the erosion process

Eight simulations were run to predict bed level changes under different values of internal friction angle (which in natural sediment varies from 0° to 30°). Results are reported in Table 7.5. The predicted time series of bed elevation is shown in Fig. 7.13.

A small variation in the erosion rate was found using a friction angle between 2° and 25° because the maximum eroded depth was reached early in the run. A significant erosion rate of about 12 cm/a was observed running the model with a friction angle equal to zero, which represents a sediment column without an increase in

resistance downward: a situation that is not representative of natural self-weight consolidated mud found in the studied area.

Tide	*Waves*	*Erosion threshold*	***Friction angle***	*Sediment export*	*Sediment input*	*Sea level changes*	***Bed level variation***
(Pa)	*(Pa)*	*(Pa)*	*(ϕ)*	*(t/a)*	*(t/a)*	*(cm)*	*(cm/a)*
Yes	Yes	0.5	**0**	0	$3.3x10^4$	No	**-12.387**
Yes	Yes	0.5	**2**	0	$3.3x10^4$	No	**-1.585**
Yes	Yes	0.5	**5**	0	$3.3x10^4$	No	**-0.573**
Yes	Yes	0.5	**10**	0	$3.3x10^4$	No	**-0.187**
Yes	Yes	0.5	**15**	0	$3.3x10^4$	No	**-0.063**
Yes	Yes	0.5	**20**	0	$3.3x10^4$	No	**-0.004**
Yes	Yes	0.5	**25**	0	$3.3x10^4$	No	**0.032**
Yes	Yes	0.5	**30**	0	$3.3x10^4$	No	**0.057**

Table 7.5. Results of bed level changes using different values of internal friction angle. Note that the eroded depth increases drastically when $\phi = 0$, suggesting an unrealistic erosion rate of 12.39 cm/a.

In all other simulations carried out during the sensitivity analysis a value of $\phi = 10°$ was used. This value, which is close to that found in Venice Lagoon by AMOS *et al.* (2000), is typical of normally consolidated sediments (LAMBE & WITHMAN, 1979).

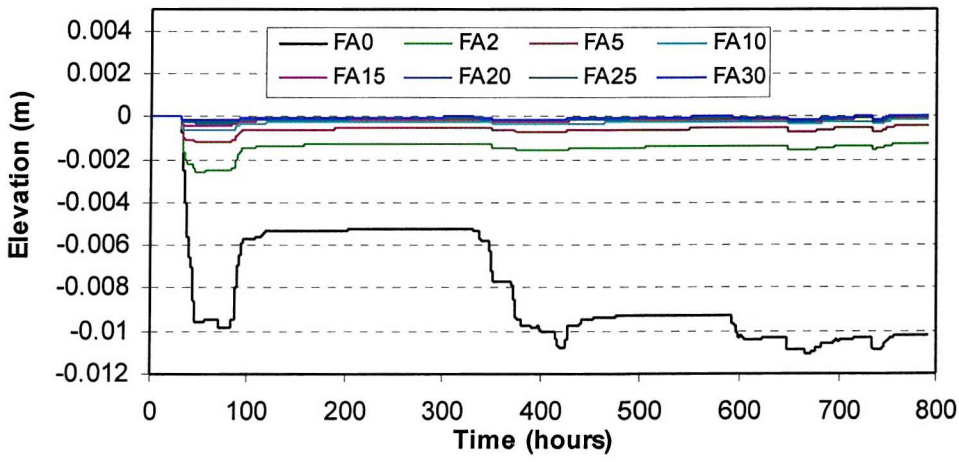

Figure 7.13. Results of bed level changes using different values of internal friction angle. Note that the black line represents the bed level simulated using a friction angle of zero degrees.

7.3.4. Effects of varying sediment input

Sediment input into Venice Lagoon from rivers was set to $3.3x10^4$ t/a based on the results of the DRAIN project (see Chap 2). Four other simulations were run using higher input rates (Table 7.6.), which resulted in a significant change in the mudflat accretion rate (Fig. 7.14.). Therefore, simply by adding suspended mass, increases in deposition rate were obtained. An accretion of the mudflat similar to the average rate monitored *in-situ* was simulated only by using a sediment input rate higher than $3.63x10^5$ t/a. A value about 11 times greater than the actual river contribution was needed in order to simulate the observed trends and the reasons for this are discussed below.

Tide	*Waves*	*Erosion threshold*	*Friction angle*	*Sediment export*	***Sediment input***	*Sea level changes*	***Bed level variation***
(Pa)	***(Pa)***	***(Pa)***	***(ϕ)***	***(t/a)***	***(t/a)***	***(cm)***	***(cm/a)***
Yes	Yes	0.5	10	0	**$3.3x10^4$**	No	**-0.187**
Yes	Yes	0.5	10	0	**$9.9x10^4$**	No	**-0.198**
Yes	Yes	0.5	10	0	**$1.98x10^5$**	No	**0.704**
Yes	Yes	0.5	10	0	**$2.97x10^5$**	No	**1.295**
Yes	Yes	0.5	10	0	**$3.63x10^5$**	No	**1.673**

Table 7.6. Results of bed level changes using sediment input rates between $3.3x10^4$ t/a and $3.63x10^5$ t/a.

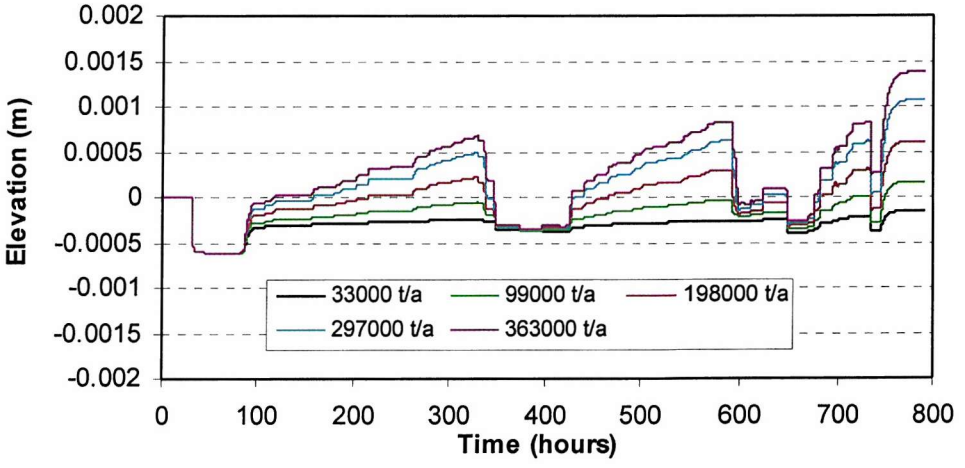

Figure 7.14. Results of bed level changes using different sediment input rates. Note the increase in the accretion rates between the three storms.

7.3.5. Effects of shear stress reduction due to plant cover

When currents and waves pass over a vegetated intertidal flat the flow velocity decreases gradually (NEUMEIER & CIAVOLA, 2001). Reduction of unidirectional currents (FONSECA *et al.*, 1982; FONSECA, 1989) and dissipation of wave motion (MÖLLER *et al.*, 1999; TSCHIRKY & HALL, 2001) occur. Consequently, the bed shear stress is reduced by the presence of sea grasses and salt marsh vegetation. This effect is related strongly to the density of the phytobenthic communities and the shape and length of their leaves (PETHICK *et al.*, 1990). Flume experiments demonstrated also that vegetation influences the velocity profile in the water column (SHI *et al.*, 1995). Therefore, a series of model runs were carried out in order to quantify the contribution of vegetation cover to tidal flat evolution.

In this study, the effect of sea grass on the bed shear stress was simulated by progressively reducing the bed shear stress up to 20 % of its original value. Six experiments were performed and the results are reported in Table 7.7. The results of the predicted time series of bed elevation are shown in Fig. 7.15. It was found that below 80 % of the original total bed shear stress accretion was predicted. No significant differences in the accretionary trend were observed for a reduction of 50, 40 and 20 % of the calculated value of bed shear stress (Fig. 7.15.).

Tide	***Waves***	*Erosion threshold*	*Friction angle*	*Sediment Export*	*Sediment input*	*Sea level changes*	***Bed level variation***
(Pa)	*(Pa)*	*(Pa)*	*(ϕ)*	*(t/a)*	*(t/a)*	*(cm)*	*(cm/a)*
Yes	**100%**	0.5	10	0	$3.3x10^4$	0	**-0.187**
Yes	**80%**	0.5	10	0	$3.3x10^4$	0	**+0.034**
Yes	**60%**	0.5	10	0	$3.3x10^4$	0	**+0.306**
Yes	**50%**	0.5	10	0	$3.3x10^4$	0	**+0.385**
Yes	**40%**	0.5	10	0	$3.3x10^4$	0	**+0.394**
Yes	**20%**	0.5	10	0	$3.3x10^4$	0	**+0.402**

Table 7.7. Results of bed level changes for reduced shear stresses. Note that the model simulates an accretion of the intertidal flat starting from a reduced bed shear stress value of 80%.

Figure 7.16. Station 6 (St6) in winter 1999. Note the unvegetated soft mud.

Figure 7.17. Station 14 (St14) in summer 1998. Note the high density *Zostera noltii* community.

Figure 7.18. Station V40 in August 1998. Note the edge of *Canale Scanello* (boat on the left) characterised by exposed mud passing rapidly to the right into seagrass communities.

The seasonal changes in *Zostera noltii* coverage are very high in *Palude della Centrega*. The intertidal flat is devoid of grasses during the winter and completely vegetated during the summer (Fig. 7.16. and Fig. 7.17.). Spatial variation of *Zostera noltii* density has also been observed in the area, particularly along the E-W orientated transect (Fig. 7.18.). The intertidal flat can abruptly pass from exposed mud (at the edge of *Canale Scanello* channel) to fully vegetated.

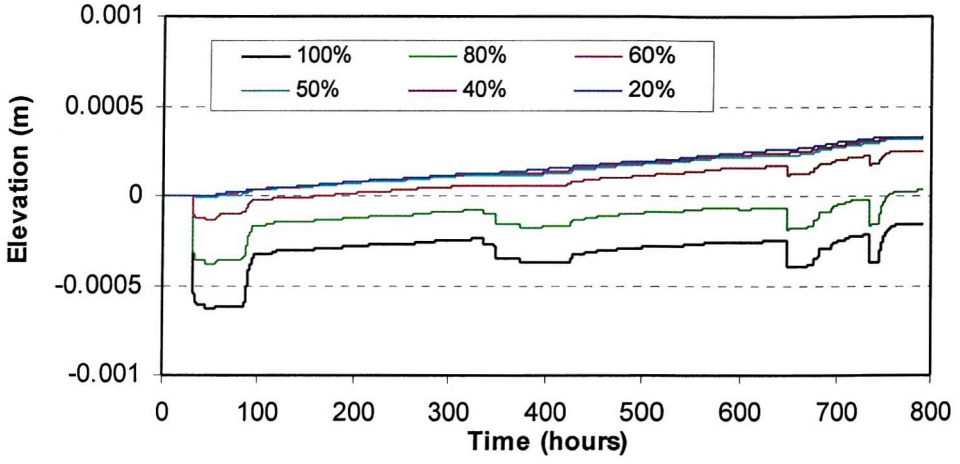

Figure 7.15. A time series of bed level predicted from bed shear stress reduction. Note that the final bed level value is not sensitive to a reduction in bed shear stress of less then 50%.

7.3.6. Effects of Bora winds on the migration of Canale Scanello

The erosion threshold derived at station V40 by the Mini Flume (between 1.16 and 2.36 Pa) is so high that sediments were not resuspended by the wave-induced shear stresses generated by SLIM on the basis of the wind speed time series used in the sensitivity analysis (Fig. 7.11.). The wind speed can occasionally blow up to 90 km/h over Venice Lagoon particularly during winter (CNV, 1992). Such events are called '*Bora*' and are capable of eroding sediments over large intertidal mud flats (evident in the elevated levels of SSC). Therefore, two tests were carried out in order to evaluate the effect of *Bora* storms on the biostabilised sediments observed at the edge of *Canale Scanello*.

In these simulations, the wind speed was multipled by a factor of two in order to generate a wind speed of about 80 km/h during storm peaks. In the first simulation, τ_c was set to 1.16 Pa (representative of the winter condition); in the second case, τ_c

was set to 2.36 Pa (representative of the summer condition). A list of the boundary conditions used for the simulations is given in Table 7.8. and the changes in bed level elevation obtained by SLIM are shown in Fig. 7.19. Results show that the mud flat is eroded by *Bora* winds when sediments are not stabilised by micro-organisms.

Tide	***Waves***	*Erosion threshold*	*Friction angle*	*Sediment export*	*Sediment input*	*Sea level changes*	***Bed level variation***
(Pa)	***(Pa)***	***(Pa)***	***(ϕ)***	***(t/a)***	***(t/a)***	***(cm)***	***(cm/a)***
Yes	**200%**	1.16	10	0	$3.3x10^4$	0	**-0.653**
Yes	**200%**	2.36	10	0	$3.3x10^4$	0	**+0.342**

Table 7.8. Results of bed level changes under *Bora* winds (wind speed was multiplied by two) at the edge of the *Canale Scanello*.

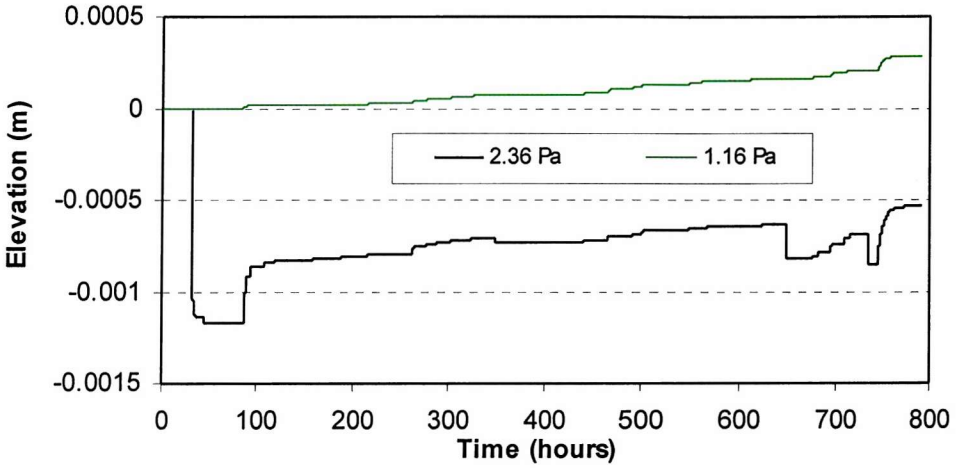

Figure 7.19. A time series of bed level changes under high wind forcing. Note that the model simulates accretion of the intertidal flat when the erosion threshold is 2.36 Pa and erosion when it is 1.16 Pa.

7.4. Results

Under the effect of tidal currents only, all material in suspension is predicted to deposit in about 24 hours. In the presence of waves, erosion of the mudflat may take place, depending on the wind speed and the sediment stability at that time. So, calm weather conditions favour the deposition of sediment and accretion of the tidal flat, which is interrupted by erosion events during storms (PETHICK *et al.*, 1990). All

results of the sensitivity analyses are illustrated in Fig. 7.20. These results show that:

- during calm conditions the bed shear stress is due only to the tidal currents which cause accretion on the intertidal mudflat;
- wind-generated waves are the prime factor causing erosion over the intertidal mudflat;
- under the combined effects of tidal currents and waves, the erosion threshold, the internal friction angle and sediment export are the most important parameters controlling the eroded depth;
- the model converged with the observed accretion rate only by increasing the sediment input (from rivers) to 3.63×10^5 t/a (which is about 11 times higher than the average rate of input);
- the accretion rate of the mudflat can also be simulated by increasing the erosion threshold or reducing the wave-induced bed shear stress in combination with the average value of sediment input provided by rivers (3.3×10^4 t/a); and
- the migration of *Canale Scanello* is caused by storms characterised by a speed above 50 km/h, which mobilise sediments during winter when the effect of biostabilisation is reduced.

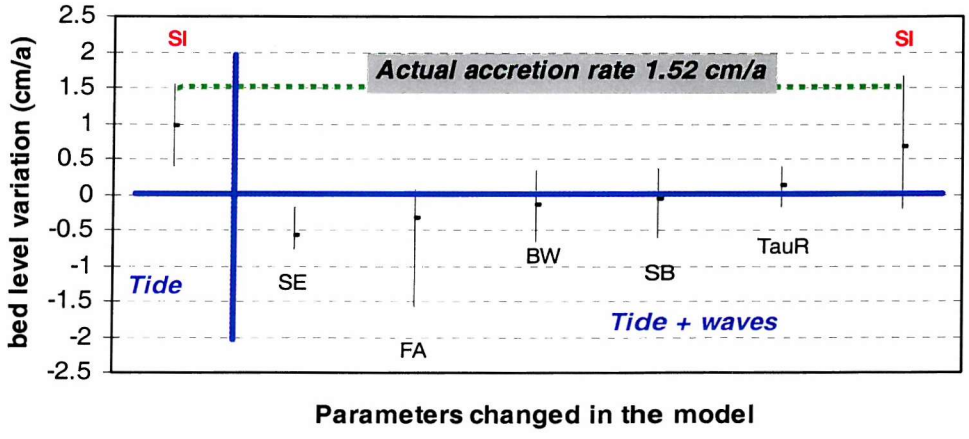

Figure 7.20. A summary of results of bed level changes obtained from the sensitivity analysis of SLIM. The vertical blue line separates the results obtained under the effect of currents only and tidal currents and waves. The horizontal blue line separates the simulations of accretion and erosion. SB = sediment stability; SE = sediment export; FA = friction angle ($0° < \phi < 30°$); SI= sediment input; BW = *Bora* wind, TauR = bed shear stress reduction. Note that maximum erosion is obtained by modifying the friction angle. Deposition can occur under the effect of tidal currents or, in the presence of waves, under a decreased elevation of the mudflat, an increase in the erosion threshold and a reduction of the bed shear stress by sea grasses. The actual accretion rate (1.52 cm/a) is represented by the green dotted line and is simulated using a sediment input of 363000 t/a.

From the results of the sensitivity analysis listed above three factors were found to be responsible for the accretion of the mudflat. These are; (1) the increase in erosion threshold, (2) the reduction of the bed shear stress by plants and (3) the sediment input by rivers (Fig. 7.20.). Sediment input plays a primary role in governing the final accretion level from the simulations. By increasing the erosion threshold or reducing the bed shear stress only, the model could not be made to simulate the accretion rate monitored *in-situ* (~1.5 cm/a).

7.5. Model calibration

The sediment input used to calibrate the model is about 11 times higher then the amount of sediment discharged by rivers into Venice Lagoon if biostabilisation is ignored. A lower value of sediment input can produce the actual accretion rate only if stress reduction due to plant cover is considered. Two experiments were run to calibrate the model under the coupled effect of sediment input, high erosion threshold and low bed shear stress. The boundary conditions used in these simulations are reported in Table 7.9.

Tide	*Waves*	*Erosion threshold*	*Friction angle*	*Sediment export*	***Sediment input***	*Sea level changes*	***Bed level variation***
(Pa)	*(Pa)*	***(Pa)***	***(ϕ)***	***(t/a)***	***(t/a)***	***(cm)***	***(cm/a)***
Yes	**50%**	0.5	10	0	**1.32×10^5**	0	**+1.556**
Yes	100%	**1.16**	10	0	**1.485×10^5**	0	**+1.597**

Table 7.9. Results of bed level changes under the effect of sediment input, bed shear stress reduction and high erosion threshold. The parameters changed in the simulations are in bold.

The results of these experiments demonstrate the tendency of macrophytobenthos on *Palude della Centrega* to enhance natural accretion of the mud flats. The effects of the dominant species on tidal flat evolution is through enhanced stability and shear stress reduction. However, these effects in isolation do not lead to the observed accretion rates. In order to simulate the observed accretion within SLIM a sediment input of about 1.4×10^5 t/a is needed (Fig. 7.21.).

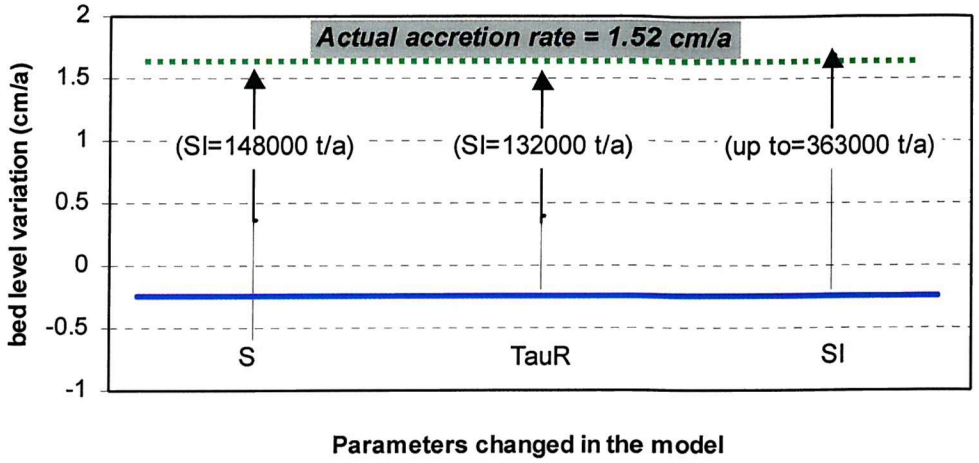

Figure 7.21. A summary of the calibration results of bed level changes obtained from the sensitivity analysis under the combined effect of high τ_c , reduction of the shear stress by plants and increase in the river sediment input. The model can be obtained using a SI of ~363000 t/a, increasing the τ_c up to 1.16 Pa (SB) and using a SI=148000 t/a, or reducing τ_o (TauR) by 50% in combination with a SI=132000 t/a. The dotted arrows represent the contribution of sediment input to the accretion rate.

7.6. Summary

Accretion of the tidal flats within the studied area takes place under the following circumstances:

- biostabilisation of surface sediments;
- reduction of the bed shear stress (by sea grasses);
- an increase in the internal friction angle; and
- elevated sediment input.

SLIM simulates both the erosion of the intertidal flat at the edges of the channel (during *Bora* events) and the accretion of the inner part colonised by sea grasses (Fig. 7.22.). A conceptual evolutionary model is proposed in Fig. 7.22., in agreement with other studies of intertidal mud flats (PETHICK *et al.*, 1990; CHRISTY *et al.*, 2001) and previous work on the evolution of mudflat-tidal channel systems in Venice Lagoon (SILVA & MOL, 1993).

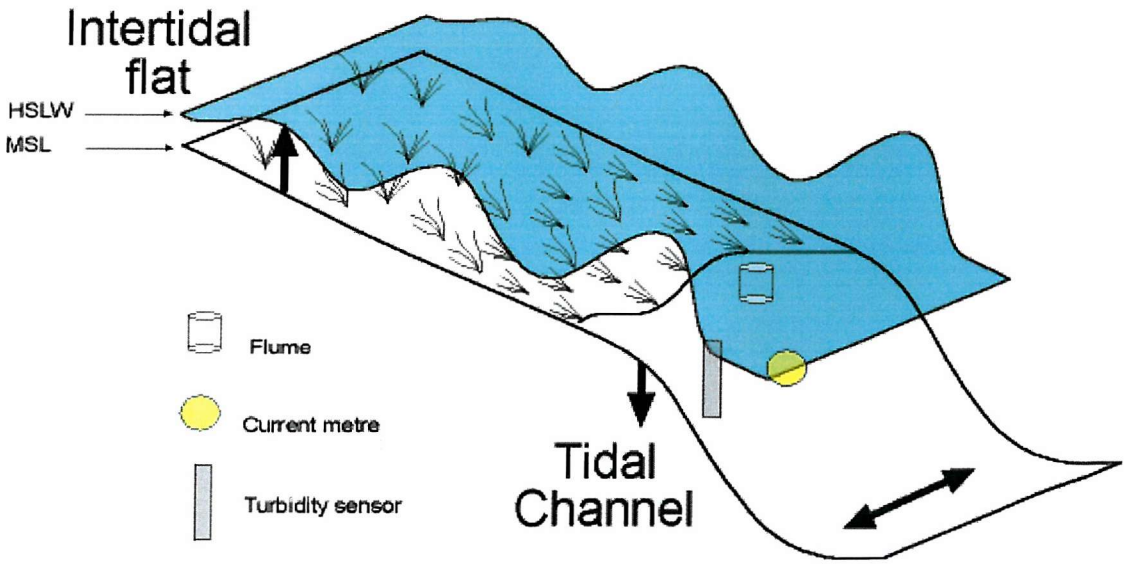

Figure 7.22. A schematic representation of an ideal E-W transect across *Palude della Centrega* during sea grass colonisation in the summer. Note that all flume measurements were carried out at the edge of the channel (the downward arrow indicates erosion). Moving westward, wave attenuation (by sea grasses) takes place (MÖLLER *et al.*, 1999), and deposition is enhanced (the upward arrow indicates accretion).

The sediment input used to tune the model (~1.4×10^5 t/a) is bigger than the average value of 3.3×10^4 t/a discharged by the present rivers entering Venice Lagoon. It suggests that *Palude della Centrega* is accreting because the material from the eroding surrounding mud flats is deposited there. If no biostabilisation was taking place in the studied area, a much higher sediment input (3.63×10^5 t/a) would be needed to account for the 1.52 cm/a of accretion measured *in-situ*. This means that biostabilisation by both micro- and macro-phytobenthos contributed about 50 % to the accretion rate of *Palude della Centrega* at the time of this study.

CHAPTER 8: CONCLUDING REMARKS AND FUTURE WORK

Conclusions

Several conclusions reached in the present study of the stability and evolution of fine-grained sediments in Venice Lagoon can be summarised as follow:

1. Turbidity in Venice Lagoon is driven by resuspension from the bed due to wind-generated waves. Its level is influenced by water depth, being lower in deep channels and higher in shallow intertidal areas. High turbidities (between 100 and 250 mg/l) were found in the northern part of the Lagoon during both the summer and winter F-ECTS field programmes, compared with the average in Venice Lagoon of less than 100 mg/l.

2. Well-preserved, fine-grained intertidal flats on which biological activity increases during the summer dominate the northern part of the Lagoon. These regions exhibit the highest erosion threshold ever measured before by annular flumes (2-3 Pa) and the τ_c derived in the present study is more than two times higher than the τ_c proposed by previous studies (0.2-1 Pa).

3. The τ_c values obtained using the Mini Flume and the Sea Carousel during the F-ECTS campaigns were very similar. Differences between the two instruments were detected during the summer campaign at intertidal sites V40 and V50, suggesting spatial heterogeneity, arising from the 'patchy' distribution of the biofilm.

4. A feed-back mechanism is proposed to explain how micro-organisms contribute to the seasonal stabilisation of sediments in the northern intertidal mudflats. The increase in chlorophyll *a* and colloidal carbohydrate was associated with increases in τ_c during the summer. These results indicate that changes in sediment stability and biological activity can be significant as they are both lower in the central and southern part than in the northern part. By contrast, physical properties of the sediments were not well correlated with τ_c due to the heterogeneous nature of the investigated sites.

5. *Palude della Centrega* (V40) has an elevation very close to the MSL and has an average sedimentation rate of 1.52 cm/a. Erosion was observed at the edge of the channel creeks (St6 and St16), suggesting that they are migrating through time. Varying accretion rates were observed in the central part of the mud flat, which was colonised by *Zostera noltii* sea grass, and the salt marsh, which was colonised by *Spartina* spp.

6. The detailed study of sediment stability of *Palude della Centrega* suggests that the physical properties of sediments play an important role in the stabilisation of sediment mudflats. In particular, the elevation and water content (i.e. bulk density) of surface sediments can be used as a proxy of sediment stability on a local scale.

7. A laboratory comparison between the CSM and Mini Flume showed that τ_c derived from the CSM (~0.2 Pa) is about 50 % smaller than τ_c obtained using the Mini Flume (~0.52 Pa) for surface sediment from *Palude della Centrega*. This is due to the large changes in shear stress generated with each increment in jet velocity in the CSM, leading to a low resolution of the device.

8. Tidal currents do not erode sediments in *Palude della Centrega* as they apply a bed shear stress which never exceeds 0.1 Pa. This value of τ_o is below the critical shear stress for deposition (τ_m = 0.1 Pa), which means, in the absence of waves, sedimentation occurs at all times and at all levels of SSC.

9. Wind-generated waves are the main cause of erosion of *Palude della Centrega*. Wave-generated bed shear stresses of 1 Pa occur during most storms and in rare events can reach 2 Pa. Winter storms are responsible for the erosion of the edge of *Canale Scanello*. Wave action due to boat traffic is negligible in this area, but is important in other parts of the Lagoon.

10. A numerical model (SLIM) has been developed to simulate the sediment processes occurring over *Palude della Centrega*. Results have shown that the erosion rate is strongly controlled by the internal friction angle of the sediment particularly when it is lower than 2°.

11. SLIM demonstrated that accretion occurs under the effect of: (1) bed shear stress reduction by *Zostera noltii*; a sea grass which colonised the majority of the study area during summer; (2) colonisation by the microphytobenthos that developed a thick biofilm at the edge of the *Canale Scanello* which increased the erosion threshold and (3) a high SSC.

12. The sediment input required to calibrate the model for *Palude della Centrega*, which is generally accreting with time, is five times higher than that supplied by rivers. Therefore, *Palude della Centrega* is accreting because material, which is eroding from surrounding areas, is deposited there. If no biostabilisation by micro- and macrophytobenthos was taking place in the studied area, a much higher sediment input would be needed to justify the observed accretion rate.

The results obtained from the SLIM model are extremely useful for the management of Venice Lagoon because even if they were restricted to a single mud flat, the factors responsible for the evolution of the whole Lagoon were found. It is possible that the same evolutionary trends could occur in other intertidal mud flats in Venice Lagoon where biostabilisation and sediment input are acting (DAY *et al.*, 1999), but it still unclear why salt marshes are well preserved only in the northern part of Venice Lagoon. The origin of sediments that are accumulating on *Palude della Centrega* is still uncertain, but they are probably eroded from the unvegetated shoals located in the northern part of the studied area which are exposed to *Bora* winds. Sea grass planting has been used for the restoration of Lagoon morphology by CNV (1996). The control of nutrients and pollutant discharges from rivers and limiting the speed of small recreational boats will be the key factors in controlling the preservation of sea grasses within the Lagoon and protecting the islands reconstructed recently using dredged material (CNV, 1996). The advantage of reducing the erosion of mudflats, other than conservation of habitats, is to lower sedimentation in the natural channels, therefore to lower the costs of dredging carried out to maintain depths of navigation. The importance of stress reduction by the phytobenthos found in this work is a topic of much ongoing research (NEUMEIER, *pers comm.*; www.sednet.org) as it provides a natural defence against sediment erosion and can be applied, worldwide, as a tool for coastline protection and habitats conservation.

Future work

The observations and experiments carried out in the present study demonstrate that an intensive field programme is needed to collect sufficient information on the environment to determine further the factors that influence the temporal and spatial variability of mudflats in Venice Lagoon. This is due to the frequent wind events (> 40 km/h which occur every two-three weeks) and the high variability of habitats that make it difficult to establish relationships between variables. The bed level measurements showed a general accretion of *Palude della Centrega*, but erosion threshold is still unpredictable due to temporal and spatial changes in sediment characteristics and the devices used for the investigation.

Despite the limitations of the present study, further understanding of the mechanisms responsible for mudflat development can only be revealed using similar approaches (e.g. FRIEND *et al.*, in press). A series of questions arise from the present study which can be used to develop future work in this field.

In-situ technology to investigate sediment stability on cohesive mud flats should be improved and upgraded. The present study pointed out that there are many logistical and technological aspects to be improved upon in order to determine τ_c more accurately. A new version of the CSM (Mk4) has already been developed. The Mk4 CSM should be tested and calibrated on cohesive sediments because the upgraded software allows smaller incremented steps in the erosive jet pressure during deployments, promising higher accuracy in determination of the erosion threshold. A detailed comparative study should also be carried out on a uniform abiotic fine-grained sediment deploying all devices used in this investigation (even more if possible). These include: the Mini Flume, the Sea Carousel (or its laboratory equivalent Lab Carousel (LC), the Cohesive Strength Meter and the Tor Vane Shear Meter.

Quantitative relationships proposed in the present study between sediment properties and τ_c in Venice Lagoon need more data to be validated. Changes in sediment stability should be monitored every two weeks in order to determine short-term trends in τ_c through time. Relationships between τ_c and sediment properties should be investigated separately for each habitat of *Palude della Centrega,* not only along transects (e.g. FRIEND *et al, in press*), and extended in time.

An accurate and intense fieldwork programme should be carried out in order to evaluate *in-situ*, the influence of *Zostera* sea grass colonies on the hydrodynamics of the area. This should include an assessment of bed shear stress reduction with plant density and height (TSCHIRKY & HALL, 2001). Measurements should be carried out at the same time within and outside sea grass colonies.

A numerical modelling assessment should be extended and linked to the 2-D model of UMGIESSER (2001). The numerical simulations carried out should be extended over a period of 12 months to be more realistic. In this way, more changes in the meteorological conditions (wind speed regimes) could be included. The one-year simulation should be carried out using a step-varying τ_c in order to simulate the seasonal fluctuations of biological activity which result in the biostabilisation of sediments during summer.

The SLIM model should also be modified to include other sedimentary processes. In particular, the *degree of retention* should be included in the deposition subroutine in order to simulate gradual settling of particles due to flow deceleration, instead of using a single deposition threshold. A more complex bed model, which considers changes in sediment properties through time and with depth should be created (e.g. ARIATHURAI, 1976). Time-varying erosion threshold linked to SLIM should also be included in order to simulate the effect of sediment consolidation (increase of τ_c) and bioturbation (decrease of τ_c).

REFERENCES

ALBEROTANZA L.G., ALDIGHIERI P., COVA C., RAMASCO C., VIANELLO A. & ZUCCHETA G. (1991a). *A method to monitor the Venice Lagoon, Water Pollution: Modelling, Measuring and Prediction.* Computational Mechanics Publication, Boston: 497-504.

ALBEROTANZA L.G., CARBOGNIN L., COVA C., RAMASCO C. & TARONI G. (1991b). *A method to monitor the Venice Lagoon, water pollution: modelling, measuring and prediction.* Computational Mechanics Publication, Boston: 481-496.

AMOS C.L., BRYLINSKY M., SUTHERLAND T.F., OBRIEN D.J., LEE S. & CRAMP, A. (1998). *The stability of a mudflat in the Humber estuary, South Yorkshire, UK.* In: Black, K.S., Paterson, D.M. & Cramp, A. (eds) *Sedimentary Processes in the Intertidal Zone.*, Geological Society, London, Special Publications, **139**: 25-43.

AMOS C.L., CLOUTIER D., CRISTANTE S., CAPPUCCI S. & LE COUTURIER M. (2000). *The Venice Lagoon Study (F-ECTS) Field Results–August, 1998.* Geological Survey of Canada open file report, **3904**: 46p.

AMOS C.L., DABORN H.A., CHRISTIAN H.A., ATKINSON A. & ROBERTSON A. (1992b). *In situ erosion measurements of fine-grained sediments from the Bay of Fundy.* Marine Geology, **108**: 175-196.

AMOS C.L., FEENEY T., SUTHERLAND T.F. & LUTERNAUER J.L. (1997). *The stability of fine-grained sediments from the Fraser River delta.* Estuarine, Coastal and Shelf Science, **45**: 507-524.

AMOS C.L. & GIBSON A.J. (1994). *The stability of dredge material at dumpsite B, Miramichi Bay, New Brunswick, Canada.* Geological Survey of Canada open file report, No. **3020**: 22p.

AMOS C.L., GRANT J., DABORN G.R. & BLACK K. (1992a). *Sea Carousel - a benthic annular flume.* Estuarine, Coastal and Shelf Science, **34**: 557-577.

AMOS C.L. & MOSHER D.C. (1985). *Erosion and deposition of fine-grained sediments from the Bay of Fundy.* Sedimentology, **32**: 815-832.

AMOS C.L., SUTHERLAND T.F., RADZIJEWSKI B. & DOUCETTE M. (1996a). *A rapid technique to determine bulk density of fine-grained sediments by x-ray computed tomography.* Journal of Sedimentary Research, **66**:1023-1039.

AMOS C.L., SUTHERLAND T.F. & ZEVENHUIZEN J. (1996b). *The stability of sublittoral, fine-grained sediments in a subartic estuary.* Sedimentology, **43**: 1-19.

AMOS C.L., VAN WAGONER N.A. & DABORN G.R. (1988). *The influence of subaerial exposure on the bulk properties of fine-grained intertidal sediment from Minas Basin, Bay of Fundy.* Estuarine, Coastal and Shelf Science, **27**: 1-13.

ANDERSON F.E. (1983). *The northern muddy intertidal: a seasonally changing source of suspended sediment to estuarine waters - a review.* Canadian Journal of Fisheries and Aquatic Science, **40**: 143-159.

ARGESE E., COCONI G, ZAGGHIA L., ZONTA R. & PINI R. (1992). *Study on redox state and grain size of sediments in a mud flat of the Venice Lagoon.* Environmental Geology Water Sciences, **20**: 35-42.

ARIATHURAI C.R. & ARULANANDAN K. (1976). *Erosion rates of cohesive soils.* Journal of Hydraulics Division, American Society of Civil Engineers, **104**: 279-282.

ARULANDAN K. (1975). *Fundamental aspects of erosion of cohesive soils.* Journal Hydraulic Division, American Society of Civil Engineers, **101**: 635-639.

BABA R.A. & KOMAR P.D. (1981). *Measurements and analysis of settling velocities of natural quartz sand grains.* Journal of Sedimentary Petrology, **51**: 631-640.

BAGNOLD R.A. (1966). *An approach to the sediment transport problem from general physics.* U.S. Geological Survey Professional Paper 422-I.

BALE A.J., MORRIS A.W. & HOWLAND R.J.M. (1985). *Seasonal sediment movement in the Tamar estuary.* Oceanologica Acta, **8**: 1-6.

BARILLARI A. (1978). *Prime notizie sulla distribuzione dei sedimenti superficiali nel bacino centrale della laguna di Venezia.* Atti dell' IstitutoVeneto di Scienze Lettere ed Arti; Tomo CXXXVI (1977-1978). Classe di scienze matematiche e naturali.

BARILLARI A. (1981). *Distribuzione dei sedimenti superficiali nel bacino meridionale della laguna di Venezia.* Atti dell' Istituto Veneto di Scienze Lettere ed Arti; Tomo CXXXIX (1980-1981). Classe di scienze matematiche e naturali.

BATTISTON G.A., GEGETTO S., GERBASI R., SBRIGNADELLO G. & TOSITTI L. (1987). *Self-absorption correction for low energy gamma rays: application to ^{210}Pb determination in marine sediments.* Science Total Environment, **77**: 15-23.

BERGER G.W., EISMA D. & VAN BENNEKOM A.J. (1987). *^{210}Pb-derived sedimentation rate in the Vlieter, a recently filled-in tidal channel in the Wadden Sea.* Netherlands Journal of Sea Research, **21**: 287-294.

BERLAMONT J., OCKENDEN M., TOORMAN E. & WINTERWERP J. (1993). *The characterisation of cohesive sediment properties.* Coastal Engineering, **21**: 105-128.

BETTINETTI A., PYPAERT P. & SWEERTS J-P. (1996). *Application of an Integrated Management Approach to the Restoration Project of the Lagoon of Venice.* Journal of Environmental Management, **46**: 207-227.

BLACK K.S. (1991). *The erosion characteristics of cohesive estuarine sediments: some in situ experiments and observations.* Unpublished Ph.D. thesis, University of Wales, UK: 313p.

BLACK K.S. & PATERSON D.M. (1996). *Measurement of the erosion potential of cohesive marine sediments: a review of current* in situ *technology.* In: PEDORZOLLI A. (eds) Proceedings Oceanology International, **3**: 129-169.

BLACK K.S., PATERSON D.M. & CRAMP A. (1998). *Sedimentary Processes in the Intertidal Zone.* Geological Society, London, Special Publications, **139**: 1-10.

BORTOLAMI G., CARBOGNIN L. & GATTO P. (1985). *The natural subsidence in the Lagoon of Venice, Italy.* International Association Hydrological Science, **151**: 777-784.

BOUMANS R. DAY J. (1993). *High precision measurements of sediment elevation in shallow coastal areas using a sedimentation erosion table.* Estuaries, **16**: 375-380.

BRIKER-URSO S., NIXON S.W., COCHRAN J.K., HIRSCHBERG D.J. & HUNT C. (1989). *Accretion rates and sediment accumulation in Rhode Island salt marshes.* Estuaries, **12**: 300-317.

BUNT J.A.C., LARCOMBE P. & JAGO C.F. (1999). *Quantifying the response of optical backscatter devices and transmissometers to variations in suspended particulate matter.* Continental Shelf Research, **19**: 1199-1220.

CAPPUCCI S., FRIEND P. & AMOS C.L. (2000). *The spatial variation of sediment stability in Palude della Centrega, Venezia Italy: a new method to calculate the erosion threshold using Cohesive Strength Meter.* International Advanced School in Coastal Management "Leonardo Da Vinci": processes in the coastal zone: links to management issues.

CARBOGNIN L. (1987). *Venezia, la laguna, i suoi problemi.* Il geologo e l'ambiente: un ruolo, una professione un impegno. In Memorie, Interventi e posters del VI Congresso Nazionale dell'Ordine dei Geologi: 239-255.

CARBOGNIN L. & CECCONI G. (1997). *The Venice Lagoon: environmental problems and remedial measures.* IAS-SEPM Meeting on Environmental Sedimentology, Venice: 71p.

CARBOGNIN L., GAMBOLATI G., MARABINI G., TARONI G., TEATINI P. & TOSI L. (1996). *Analisi del processo di sibsidenza nell'area veneziana e sua simulazione con un modello tridimensionale non lineare.* Relazione finale della Linea di ricerca 2.7, Worhshop Progetto "Sistema Lagunare veneziano": 32p.

CARBOGNIN L., GATTO P. & MARABINI F. (1984). *The city and the Lagoon of Venice. A Guidebook on the Environment and Land Subsidence.* Third International Symposium on Land Subsidence, Venice: 36p.

CARBOGNIN L., GATTO P. & MOZZI G. (1981). *La riduzione altimetrica del territorio veneziano e le sue cause.* Istituto Veneto di Scienze, Lettere ed Arti, Rapporti e Studi, **VIII**: 55-83.

CARBOGNIN L., GATTO P., MOZZI G., GAMBOLATI G. & RICCERI G. (1976). *New trend in the subsidence of Venice.* Second International Symposium on Land Subsidence, Anaheim, CA, U.S.A., International Association Hydrological Science, **121**: 65-81.

CARBOGNIN L., MARABINI P. & TOSI L. (1995b). *Land subsidence and degradation of the Venice littoral, Italy.* Proceedings of the Fifth International Symposium on Land Subsidence, The Hague, International Association Hydrological Science, **234**: 391-402.

CARBOGNIN L., TEATINI P. & TOSI L. (1995a). *Analysis of Actual Land Subsidence in Venice and its Hinterland (Italy).* In: BARENDS BROWER & SCHOEDER (eds). Land subsidence: 129-138.

CAVALERI L. (1980). *Sediment transport in shallow lagoons.* Il Nuovo Cimento, **3C**: 527-540.

CAVALERI L. & HUBBARD D.H. (1981). *Velocity profiles and turbulence characteristics at the Lido entrance of the Venice Lagoon.* Il Nuovo Cimento, **4C**: 603-617.

CAVALERI L. & MALANOTTE RIZZOLI P. (1981). *Wind prediction in shallow water: theory and applications.* Journal of Geophysical Research, **86**:10961-10973.

CAVAZZONI S. (1977). *Variazioni batimetriche e idrografiche nella laguna di Venezia intercorse tra il 1933 ed il 1971.* Istituto Veneto di Scienze, Lettere ed Arti - Rapporti e studi, **VII**: 1-18.

CHRISTIE M.C., DYER K.R., BLANCHARD G., CRAMP A., MITCHENER H.J. & PATERSON D.M. (2000). *Temporal and spatial distributions of moisture and organic contents across a macrotidal mudflat.* Continental Shelf Research, **20**: 1219-1241.

CHRISTIE M.C., DYER K.R. & TURNER P. (2001). *Observations of long and short term variations in the bed elevation of a macro-tidal mudflat.* In: McANALLY & METHA (eds): *Coastal and Estuarine Fine Sediment Processes.* Elsevier. Proceedings in Marine Science, **3**: 323-342.

CIAVOLA P. & COVELLI S. (2000). *Detail report of field operations in Venice Lagoon. Sedimentological Characterisation of Sites.* University of Ferrara. Open file F-ECTS-REL (wp1b)-T026.0: 32p.

CIAVOLA P., ORGANO C., VINTRÒ L.L. & MITCHELL P.I. (in press). *Sedimentation processes on intertidal areas of the Lagoon of Venice: identification of occasional events (acqua alta) using radionuclides.* Journal of Coastal Research, Special Issue from International Coastal Symposium 2002.

COCHRAN J.K., FRIGNANI M., SALAMANCA M., BELLUCCI L.G. & GUERZONI S. (1998). *Lead-210 as a tracer of atmospheric input of heavy metals in the northern Venice Lagoon.* Marine Geochemistry, **62**: 15-29.

CONSORZIO VENEZIA NUOVA (1992). *Progetto generale degli interventi sulla morfologia.* Rapporto finale, **3**: 206 p.

CONSORZIO VENEZIA NUOVA (1996). *The morphological restoration of the Venice Lagoon.* Supplemento ai Quaderni Trimestrali, **4**: 24p.

CRAIG R.F. (1992). *Soil Mechanics* (5^{th} edn). Chapman & Hall, London, UK.

CROUDACE I.W. & CUNDY A.B. (1995). *Heavy metal and hydrocarbon pollution in Recent sediments from Southampton water, Southern England: a geochemical and isotopic study.* Environmental Science and Technology, **29**: 1288-1296.

CUNDY A.B., COLLINS P.E.F., TURNER S.D., CROUDACE I.W. & HORNE D. (1998). *Recent environmental change, southeast Sicily*: In: BLACK K.S., PATERSON D.M. & CRAMP A. (eds) *Sedimentary Processes in the Intertidal Zone.*, Geological Society, London, Special Publications, **139**: 243-254.

CUNDY A.B. & CROUDACE I.W. (1995). *Sediment accretion and recent sea-level rise in the Solent. Southern England: interference from radiometric and geochemical studies.* Estuarine Coastal and Shelf Science, **43**: 449-467.

DABORN G.R., AMOS C.L., BRYLINSKY M., CHRISTIAN H., DRAPEAU G., FAAS R.W., GRANT J., LONG B., PATERSON D.M., PERILLO G.M.E. & PICCOLO M.C. (1993). *An ecological cascade effect: migratory birds affect stability of intertidal sediments.* Limnology and Oceanography, **38**: 225-231.

DADE B.W., DAVIS J.D., NICHOLS P.D., NOWELL A.R., TISTLED D., TREXLER M.B. & WHITE D.C. (1990). *Effects of bacterial exopolimer adhesion on the entrainment of sand.* Geomicrobiology, **8**: 1-16.

DAZZI R., GATTO G., MOZZI G. & ZAMBON G. (1994). *La rete di monitoraggio delle pressioni di strato.* In: *Lo sfruttamento degli acquiferi artesiani di Venezia e i suoi riflessi sulla situazione altimetrica del suolo, Part 2.* Linea di ricerca 2.8. Progetto Sistema Lagunare Venziano, CNR, ISDGM, Venezia.

DAY J.W.Jr., RISMONDO A., SCARTON F., ARE D. & CECCONI G. (1998a). *Relative sea level rise and Venice Lagoon wetlands.* Journal of Coastal Conservation, **14**: 583-590.

DAY J.W.Jr., SCARTON F., RISMONDO A. & ARE D. (1998b). *Rapid deterioration of salt marsh in Venice Lagoon, Italy.* Journal of Coastal Research, **14**: 583-590.

DAY J. W.Jr., RYBCZYK J., SCARTON F., RISMONDO A., ARE D. & CECCONI G. (1999). *soil accretionary dynamics, sea-level rise and the survival of wetlands in Venice Lagoon: a field and modelling approach.* Estuarine, Coastal and Shelf Science, **49**: 607-628.

DE BROUWER J.F.C., BJELIC S., DE DECKERE E.M.G.T. & STAL L.J. (2000). *Interplay between biology and sedimentology in a mudflat (Biezelingse Ham, Westershelde, The Netherlands).* Continental Shelf Research, **20**: 1159-1177.

DE CASABIANCA M.L., LAUNGIER T. & MARINHO-SORIANO E. (1997). *Seasonal Changes of nutrients in water and sediment in a Mediterranean lagoon with shellfish farming activity (Thau Lagoon, France).* ICES Journal of Marine Science, **54**: 905-916.

DECHO A.W. (1990). *Microbial exopolymer secretions in ocean environments: their role(s) in food webs and marine processes.* Oceanography and Marine Biology, Annual Review, **28**: 73-153.

DECHO A.W. (2000). *Microbial biofilms in intertidal systems: an overview.* Continental Shelf Research, **20**: 1257-1273.

DELO E.A. & OCKENDEN M.C. (1992). *Estuarine Muds Manual.* HR Wallingford Report, SR **309**.

DENEIX A. (1896). *Carta Topografica Idrografica Militare della Laguna di Venezia.* Istituto Geografico Militare, Italy.

DHI (1991). *Morphological Study, Phase II, second intermediate report.* Danish Hydraulic Institute.

DI SILVIO G. & GAMBOLATI G. (1990). *Two dimensional model of the long-term morphological evolution of tidal lagoons.* 8th International Conference on Computational Methods in Water Resources. June, Venice, Italy.

DONAZZOLO R., ORIO A. & PAVONI B., (1982). *Radiometric dating and pollutant profiles in a sediment core from the Lagoon of Venice.* Oceanologica Acta, International Symposium on coastal lagoons, SCOR/IABO/UNESCO: 101-106.

DUNN I.S. (1959). *Tractive resistance of cohesive channels.* Journal of the Soil Mechanics and Foundations Division, American Society of Civil Engineers, **3**: 1-24.

DYER K.R. (1979). *Estuarine Hydrography and Sedimentation.* Cambridge University Press.

DYER, K.R. (1986). *Coastal and Estuarine Sediment Dynamics.* Wiley-Interscience: 342 p.

DYER, K.R. (1996). Mud, Glorious Mud. *Ocean Challenge.*

DYER K.R. (1998). *The typology of intertidal mudflats.* In: BLACK K.S., PATERSON D.M. & CRAMP A. (eds) *Sedimentary Processes in the Intertidal Zone.* Geological Society, London, Special Publications, **139**: 11-24.

DYER K.R., CHRISTIE M.C., WRIGHT E.W. (2000). *The classification of intertidal mudflats.* Continental Shelf Research, **20**: 1039-1060.

EVANS A.W. & HARDISTY J. (1989). *An experimental investigation of the effect of bedslope and grain pivot angle on the threshold of marine gravel transport.* Marine Geology, **89**: 163-167.

FAVERO V. (1992). *Evoluzione morfologica e trasformnazioni ambientasli della conterminazione lagunareal nostro secolo.* In: *Conterminazione lagunare: storia, ingegneria, politica e diritto nella laguna di Venezia.* Proceedings of the Conference "Convegno di studio nel bicentenario della conterminazione lagunare" Venice, Italy.

FLEMMING B.W. (2000). *A revised textural classification of gravel-free muddy sediments on the basis of ternary diagrams.* Continental Shelf Research, **20**: 1125-1139.

FONSECA M.S. (1989). *Sediment stabilization by Halophila decipiens in comparison to other seagrasses.* Estuarine, Coastal and Shelf Science, **29**: 501-507.

FONSECA M.S., FISHER J.S., ZIEMAN J.C. & THAYER G.W. (1982). *Influence of the seagrass Zostera marina on current flow.* Estuarine, Coastal and Shelf Science, **15**: 351-364.

FRIGNANI M. (1999). *Programma Generale delle attivita' di approfondimento del quadro conoscitivo di riferimento per gli interventi ambientali.* Consorzio Venezia Nuova. *Inquinamento e dinamica dei sedimenti.* Stralcio attuativo (2023-C-REL) del Progetto 2023: 55 p.

FRIGNANI M, BELLUCCI LG, LANGONE L. & MUNTAU H. (1997*). Metal fluxes to the sediments of the northern Venice Lagoon.* Marine Chemistry, **58**: 275-292.

FRIEND L.P. (2001). *Biological influences on the stability of intertidal flat sediments.* Unpublished Ph.D. thesis, University of Southampton, UK: 227 p.

FRIEND P.L., CIAVOLA P., CAPPUCCI S., SANTOS R. & CASTELLANI G. (in press). *Bio-dependent bed parameters as a proxy tool for sediment stability in mixed habitat intertidal areas.* Nearshore and Coastal Oceanography.

FROSTICK L.E. & McCAVE I.N. (1979). *Seasonal shifts of sediment within an estuary mediated by algal growth.* Estuarine and Coastal Marine Science, **9**: 569-576.

FUNG A. (1997). *Calibration of flow field in Mini-Flume.* Contract No. 23420-7-M339, Technical University of Nova Scotia, Canada.

GAMBOLATI G., GATTO P. & FREEZE R.A. (1974). *Mathematical simulation of the subsidence of Venice.* Water Resources Research, **10**: 563-577.

GATTO P. & CARBOGNIN L. (1981). *The lagoon of Venice: natural environmental trend and man-induced modification.* Hydrology Science Bulletin, **26**: 379-391.

GENNARO M.C., ABRIGO C., GIACOSA D., SAINI G. & AVIGNONE M.T. (1994). *The role of tide in the composition of Venice Lagoon water-determination of Phosphate, Silicate, Nitrite, Nitrate, Iodide, Bromide and Sulphate by spectrophotometry and HPLC ion-interaction chromatography.* Journal of Environmental Science and Engineering & Toxic and Hazardous Substance Control, **29**: 967-981.

GHERMANDI G., CAMPOLIETI D., CECCHI R., COSTA F., ZAGGIA L. & ZONTA R. (1993). *Trace metals behaviour during salt and fresh water mixing in the Venice Lagoon.* Nuclear instrument & Methods in Physics Research Section B-beam Interactions with Materials and Atoms, **75**: 330-333.

GIBBS R.J., MATTHEWS M.D. & LINK D.A. (1971). *The relationship between sphere size and settling velocity.* Journal of Sedimentary Petrology, **41**: 7-18.

GOMEZ E.A. (1996). *Erodibility of cohesive sediment beds under unidirectional currents.* ACER publication No. **40**, Acadia Centre for Estuarine Research, Wolfville, Nova Scotia, Canada: 24 p.

GOTTARDO D. & CAVAZZONI S. (1981). *Osservazioni sulla propagazione della marea nella laguna di Venezia.* Istituto Veneto di Scienze Lettere ed Arti. In: Rapporti e Studi, **VIII**: 31-37.

GRANT J. (1988). *Intertidal bedforms, sediment transport and stabilisation by benthic microalgae.* In: DE BOER P.L. *et al.* (eds). *Tide influenced Sedimentary Environment and Facies.* D. Reidel Publishing Company: 499-510.

GRANT J. & GUST G. (1987). *Prediction of coastal sediment stability from photopigment content of mats of purple sulpher bacteria.* Nature, **330**: 244-246.

GREEN M.O. & BOON III J.D. (1993). *The measurement of constituent concentrations in non-homogeneous sediment suspension using optical backscatter sensors.* Marine Geology, **110**: 73-81.

HATCHER A., HILL P., GRANT J. & McPHERSON P. (2000). *Spectral optical backscatter of sand in suspension: effects of particle size, composition and colour.* Marine Geology, **168**: 115-128.

HOLLAND K.D., ROSOWSKI J.R., GRETZ M.R. & ROEMER S.C. (1974). *Quantitative evidence concerning the stabilisation of sediments by marine benthic diatoms.* Marine Biology, **27**: 191-196.

HJÜLSTROM F. (1939). *Transportation of detritus by moving water.* In: P.D. TRASK (eds). *Recent Marine Sediments.* Dover: 5-31.

JEFFREY S.W. & VESK M. (1997). *Introduction to marine phytoplankton and their pigment signatures.* In: JEFFREY S.W., MANTOURA R.F.C. & WRIGHT S.W. (Eds). *Phytoplankton Pigments in Oceanography.* Paris, UNESCO: 37-84.

KIRBY R. (1990). *The sediment budget of the erosional intertidal zone of the Medway Estuary, Kent.* Proceeding of Geologists Association, **101**: 63-77.

KIRBY R. (2000). *Practical implications of tidal flat shape.* Continental Shelf Research, **20**: 1061-1077.

KIRBY R., BLEAKLEY R.J., WEATHERUP S.T.C., RAVEN P.J. & DONALDSON N.D. (1993). *Effect of episodic events on tidal mud flat stability, Ardmillan Bay, Strangford Lough, Northern Ireland.* In: METHA A.J. (eds). *Nearshore and Estuarine Marine Cohesive Sediment Transport, Coastal and Estuarine Studies 42*, American Geophysical Union, Washington D.C.: 378-392.

KJERFE B. (1994). *Coastal Lagoons.* In: KJERFE B. (eds). *Coastal Lagoon Processes.* Elsevier Oceanography Series, **60**: 1-8.

KOMAR P. & REIMENRS (1978). *Grain shape effects on settling rates.* Journal Geology, **86**: 193-209.

KRONE R.B. (1962). *Flume studies of the transport of sediment in estuarine shoaling processes.* Final report to the Hydraulic Engineering Laboratory and Sanitary engineering Research Laboratory, University of California, Berkeley, CA: 118p.

LABORATORIO VENEZIA (1996). *66-96 Laboratorio Venezia; La laguna, I fiumi, le citta` e il mare*. CD ROM I & II.

LAMBE T.W. & WHITMAN R.V. (1979). *Soil Mechanics*. John Wiley & Sons: 547p.

LASSERRE P. & MARZOLLO A. (2000). *The Venice Lagoon ecosystem. inputs and interactions between land and sea*. UNESCO (eds.): Man and Biosphere series, **25**: 387pp.

LAVELLE J.W. & MOFJELD H.O. (1987). *Do critical erosion stresses for incipient motion and erosion really exist?* Journal of Hydraulic Engineering., **113**: 370-393.

LORING D.H. & RANTALA R.T.T. (1992). *Manual for geochemical analysis of marine sediments and suspended particulate matter*. Earth Science Review, **32**: 235-283.

MADSEN K.N., NILSSON P. & SUNDBACK K. (1993). *The influence of benthic microalgae on the sediment stability of a subtidal shallow water sediment*. Journal Experimental Marine Biology Ecology, **170**: 159-177.

MANZENRIEDER H. (1983). *Die Biologische Verfestingungen von Wattflachen aus der sicht des Ingenieurs, Miteilungen des Leichtweiss-Instituts fur Wasserbau*, TU Braunschweig, **79**: 135-193.

MARCOMINI A., GEATTI A., ARGESE E. & DEGETTO S. (1997). *Passato e presente dell'inquinamento lagunare attraverso l'analisis di carote sedimentarie radiodatate*. Convegno "Salvaguardia Ambientale e Sviluppo Sostenibile: Contributi Scientifici al Progresso delle Conoscenze sulla Laguna di Venezia, Italy.

McANALLY W.H. & METHA A.J. (2001). *Coastal and Estuarine Fine Sediment Processes*. Elsevier. Proceedings in Marine Science, **3**: 506p.

McCAVE I.N. (1971). *Sand waves in the North Sea off the coast of Holland*. Marine Geology, **10**: 199-225.

McCAVE I.N. (1984). Erosion, transport and deposition of fine-grained marine sediments. In *Fine-Grained Sediments: Deep Water Processes and Facies* (STOW, D. AND PIPER, D.J.W., Eds.). Geological Society of London Special Publication, **15**: 35-69.

McCHARTY D.F. (1993). *Essentials of Soil Mechanics and Foundations* (4th edn). Prentice Hall Carer & Technology, New York: 788p.

MEADOWS P.S. & TAIT J. (1989). *Modification of sediment permeability and shear strength by burrowing invertebrates*. Marine Biology, **101**: 75-82.

MEHTA A.J. & PARTHENIADES E.M. (1975). *An investigation of the depositional properties of flocculated fine sediments*. Journal of Hydraulic Research, **13**: 361-381.

MEHTA A.J. & PARTHENIADES E.M. (1982). *Resuspension of deposited cohesive sediment beds*. Eighteenth Conference Coastal Engineering: 1569-1588.

MERLIN H.O., MENEGAZZO V.L. & SEMENZATO G. (1978). *Contributo alla conoscenza dei sedimenti superficiali della laguna veneta*. Atto dell'Istituto Veneto di Scienze, Lettere ed Arti; Tomo CXXXVII (1978-1979). Classe di scienze Fisiche, Matematiche e Naturali)

MILLER M.C., McCAVE I.N. & KOMAR P.D. (1997). *Threshold of sediment motion under unidirectional currents*. Sedimentology, **24**: 507-527.

MITCHENER H.J., TORFS H. & WHITEHOUSE R.J.S. (1996). *Erosion of mud-sand mixtures*. Journal of Coastal Engineering, **29**: 1-25.

MOOK D.H. & HOSKIN C.M. (1982). *Organic determinations by ignition: caution advised.* Estuarine, Coastal and Shelf Science, **15**: 697-699.

MÖLLER I., SPENCER T., FRENCH J.R., LEGGETT D.J. & DIXON M. (1999). *Wave transformation over salt marshes: a field and numerical modelling study from north norfolk, England.* Estuarine, Coastal and Shelf Science, **49**: 411-426.

MOORE W.M. & MASCH D.M. (1962). *Experiments on the scour resistance of cohesive materials.* Journal of Geophysical Research, **67**: 1437-1499.

MOSS B. (1989). *Water Pollution and the management of ecosystem: a case study of science and scientist.* In: GRUBB OCH WHITTAKER (eds). *Toward a more exact ecology.* Blackwell: 401-422.

MUSKANANFOLA M. R. (1994). *The influence of biological, sedimentological and physical factors on sediment stability in intertidal waters.* Un-published Ph.D. thesis, University of Southampton, UK: 243 p.

NEUMANN A.C., GEBELEIN C.D. & SCOFFIN G.P. (1970). *The composition, structure, erodibility of subtidal mats, Abaco, Bahamas.* Journal of Sedimentary Petrology, **40**: 272-297.

NEUMEIER U. & CIAVOLA P. (2001). *Influence of intertidal vegetation on sedimentary processes in a coastal lagoon (Ria Formosa, Southern Portugal).* IAS-2001. 21st Meeting of Sedimentologist, Davos, CH.

O'BRIEN D. (1998). *The sediment dynamics of a microtidal mudflat on varing timescales.* Unpublished PhD Thesis, University of Wales Cardiff, UK: 111p.

O'BRIEN D., WHITEHOUSE R. & CRAMP A (2000). *The cyclic development of a macrotidal mudflat on varying time scales.* Continental Shelf Research, **20**: 1593-1619 .

OCKENDEN M.C. & DELO E.A. (1991). *Laboratory testing of muds.* Geo-Marine Letters, **11**: 138-142.

ORSI T.H., EDWARDS C.M. & ANDERSON A.L. (1994). *X-Ray computed tomography: a non destructive method for quantitative analysis of sediment cores.* Journal of Sedimentary Research, **64**: 690-693.

PANAGIOTOPOULOS I., VOULGARIS G. & COLLINS M.B. (1997). *The influence of clay on the threshold of movement of fine sandy beds.* Coastal Engineering, **32**: 19-43.

PARCHURE T.M. & MEHTA A.J. (1986). *Erosion of soft cohesive sediments.* Journal of Hydraulic Engineering, **10**: 1308-1326.

PARTHENIADES E. (1971). *Erosion and deposition of cohesive material.* In: H.W. SHEN (eds). *River Mechanics II*: 25-91.

PARTHENIADES E. (1986). *A fundamental framework for cohesive sediment dynamics.* In: MEHTA A.J. (eds*) Estuarine Cohesive Sediment Dynamics.* Springer-Verlag: 219-250.

PATERSON D.M. (1989). *Short-term changes in the erodibility of intertidal cohesive sediments related to the migratory behaviour of epipelic diatoms.* Limnology and Oceanography, **34**: 223-234.

PATERSON D.M. & BLACK K.S. (1999). *Water Flow, Sediment Dynamics and Benthic Biology.* Advances in Ecological Research, **29**: 155-193.

PATERSON D.M. & DABORN G.R. (1991). *Sediment stabilization by biological action: significance for coastal engineering.* Developments in Coastal Engineering, University of Bristol: 111-119.

PATERSON D.M., TOLHURST T.J., KELLY J.A., HONEYWILL C., DE DECKERE E.M.G.T., HUET V., SHAYLER S.A., BLACK K.S., DE BROUWER J. & DAVIDSON I. (2000). *Variations in sediment properties, Skeffling mudflat, Humber Estuary, UK.* Continental Shelf Research, **20**: 1373-1396.

PATERSON D.M. & UNDERWOOD G.J.C. (1990). *The mudflat ecosystem and epipelic diatoms.* Proceedings of the Bristol Naturalist's Society, **50**: 74-82.

PAVONI B., DONNAZZOLO R., MARCOMINI A., DEGOBBIS D. & ORIO A.A. (1987). *historical development of the Venice Lagoon contamination as recorded in radiodates sediment cores.* Marine Pollution Bullettin, **18**: 18-24.

PERILLO G.M.E. (1995). *Geomorphology and Sedimentology of Estuaries.* Elsiever: 471p.

PETHICK J.S. (1992). *Saltmarsh geomorphology.* In: ALLEN J.R. & PYE K. (eds) *Saltmarshes: Morphodynamics Conservation and Engineering Significance.* Cambridge University Press, UK: 41-62.

PETHICK J., LEGGETT D. & HUGAN L. (1990). *Boundary layers under salt marsh vegetation development in tidal currents.* In: J.B. THORNES (eds). *Vegetation & Erosion: Processes and Environments.* John Wiley & Sons: 113-125.

PIGNATTI S. (1966). *La vegetazione alofila della Laguna di Venezia.* Memoria Istituto Veneto di Scienze, Lettere ed Arti, **33**: 1-74.

PIRAZZOLI B. (1997). *Recent sea-level changes and related engineering problems in the Lagoon of Venice, Italy.* Progress in Oceanography, **18**: 323-346.

POLAND J.F., FIGUERO A, VEGA G., CARBOGNIN L., JOHNSON A.I. & YAMAMOTO S. (1984). *Guidebook to studies of Land Subsidence due to ground water withdrawal.* Studies and Reports in Hydrology, UNESCO: 305p.

PRICHARD D.W. (1989). *Estuarine classification - a help or a hindrance.* In: NEILSON B.J., KUO A. & BRUBAKER J. (eds). *Estuarine circulation.* Humana Press: 1-38.

PULLIERO A. (1987). *Canal Grande mare forza tre.* Helvetia (eds), Venezia: 181p.

RAMASCO C. (1991). *Qualita` del acque del bacino Centrale della Laguna di Venezia: variazioni relative a cinque anni di misure.* CNR-ISDGM, Venezia, Technical Report, **161**: 54p.

RANWELL D.S. (1964). *Spartina salt marshes in Southern England. Rate and seasonal pattern of sediment accretion.* Journal of Ecology, **52**: 79-94.

RIETHMULLER R., HEINEKE M., KUHL H. & KEUKER-RUDIGER R. (2000). *Chlorophyll-a concentration as an index of sediment surface stabilisation by microphytobentos?* Continental Shelf Research, **20**: 1351-1372.

RITCHIE J.C., McHENRY J.R. & GILL A.C. (1973). *Dating recent reservoir sediments.* Limnology and Oceanography, **18**: 254-263.

ROBERTS W. & WHITEHOUSE R.J.S. (1997). *Long-term morphodynamic modelling of intertidal mudflats*: Interim report on morphology, processes and assessment of modelling approaches. HR Wallingford, Technical Report, **48**: 27 p.

ROLINSKI S. & SÜNDERMANN J. (2001). *Description of the suspended particulate matter phytobenthos reaction model.* Feed backs of estuarine circulation and transport of sediments on phytobenthos (F-ECTS), Institute of Oceanography, Hamburg University, 2001.

RUNCA E., BERNSTEIN A., POSTMA L. & DI SILVIO G. (1993). *Control of macroalgae blooms in the lagoon of Venice.* Proceedings Meadcost '93 Conference, Antalya, Turkey.

SARGUMAN A., RILEYP., ARULANDAN K., & KRONE R.B. (1973). *Physicochemical factors in the erosion of cohesive soils.* Journal Hydraulics Division, Proceedings of American Society of Civil Engineers, **99**: 555-558.

SEROTA S. & JAGLE A. (1972). *A direct-reading pocket shear vane.* Civil Engineering - American Society of Civil Engineers, **42**: 73-76.

SFRISO A., DONNAZZOLO R., CALVO C. & ORIO A.A. (1991). *Field resuspension of sediments in the Venice lagoon.* Environmental Technology, **12**: 371-379.

SFRISO A. & PAVONI B. (1994). *Macroalgae and Phytoplankton competition in central Venice lagoon.* Environmental technology, **15**: 1-14.

SFRISO A., PAVONI B. & MARCOMINI A. (1995). *Nutrient distribution in the surface sediment of the central lagoon of Venice.* Science of the Total Environment, **172**: 21-35.

SHAIKH M.A., MEADOWS A. & MEADOWS P.S. (1998). *Biological control of avalanching and slope stability in the intertidal zone.* In: BLACK K.S., PATERSON D.M. & CRAMP A. (eds) *Sedimentary Processes in the Intertidal Zone.* Geological Society, London, Special Publications, **139**: 1-10.

SHARMA P., GARDENER L.R., MOORE W.S. & BOLLINGER M.S. (1987). *Sedimentation and bioturbation in a salt marsh as revealed by ^{210}Pb ^{137}Cs and ^{7}Be studies.* Limnology and Oceanography, **32**: 313-326.

SHENG Y.P. & LICK W. (1979). *The transport and resuspension of sediments in a shallow lake.* Journal of Geophysical Research, **84**: 1809-1826.

SHI Z., PETHICK J.S. & PYE K. (1995). *Flow structure in and above the various heights of a saltmarsh canopy: A laboratory flume study.* Journal of Coastal Research, **11**: 1204-1209.

SHIELDS A. (1936). *Anwendung der Ähnlichkeits Mechanik und der Turbulenzforschung, auf die Geschiebe Bewegung.* Preuss Versuchanstalt fur Wasserbau und Schiffbau. Berlin: 20p.

SILVA P. & MOL. A. (1993). *Development of the Venice morphological system.* In: EDGE B.L. (eds). *Coastal Engineering.* Proceedings of the twenty-third international conference of American Society of Civil Engineers, **2**: 1812-1825.

SUNDBÄCK K., ODMARK S., WULFF A. & NILSSON C. (1997). *Effects of enhanced UVB radiation on a marine benthic diatom mat.* Marine Biology, **128**: 171-179.

SUTHERLAND A.J. (1967). *Proposed mechanisms for sediments suspension by turbulent flow.* Journal of Geophysical Research, **72**: 6183-6194.

SUTHERLAND T.F. (1996). *Biostabilization of estuarine subtidal sediments.* Unpublished PhD Thesis, Dalhousie University, Nova Scotia, Canada: 184p.

SUTHERLAND T.F., LANE P.M., AMOS C.L. & DOWNING J. (1999). *The calibration of optical backscatter for suspended sediment of varying darkness levels.* Marine Geology, **162**: 587-597

SUTHERLAND T.F., AMOS C.L. & GRANT J. (1998a). *The effect of buoyant biofilms on the erodibility of sublittoral sediments of a temperate microtidal estuary.* Limnology and Oceanography, **43**: 225-235.

SUTHERLAND T.F., GRANT J. & AMOS C.L. (1998b). *The effect of carbohydrate production by the diatom Nitzschia curvilineata on the erodibility of sediment.* Limnology and Oceanography, **43**: 65-72.

TEATINI P., GAMBOLATI G. & TOSI L. (1995). *A new three-dimensional non linear model of the subsidence at Venice.* Proceedings of the Fifth International Symposium on Land Subsidence, The Hague, International Association Hydrological Science, **234**: 353-361.

TEISSON C., OCKENDEN M., LE HIR P., KRANENBURG C. & HAMM L. (1993). *Cohesive sediment transport processes.* Coastal Engineering, **21**: 129-162.

THETIS (1997). *F-ECTS-(Feed-back of estuarine circulation and transport of sediments on Phytobentos).* A proposal to the EC Mast III Programme: 37p.

THOMPSON C. E. L. & AMOS C. L. (in press). *The impact of mobile disarticulated shells of Cresterderma edulis on the erosion of a cohesive substrate.* Estuaries.

TOLHURST T.J. (1999). *Microbial mediation of intertidal sediment erosion.* University of St. Andrews, Un-published PhD. thesis.

TOLHURST T.J., BLACK K.S., PATERSON D.M., MITCHENER H.J., TERMAAT G.R. & SHAYLER S.A. (2000). *A comparison and measurement standardisation of four in situ devices for determining the erosion shear stress of intertidal sediments.* Continental Shelf Research, **20**: 1397-1418.

TOLHURST T.J., BLACK K.S., SHAYLER S.A., MATHER S., BLACK I., BAKER K. & PATERSON D.M. (1999). *Measuring the in situ erosion shear stress of intertidal sediments with the Cohesive Strength Meter (CSM).* Estuarine, Coastal and Shelf Science, **49**: 281-294.

TOORMAN E.A. (1996a). *Sedimentation and self-weight consolidation: general unifying theory.* Geotechnique, **46**: 103-113.

TOORMAN E.A. (1996b). *Sedimentation and self-weight consolidation: general unifying theory.* Geotechnique, **48**: 295-298

TORFS H. (1994). *Erosion of layered sand mud beds in uniform flow.* Proceedings of the 24th International Conference on Coastal Engineering, Kobe, Japan.

TSCHIRKY P. & HALL K. (2001). *A field investigation of wave height reduction by bulrushes.* Proceedings of the 2001 Canadian Coastal Conference, Quebec, Canada.

UMGIESSER G. (2000). *Modelling residual currents in the Venice lagoon.* In: YANAGY T. (eds). *Interactions between Estuaries, Coastal Seas and Shelf Seas*: Terra Scientific Publishing Company, Tokyo: 107-124.

UNDERWOOD G.J.C., PATERSON D.M. & PARKES R.J. (1995). *The measurement of microbial carbohydrate exopolymers from intertidal sediments.* Limnology and Oceanography, **40:** 1243-1253.

VILLARET C. & PAULIC M. (1986). *Experiments on the erosion of deposited and placed cohesive sediments in an annular flume and a rocking flume.* Report to Coastal and Oceanographic Engineering Department, Gainesville: University of Florida.

VOS P.C., DE BOER P.L. & MISDORP R. (1988). *Sediment stabilisation by benthic diatoms in intertidal sandy shoals.* In: DE BOER P.L. *et al.* (eds). *Tide influenced Sedimentary Environment and Facies.* D. Reidel Publishing Company: 511-526.

WARRICK R. & OERLEMANS J. (1990). *Sea level rise.* In: HOUGHTON J., JENKINS G. & EPHRAMAUS J. *Climate Change: the Scientific Assessment*, Cambridge University Press, Cambridge: 257-281.

WEBB J.E. (1969). *Biologically significant properties of submerged marine sands.* Proceeding Royal Society London, **B174**: 355-402.

WIDDOWS J., BROWN S., BRINSLEY M.D., SALKELD P.N. & ELLIOT M. (2000). *Temporal changes in intertidal sediment erodability: influence of biological and climatic factors.* Continental Shelf Research, **20**: 1275-1289.

WHITEHOUSE R.J.S., SOULSBY R.L., ROBERTS W. & MITCHENER H.J. (1999). *Dynamics of Estuarine Muds. A Manual for Practical Applications.* HR Wallingford Scientific Report **527**: 74p.

WHITEHOUSE R.J.S., BASSOULET P., DYER K.R., MITCHENER H.J. & ROBERTS W. (2000). *The influence of bedforms on flow and sediment transport over intertidal mudflats.* Continental Shelf Research, **20**: 1099-1124.

WHITEHOUSE R.J.S. & WILLIAMSON W. (1996). *The relative importance of tide and wave influences on bed level change at an intertidal cohesive mudflat site.* H.R. Wallingford Report Scientific Report **445**: 17p.

XU J.P. (1997). *Converting near-bottom OBS measurements into suspended sediment concentrations.* Geo-Marine Letters, **17**: 154-161.

YALLOP M.L., DE WINDER B., PATERSON D.M. & STAL L.J. (1994). *Comparitive structures, primary production and biogenic stabilization of cohesive and non-cohesive marine sediments inhabited by microphytobenthos.* Estuarine, Coastal and Shelf Science, **39**: 565-582.

YOUNG R.A. (1977). *Seaflume: a device for in situ studies on threshold erosion and erosional behaviour of undisturbed marine muds.* Marine Geology, **23**: 11-18.

ZAGO C., COSTA F., ZAGGIA L., ZONTA R., GHERMANDI G. & CECCHI R. (1994). *Heavy-Metal Distribution in Pore Waters of the Cona Marsh: A Preliminary Investigation on Surface Sediments.* Il Nuovo Cimento, **17C**: 503-510.

ZAGGHIA L., ARGESE E. & ZONTA R. (1996). *Extraction of anthropogenic heavy metals from reduced sediments: indeterminations due to authigenic sulphides and clay minerals.* Toxicology and Environmental Chemistry, **54**: 11-21.

ZAGGHIA L. & ZONTA R. (1997). *Metal-sulphide formation in the contaminated anoxic sludge of the Venice canal.* Applied Geochemistry, **12**: 527-536.

ZONTA R. (2000). *DRAIN project (DeteRmination of pollutAnts INput from the drainage basin to the Venice Lagoon).* International Advanced School "Leonardo da Vinci": processes in the coastal zone: links to management issues.

ZONTA R., ARGESE E., COSTA F. & ZAGGIA L. (1995). *Useful tracer parameters to investigate the environmental conditions in areas of the Venice Lagoon.* Wetlands Ecology, **3**: 139-147.

ZONTA R., CECCHI R., COSTA F., SIMIONATO F. & GHERMANDI G. (1994a). *A filtration system for the size separation of freshwater samples.* The Science of the Total Environment, **143**: 163-172.

ZONTA R., ZAGGIA L. & ARGESE E. (1994b). *Heavy metal and grain-size distributions in estuarine shallow water sediments of the Cona Marsh (Venice Lagoon, Italy).* The Science of the Total Environment, 151: 19-28.

APPENDIX I

Analytical Methods and definition of parameters

Sediment suspended concentration

Suspended Sediment Concentration (SSC) was determined by filtering a known volume of water (between 10-50 ml) through Whatman ® 47 mm filters. Filters were pre-weighed and placed in a millipore® pump system; 10 ml of fresh water were flushed through filters at the end of filtration to remove the salts (if salt water was filtered). Filters were dried in an oven for 24 hours at 60°C then re-weighted. SSC was calculated using the following equation:

$$SSC = [(M_{fs} - M_f) / V]*1000 \ (mg/l)$$

where: M_{fs} is the weight of the filter plus sediment (g); M_f is the weight of the filter (g) and V is the volume of water (l).

Grain size

Surface sediment samples were treated at high temperature (375°C) for about 12 hours to remove the organic matter. After this treatment, samples were wet-sieved with tap water using two sieves, which had openings of 2 mm and 62.5 µm. The first one was used to remove coarse fragments of gravel, the second one to separate sand from mud. The sand : mud ratio was determine gravimetically. Sequentially, grain size distributions were determined using the Coulter® Laser counter in triplicates.

Water and organic content

BACKGROUND INFORMATION ON WATER CONTENT, wc (%); is defined as the ratio between the mass of water and dry sediment. The water content in sediment depends by the porosity (i.e. packing of particles) as water can saturate the voids left between grains.

BACKGROUND INFORMATION ON LOSS ON IGNITION, LOI (%); The organic matter in the soil is made up of the partially decomposed remains of plant and animal tissues as well as the bodies of living micro-organisms and plant roots. It can be determined

by measuring the weight loss of dry sediments by combusting the organic matter (trapped within particles) by ignition at 375 °C for 4 hours. The limitation of this technique is that part of the structural water (locked within the lattice structure of the clays) may be driven off (MOOK & HOSKIN, 1982).

ANALYTICAL METHOD: Determination of water content was performed on fully saturated subsamples of sediment following the method outlined by LORING & RANTALA (1992). Approximately 2 g of wet sediment were placed in a drying oven for 24 hours at 105°C. After drying, samples were replaced in a desiccator until they reached room temperature. Water content (wc) was derived from the following equation:

$$wc = [(w_w - w_d) / w_d] \times 100\ (\%)$$

Where w_w and w_d are respectively wet weight and dry weight.
Dry sediment samples were then used to determine organic content on the basis of the "Loss On Ignition" (LOI). About 2 g of dried samples were placed in a oven for 4 hours at 375°C (±5°C). The LOI, (%), was determined as for the water content.

Bulk Density

BACKGROUND INFORMATION ON WET BULK DENSITY, ρ (kg/m^3); is defined as the mass of saturated sediments per unit of volume. The soil particles may consist of many kinds of minerals with a wide range in particle densities. The average particle density for most minerals varies between 2600 and 2750 kg/m^3. The average density of organic-rich particles range between 1200 and 1400 kg/m^3. Bulk density of natural sediments depends on the heterogeneity of material (i.e. % of particles and organic material).

ANALYTICAL METHODS: The density of sediment has been measured using x-ray computed tomography and sub-samples from syringe cores.

Computed tomography is non-destructive, digital, three dimensional and gives greater spatial resolution compared to other standard methods (AMOS *et al.*, 1996a). Syringe cores were tomographically sliced at 1.5 mm intervals from the top

to a depth of 15 mm (Figure A). Thereafter, slices were taken each 10 mm. More than 10,000 independent analyses were made across each 1.5 mm thick tomographic slice, due to the high plane resolution (0.035 mm^2) of the CT scanner.

The mean value and standard deviation of the fresh-water, wet bulk density were calculated using the following relationship of AMOS *et al.* (1996a).

$$\rho = 390 + 670\ (CT)\ \ kg/m^3$$

where CT is a Computed Tomographic number derived using the expression of ORSI *et al.* (1994), reported as follows:

$$CT = 1 + (HU/1000)$$

where HU is the Hounsfield Unit for any voxel and is defined as:

$$HU = 1000\ (\mu_s - \mu_w)/\mu_w$$

where μ_s and μ_w are respectively the x-ray linear attenuation coefficients of sediment and fresh water, respectively. According to Beer's Law, μ_s is a function of sediment bulk density, ρ_s. Results were plotted against core depth for each sample to produce the profile of each core.

Wet bulk density was also derived from saturated sub-samples using the following equation:

$$\rho = (W_w + W_s) / V$$

where W_w is the weight of the water and W_s is the weight of the sediment and V is the Volume of the sample.

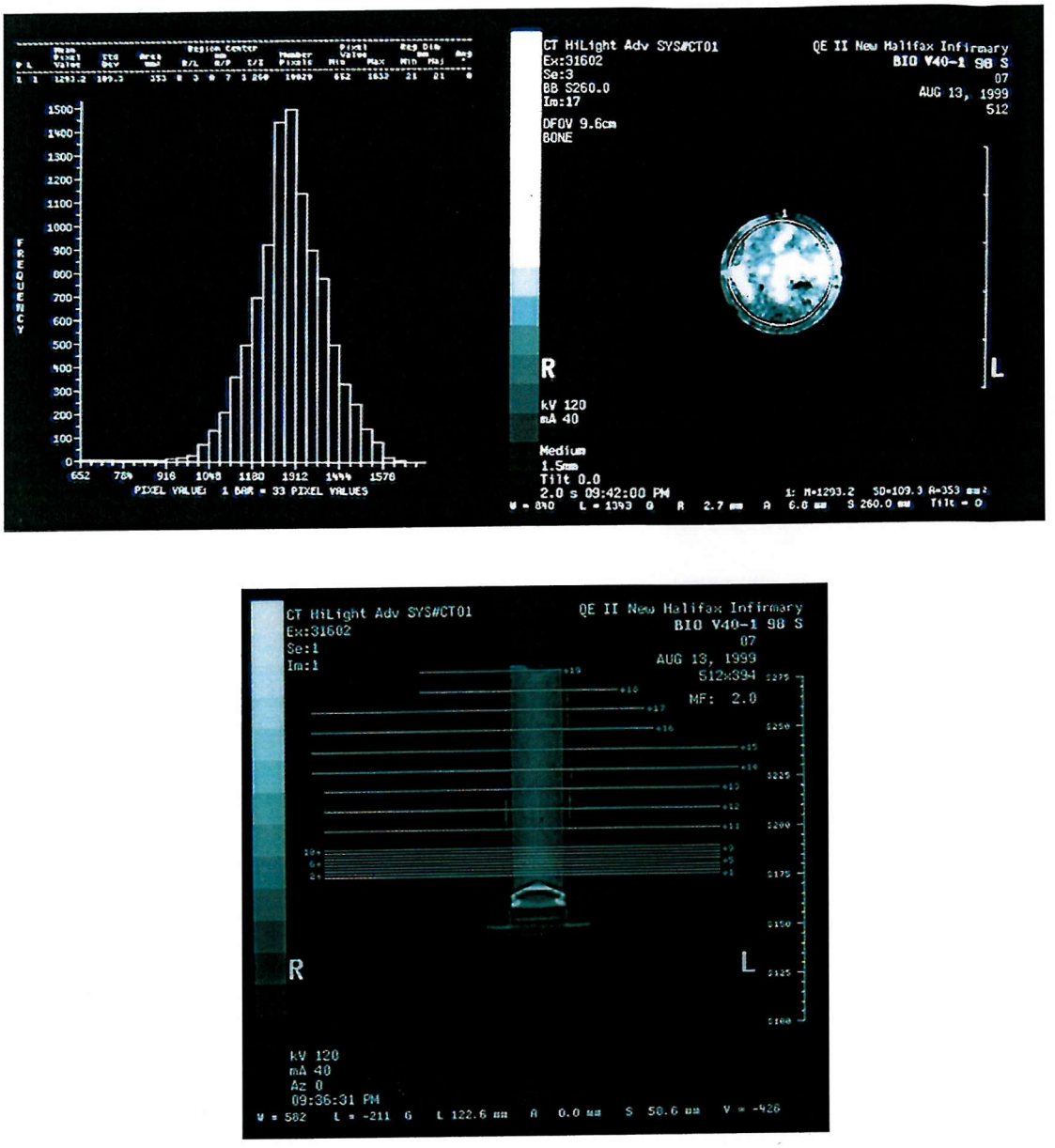

Figure A. Section of syringe core V40 at 9 mm (1.5 mm) of depth from CT scanner image (top). Frequency diagram (top left) show a unimodal distribution of HU values. Typical profile of scanning procedure to determine bulk density with depth (bottom).

Colloidal carbohydrate

BACKGROUND INFORMATION, EPS gluc. eq. ($\mu g/g_{DW}$). Extra polymeric substances (EPS) are secreted by diatoms, bacteria and cyanobacteria. Carbohydrates represent about 70% of the gluey substances (EPS) and are largely made of polysaccharides, produced by the diatoms in order to stick to the sediment grains and/or facilitate their own movement.

ANALYTICAL METHOD: The top 10 mm of sediment from a frozen 60 ml syringe core was subsampled and freeze-dried (lyophilised sediment yielded more carbohydrate than wet samples UNDERWOOD *et al* (1995)). Approximately 0.1 g of material was then put into a centrifuge cuvette and 3 ml of 25% saline solution added. The solution was mixed using a Roter Shaker for 10 seconds and incubated for 15 minutes to complete the dissolution before centrifuging at 3500 rpm for 10 minutes. 1 ml of supernatant fluid was transferred in a clean centrifuge cuvette. 0.4 ml of 5 % (by weight) phenol solution was added. After mixing, 2 ml of concentrated H_2SO_4 was rapidly added. After about half-hour (when the exothermic reaction was completed) the absorbance at 485 nm was measured using a spectrophotometer. To be sure all the carbohydrate was extracted from the samples, extractions were repeated three times. Total carbohydrate content is derived by:

$$Carb_{TOT} = (Carb1+Carb2+Carb3) \qquad (\mu gGE/g_{DW})$$

where *Carb1, Carb2 and Carb3* are the concentrations determined by the three repeated extractions. They are calculated using the following relationship

$$Carb\ n = ((a*ext\ n)+b) / W_d \qquad (\mu gGE/g_{DW})$$

Where *a* and *b* are respectively the coefficient and constant of the linear calibration curve ($Y = aX+b$) and W_d is the dry weight of the sample. A calibration curve is produced with dilutions of glucose solution containing 0, 5, 10, 25, 50, 75, 100 µg/ml glucose.

Chlorophyll *a*

BACKGROUND INFORMATION, ($\mu g/g_{DW}$); Chlorophyll *a* is the principal pigment converting light energy into chemical energy by the following reaction:

$$2H_2O+C_2O+light \rightarrow (CH_2O)+H_2O+O_2$$

Photosynthetic pigments are in all plants and they absorb the light between 400 and 700 nm (JEFFREY & VESK, 1997).

ANALYTICAL METHOD: Approximately 2 g of superficial sediments were collected from the topmost 1 cm of a syringe core. The tip of the syringe was cut to facilitate the sediment's collection. 10 ml of 90% acetone was immediately added to the samples. These samples were stored in a fridge at 4 °C temperature.
The samples were accurately weighed before the analysis, then mixed and treated in an ultrasonic bath for 30 minutes. The supernatant fluid was poured into a quartz cuvette and three values of absorbance were determined using a spectrophotometer. The values were obtained at 664, 647, 630 μm and then used in the following formula to determine the amount of chlorophyll-a:

$$C=11.85\ E_{664}-1.54\ E_{647}-0.08\ E_{630}$$

The following relation was used in order to determine the absolute value of chlorophyll-a concentration in the sediments:

$$Cla = (CV)/P \qquad (\mu g/g_{DW})$$

were C = chlorophyll amount units; V = volume of acetone (ml); P = weight of the sediment (mg).

APPENDIX 2

Description of investigated sites in Venice Lagoon

A summary of site positions and depth from the F-ECTS field campaigns is reported in the Table below. A map showing the position of the station within Venice Lagoon is reported in the text (Fig 3.1.). A brief description of the type of environment, biological covering and ambient conditions are listed for each site as follow.

Site	*Name*	*Latitude*	*Longitude*	*Depth (m)*	*Sub-Basin*
V 20	S.Giacomo	45° 28' 31"	12° 23' 11"	1	Northern
V 30	Cona	45° 30' 30"	12° 23' 12"	1.4	Northern
V 40	Centrega	45° 29' 40"	12° 26' 23"	0.2	Northern
V 50	Saline	45° 30' 34"	12° 28' 28"	0.2	Northern
V 60	S.Maria del Mare	45° 19' 58"	12° 18' 13"	2	Central
V 70	S.Leonardo	45° 21' 25"	12° 15' 45"	2.4	Central
V 80	S.Spirito	45° 24' 08"	12° 20' 10"	1.7	Central

V 20 - *S. Giacomo* is a subtidal area located on the northern side of the channel that links the City of Venice to Burano. Diatoms cover the surface of the soft mud. Fragments of shells were also observed.

V 30 - *Rosa* is a subtidal station located in the mouth of the Dese River. It is subject to the lowest salinity due to the discharge of the river. In this station floating aggregates were observed (Fig B.). Their origin is unknown, but bubbles of O_2 probably support them. They may also contribute significantly to the total sediment budget of Venice Lagoon.

V 40 - *Palude della Centrega* is probably the site presenting the most variability and is a well preserved intertidal region of Venice Lagoon. For this reason it has been studied in detail in the present study. An accurate description can be found in Chapter 4. Diatoms, cyanobacteria filaments, *Zostera noltii* cover the very soft mud in the area. Salt marsh vegetation is represented by Spartina and Salicornia.

V 50 – *Saline* is the northernmost investigated site. The area is intertidal and was open to tidal inundations after the second war CVN (1996). Before that time it had been reclaimed from the sea and used to produce marine salt. The site is characterise by filamentous algae, diatoms, wormholes, and birds prints.

Fig B. Floating organic aggregates (1-5 cm in diameter) supported by O_2 bubbles.

V 60 - *S. Maria del Mare* is the southernmost investigated site, and is located on the eastern side of Malamocco inlet. The site is subtidal and is characterised by sandy silt.

V 70 - *S. Leonardo* is located on the left side of *Malamocco* Canal *(Canale dei Petroli)*. Before dredging of the channel the area was covered with a Zostera marina community (CVN, 1996). The average depth is more than 1 m and no algae coverage have been observed in summer or winter due to the high turbidity of the area.

V 80 - *S.Spirito* is a subtidal area located in the south of the City of Venice. It is characterises by very fine sediments covered by macroalgae (Ulva).